1987

The Crixas Gold Deposit, Brazil: Metamorphism, Metasomatism And Gold Mineralization

Margaret Lee Thomson

NOTICE

The quality of this microform is heavily dependent upon the quality of the original thesis submitted for microfilming. Every effort has been made to ensure the highest quality of reproduction possible.

If pages are missing, contact the university which granted the degree.

Some pages may have indistinct print especially if the original pages were typed with a poor typewriter ribbon or if the university sent us an inferior photocopy.

Previously copyrighted materials (journal articles, published tests, etc.) are not filmed.

AVIS

La qualité de cette microforme dépend grandement de la qualité de la thèse soumise au microfilmage. Nous avons tout fait pour assurer une qualité supérieure de reproduction.

S'il manque des pages, veuillez communiquer avec l'université qui a conféré le grade.

La qualité d'impression de certaines pages peut laisser à désirer, surtout si les pages originales ont été dactylographiées à l'aide d'un ruban usé ou si l'université nous a fait parvenir une photocopie de qualité inférieure.

Les documents qui font déjà l'objet d'un droit d'auteur (articles de revue, tests publiés, etc.) ne sont pas microfilmés.

THE CRIXAS GOLD DEPOSIT, BRAZIL: METAMORPHISM, METASOMATISM AND GOLD MINERALIZATION

by

Margaret Lee Thomson

Department of Geology

Submitted in partial fulfillment of the requirements for the degree of Doctor of Philosophy

Faculty of Graduate Studies
The University of Western Ontario
London, Ontario

September 1987

ISBN 0-315-40796-4

ABSTRACT

The Crixas gold deposit is located in central Goias State, approximately 400 km NW of Brasilia. The hosting Crixas Greenstone Belt is underlain by a typical Archean volcanic-sedimentary sequence surrounded by granite gneiss terrains. The interpreted stratigraphic sequence consists of a basal ultramafic volcanic unit (Corrego do Alagadinho Formation), locally spinifex textured, which is overlain by the Rio Vermelho Formation of komatiitic and tholeiitic basalts. This unit is in turn overlain by a sedimentary sequence consisting dominantly of chloritic schists and graphitic pelites (Ribeirao das Anta Formation). The Ribeirao das Anta Formation is unconformably overlain by the Proterozoic age Araxa Group.

The Crixas Gold Deposit occurs at the contact of metavolcanics and metasediments. The lithologic sequence from the structural hanging wall to footwall is: Foliated Amphibolite transitional to Ferroan Dolomite-Chlorite-Biotite-Quartz Schist (FDCBQS), veined Ferroan Dolomite-Chlorite-Sericite-Biotite-Quartz Schist (veined FDCSBQS) and Massive Ferroan Dolomite. These ferroan dolomite rocks are in sharp contact with and envelope Sericite-Chlorite and Chlorite-Magnetite Schist which is distinguished by the presence of grunerite, magnetite and massive sulphides of pyrrhotite, arsenopyrite. Underlying these units are alternating units of Silicified Dolomite and Graphitic Pelite. A distinct marker horizon of Banded Chlorite-Sericite-Garnet Schist is in sharp upper contact to Graphitic Pelite and sharp lower contact to Banded Quartz-Biotite-Chlorite-Plagioclase

Schist.

Gold occurs within an Upper Ore Zone of FDCBQS, veined FDCSBQS, Massive Ferroan Dolomite, Sericite-Chlorite Schist and Magnetite-Chlorite Schist and a Lower Ore Zone of Quartz Cemented Graphitic Pelite Breccia located at or near the contact of the Graphitic Pelite and the Banded Chlorite-Sericite-Garnet Schist. Gold occurs associated with both massive and disseminated arsenopyrite and pyrrhotite.

The Upper and Lower Ore Zones are interpreted as metasomatically altered parent lithologies. Metasomatism post-dates a maximum regional metamorphism of Biotite-Garnet Grade or Epidote Amphibolite Facies and consists of carbonatization, sericifization, Fe-metasomatism and sulphidization. The Foliated Amphibolite is the carbonatized parent to the FDCBS, veined FDCSBQS and Massive Ferroan Dolomite and sericitized, Fe-metasomatised and sulphidized parent to the Sericite-Chlorite Schist and Chlorite-Magnetite Schist. The Graphitic Pelite is the sericitized and sulphidized parent to the Quartz Cemented Graphitic Pelite Breccia.

Gold deposition resulted from reduced f_{S2} due to the reaction of S of the metasomatic fluid and Fe-silicate minerals to form sulphides. f_{O2} is constrained by the presence of graphite and magnetite.

Geothermometric calculations of coexisting garnet and biotite, inclusions within garnets and coexisting mineral assemblages all indicate that the Lower Ore Zone represents a major structural and geothermal discontinuity. It is proposed that shearing related low angle thrusting is the most likely model which accounts for the development of both the Upper and Lower Ore Zones. The age of this thrusting is not known, but is speculated to be Brasiliano Cycle in age (570 Ma).

ACKNOWLEDGEMENTS

I want to express my sincerest appreciation to Dr. W.S. Fyfe for his advice when facing impasses and for the freedom he granted me in doing this research. Dr. J.P. Golightly is thanked for his continued support and for critisms which always resulted in the advancement of my work. Drs. W.R. Church, H.W. Nesbitt and R.W. Hodder provided me with their valuable guidance, and they are warmly acknowledged.

INCO Metals, and in particular Mr. T. Podolsky, is acknowledged for giving me the opportunity and partially supporting this study on the Crixas Gold Deposit.

Special gratitude is given to Mr. R.L. Barnett who provided helpful instruction on the use of the electron microprobe and his continued friendship. Dr. T.C. Wu gave me able assistance in completing the whole rock analysis. Mr. J. Forth and Mr. W. Harley are thanked for making superb thin sections at the most critical times. Mr. I. Craig provided the photographic expertise for which I am grateful.

I want to thank my fellow graduate students for educating, helping and distracting me. Dr. A. Kishida, Dr. E. Van der Flier-Keller, Dr. W. Shotyk are thanked in absentia. The time, inspiration and insight provided by Mr. G. Albino cannot go without a mention. Mrs E. Malik, Mrs. T. Weerasooyria, Mr. E. Prosh and Ms. K. Cunnison are warmly thanked for their friendship and tolerance.

The encouragement and support of my five sisters and brother is deeply appreciated.

Finally I want to acknowledge Dr. T.E. LaTour who instilled in me the desire to pursue a graduate degree. I am truly indebted to him.

TABLE OF CONTENTS

Page

Page

Page

Page

LIST OF PHOTOGRAPHIC PLATES

LIST OF TABLES

LIST OF FIGURES

Figure	Description	Page
6.3	AFM diagram of Fe-Silicate assemblage of Sericite-Chlorite-Schist	218
6.4	$-\log f_{O2}$ versus $-\log {}_{S2}$ in the system Fe-Ti-S-O-C at 500°C and 5Kb	221
6.5	X-CO_2 versus T°C for a dolomite system	226
6.6	AFM diagram of Graphitic Pelite	230
7.1	$-\log f_{O2}$ versus pH for the system Au-Na-Cl-S-H_2O at 250°C	239
7.2	$-\log f_{O2}$ versus $-\log f_{S2}$ in the system Au-As-Fe-S-H_2O at 500°C and 5Kb	242
7.3	$-\log f_{O2}$ versus T°C for Reaction (4)	244
8.1	Block diagram of Minas III showing the metamorphic isograd	248

Chapter One

1.1 Introduction

This thesis presents a study of the geology of the Crixas Gold Deposit, known locally as Minas III. The deposit is located within central Goias State, approximately 400 km north-west of the capital of Brazil, Brasilia. The nearest town is its namesake, Crixas. Crixas is a small farming community with a population of 3000, accessible by road and air.

The deposit is currently being brought into production by the operators, Anglo American Corporation, in joint venture with INCO Metals. The published reserves are 7 million metric tonnes, with a grade of 10-12 grammes/tonne (INCO Annual Report, 1986).

1.2 Purpose

1.2.1 Regional Scale

After the Republic of South Africa, gold from lode gold deposits of Archean rocks is mined predomoninatly in Canada (86 tonnes), United States (79 tonnes), Brazil (63.3 tonnes) and Australia (57 tonnes) (Mining Journal, 1985 figures, Milling-Stanley, 1986). To date, the bulk of Brazil's gold production has been from surficial gold produced by garimpos (non-mechanised miners) representing 55 tonnes/year. Hard rock production has historically come from the Quadrilatero Ferrifero, with Morro Velho representing a major producer. Recent discoveries elsewhere in Brazil, such as the Crixas Gold Deposit, confirm the tremendous potential for gold production within Brazil.

The most detailed mapping of the geology of Brazil is limited to populated areas and major mineral producing areas, leaving vast tracts of land mapped in limited detail. Geologic mapping in Brazil is further complicated by pervasive saprolitic and lateritic weathering which confounds rock identification. It is by default, therefore, that studies of diamond drill-core and mine workings provide much of the detailed geologic information.

The advent of gold exploration within the Crixas Greenstone Belt and the discovery of the Crixas Gold Deposit itself have sparked considerable interest in the geology of the area; however, little is as yet understood. This study presents the first extensive and systematic petrographic and geochemical investigation of rocks belonging to the Crixas Greenstone Belt and the Crixas Gold Deposit. As a result of the pioneering nature of this work, many of what seem to be fundamental questions are not answered. Simply, many crucial details are not yet available. One principal aim of this study is to establish a body of data and knowledge of the Crixas Greenstone Belt and the Crixas Gold Deposit around which future workers can build.

1.2.2 Deposit Scale

As matters currently stand, two schools of thought exist regarding the genesis of gold deposits: 1) gold deposition is primary, occurring essentially coevally with deposition of the host rocks and 2) gold deposition is secondary, occurring significantly later then host rock deposition. An excellent example of the application of these two models to the same deposit is the Kerr Addison Gold Mine in the Larder Lake Camp, Ontario.

Ridler (1972) proposes that the ubiquitous "green carbonate" associated with gold mineralization is the product of primary carbonate sedimentation, a carbonate facies iron formation. Kishida (1984), however, proposes that the "green carbonate" is a product of carbonatization of ultramafic and mafic rocks.

Similar conflicting arguments could be presented for the Crixas Gold Deposit. It might be suggested the carbonate and magnetite rich rocks of the Upper Ore Zone are the products of either primary or secondary processes, and similarly for the quartz breccia of the Lower Ore Zone is the product of either primary or secondary processes. It is an aim of this study to determine the nature of these rock units and to evaluate which style of genesis is best applied to the Crixas Gold Deposit.

1.3 Statement of the Problems

1) What are the nature of the rock types of the Crixas Gold Deposit?

2) Do these rock types represent essentially primary lithologies or have they undergone alteration resulting in a secondary lithology?

3) What are the geologic processes which have affected the primary rock types?

4) Do any of these processes relate to the deposition of gold?

1.4 Approach

Chapter Two presents a summary of the previous work in the area leading up to the recognition of the Crixas Greenstone Belt as a typical Archean greenstone belt. The geology of the adjacent greenstone belts and the Crixas Greenstone Belt itself are also described. Although merely a summary this simple review does effectively represents the current understanding of the geology of this area.

Chapter Three is a detailed petrographic description of the rock types of the Crixas Gold Deposit. This body of work is the cornerstone of the thesis. Its design is objective and its intent is to provoke further inquiry beyond this initial study.

Chapters Four and Five are not unlike Chapter Three. They present initial whole rock geochemical data and mineral chemistry data obtained on the lithologies of the Crixas Gold Deposit. In addition, mass balance calculations are applied to the geochemical data to better understand the nature and relationships of the various rock types, and gain insight into their possible primary or secondary genesis. Garnet and biotite geothermometyr is further used to establish the conditions of metamorphism of several rock types.

Chapter Six is a synthesis of all data relevant to the metamorphic and metasomatic histories of the rock types. Whereas the previous chapters are broad in their scope, presenting large bodies of data, Chapter Six is intended to be much more specific, dealing with the nature of metamorphism and the reactions involved in metasomatism.

Chapter Seven summarizes the available data on gold solubility, and presents a model for gold deposition within the Crixas Gold Deposit.

Chapter Eight is not intended to be a rigorous discussion on the structural development of the Crixas Gold Deposit. Rather, it is presented as a review of the available data as they pertain to the proposed model for the genesis of the Crixas Gold Deposit.

CHAPTER TWO.

Regional Geology.

2.1 Introduction

The Precambrian of Brazil consists of the large Guapore, Sao Francisco and Atlantic Cratons with the smaller Rio de La Plata, Sao Luis and Luis Alves Cratons fringing the larger ones (Figure 2.1). Two complex terrains known as the Guaxupe and Goias Massifs flank the western margin of the Sao Fransisco Craton (Figure 2.1) and are believed to be older basement crust than that of the Sao Fransisco Craton (Schobbenhaus et al., 1984). The Paraguai-Araguaia Fold Belt (Brasiliano Event, 450-700 Ma, ibid) separate the Guapore and Sao Fransiciasco Cratons.

The geologic evolution of the Precambrian of Brazil is shown in Table 2.1. The Archean consists of greenstone belts made up of volcano-sedimentary rocks, surround by granite and granite-gneiss. Thick sequences of Proterozoic sediments overly the Archean. (Figure 2.1)

2.2. Previous Work

Prior to 1978 the geology of central Goias State was considered to be part of the Araxa Group (of probable Precambrian age) represented by amphibolites, quartzites and mica schists (Almeida, 1968). Ultramafic rocks were interpreted to be alpine ultramafic suites emplaced within the Araxa Group during the Uruacuano-Espinhaco Tectonic Event dated at 1400-1100 Ma by K/Ar dating method. (Almeida et al.,1976).

Table 2.1. Geologic Evolution of the Precambrain of Brazil.

570 Ma **BRASILIAN EVENT** Upper Proterozoic

Geosynclinal Sediments (pelite and carbonate)
Syntectonic Granite-Granitoid

1100 Ma **ESPINHACO EVENT** Middle Proterozoic

Alpine Ultramafic Intrusions
Acid to Intermediate Volcanism
Granite Intrusions

1900 Ma **TRANSAMAZONIAN EVENT** Lower Proterozoic

Basin Sediments BIF (Superior Type),
Graphitic Schists and Dolomite

Metaconglomerate (Witswatersrand Type)
Volcano-Sedimentary Greenstone Belt

2600 Ma **JEQUIE EVENT** Archean

Volcano-Sedimentary Greenstone Belt
Mafic-Ultramafic Complexes
Granitoid, Granite-Gneiss, Migmatite

after Schabbenhaus et al., 1984

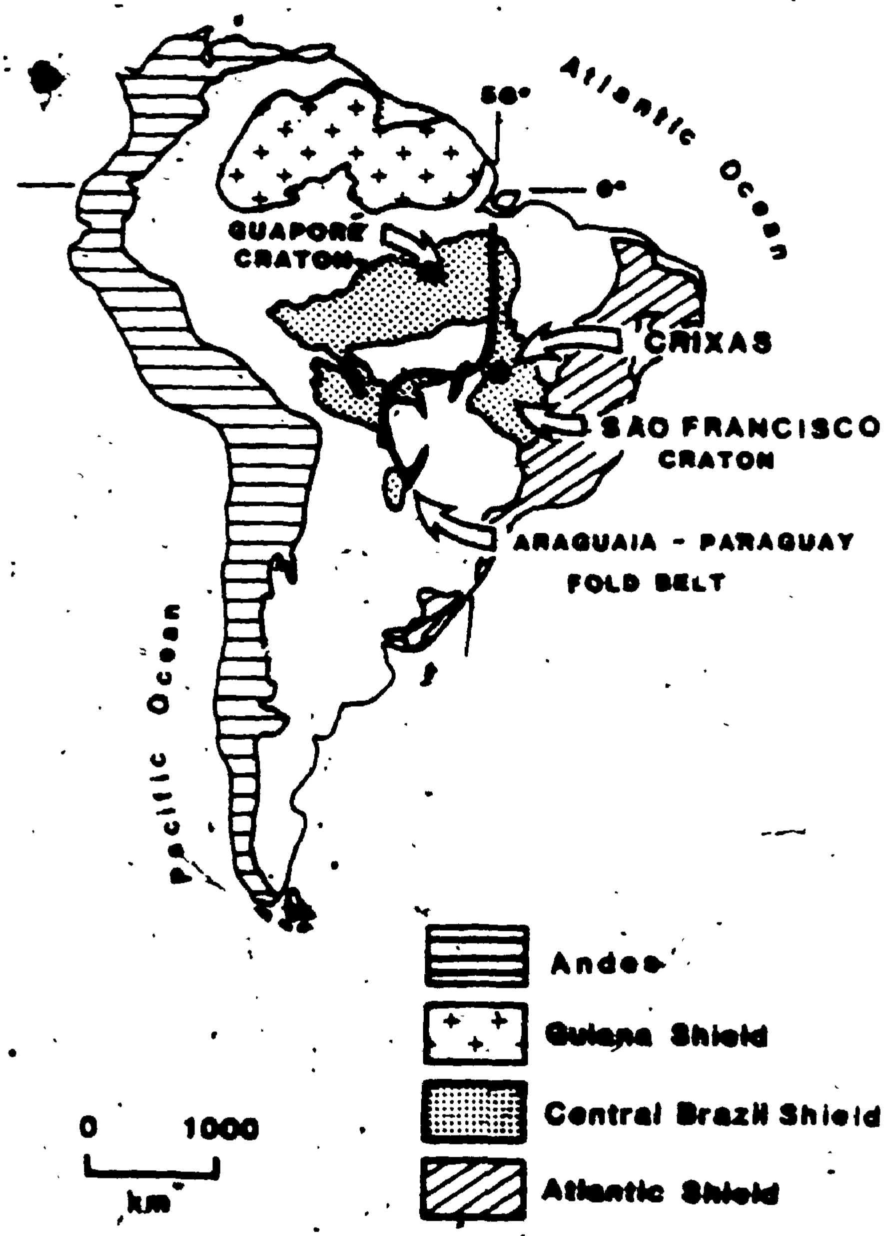

Figure 2.1. Geologic map of South America indicating the location of the Precambrian Cratons and the town of Crixas. (after Schobbenhaus et al., 1984)

Regional mapping by Schobbenhaus et al. (1975) grouped the Arai Group, Canastra Formation and the Araxa Group into an informal "Araxa System". They recognized a basal portion to the Araxa System, termed "amphibolite rocks" consisting of hematitic quartzites and amphibolite schists.

Danni and Ribeiro (1978) first suggested an Archean age for the greenstone belt in central Goias State. They described the geology in the region of the towns of Pilar de Goias and Guarinos (Figure 2.2). as a volcanic-sedimentary rock sequence (Pilar de Goias Group) consisting of, in part, komatiitic volcanics. The association of komatiitic volcanics suggested, to these authors, an Archean age but they did not commit themselves to this interpretation. They did, however, recognize the Pilar de Goias Group as an older sequence of rocks than the Araxa Group.

Ribeiro et al.(1978), studying in the Pilar de Goias and Mara Rosa regions, divided the Precambrian stratigraphy (formally all Araxa Group, Almeida, 1968) into three separate units with discordant contacts. These are: the Basal Complex (lowest PC) consisting of granites, granite gneisses and migmatites; the "Metamorphic Association of Pilar de Goias" (lower-mid PC), consisting of volcanic and sedimentary rocks and the Araxa Group (mid-upper PC) consisting of a poorly defined sequence of complexly folded schists.

de Saboia (1979) first described the volcanic and sedimentary rocks of the Crixas area as a greenstone belt, comparing it to the Archean greenstone belts described in the Superior Province of Canada (ie. Goodwin, 1968) and Barberton Mountain Land of Republic of

South Africa (ie. Anhaeusser,1969). The granite and granite gneisses surrouuding the greenstone belts are considered to be basement sialic crust and the Araxa Group is interpreted to unconformably overlie the greenstone belt rocks and be of a Proterozoic age.

It is de Saboia's (1979) interpretation of the regional geology which is used in this study.

2.3. Geology of Crixas, Guarinos, and Pilar Greenstone Belts

As defined by de Saboia (1979), the Crixas Greenstone Belt is composed of three N-S trending elongate (40 km long, 10 km wide), arc-shaped belts containing a similar sequence of volcanic and sedimentary rocks (Figure 2.2). However, it is recommended that each "belt" be referred to as separate Greenstone Belts, thereby eliminating the collective term Crixas Greenstone Belt.

The most easterly belt is the Pilar Greenstone Belt, the central is the Guarinos Greenstone Belt and the westerly is the Crixas Greenstone Belt, all named after the local towns. Each is surrounded by complex terrains of granite, granodiorite, tonalite and granite gneiss of the Goiano Basal Complex (Almeida et.al.,1976). After de Saboia (1979) and de Saboia and Teixeira(1983) these granite granite-gneiss terranes are: Hidrolina Dome east of the Pilar Greenstone Belt, Muquem Dome separating the Pilar and Guarinos Greenstone Belts, Caiamar Dome separating the Guarinos and Crixas Greenstone Belts and the Anta Dome west of the Crixas Greenstone Belt.

Figure 2.3 schematically correlates the geologic columns of the Crixas, Gurarinos and Pilar Greenstone Belts (after de Saboia et al.,1981 and Danni and Ribeiro,1978). In all three belts the gross

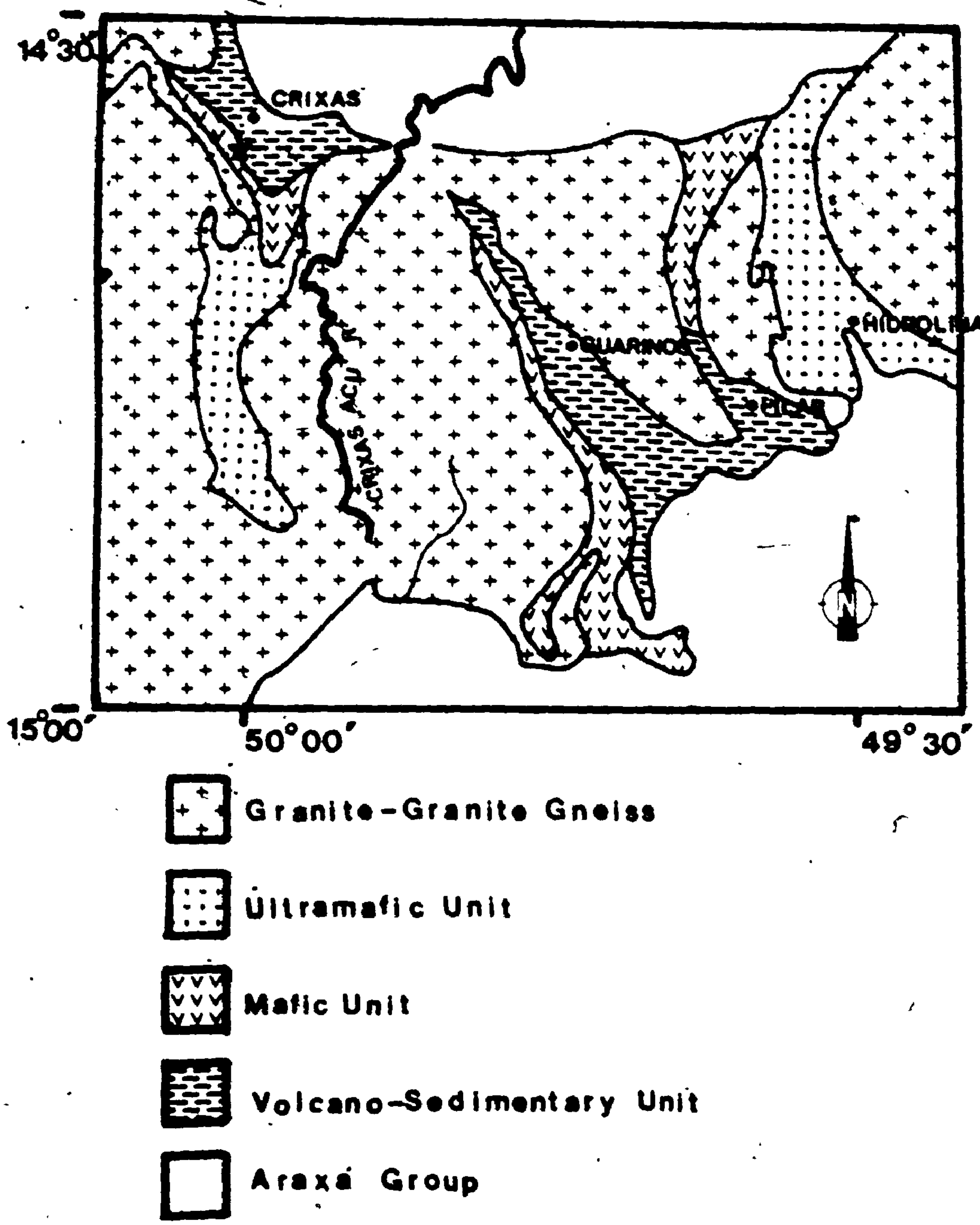

Figure 2.2. Geolgic map of Crxas, Guarinos and Pilar Greenstone Belts. Star indicates location of Minas III. (after de Saboia, 1979).

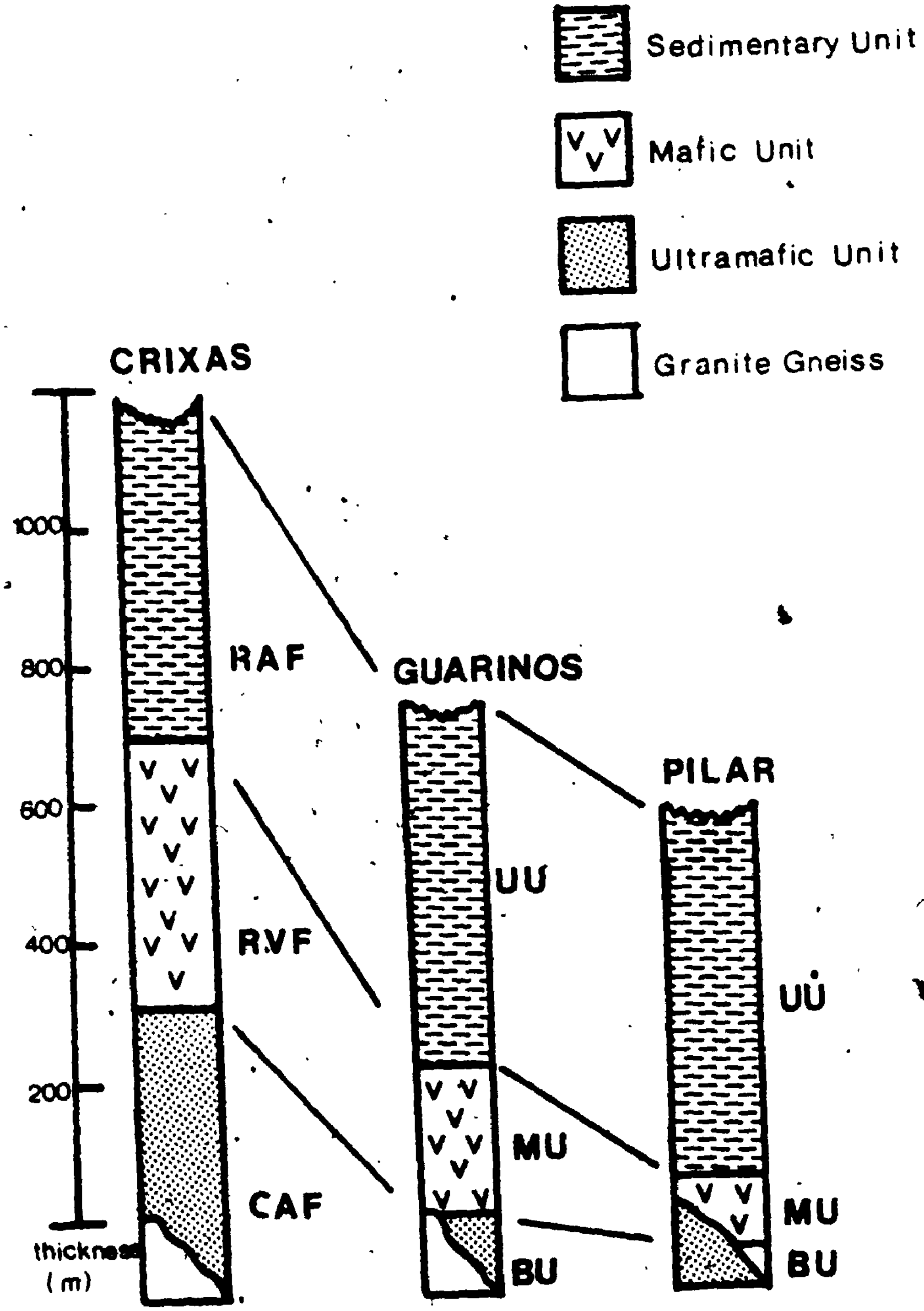

Figure 2.3. Schematic correlation of geologic profiles of Crixas, Guarínos and Pilar Greenstone Belts. CAF, Corrego do Alagadinho Formation; RVF, Rio Vermelho Formation; RAF, Ribeirao das Antas Formation; BU, Basal Unit; MU, Middle Unit; UU, Upper Unit. (after de Saboia, 1979; Danni and Ribeiro, 1978)

stratigraphy from base to top consists of metamorphosed ultramafic rocks which are overlain by metamorphosed mafic rocks which are inturn overlain by metamorphosed sediments consisting dominantly of chlorite-quartz, chlorite-sericite-quarts and graphitic schists.

2.3.1. Geology of the Pilar and Guarinos Greenstone Belts.

The geology of the Pilar de Goias and Guarinos Belts are similar and may be described as a metamorphosed pile of volcanic and sedimentary rocks. Ultramafic rocks occur at the stratigraphic base (Basal Unit), mafic and felsic volcanics occur in the middle (Middle Unit), with chemical sediments, felsic pyroclastics and fine to medium grained clastics occurring at the top (Upper Unit, Ribeiro Filho, 1978; Danni and Ribeiro, 1978).

The Basal Unit consists of intercalations of talc-carbonate schist, tremolite-actinolite schist, serpentinite, metacherts and dolomites locally metamorphosed to calcsilicate assemblages. The Middle Unit consists of amphibolite schists with intercalations of chlorite and chlorite-quartz schists. Near the top of the Middle Unit are graphitic metasediments with frequent intercalations of "gneissic felsics" interpreted as acid metavolcanics (Ribeiro Filho, 1984). The Upper Unit is composed dominantly of metasediments which include muscovite-sericite schists, carbonates, graphitic schists, metacherts with graphite or carbonate, magnetite rich schists and garnet-chloritoid schists. Chlorite-quartz schist with graphite and greywacke top the Upper Unit.

The Pilar de Goias Belt takes the form of a N-S trending synclinal trough flanked to the west and to the east by major faults.

To the west the Upper Unit sediments are in fault contact with the Muquem Dome and to the east ultramafics of the Basal Unit are faulted against the Hidrolina Dome exposing the complete sequence (Ribeiro Filho, 1984)

At Cachoeira do Ogo (waterfalls near the town of Ogo) the base of the exposed sequence consists of ultramafic rocks intercalated with calcsilicates (Basal Unit). This is overlain by a 1 km maximum thickness of amphibolites intercalated with possible acid volcanics (Middle Unit). The contact zone of the Middle Unit and Upper Unit is distinct and is typified by a black-green muscovite-chlorite schist with quartz and a boxwork of oxidized magnetite and garnet (ibid). It is interesting to note that where the amphibolite sequence is thin the thickness of a fine-grained sericite schist increases which in turn grades to a massive magnetite-garnet rock (see Section 3.3.3.6 for comparison to Minas III). Ribeiro Filho (1984) furthur comments that ample carbonate is present at this contact and proposes it as a product of alteration, but adds that it is difficult to document due to surface weathering. Quartz is common in this portion of the sequence as veins and veinlets parallel to foliation. Graphitic schists with quartz lenses predominate above the contact zone, and pass into a capping sequence of chlorite-sericite greywacke.

Significant Au mineralization (3-5 g/m^3 extracted) occurs within the sericite-quartz schist with magnetite-garnet and chloritoid. Minor values are reported from the graphitic schist where quartz is significant (Ribeiro Filho,1984). The strike of the mineralized zone is N10-20 $^{\circ}$ W with a known length of 10 km.

The geology of the Guarinos Greenstone Belt is very similar to that of the Pilar de Goias Belt (Ribeiro Filho, 1984). A sequence of volcanic and sedimentary rocks is confined to a fault bounded trough-like structure flanked to the east by the Muquem Dome and to the west by the Caimar Dome. Approximately 5 km to the south of the town of Guarinos the sequence is well exposed and consists of a coarse grained grey-white granite gneiss, locally mylonitic, in fault contact with amphibolites of the Middle Unit of the Pilar de Goias Group. The Basal Unit ultramafics are apparently faulted out. Seven hundred meters above the amphibolite-gneiss contact occurs the contact of the amphibolites with the metasediments of the Upper Unit. The contact is sharp and the unit consists of 10 m of biotite-muscovite-chlorite-quartz schist which rapidly passes into 30-40 m of magnetite-chlorite-sericite schist with lenses of carbonate and rare chloritoid. This unit is in sharp contact with a chlorite and carbonate rich greywacke which caps the sequence.

The Au mineralization at this location grades 8-10 g/m^3 extracted (Ribiero Filho, 1984). It occurs within a 2 to 30 m thick unit of sericite schist with fine intercalations of chlorite and chlorite-magnetite-garnet schist, both with abundant pyrrhotite and arsenopyrite. Quartz veins are frequent but discontinuous, varying from 0.3 to 1.0 m in thickness, and parallel the foliation at $N10^{\circ}W/50^{\circ}SW$. These two auriferous schists compare well with the Sericite-Chlorite and Chlorite-Magnetite Schists of Minas III (Sections 3.3.3.5 and 3.3.3.6).

2.3.2 Geology of the Crixas Greenstone Belt

The geology of the Crixas Greenstone Belt consists of the Corrego do Alagadinho Formation, the Rio Vermelho Formation and the Ribeirao das Antas Formation (de Sabioa,1979). Figure 2.2 is a regional geologic map after de Saboia, 1979.

The Corrego do Alagadinho Formation (CAF) is the lower most unit and has a calculated thickness of 600 m thinning to the north and north-west (de Saboia,1979). It is best exposed in the southern portion of the belt with the type location occurring at the Alagadinho Creek. It consists of a series of ultramafic flows displaying spectacularly developed spinifex texture. Three types of flows have been recognized and described (ibid). The first type is characterized by an upper or A-zone of quenched, aphanitic and fractured ultrabasic rock (A1) which is transitional into triangulary shaped sheaths of olivine spinifex (A2) which is in turn transitional to subparallel to skeletal olivine (A3). The lower or B-zone is characterized by skeletal olivine developed parallel to the margins of the flow (B1). It is underlain by massive cumulous textured peridotite. This type of flow has been studied by Pyke et al.(1973).

The second type, apparently unique to this area (ibid) consists of a quenched top (A1) transitional to clinopyroxene spinifex (A2) and ends in a basal zone of massive peridotite with pseudo-polyhedral jointing.

The third type of flow is similar to the ultramafic flows described by Arndt(1976) and Arndt et al.(1977) from Munroe Township, Ontario (ibid). It consists of a spinifex textured upper zone (A) which is locally contorted and cut by veins of spinifex textured ultramafic, suggesting a later injection after the flow cooled. The lower zone (B) is massive pseudo-polyhedral jointed peridotite.

Elsewhere in the Crixas Greenstone Belt the CAF occurs as serpentinites and varying proportions of talc, tremolite and chlorite schists. The serpentinites are found to the west of the undeformed ultramafics near the contact with the Anta Dome (de Saboia & Teixeira, 1983). No primary textures are evident making it unclear as to whether or not they are intrusive or extrusive in origin. In areas of minor deformation the talc schists are noted to be transitional into spinifex textured ultramafic lavas (de Saboia, 1979).

Intercalated with the ultramafic units are ferruginous cherts, quartz-chlorite schists and tremolite-albite-quartz-carbonate schists interpreted to be deformed mafic flows or sills (ibid, Kuymjian,1981).

The Rio Vermelho Formation (RVF) is approximately 800 m thick and is in both gradational and sharp contact with the CAF. It consists dominantly of mafic schists but rare exposures of pillowed basalts occurring along the Vermelho River 8 km south of the town of Crixas and in a farmers field along the road leading west from Crixas.

The pillow shapes are slightly elongate in the horizontal direction, with the median size 0.5 m wide and 1.5 m long. Amygdules developed concentrically at the margins of the pillows are filled by quartz, chlorite, calcite and epidote. Unusual "swallow tail" textured plagioclase needles replaced by epidote are noted to fill the amygdules and are interpreted to represent quench texture (Teixeira et al.,1981). The cores of the pillows are composed of fine grained actinolite-tremolite, Na-plagioclase, chlorite, calcite and ilmenite with clusters of radial actinolite thought to be after quenched clinopyroxene (ibid). Teixeira et al. (1981) describe hollow elongate cavities lined with quartz within the pillow lavas and interprets these to be lava tubes as described by Viljeon & Viljeon (1969). The interpillow material includes calcite, tourmaline and quartz. At one outcrop location the rocks appear to be overturned but this is not unequivocal.

Along strike the pillow lavas can be seen to grade into tremolite-actinolite-albite-chlorite-carbonate schists which are the most representative of the RVF. Locally hornblende-albite-quartz-epidote assemblages have been noted (Kuymjian,1981, Section 5.2.1). Intercalated with the mafic schists are graphitic schists, crystalline quartz bodies with rare fuchsitite, iron formation of banded quartz and magnetite, and quartz-chlorite schists and talc schists. These intercalations make up approximately 20-30% of the rock unit, and vary in width from one to 10's of meters and in strike length from 1 to several hundreds of meters.

The Ribeiro das Antas Formation (RAF) has a calculated thickness of 1600 m and concordantly overlies the RVF at most localities. In the extreme north however it is in contact with the Antas Dome granites, and in the extreme south it overlies the CAF (Kuymjian,1981). The lithologies of the RAF are dominantly detrital and chemical sediments, including quartz-graphitic schists and biotite-chlorite schists. Magalhaes et. al. (1984) suggests a facies variation at the the base of the RAF of graphitic carbonate schists which include: graphitic schists, dolomites, metacherts and graphite-magnetite-garnet-chlorite-chloritoid schists; and graphitic-Mn rich schists which include: garnet-graphite schists, quartz-garnet schists and garnet schists. Overlying the graphitic schists is a greywacke, consisting of feldspar, quartz, calcite and graphite (Magalhaes et al, 1984).

Overlying the RAF, Kuymjian (1981) names an Upper Ultramafic Unit composed of serpentinites, talc schists, talc chlorite schists with intercalation of metacherts, iron formations, graphitic schists. It occurs as elevated N-S ridges in the northern region of the belt and as a thin ridge running E-W in the central portion to the SE of the town of Crixas. The lower contact is abrupt to the RVF (ibid). It is not clear as to whether or not this unit should be considered apart from the CAF as described above. It is possible that this unit may represent a thrust sheet of the CAF and therefore should not be given

2.4. Araxa Group

Overlying the rocks of the Crixas Greenstone Belt are the highly schistose rocks of the Araxa Group (de Saboia,1979, Kuyumjian,1981). The Araxa Group is traceable to the east of the Pilar Greenstone Belt and northward to the northern most portion of Goias State (Figure 2.2). North of the town of Crixas the Araxa Group is represented by quartz-biotite-muscovite (sometimes garnet) schist whereas to the west it occurs as a banded meta-quartzite.

The age of the Araxa Group is in dispute. Fuck and Marini (1981) suggest a Proterozoic age (1.8-1.2 Ga) based on correlation with the Espinhaco Super Group of the Quadrilatero Ferrifero. Almeida (1976) and Ribeiro Filho (1981) suggest an age of 1.4-1.6 Ga based on cross cutting granitic bodies. Richardson et al.(1986) suggest an age of 561+/-9 Ma (Rb/Sr) for the Mara Rosa Sequence at Chapada (east of the Pilar Greenstone Belt). Clearly, considerable work is needed to be done to clarify these conflicting dates.

Throughout the region the Araxa Group unconformably overlies the basement consisting of granite and granite-gneiss terrains and greenstone belts (Fuck & Marini,1981). Danni and Ribeiro (1978) describe the Araxa Group as being in thrust contact with the Pilar Group. The observable contact of the Araxa Group and the underlying volcanic and sedimentary rocks within the Crixas Greenstone Belt is seen to be a low angle thrust contact. Where well exposed, talc schist of the Upper Ultramafic Unit of Kuyumjian (1981) uncomformably underlies a folded, banded meta-quartzite. The foliation of the CAF talc schist is clearly truncated by the contact with the Araxa Group meta-quartzite.

2.5. Geology of the Anta Granite-Granite Gneiss Terrain.

Very little is known about the specific nature of the Anta Granite-Granite Gniesses Terrane surrounding the Crixas Greenstone Belt. Kuymujian(1981) classified seven samples according to Streckeisen (1976) as tonalites and granodiorites with subordinate granite and migmatites. During this author's limited field work in the Anta Granite-Granite Gneiss Terrane several rock types were noted. Approximately 25 km west of the town of Crixas occurs a feldspar augen gneiss cut by pegmatite consisting of 5-7 cm crystals of feldspar with coarse grained biotite. A large pavement outcrop of tonalite (?)

consisting of 85% grey-pink feldspar, 10% quartz and 5% black biotite occurs 15km north west of the town of Crixas. It varies in texture from medium grained and equigranular to variably fine to medium grained, foliated or banded in appearance. One Rb/Sr whole rock age date of 2929 +/_ 105 Ma has been determined by Tassinari & Montavao (1980) on a granodiorite sample collected from the Anta Granite-Granite Gneiss Terrain.

CHAPTER THREE

Geology of the Crixas Gold Deposit or Minas III.

3.1 Introduction

The Crixas Gold Deposit is one of four areas in which Minerasul (INCO Metals in Brazil) is actively exploring south of the town of Crixas. For convenience the areas are numbered from I to IV using the prefix "Minas" which translates in English as "Mine" or less precisely to "mineralized area". Throughout the thesis the gold deposit herein studied will be referred to as Minas III.

Minas III is located approximately 4 km south of the town of Crixas and covers an area of about 14 km^2 (Figure 3.1). The western and northern boundaries are the Vermelho River. The eastern boundary is the eastern limit of Minerasul's manifesto. The southern boundary is arbitrarily established by this author at the southern limit of the 18^{th} Century , open pit workings as illustrated in Figure 3.1.

3.2. Surface Geology

Over 75% of the outcrop exposure within the boundaries of Minas III consists of rocks weathered to varying degrees, within which rare islands of fresh rock are exposed. The depth of weathering ranges from centimeters to 30 meters, with 5 meters the average. By far the best exposures of rock or weakly developed saprolite occur within the trenches and galleries dug out by the enslaved workers of the Portuguese adventurers of the eighteenth century.

Six rock types have been recognised at surface. From west to east these are:

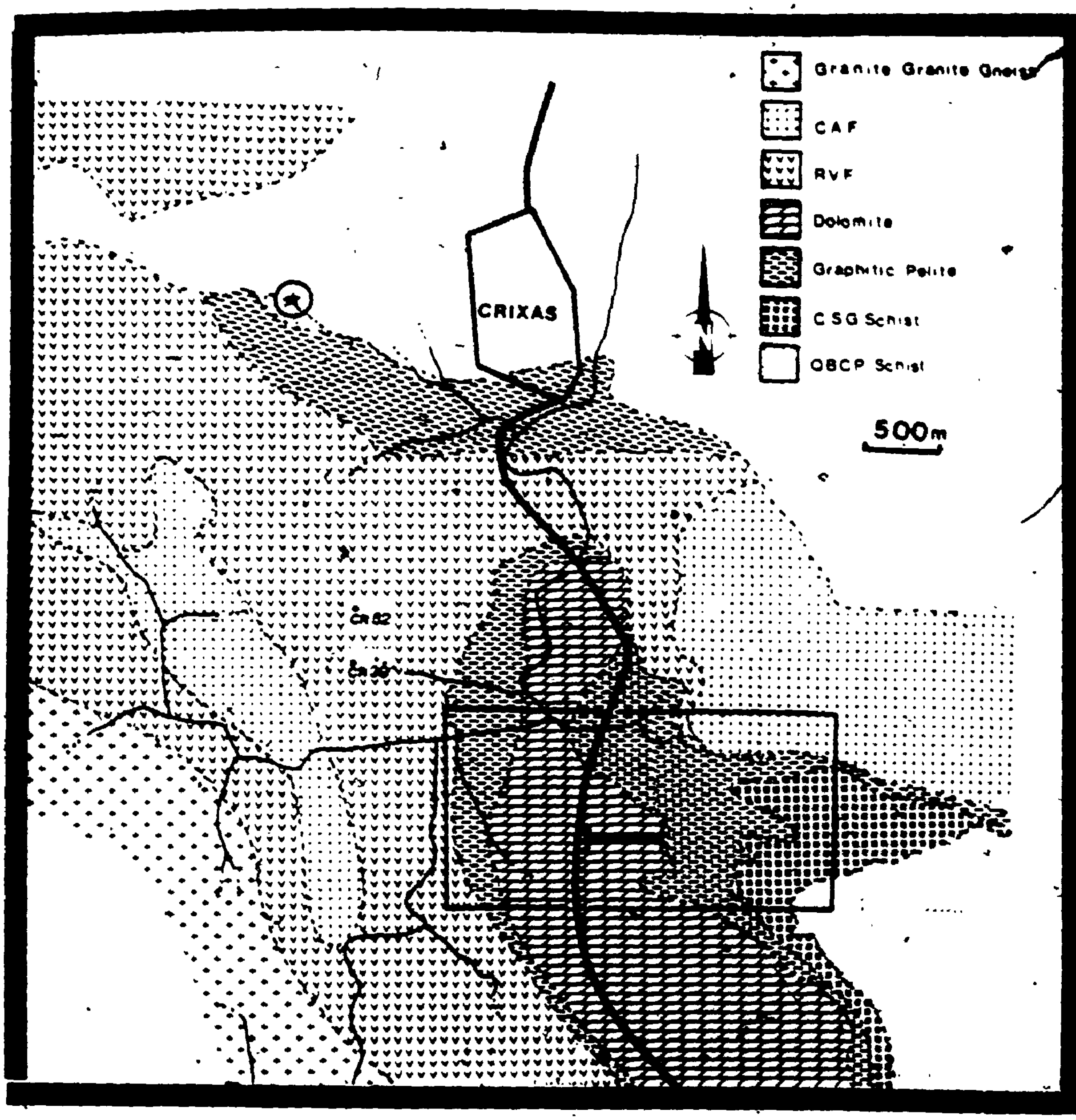

Figure 3.1. Geological Map of the southern portion of the Crixas Greenstone Belt within the region of the town of Crixas. Large box marks out the areal extent of Minas III. Small bar indicates the location of the cross-section in Figure 3.2. Circled star marks the location of the Archean-Araxa Group contact exposure. Abbreviation in legend as in text. (after de Saboia, 1979; Kuymjian, 1981; Minerasul Staff, 1983).

1) Foliated Amphibolite with Chloritic Schist,
2) Chloritic Schist often intercalated with Graphitic Pelite,
3) Dolomite,
4) Porphyroblastic Chlorite-Magnetite-Garnet Schist locally with arsenopyrite, chloritoid and grunerite porphyroblasts,
5) Graphitic Pelite with intercalations of Chloritic Schist,
6) Banded Chlorite-Sericite-Garnet Schist.

Figure 3.2 is an idealized block diagram which includes the surface geology, as interpreted from a detailed outcrop map produced by Mineralsul Staff (1983).

A rigorous discussion of surface lithologies is without merit in view of the degree of weathering. The surface geology is well represented by the diamond drill core samples used for this study. All further discussion will be based on data obtained from the collected diamond drill core samples.

3.3. Subsurface Geology.

3.3.1. General Statement

As of July 1985 over 200 diamond drill holes, ranging in depth from 50 to 300 m, had been drilled from surface into the Minas III working area, totalling approximately 25 kilometers of core. The drilling has extended along the E-W direction for 1700 m and along the N-S direction for 700m, covering 1.2 km^2. This author reviewed diamond drill core of over 100 boreholes and detail logged and sampled 30 boreholes. The location of these holes are illustrated in Appendix III. It should be noted that the study area is east of the main road (Figure 3.1). It does not include the area to the west of the road where drilling subsequent to this author's field work has indicated continued mineralization.

3.3.2. Description of Lithologies.

In total there are twelve unique rock types which have been recognized in all boreholes. These are:

1) Foliated Amphibolite,
2) Ferroan Dolomite-Chlorite-Biotite-Quartz Schist,
3) veined Ferroan Dolomite-Chlorite-Biotite-Quartz Schist,
4) Massive Ferroan Dolomite with chlorite-sericite partings,
5) Sericite-Chlorite Schist,
6) Chlorite-Magnetite Schist,
7) Silicified Dolomite,
8) Graphitic Pelite,
9) Quartz Cemented Graphitic Pelite Breccia or Lower Ore Zone (LOZ),
10 Chlorite-Plagioclase-Quartz-Ferroan Dolomite Schist,
11) Banded Chlorite-Sericite-Garnet Schist,
12) Banded Quartz-Biotite-Plagioclase Schist.

Each rock type will be described separately in the following section. The spatial relationships of the rock types are illustrated in Figure 3.2 which is an idealized and simplified geologic block diagram compiled from several boreholes.

3.3.3.1. Foliated Amphibolite

The Foliated Amphibolite occurs within the western and northern portions of the study area (Figure 3.1 and Figure 3.2) and is restricted to the upper portions of the geologic profile (Figure 3.2). It thins and wedges out toward the south and east. It makes up 5% of the rock volume and has a maximum thickness of 13 m.

The Foliated Amphibolite is in contact with overlying saprolitic soil. The lower contact is transitional to a chlorite-calcite schist. More rarely the Foliated Amphibolite occurs as 5 to 10 cm thick, islands within Ferroan Dolomite-Chlorite-Biotite-Quartz Schist, and shows contacts which are chlorite-calcite rich and transitonal over 1 to 5 cm.

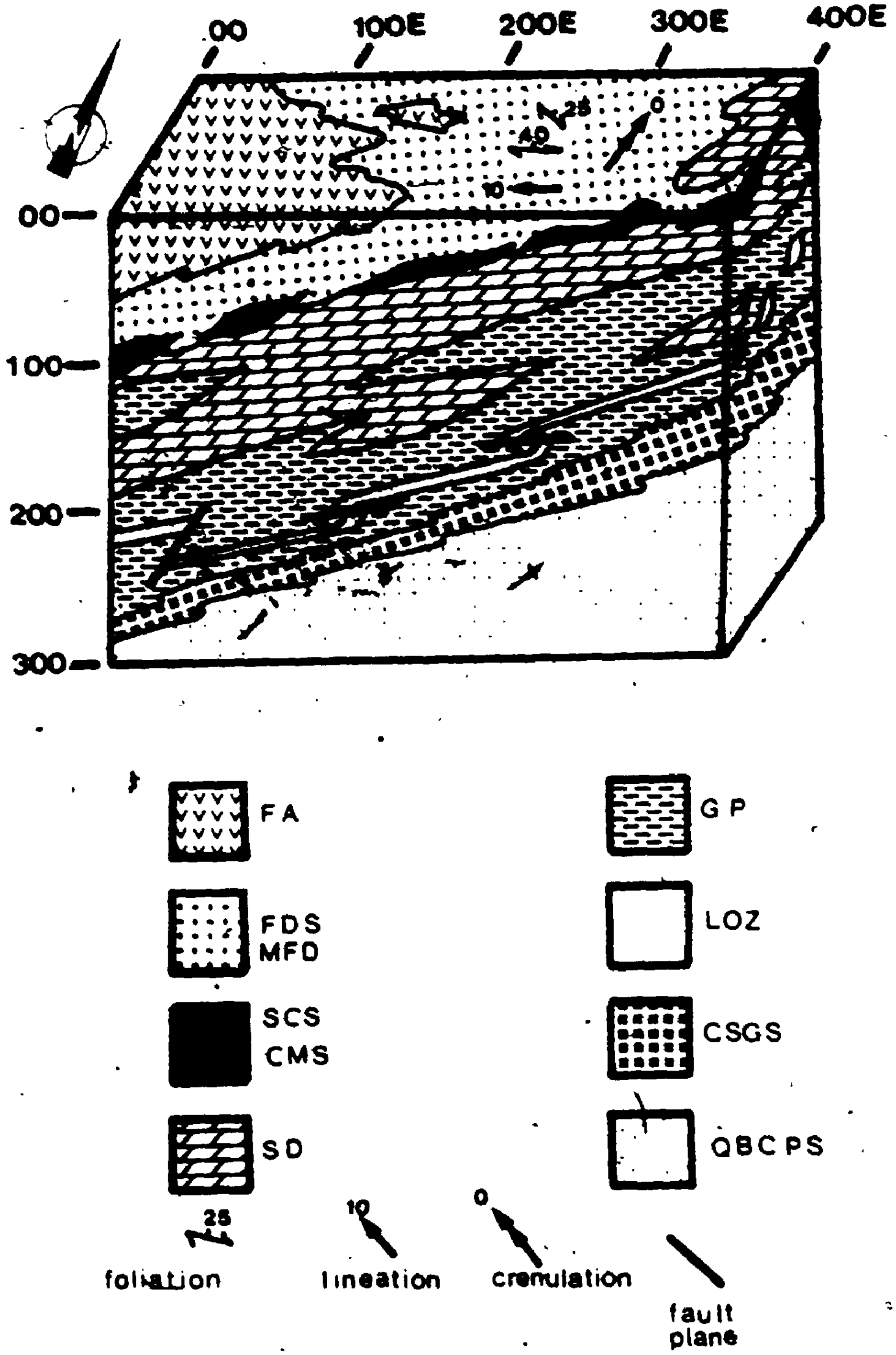

Figure 3.2. Block diagram of idealized geology of Minas III. Horizontal and vertical distances in metres. FA, Foliated Amphibolite; FDS, Ferroan Dolomite Schist; MFD, Massive Ferroan Dolomite; SCS, Sericite-Chlorite Schist; CMS, Chlorite-Magnetite Schist; SD, Silicified Dolomite; GP, Graphitic Pelite; LOZ, Lower Ore Zone; CSGS, Chlorite-Sericite-Garnet Schist; QBCPS, Quartz-Biotite-Chlorite-Plagioclase Schist.

In hand sample the Foliated Amphibolite is medium to dark olive green, homogeneous, fine to medium grained and moderately foliated. Rarely, the rock may show a mottled texture, interpreted to be relict subophitic texture. Minor quartz veining is noted, but comprises up less than 1% of the rock.

In thin section the Foliated Amphibolite is characterized by poikiloblastic amphibole (50%) in a matrix of chlorite (20%), quartz (20%), plagioclase (10%) and ilmenite (3%). The amphibole occurs as uniform poikiloblastic blades, 300-400 um long, and includes quartz and ilmenite (Plate 1a). The blades form an open, often discontinuous, anastomosing cleavage. Chlorite blades of similar size are developed epitaxially to the amphibole, paralleling foliation.

Intergranular to the hornblende poikiloblasts and chlorite is a matrix consisting of equant to slightly elongate, 100 um wide, mosaic textured quartz and plagioclase (Plate 1a). Quartz may form three to four grain composite patches or occur individually. Untwinned plagioclase grains are difficult to distinguish from quartz, and occur in much the same manner as described for the quartz. Twinning of the plagioclase is rare, with twinned grains slightly coarser and showing subgrain development to new grains similar in size to those noted above. Myrmekite is also rarely noted at the margins of deformed twinned plagioclase grains.

Ilmenite occurs as 100 um blebs oriented parallel to the foliation. It is invariably in contact with amphibole and may be partially included in the amphibole. Trace chalcopyrite is noted as

PLATE ONE: Foliated Amphibolite

1a. Overview showing subhedral outline of magnesio-hornblende blades (dark grey) set in a plagioclase+calcite with minor chlorite matrix. Opaque pyrrhotite and ilmenite. (ppl, Scale Bar = 1.0mm)

1b. Coarse grained garnet poikiloblast.(ppl, Scale Bar = 1.0mm)

1c. Overview showing matrix of transitional rock consisting of dominatly chlorite and carbonate. Opaque ilmenite. (ppl, Scale Bar = 1.0mm)

1d. Example of plagioclase glomerocrysts with calcite alteration. Note albite twinning. (xpl, Scale Bar = 0.30mm)

1e. Overview showing calcite eye with plagioclase inclusions. (xpl, Scale Bar = 1 mm).

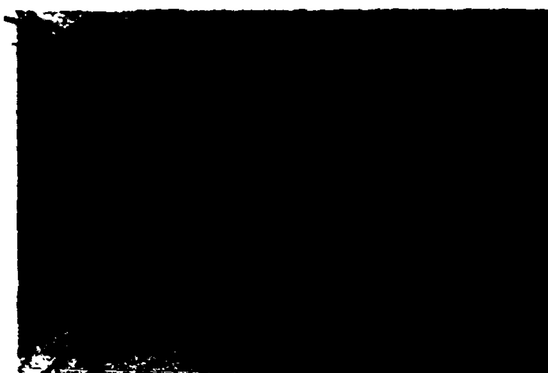

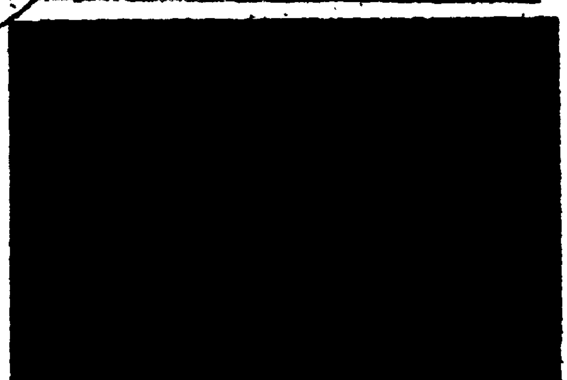

is calcite. In one thin section a single garnet porphyroblast is noted (Plate 1b).

With increasing proximity to the Ferroan Dolomite-Chlorite-Biotite-Quartz Schist the Foliated Amphibolite becomes chlorite and calcite rich. It consists of amphibole (0-15%), chlorite (20-45%), calcite (20%), quartz (20%), plagioclase (15%), biotite (5%) and ilmenite (3%).

The amphibole is strongly pleochroic, medium olive green to blue green and occurs as fish-net textured poikiloblasts ranging in size from 1-5 mm in diameter and averaging 3 mm. The poikiloblasts define an open anastomosing foliation and include the matrix minerals. Pleochroic meduim to light green chlorite also defines the anastomosing foliation. It occurs as 0.7-1.0 mm epitaxial blades to the amphibole or completly replaces the amphibole (Plate 1c). Greenish brown biotite forms as poikiloblasts overgrowing both chlorite and amphibole and includes matrix quartz and plagioclase.

The matrix is a combination of quartz, plagioclase and calcite. The quartz occurs as variably sized grains (50-200 um), generally elongate parallel to the foliation. Finer grained quartz appears to have developed from grain reduction of the coarser grained quartz. The plagioclase grains are difficult to distinguish from quartz. They occur as weakly twinned, coarser grained, inclusion rich grains, often showing mortar-textured finer grained feldspar rims. Calcite is much coarser grained than the quartz and feldspar. It occurs as 400-500 um elongate grains, forming fairly continuous trails parallel to the foliation.

Ilmenite forms distinct 1 mm linear trails made up of single 70-100 um blebs paralleling the foliation. Trace pyrrhotite is noted as thin, continuous, irregularily shaped 500 um blebs associated with biotite.

The subophitic textured Foliated Amphibolite has a bimodal size distribution of minerals. Plagioclase (20%) and amphibole (5%) porphyroblasts are set in a finer grained matrix of amphibole (25%), chlorite (15%), plagioclase (20%) and quartz (5%). Amphibole blades are colourless to very pale green and range in size from 400-700 um. They are oblique to the weakly developed matrix foliation. Plagioclase porphyroblasts range in size from 0.7-1.0 mm with the average 0.8 mm. They are usually well twinned, subhedral and have cuspate grain boundaries with the matrix minerals. The well twinned plagioclase phenocrysts are generally inclusion free (<1%), but those which are poorly twinned have an inclusion content as high as 25%. The inclusions are dominantly amphibole, with minor chlorite and clinozoisite. The well twinned plagioclase are interpreted as either pseudomorphed or relict igneous feldspars, whereas, poorly twinned plagioclase are interpreted as poikilobasts. Plagioclase may also form decussate glomerocrysts which range in size from 1-2 mm with 1 mm the average (Plate 1d). The plagioclase glomerocryst are often replaced by coarse grained radiating chlorite and calcite.

The matrix component is less than 50 um in size and not homogeneous, with local zones of chlorite and amphibole defining a weak foliation separating quartz and plagioclase zones. Ilmenite is the dominant opaque, occuring as 200 um single blebs or up to 600 um long composite blebs, developed parallel to the foliation. Trace calcite is noted with the feldspar.

A variation of this rock type occurs with the development of 1.5-2.5 mm composite calcite eyes making up 25 volume % of the rock. The calcite is poikiloblastic with inclusions of amphibole and quartz and rarely plagioclase. This rock type tends to be more foliated but is otherwise very similar to the relict subophitic textured rock described above (Plate 1e).

3.3.3.2. Ferroan Dolomite-Chlorite-Biotite-Quartz Schist

The Ferroan Dolomite-Chlorite-Biotite-Quartz Schist (FDCBQ Schist) makes up 5 % of the subsurface rock volume, most often occurring in the structural upper half of the geologic profile. Where in contact with Foliated Amphibolite the contact is transitional over 1-2 cm and is characterised by chlorite-calcite Foliated Amphibolite. The FDCBQ schist is intimately associated with the veined-FDCSBQ schist with transitional contacts. The FDCBQ schist more rarely occurs in the medium to lower portions of the geologic profile. It is in sharp contact with the Graphitic Pelite and in transitional contact with the Chlorite-Plagioclase-Quartz-Ferroan Dolomite Schist.

The FDCBQ Schist varies in thickness from one to ten metres with the average thickness of three metres. There appears to be a limited control over the variability of its thickness in relation to the contacting rock types. For instance, where associated with Foliated Amphibolite it is significantly thicker than when associated with the Chlorite-Plagioclase-Quartz-Ferroan Dolomite Schist.

In hand sample the rock consists of a fine-grained medium olive green matrix with 5-10 % weakly alligned, 1.0-5.0 mm grey-white eyes of ferroan dolomite and dark green-black flakes of biotite (Plate 2a). Locally, the rock takes on a more banded appearance. Darker green bands of chlorite and sericite separate lighter green bands of ferroan dolomite, with biotite forming coarser grained flakes.

In thin section the FDCBQ Schist consists of poikiloblasts of ferroan dolomite (20%), biotite (10%) and plagioclase (5%) in a finer grained matrix of quartz (35%), chlorite (20%), plagioclase (5%) and sericite (0-10%). Acessory minerals are less than 1% and include tourmaline, ilmenite, pyrrhotite and chalcopyrite.

Ferroan dolomite poikiloblasts occur as 1.5 mm elipsoid eyes oriented with their long direction parallel to the foliation (Plate 2b). The eyes are composite grains showing different orientations of twinning but have a "wave" extinction pattern suggesting that the eyes may have been single grains. Quartz is the most common inclusion, often making up 20% of the ferroan dolomite poikiloblast. Characteristic of the ferroan dolomite poikiloblasts are dense clusters of bubble-like inclusions. The compositon of the "bubbles" is ferroan dolomite. The ferroan dolomite poikiloblasts are often surrounded by a one grain thick (100 um wide) mantle of quartz along the edge parallel to the foliation and five or six quartz grains in the pressure shadow zones. The pressure shadow quartz may be coarser grained than the matrix quartz.

Biotite occurs as pleochroic medium yellow brown to dark orange brown, 1-2 mm blades and flakes (Plate 2c). Inclusions may make up

PLATE TWO: FERROAN DOLOMITE SCHIST

2a. Core sample of FDCBQ Schist with minor veining. Ferroan dolomite eyes well developed. (Core width 7 cm).

2b. Composite ferroan dolomite eyes in well foliated matrix. (xpl, Scale Bare = 1 mm).

2c. Fine chlorite blades with larger biotite blades, forming dense mat with ferroan dolomite and quarzt as the matrix. (ppl, Scale Bar = 1 mm).

2d. Tourmaline in ferroan dolomite and chlorite matrix. Locally tourmaline appears to overgrow the ferroan dolomite. (ppl, Scale Bar = 0.30 mm).

2e. Core sample of veined FDCSBQ Schist. Veins consist of ferroan dolomite and quartz. Note ferroan dolomite eyes in matrix and the complex folding of the veins. (Core width 7 cm).

2f. Chlorite and sericite blades intimately intergrown with ilmenite as the opaque. (xpl, Scale Bar = 0.30 mm).

2g. Core sample of Massiver Ferroan Dolomite. Curvilinear chlorite-sericite partings are clearly evident. (Core width 7 cm).

2h. Matrix of ferraon dolomite cut by splays of curvilinear sericite and chlorite blades. (xpl, Scale Bar = 0.5 mm).

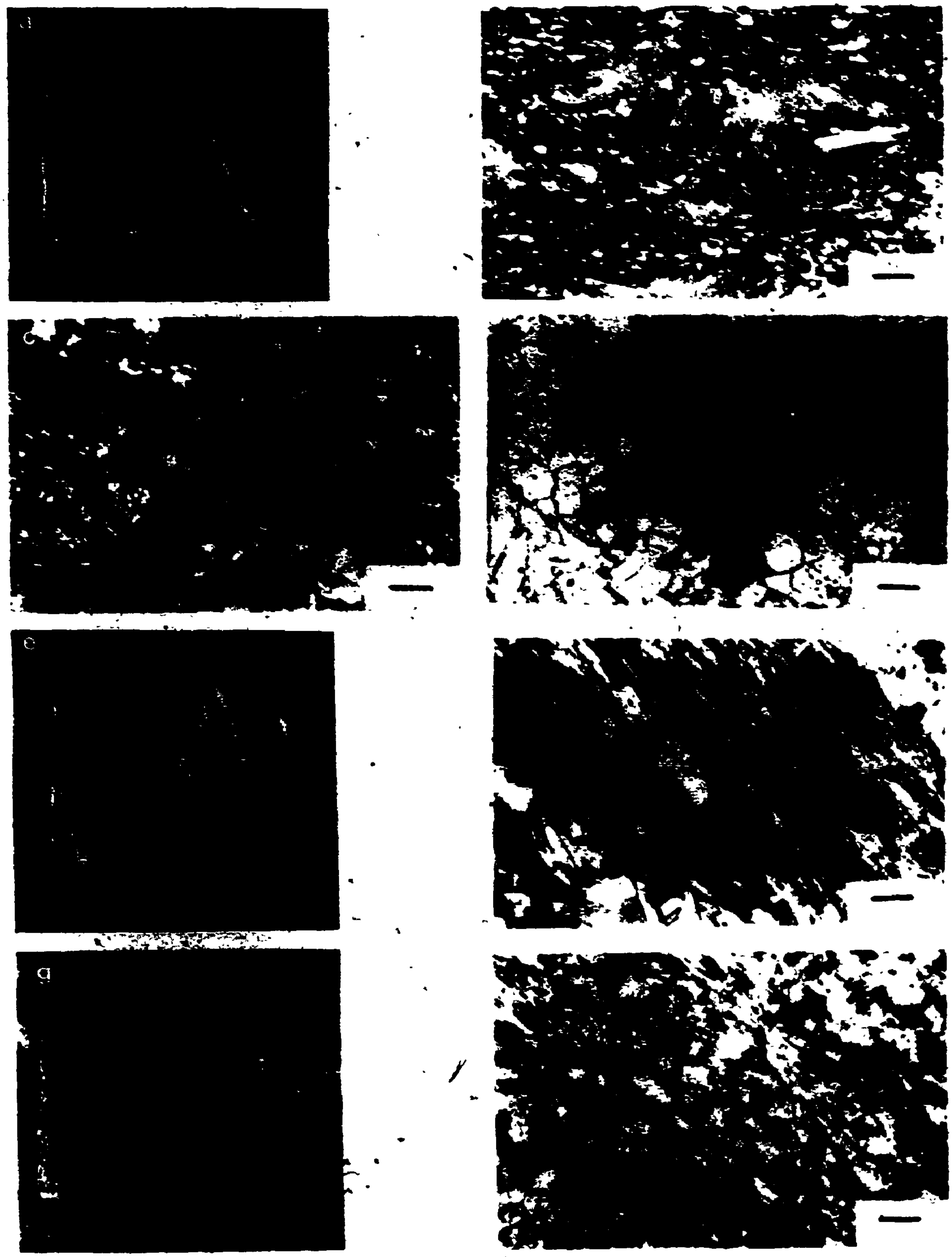

to 10% of the flake and consist of dominantly rounded quartz grains, although carbonate and chlorite are rarely noted. The contact boundaries of the biotite to the chlorite matrix are sharp and occasionaly slightly cross-cutting parallel to the (001) cleavage; however, perpendicular to the (001) cleavage the biotite blades are epitaxial to the chlorite with the boundary interface frayed. For the most part, biotite appears to overgrow chlorite but there are instances where this relationship is not clear.

Plagioclase makes up a maximum of 2 modal percent when occurring as pophyroblasts. It appears to have two modes of occurrence. The most common is as relict and altered twinned plagioclase feldspar (500 um) reminiscent of the glomerocrysts described in the Foliated Amphibolite. The alteration is most often to carbonate as fine dustings. The grains are commonly subgrained and surrounded by new grains of feldspar resulting in very cuspate grain boundaries. Plagioclase also occurs as rounded, concentrically zoned, porphyroblasts, 100 um in diameter, growing out of and overgrowing the matrix chlorite. The grain boundaries may be smooth but may also mimic the chlorite, developing a frayed boundary. This type of plagioclase occurs where sericite is noted within the matrix.

Quartz occurs as 100 um wide, equigranular, mosaic texture grains showing minor undulose extinction. The grains occur in 1-2 mm elipsoid zones surrounded by either anastomosing chlorite or poikiloblasts. Fifty micron chlorite blades occur at the margins of the mosaic quartz grains. In several instances, quartz occurs as very fine grained (<10 um) zones. More coarse grained quartz grains

(100 um) show distinct subgrain development to the <10 um grain size. Quartz is also noted to rarely (<1%) occur as discontinuous 2-3 mm trails consisting of single 0.5-1.0 mm long and 0.2 mm wide grains. The grains are slightly subgrained, have undulose extinction and are interpreted as dismembered quartz veins.

Plagioclase is also a component of the matrix but its modal abundance is difficult to establish as it is usually untwinned and occurs in much the same manner as quartz. Where identified it appears as 100 um equigranular, mosaic to weakly sutured grains and is distinguished from quartz by the presence of inclusions of carbonate.

Medium green chlorite may comprise to 40% of the rock with 20% the average. It occurs as 100 um long blades of variable width (50-700 um), forming an anastomosing, zonal cleavage (Plate 2c). Where only 50 um wide, the chlorite flakes are individual occurring at quartz or plagioclase margins. The increase in width of the chlorite blades shows a progressive alignment of the chlorite until the chlorite is a discontinuous mat of parallel blades with rare inclusions of quartz.

Sericite may occur at the expense of chlorite. Where first recognized at less than 5 modal%, it occurs as 300 um long individual, colourless blades parallel to chlorite blades. With increasing abundance the sericite forms continuous anastomosing zones similar to that of chlorite.

Colour zoned tourmaline euhedra with blue green cores and dark olive green rims, commonly occur in quartz ~~rich~~ regions. It is also noted to occur with biotite poikiloblasts. In one instance it can be seen as a composite grain with ferroan dolomite, strongly suggesting replacement of the ferroan dolomite by tourmaline (Plate 2d).

The accessory opaque mineralogy consists of ilmenite, pyrrhotite, and chalcopyrite in decreasing order of modal abundance. The ilmenite usually occurs as 100 um long ragged edged blades. These may form up to 10 blade, randomly oriented concentrations or single blade linear trails. They are often included in biotite, ferroan dolomite and tourmaline and appear to be altered to rutile where included.

Pyrrhotite and chalcopyrite occur as elongate composite blebs paralleling foliation. They are commonly in association with chlorite and biotite, showing complex contact boundaries. Where in contact with quartz and carbonate the sulphides are intergranular and take on the shape of the contacting minerals. Chalcopyrite most often form as blebby inclusions in the pyrrhotite and as flames in the pyrrhotite. It rarely occurs as singular grains, taking on the same shape of the pyrrhotite.

<u>3.3.3.3. Veined Ferroan Dolomite-Chlorite-Sericite-Biotite-Quartz Schist</u>

The veined Ferroan Dolomite-Chlorite-Sericite-Biotite-Quartz Schist (veined FDCSBQ Schist) represents two percent of the subsurface rock volume. It is considered to be a veined equivalent to the FDCBQ Schist described in Section 3.3.3.2. It shares the same geologic profile position with and is in transitional contact to the FDCBQ Schist (Figure 3.2). It alternates with the FDCBQ Schist in

1-2 cm zones (Plate 2e) over 2-10 metres with 3 metres the average. This unit is significant in that it is frequently contains gold, making it part of the Upper Ore Zone.

The mineralogy of this unit can be divided into host rock mineralogy, vein and vein wallrock mineralogy. The host litholgy is comparable to the FDCBQ Schist described above but does have some significant differences. The most significant difference is the almost complete loss of chlorite in the matrix and the dominance of sericite giving the rock a grey sheen. The sericite, which forms continuous linear zones, defines a weakly anastomosing foliation (Plate 2f). Associated with sericite is trace pyrrhotite, chalcopyrite and tourmaline. Biotite and ferroan dolomite remain as poikiloblasts but in more foliated rocks the biotite does not cross cut the foliation and the (001) cleavage direction parallels the foliation. The vein portion of the rock may represent up to 40% of the volume and averages 20%.

The veins form a folded "boxwork" networks (Plate 2e) and vary in density from less then 1% up to 20%. The veins are 1-2 cm in width and show sharp, often rimmed boundaries to the matrix. The boundaries are not linear and tend to be irregular and folded, reflecting the cleavage-slip style of deformation common to most of the rock types described. The veins are a greyish-white colour, mottled by faint yellow patches and frequently can be seen to contain ghost-like inclusions of the host FDCSBQ Schist. The alteration marginal to vein appears as a colour variation and ranges in width from zero to several centimetres.

The vein mineralogy consists dominantly of quartz, ferroan dolomite and plagioclse, but the portions vary. Quartz dominated veins make up 60% of this vein type; ferroan dolomite dominated veins make up 30% and plagioclase dominated veins make up 10%. Biotite, chlorite, tourmaline, pyrrhotite, arsenopyrite, chalcopyrite and gold make up the accessory and trace minerals of the assemblage.

Where quartz makes up 70% of the vein the individual grains are 500-700 um in length and 200-300 um in widths and are elongate parallel to the rock foliation. They show distinct undulose extinction and although the grain boundaries are locally sharp, they may show undulose extinction. Ferroan dolomite occurs as 200 um long, intergranular grains to quartz making up the remaining 30% of the vein. Trace pyrrhotite and chalcopyrite occurs associated with the ferroan dolomite. In this assemblage the alteration marginal to the vein is limited to minor grain size reduction and the development of tourmaline. Plagioclase may occur as isolated grains at the margin of the quartz vein associated with ferroan dolomite of the host FDCSBQ Schist.

Ferroan dolomite may occur as the dominant mineral (90%) with minor quartz (5%) and sulphide(5%). It is much the same as the quartz dominated vein type. The ferroan dolomite grains average 500 um in size and are equigranular and mosaic textured. Quartz occurs intergranular to the ferroan dolomite as 200 um, equigranular grains. Pyrrhotite is the dominant sulphide occuring intergranular to the ferroan dolomite. Chalcopyrite and more rarely pyrite are associated with the pyrrhotite. The vein boundaries are rimmed by 500 um of sericite containing a 2% dusting of rutile giving it a faint orange colour. Arsenopyrite occurs as 200 um, diamond shaped grains in the sericite rim to the vein. It is most often a trace mineral but may make up to 1 modal % of the rock. Anomalous Au values are common to this vein type.

Plagioclase dominated veins are the third type of vein. The plagioclase ranges in modal abundances from 15 to 90%. Where plagioclase is greater than 80% of the rock the grains are <300 um in diameter and show no twinning. They commonly have a fine grain dusting of carbonate. The grain boundaries of composite grains show undulose extinction and the rims have significant subgrain development. Randomly oriented blades (<500 um) of sericite and less commonly chlorite occurs intergranular to the plagioclase. Minor apatite is also noted to be intergranular to the quartz of this vein type. Trace diamond shaped arsenopyrite (0.5-1.0 mm), pyrrhotite, chalcopyrite occur within the vein and at the margin. Tourmaline often rims the vein as well.

A second, but less common plagioclase-rich vein type is also noted. It is 1-2 cm in diameter and 2-5 cm long with contact boundaries which are often transitional to the matrix with ghosts of the host FDCSBQ Schist. In thin section the veins are 60% plagioclase, 30-40% ferroan dolomite, 5% combined tourmaline, biotite and chlorite and 0-10% sulphide. The plagioclase grains range in size from 1.0 to 5.0 mm with 1.5 mm the average. They commonly show a random orientation with discontinuous and bent albite twinning. They may be composite grains with severe grain size reduction at interior grain boundaries. Subgrain reduction and new grain development is also apparent along the margins of the coarse grains and in several instances can be seen to almost completely consume the grain. Where the plagioclase grains are marginal to ferroan dolomite and associated with arsenopyrite, they may contain 200 um long needles of rutile.

Ferroan dolomite occurs as coarse grained (1-2 mm) patches, exhibiting radial, wavy extinction. The carbonate-carbonate grain boundaries are cuspate, locally showing subgrains and more rarely new grains. Where in contact with feldspar the relationship appears to suggest ferroan dolomite replacing the plagioclase. Included plagioclase shows very embayed corroded boundaries and is partially dismembered by the ferroan dolomite.

Pleochroic brown to colourless biotite forms distinct 100 um wide anastomising zones commonly cutting the plagioclase rich portion and less commonly the carbonate rich portions of the rock. It also occurs as randomly oriented blades marginal to the sulphide minerals. Chlorite is uncommon, occurring associated with the biotite. Coarse grained (1 mm) olive green tourmaline occurs in clusters associated with ferroan dolomite, biotite and sulphide. The clusters often form non-continuous linear trails paralleling the vein boundaries and cross-cut the plagioclase patches.

Arsenopyrite is the dominant sulphide type, occuring as 1-2 mm sub-diamond shaped blebs which commonly coalesce. Pyrrhotite, chalcopyrite are minor phases. The sulphides are associated with ferroan dolomite, tourmaline and biotite. Ilmenite occurs in close association with arsenopyrite, often forming irregular composite patches (200–300 um). Rutile may penetrate the ilmenite clusters, and is generally restricted to the carbonate regions but does occur along boundaries of the plagioclase.

Gold is very rarely seen in this rock type, but anomalous assay values are common. Where it is seen, it occurs at the boundary of rare quartz patches within ferroan dolomite. The boundary of the ferroan dolomite is marked by fine flakes of biotite.

The alteration marginal to the plagioclase rich vein type is far more significant than the other vein types, extending up to several centimetres on either side of the vein. The altered rock is foliated, homogeneously textured, consisting of biotite, plagioclase and ferroan dolomite. Pleochroic light brown to dark orange brown biotite blades (1-2 mm, 40%), define an open anastomosing cleavage, wrapping around the plagioclase and ferroan dolomite. The plagioclase (20%) occurs as either elipsoidal patches (0.5–1.0 mm) made up of untwinned grains or as single, strongly subgrained elipsoid eyes. Fine biotite flakes and carbonate grains occur as inclusions in the plagioclase. Ferroan dolomite (10%) occurs in zones as mosaic textured grains, 300 um in diameter, intergranular to the plagioclase. The opaque mineralogy consists of ilmenite as 100 um long blebs; pyrrhotite occurs as thin elongate blebs associated with biotite; and arsenopyrite, as a trace mineral associated with pyrrhotite.

3.3.3.4. Massive Ferroan Dolomite with Chlorite-Sericite Partings

The Massive Ferroan Dolomite is generally restricted to the structural upper portions of the geologic profile (Figure 3.2). It is commonly associated with the veined FDCSBQ Schist and Sericite-Chlorite Schist but also occurs with Silicified Dolomite and Graphitic Pelite. It is in transitional contact with the veined FDQCSBQ Schist and may alternate with it over several metres. The contact to the Sericite-Chlorite Schist is sharp. The Massive Ferroan Dolomite is the only carbonate rock noted to occur in contact with the Sericite-Chlorite Schist and is locally interpreted to completely envelope it (Figure 3.2). The true shape of the Massive Ferroan Dolomite is not clear, but it does not appear to be regular in shape or dimension, varying in thickness from 0.5 m to 3.0 m and averaging at 1.5 m.

In hand sample the Massive Ferroan Dolomite is buff grey to pink. It is characterized by curvilinear green-grey chlorite-sericite partings (Plate 2g).

In thin section this rock type consists of ferroan dolomite (80%), combined chlorite and sericite (20%), trace plagioclase and arsenopyrite. Elongate, mosaic textured coarse ferroan dolomite grains (0.7 mm long) are often decorated at their edges by finer grains (0.2 mm across) of ferroan dolomite (Plate 2h). Trace quantities of black carbonaceous material may dust the grain boundaries. Chlorite forms characteristic linear zones or partings which are 1-2 cm long and 1 mm wide. Significant grain size reduction of ferroan dolomite is noted at the margins of these zones or partings. Sericite may replace chlorite or form distinct zones within the chlorite. Trace plagioclase porphyroblasts (0.2 mm across) may overgrow the chlorite. Euhedral grains of arsenopyrite (up to 5 mm across) and euhedral grains of tourmaline (0.1-0.5 mm across) occur in the ferroan dolomite matrix marginal to the chlorite-sericite partings. In several instances tourmaline is seen to pseudomorph ferroan dolomite grains. Trace ilmenite, pyrrhotite, chalcopyrite and arsenopyrite are associated with the chlorite partings.

3.3.3.5 Sericite-Chlorite Schist

The Sericite-Chlorite Schist is generally restricted to the structural upper portions of geologic profile. It is in upper sharp contact to Mássive Ferroan Dolomite or veined FDCSBQ Schist and is in transitional lower contact to Chlorite-Magnetite Schist. (Figure 3.2) It is characterized by its fissile nature, tiger-striped pattern of interfingered sericite and chlorite (Plate 3a) and the development of large, up to 2 cm wide, porphyroblasts of chloritoid, garnet, plagioclase and arsenopyrite. It ranges in thickness from 0.5 to 3 m with 1.5 m the average. It often contains significant Au and is an intergral part of the Upper Ore Zone. Surface exposure, longitudinal and cross-section interpretations suggest that it is cigar or pod-like in shape with the long dimension plunging 10-15^{o}, approximately east-west.

The Sercite-Chlorite Schist consists of sericite (70-50%), chlorite (15-35%), biotite (2-5%), chloritoid (0-5%), garnet (0-5%), plagioclase (0-2%), arsenopyrite (0-2%), ilmenite (1-2%) and minor

PLATE THREE: BANDED SERICITE-CHLORITE SCHIST

3a. Core sample of typical rock. Matrix dominantly sericite.. Whitish zones are albite. Note complex, irregular "controtion/folding" in matrix. (Core width 7 cm).

3b. Overview showing matrix dominated by chlorite with ellipsoidal sericite patches. Opaque ilmenite. (ppl, Scale Bar = 1 mm).

3c. Blades of chloritoid (right of photo) are altered to sheaths of chlorite (left of photo). The sheaths of chlorite are altered to finer grained chlorite and sericite. (ppl, Scale Bar = 1 mm).

3d. Garnet porphyroblasts with inclusions of quartz and ilmenite in contact with chloritoid blade. Contact boundaries are irregular but smooth. Ilmenite generally shows a helicitic texture. (ppl, Scale Bar = 1 mm).

3e. Oligoclase porphyroblasts in sericite-chlorite matrix. Note the zoned and more sericitic boundaries to the plagioclase. (xpl, Scale Bar = 1 mm).

3f. Chloritoid porpyroblast showing the re-orientation of. ilmenite inclusions relative to ilmenite in the sericite matrix. (xpl, Scale Bar = 1 mm).

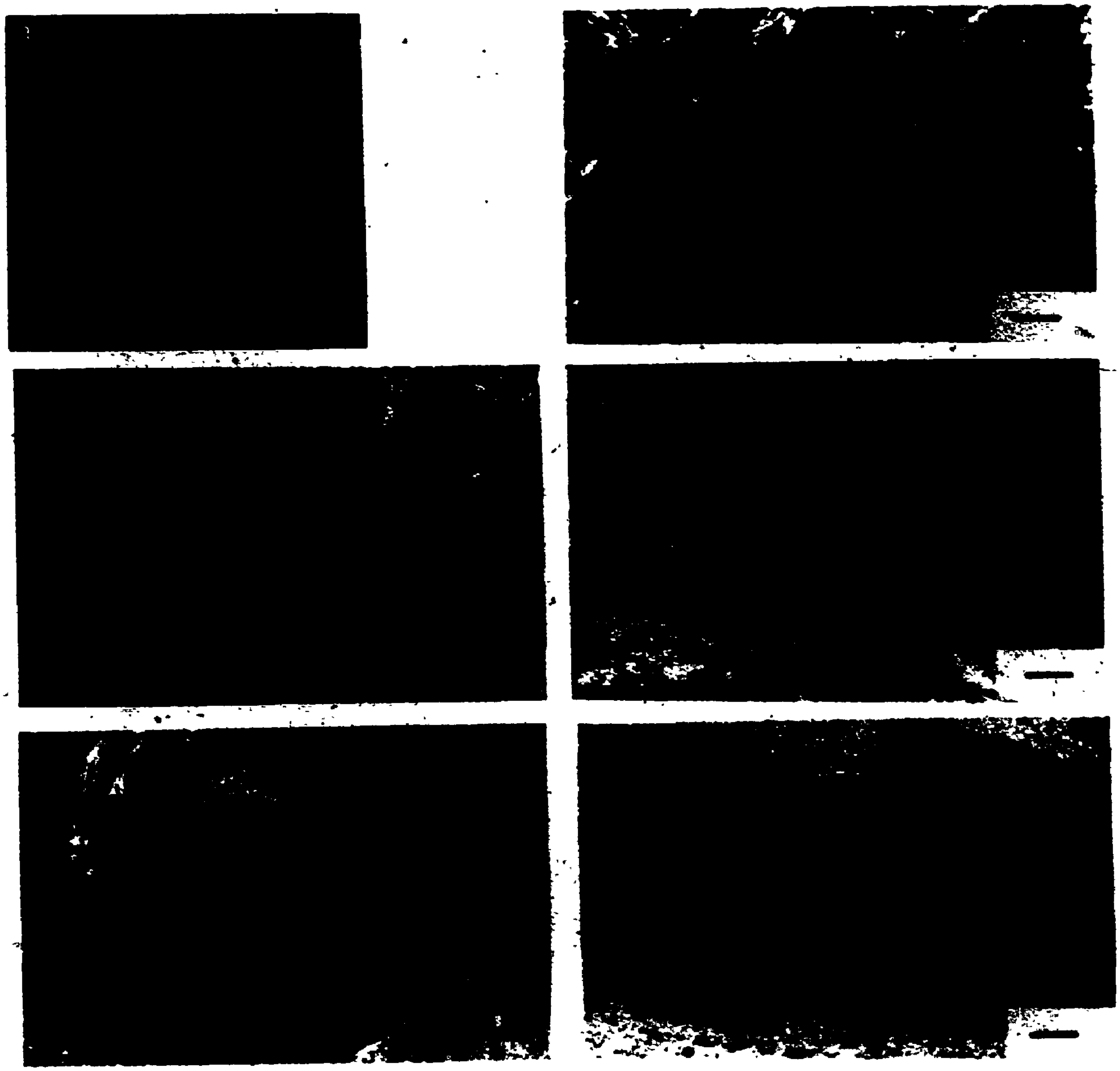

pyrrhotite, chalcopyrite and Au. Fine grained, 20-50 um long, colourless sericite and dark green chlorite blades form a continuous, aligned mat forming the characteristic tiger striped pattern (Plate 3b). Blebs of ilmenite (100 um long) are included in the sericite and are alligned parallel to the sericite foliation (Plate 3b). Poikiloblasts (0.5 mm across) of brown biotite are randomly oriented in the sericite mat and grain boundaries are usually sharp. Locally they have a beard-like growth of mixed sericite, chlorite and biotite which is oriented parallel to the foliation. Chloritoid poikiloblasts (0.5-2 cm across) occur in much the same fashion as the biotite poikiloblasts (Plate 3c). They generally include helicitic trails of biotite and ilmenite and are fringed by sericite and chlorite beards. Sheaths of chlorite may psueudomorph the chloritoid poikiloblasts (Plate 3d). Subhedral almandine garnet porphyroblasts (0.5 to 4.0 cm across) commonly contain inclusions of ilmenite, quartz and more rarely biotite and sericite (Plate 3c). Strongly optically zoned plagioclase porphyroblasts (0.3-0.6 mm across) may overgrow the sericite-chlorite dominated matrix (Plate 3e). Euhedral to slightly ellipsoidal arsenopyrite grains (1-5 mm across) occur with pyrrhotite forming in the pressure shadow regions. Visible gold is commonly noted with the pyrrhotite. The abundance of arsenopyrite is directly proportional to the gold content of the sample but no gold has been observed in arsenopyrite.

3.3.3.6. Chlorite-Magnetite Schist

This rock may or may not be present in the geologic profile. It is a variable unit but is distinguished by the presence of magnetite and very dark green chlorite. It is generally restricted to the upper portions of the geologic profile and is invariably enveloped by Sericite-Chlorite Schist or Massive Ferroan Dolomite (Figure 3.2). It is noted to occur within Graphitic Pelite in one borehole (159) where it is enveloped by Sericite-Chlorite Schist. In handsample the contact to the Sericite-Chlorite Schist is marked by a progressive increase in chlorite and the appearance of magnetite over centimetres. The contact with the Massive Ferroan Dolomite is sharp and parallel to foliation. The unit ranges in thickness from 0.5 to 2.5 metres and is interpreted to form cigar shaped pods.

Although, it makes up less than 1% of the subsurface rock volume, it is economically important, often hosting significant gold mineralization. Several sections have graded well over 70 g Au/tonne. It is considered to represent the core of the Upper Ore Zone.

The variability characteristic of this rock unit is due to the presence or absence of garnet, grunerite, biotite, plagioclase, arsenopyrite, pyrrhotite, chalcopyrite, pyrite and gold. Dark green chlorite and sub-to euhedral octahedra of magnetite are ubiquitous throughout, varying in modal porportion depending on the coexisting mineral assemblage. Figure 3.3 illustrates the internal heterogeneity of the unit as well as the heterogeneity from borehole to borehole. Within Borehole 156 the proportion of sulphide (aspy,po,cpy) varies with garnet content while within Borehole 159 the proportion of sulphide varies with abundance of chlorite, magnetite as well as the presence or absence of grunerite. In Borehole 60 both biotite and plagioclase feldspar are present with

Figure 3.3. Examples of Chlorite-Magnetite Schist from Various Boreholes.

	(metres)	Borehole 156	Borehole 60	Borehole 159
Au Grade (g/m)		43.80/2.05	nil	3.04/1.4
		Sericite-Chlorite Schist	Massive Ferroan Dolomite	Massive Ferroan Dolomite
Upper Contact	0.0	****************	****************	****************
			70% chl, 20% mt 10% po,cpy,aspy	50% chl, 15% mt, 10% grun, 5% gnt 5% po
		20%aspy, 20%po, 10%cpy, Au	****************	
	0.5	20%chl, 5% mt; 5% gnt	Silicified Dolomite	----------------
				Massive Ferroan Dolomite

		70%gnt, 20%chl,		----------------
	1.0	5% mt 5% aspy, tr. po		60% chl, 10% mt, 10% gnt, 5% po, 5% aspy, Au
				****************
	1.5			Sericite-Chlorite Schist
	2.0			
Lower Contact		****************		
		Sericite-Chlorite Schist		

only pyrrhotite as the sulphide. In all three boreholes the presence or absence of Au appears to be related to the arsenopyrite and chalcopyrite contents. Plates 4a and 4b show the variability of sulphide within the unit.

The abundance of chlorite varies from 10-90%. In thin section it occurs as pleochroic, very dark green to medium green blades, defining the foliation where abundant (Plate 4c). It may also occur as nonoriented fibrous mats intergranular to the other minerals or overgrowing the matted, fibrous chlorite.

Almandine garnet may or may not be present in this unit. It ranges in abundance from 0-70% with the average at 10%. It occurs most often as coalesced, irregular, anhedral poikiloblasts (0.5-1.0 mm) which include octahedra of magnetite, blebs of ilmenite, and grains of grunerite and quartz, all forming a continuous helicitic texture with the fabric of the matrix (Plate 4d). Where the rock is more foliated the garnet occurs as fish-net textured bands riddled with only quartz as the inclusion.

The contact boundaries of garnet with other minerals are generally sharp although not necessarily smooth. Chlorite may form a discontinuous rim around magnetite included in garnet (Plate 4d). In addition, fine grained matted chlorite may form along cracks within the garnet. Locally garnet is noted to pseudomorph the bladed matrix chlorite.

Grunerite ranges in abundance from 0-20%. Where present it occurs in patches of 0.5 mm long, well twinned radiating fibre bundles (Plate 4e). Locally the twin planes appear to be displaced

PLATE FOUR: CHLORITE-MAGNETITE SCHIST

4a. Core sample of Chlorite-Magnetite Schist represented by > 50% sulphide. Sulphides consist of euhedral arsenopyrite, pyrrhotite, chalcopyrite and galena. Sample is ore. (Core width 7cm).

4b. Core sample of Chlorite-Magnetite Schist represented by 90% sulphide. Sulphides consist of arsenopyrite, pyrrhotite and chalcopyrite and galena. Sample is ore. (Core width 7cm)

4c. Subhedral magnetite rimmed by quartz in a matrix of chlorite and ilmenite. (ppl, 1cm = 0.3mm).

4d. Euhedral magnetite in a matrix of garnet (light grey) separated by chlorite (darker grey). To upper right patch of grunerite with inclusion of magnetite and ilmenite. (ppl, Scale Bar = 0.3mm).

4e. Large dark grain of garnet in intimate contact with grunerite locally showing characteristic twinning (light grey). (xpl, Scale Bar = 0.3mm).

4f. Opaque consists of dominantly arsenopyrite with pyrrhotite, chalcopyrite and galena. Darker grey silicate is albite, which is clearly included in the sulphide. (xpl, Scale Bar = 0.3mm).

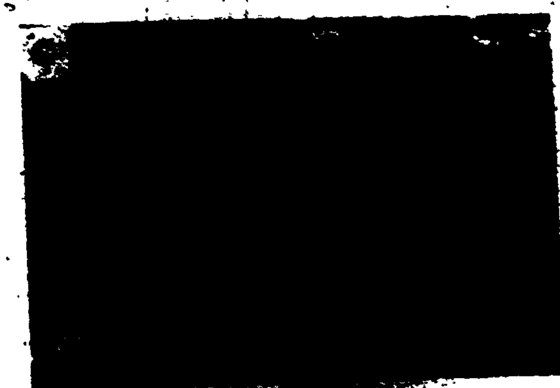

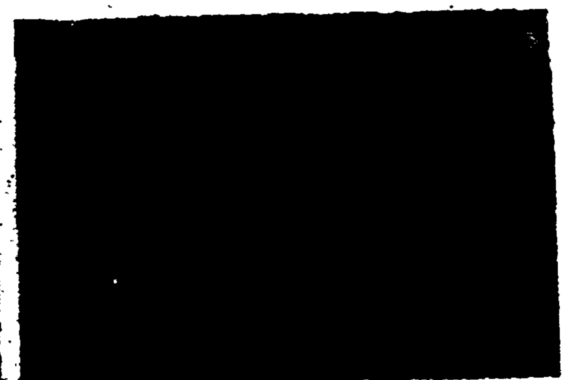

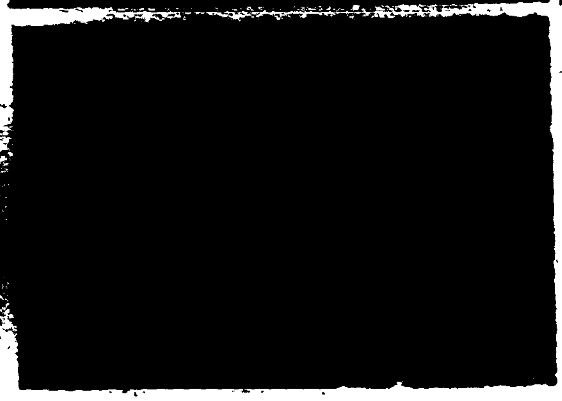

to various degrees giving the impression of brittle deformation. The grunerite invariably contains euhedral octahedra of magnetite and blebs of ilmenite which show a helicitic texture with that of the matrix.

Grunerite is most commonly in contact with chlorite, often cross-cutting the foliation direction defined by chlorite. Close examination of the contact of the grunerite and chlorite reveals a fine grained fringe or interface of chlorite and quartz oriented parallel to the (010) cleavage direction of grunerite. Grunerite is also in contact with the almandine garnet poikiloblasts. Here the contacts are generally sharp and well defined with minor development of interfacing chlorite. In one instance garnet can be seen to envelope grunerite at grain boundaries giving the impression of incipient replacement of grunerite by garnet (Plate 4e). Grunerite is also rarely noted to occur as inclusions in garnet and here too the contacts are sharp and well defined.

The abundance of ferroan-dolomite varies from 0-15% and appears to be related to the degree of deformation of the grunerite. That is, the more the twin planes are displaced the greater the amount of ferroan dolomite. Ferroan dolomite also occurs as an accessory mineral at grain boundaries of grunerite to grunerite or magnetite to grunerite. It rarely occurs associated with chlorite and was not noted associated with garnet.

Quartz occurs as an accessory mineral (1-5 modal%), frequently as isolated grains or mosaic textured patches intergranular to the other silicate minerals without any obvious preferred association.

In other instances, quartz occurs as mosaic textured grains with intergranular anastomosing chlorite blades and rare magnetite octahedra, grunerite and garnet. Similarily it occurs as mosaic grains within fish-net textured garnet as described above.

Magnetite is ubiquitous, occuring as euhedral to subhedral octahedra. Its abundace ranges from 5 to 20% with 5% the average. It is not restricted in association, occuring as inclusions in both silicate and sulphide phases. Ilmenite is also ubiquitous with an abundace of 1%. It occurs as evenly distributed 200-500 um blebs often containing worm-like inclusions of quartz. Rutile is rarely noted.

Plagioclase is fairly rare in this unit occurring with abundant chlorite or abundant massive sulphide. Its abundance ranges from 0-10%. The grains are 0.5-1.0 mm in diameter, circular in cross-section and moderately well twinned. The grains are visibly zoned, showing a continuous undulose extinction pattern. When in contact with chlorite the edges of the plagioclase are frayed-looking, whereas when in contact with the sulphides the contact boundaries are sharp.

Arsenopyrite, pyrrhotite, chalcopyrite, galena and pyrite (Plates 5a, 5b, 5c, Au and Ag (Plate 5d)make up the sulphide and precious metal component of this unit. Arsenopyrite is the dominant sulphide with its abundance ranging from 2-50%; pyrrhotite is next at 2-10% with chalcopyrite following at <1-2%. Galena and pyrite are the least common at 0-<1%. Where the sulphides represent less than 5% of the rock volume they occur as isolated blebs, evenly

PLATE FIVE: CHLORITE-MAGNETITE SCHIST

5a. Backscatter SEM image of sulphides. Magnetite occurs as euhedral graims. (Scale Bar = 20.4 um).

5b. Backscatter SEM image of coarse, fractured, arsenopyrite grains surrounded by pyrrhotite and chlcopyrite. Darker grains are magnetite. (Scale Bar = 69.0 um).

5c. Backscatter SEM image of pyrite (light grey) included in pyrrhotite. (Scale Bar = 43.5 um).

5d. Backscatter SEM image of native silver, showing well developed granular morphology in crack of magnetite.

5e. Backscatter SEM image of bleb of Jamesonite within magnetite.

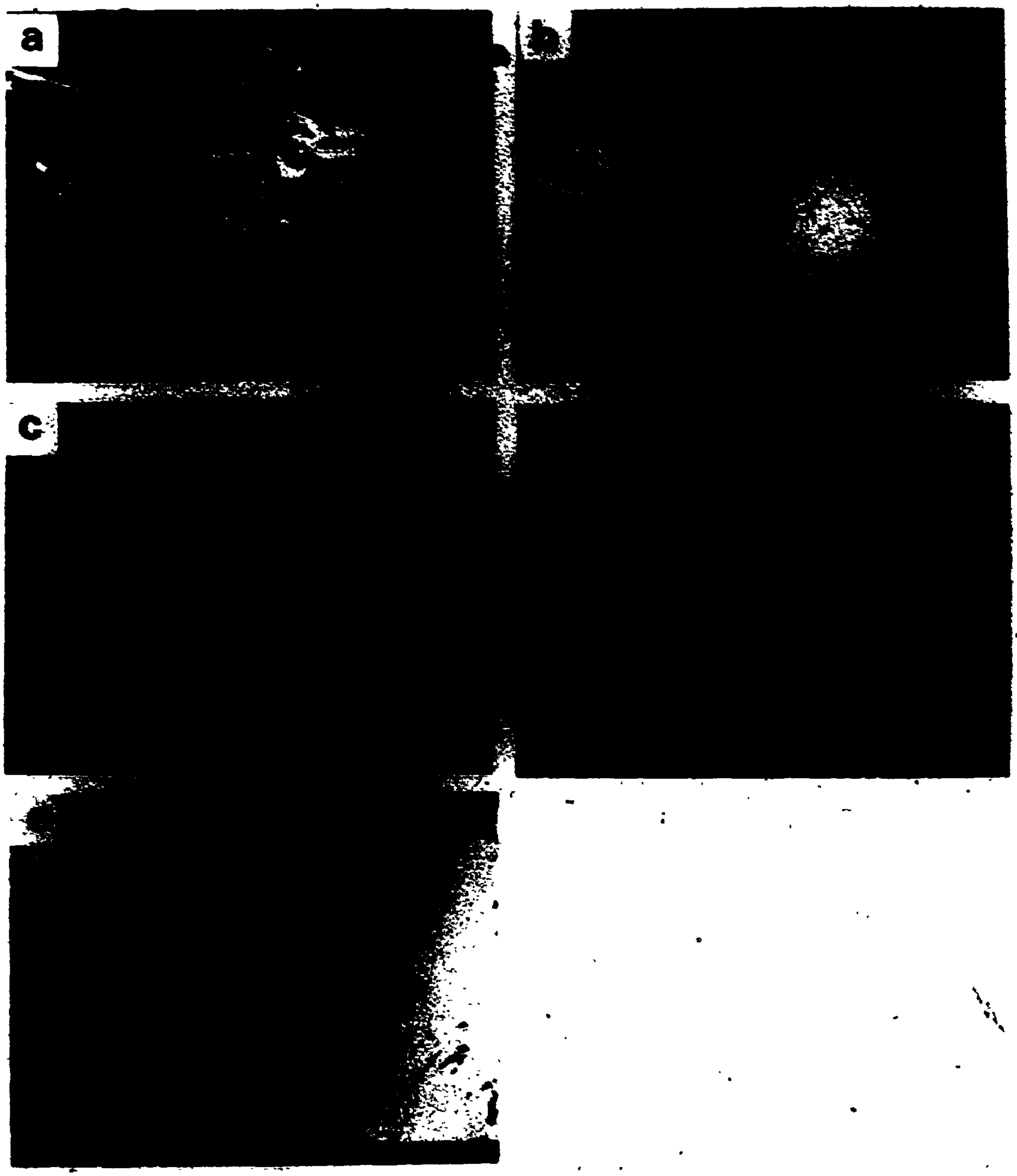
a
b
c

distributed in the rock. Where they are more abundant they coalesce into massive patches, including the silicate assemblage (Plate 4f). Increasing sulphide abundace is at the expense of the silicate assemblage, but does not indicate a decrease in the oxide assemblage.

Texturally the sulphides show an intimate relationship to one another. Plates 5a and 5b show magnetite as subhedral grains with arsenopyrite as fractured, sub-cubic grains and pyrrhotite and chalcopyrite as irregular grains.

Visible gold is fairly rare, but is more typical than in any other rock type of the Upper Ore Zone. It appears to be related to the presence of both magnetite and arsenopyrite, as it is not significant in those rocks with only magnetite or only arsenopyrite. In one sample gold can be seen to occur within magnetite along a crack.

Native silver is noted to occur within cracks and along the edge of magnetite (Plate 5d) as very granular almost blade like grains.

Several grains of Jamesonite (a lead sulphosalt) is noted to occur within magnetite (Plate 5e).

3.3.3.7 Silicified Dolomite

The Silicified Dolomite represents approximately 25% of the subsurface rock volume, ocurring in the central portions of the geoligic profile (Figure 3.2). The upper contact is sharp to Sericite-Chlorite Schist; however, where in contact with Massive Ferroan Dolomite the contact is transitional, distinguished by a colour change from buff to white grey. Silicified Dolomite is in sharp contact to, and alternates with, Graphitic Pelite at 10-20 m

PLATE SIX: SILICIFIED DOLOMITE

6a. Core samples of varying textural types of Silicified Dolomite. From left to right, Spotted Dolomite, Fragmented Dolomite, Fragmental Dolomite and Fragmental Dolomite with quartz vein.

6b. Core sample of Fragmental Dolomite with patches of Spotted Dolomite. (Core width 7cm).

6c. Opaque is carbonaceous fragment, which is more of a dense dusting overgrowing the dolomite matrix. (ppl, Scale Bar = 0.30mm).

6d. Overview of Massive Dolomite of carbonceous dustings developed into a styloitic texture. (ppl, Scale Bar = 0.30mm).

6e. Overview of Spotted Dolomite. Carbonaceous dusting follows grain boundaries. (ppl, Scale Bar = 0.30mm).

6f. Spotted Dolomite texture of radial dolomite with ferroan dolomite core. Texture forms spheroids. (xpl, Scale Bar = 0.30mm).

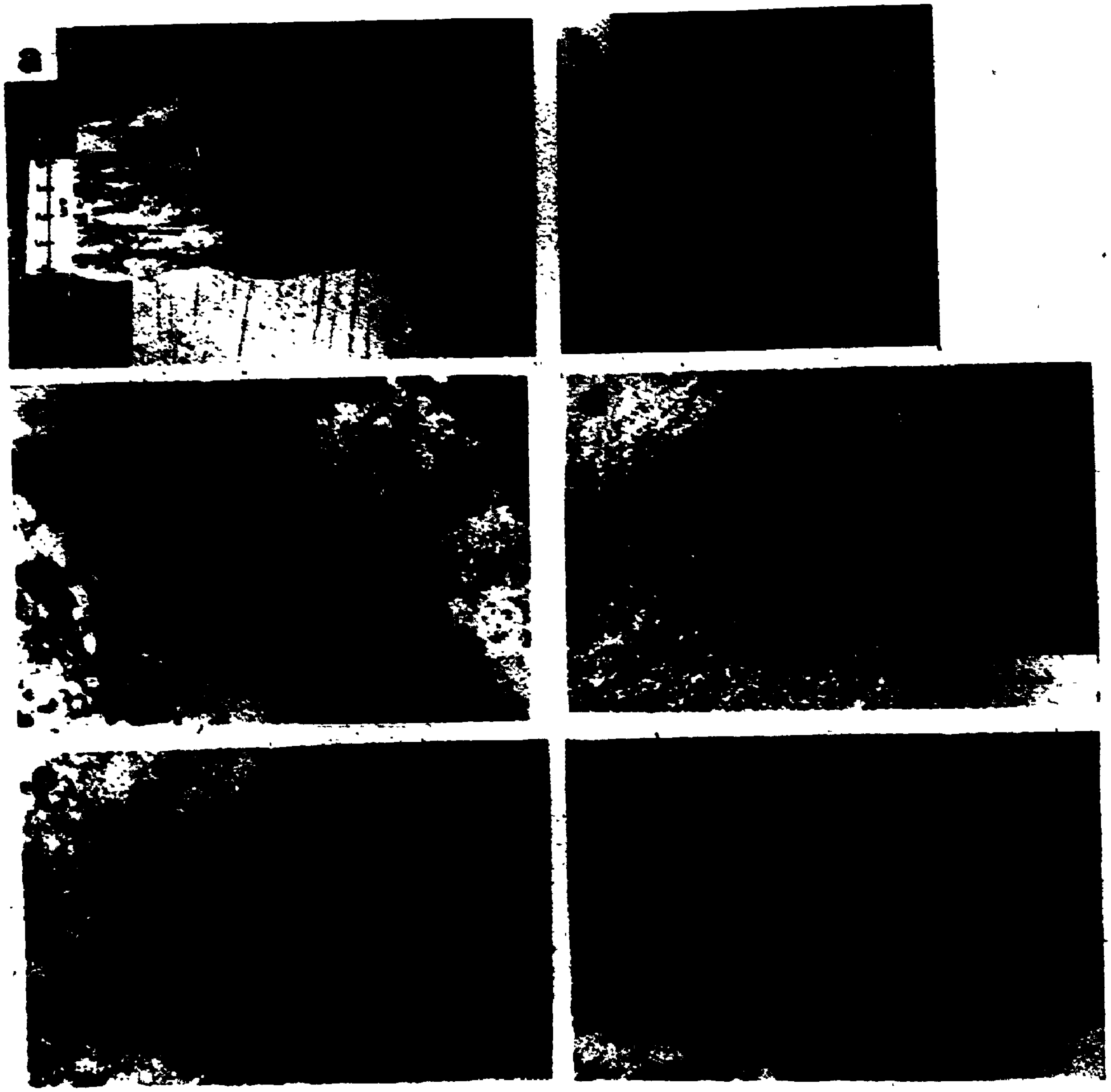

intervals. It ranges in thickness from 0.5 m to 50 m with an average of 10 m. It is interpreted as large but discontinuous bodies enveloped by graphitic pelite (Figure 3.2).

There are four textures developed within the silicified dolomite. In order of abundance of these are:

i) fragmented dolomite (40%) (Plate 6a),
ii) fragmental dolomite (30%) (Plate 6a),
iii) massive to slightly banded dolomite (20%),
iv) spotted dolomite (10%) (Plate 6a, 6b).

i) Fragmented Dolomite

In hand specimen the fragmented dolomite consists of 80-90%, elongate, angular grey-white carbonate fragments, 5 mm wide and 20 mm long. The fragments appear to have once formed a continuous rock mass and are separated by well defined, thin, <1 mm wide, black carbonaceous material or graphite (Plate 6a, 6d). The elongation direction of the fragments is sub-parallel throughout the rock with the width to length ratio of the fragments varying from 2:3 to 1:6 with 1:5 the average. Quartz makes up to 10% of the rock, ocurring as interfragmental 1x3 mm patches and as 1 mm wide veins frequently cutting the fragments.

In thin section the fragmented dolomite consists of 80-90% dolomite, 10-15% quartz, 1-2% graphite, 1-2% sericite and rare plagioclase and calcite. The fragments are composed of medium grained, 300-500 um wide, equigranular to slightly elongate dolomite grains. Separating the fragments is a thin carbonaceous boundary composed of very fine grained, spherical grains forming a discontinuous train at dolomite grain boundaries (Plate 6d). Commonly associated with the graphite are 200 um long, blades of sericite which also form discontinuous , linear trails along dolomite grain boundaries. Locally the graphite and sericite concentrate to form more continuous, anastomosing trails. The contacting dolomite shows moderate subgrain development along these zones.

Quartz is most often developed as one or two grain, 200-300 um wide, discontinuous trails, often associated with the graphite and sericite. Where quartz makes up to 15% of the rock the grains are highly sutured, and form elongate vein-like patches. Finer grained, 100 um wide quartz is developed within the interior of the patches, often showing a ribbon texture.

Plagioclase, is associated with the graphite-sericite zones described above. It is usually equigranular, 300-500 um in diameter, untwinned, highly dusted by graphite and appears to be incipiently replacing dolomite.

Coarse grained (0.7-1.0 mm wide) calcite veins are rarely noted to cut the fragmented dolomite. Inclusions of finer grained dolomite with graphitic dusting occur within these veins. These are interpreted to be late.

<u>ii) Fragmental Dolomite</u>

In hand specimen the fragmental dolomite is a mottled looking rock (Plate 6[illegible] The fragments are commonly losenge shaped, ranging in length from 1 mm to 2 cm. The long dimension defines the foliation. The fragments are dominantly light grey dolomite with abundance of 70 to 80%, medium to dark grey quartz at 10 to 15% and black graphitic fragments at 5%. The matrix to the fragments makes up 10% of the rock and is fine grained, medium-grey and wispy textured often wrapping around the fragments giving the rock a very fluid appearance.

In thin section the dolomite fragments are similar to those of the fragmented dolomite. They are made up of equigranular to slightly elongate dolomite grains which tend to be coarser grained than the dolomite of the matrix. The margins of the fragments are usually defined by a contact with quartz and may be marked by grain size reduction. The quartz fragments are made up of elongate (width:length=1:2), medium grained (0.5-0.7 mm wide), highly sutured, quartz grains with undulose extinction. Fine blades of sericite (200-300 um long) are intergranular to quartz and parallel the rock fabric. The quartz fragments are variably sized patches which are rarely completely isolated from one another; joined by multi- or single grain wide trails of quatrz or by graphitic dusting. Frequently the quartz patches are cut by dense, anastomosing zones of graphite. Here the quartz is finer grained, more elongate, taking on an almost ribbon-like texture.

The graphitic fragments are not well defined. They are usually linear, parallel to the rock fabric, consisting of a dense near-opaque graphite dusting of dolomite and more rarely quartz (Plate 6c). The margins of the fragments are sharp, parallel to the rock fabric but are transitional perpendicular to the foliation at their ends. Several graphitic fragments show a colour zoning from black to grey toward the edges and others are seen to be folded or dismembered.

The matrix to the fragments is similar to that of the fragmented dolomite but is more developed. It consists of fine grained, 100 um wide, dolomite grains cut by anastomosing 1 mm wide zones of graphite (10%), sericite (5-10%) and rarely biotite (0-5%). In the extreme, sericite may form well defined (1-2 mm) anastomosing bands with up to 10% stubby yellow-brown euhedral cyrstals of rutile randomly dispersed within it. Dense graphite may develop at the margins of these zones.

iii Massive Dolomite

In handsample the massive dolomite is grey-white, equigranular and homogeneously textured. Locally it takes on a banded appearance. The bands are dark-grey, 1 to 5 mm wide, alternating with 1-3 cm wide grey white bands.

In thin section the massive dolomite consists of 90% dolomite, 4% quartz and 1% graphite. The dolomite forms as equant to slightly elongate (0.5 mm long) grains. Grain boundaries are sutured and irregualar, showing grain size reduction. They are also often dusted by fine grained spherical grains of graphite. Locally the graphite grains are continuous trails giving the rock a stylolitic appearance (Plate 6d). Quartz occurs as 300 um wide, three to four grained patches intergranular to the dolomite.

iv Spotted Dolomite

Although not abundant, the spotted dolomite texture is fairly ubiquitous, ocurring in close association with the massive dolomite. In hand sample it appears as 0.5 mm wide, medium-grey, spheroidal dolomite grains making up 20% of the rock in a dark grey to black, fine grained matrix consisting of 70% dolomite, 5% graphite, and 5% sericite with rare plagioclase (Plate 6a, 6b). It is interesting to note that the dolomite spheroids are occasionally elongate rods perpendicular to the spherical cross-section and parallel to the foliation direction.

In thin section the rock shows a complex texture. Round, coarse dolomite grains (0.5–0.8 mm in diameter), frequently subgrained into three or four sections are rimmed by finer grained (200–300 um wide), mosaic textured dolomite. A thick (locally opaque) dusting of graphite occurs at the boundaries of the finer grained dolomite and the coarser grained carbonate, giving the spotted appearance to the rock (Plate 6e, 6f). The degree to which the coarse grained carbonate grains are rimmed by finer grained mosaic carbonate varies. Where in direct contact with other coarse grained carbonate grains the boundaries are smooth with a graphite dusting defining the boundary. At the boundary of the coarse grained carbonate grains with the finer grains the rim are sutured and cuspate, although still clearly defined. Locally, the coarse grained carbonate grains are isolated in a fine grained carbonate matrix with a contact boundary that is ill defined giving the appearance of progressive grain size reduction.

Quartz occurs dominantly as fine to medium grained (200–500 um wide), mosaic textured patches within the matrix. Rare dolomite is intergranular ~~to the~~ quartz grains and a graphitic dusting occurs only at the margins of the patches. Graphite occurs in the same fashion as in the fragmented dolomite. Sericite is noted to occur as thin, 1 mm long, linear, weakly anastomosing zones margined by fine grained, mosaic textured to slightly elongate matrix dolomite.

Plagioclase feldspar may occur overgrowing sericite blades as described for the fragmental dolomite. The grains are rounded, irregularly shaped, ranging in size from 100–300 um wide and include a fine brownish dusting. Plagioclase can also be seen to rarely occur within the dolomite matrix where the margins of the coarse grained dolomite grains show marked subgrain development. The grains appear to be partially replacing the matrix dolomite.

3.3.3.8 Graphitic Pelite

Graphitic Pelite generally occurs in the middle of the geologic profile (Figure 3.2). It alternates with the Silicified Dolomite over 10 to 20 m intervals and has an average thickness of 15 m. It is in sharp contact with the Silicified Dolomite, with the contact boundary parallel to the foliation direction. It is in transitional contact to the Quartz Cemented Graphitic Pelite Breccia, which is marked by increasing quartz vein density. It is interpreted to form the enveloping matrix to the Silicified Dolomite.

In hand sample the Graphitic Pelite is black to dark grey, fine grained, and foliated. It is typically homogeneous (Plate 7a) except where ellipsoidal, (2-3mm) grey 'eyes' give it a fragmental appearance (Plate 7a). Pyrrhotite is ubiquitous occurring as 1-3mm elongate trails parallel to the foliation; biotite porphyroblasts (1-2mm long occur evenly throughout the unit, and garnet porphyroblasts (1-2mm in diameter) are developed in zones with increasing frequency toward the lower contact (Plate 7a). The Graphitic Pelite is locally cut by folded 1-5 cm quartz-ferroan dolomite veins which become more common near the Quartz Cemented Graphitic Pelite Breccia (Plate 7d). Within 2 m of the Quartz Cemented Graphitic Pelite Breccia the Graphitic Pelite becomes lighter grey and euhedral arsenopyrite become more abundant and coarser in grain size from 0.5 mm to 5 mm.

PLATE SEVEN: GRAPHITIC PELITE

7a. Core sample of typical Graphitic Pelite. Small light grey elipsoids ferroan dolomite and small light grey spheroids garnet. (Core width 7cm).

7b. Core sample of Graphitic Pelite with intercalations of Sericite-Chlorite-Quartz Schist. (Core width 7cm).

7c. Euhedral garnet in matrix of chlorite, sericite and quartz dusted by carbonaceous material. (ppl, Scale Bar = 1mm).

7d. Core sample of contorted quartz-ferroan dolomite veins typical proximal to the LOZ. (Core width 7cm).

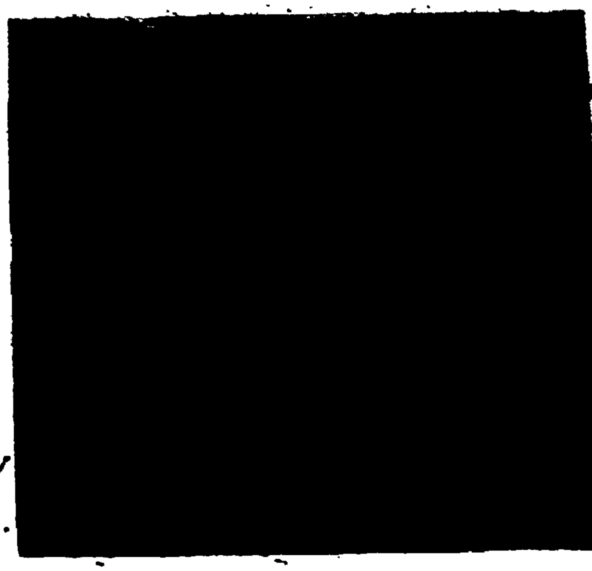

A sub-unit, termed Sericite-Chlorite-Quartz Schist occurs interlayered with the Graphitic Pelite (Plate 7b). It makes up 20% of the unit and is in sharp contact with the Graphitic Pelite. It occurs as 0.5-1 mm long fingers or as isolated 2-3cm "fragments". It is texturally similar to the Graphitic Pelite but is grey-green in colour with distinct brown biotite porphyroblasts (1-2 mm). Garnet porphyroblasts are developed in this sub-unit as well as trace pyrrhotite. The most significant difference is the absence of graphite.

In thin section (Plate 7c) the Graphitic Pelite consists of quartz(40%), sericite(20%), biotite(20%), graphite or carbonaceous material(5%) and pyrrhotite (2-5%) with minor chlorite(2%), ferroan dolomite and calcite (2-10%), garnet (0-5%), plagioclase (0-2%). Fine grained (50-200 um wide) quartz grains are equant to slightly elongate and show a mosaic texture. Locally quartz occurs as coarser grains, 300 to 500 um wide, forming elongate patches, interpreted to be dismembered veins. Sericite occurs as 200 um long blades defining a tight, continuous, planar foliation. The carbonaceous material is evenly distributed, locally obscuring the other matrix minerals. Coarser grained, 0.3 to 6 mm long, brown biotite blades parallel the sericite foliation, but are rare.

Porphyroblasts of brown biotite (1-2 mm long) cross-cut the sericite defined foliation and often contain sigmoidal trails of carbonaceous inclusions. Locally the biotite porphyroblasts are cut by biotite flakes which parallel the foliation.

Subhedral almandine garnet porphyroblasts, 0.5 to 2 mm in diameter, occur in 2 to 5 cm zones (Plate 7c). They contain very few inclusions and often have a dense rimming of carbonaceous material. The matrix fabric rarely wraps around the garnets and more commonly abuts against the garnet edge.

Chlorite occurs as 100-300 um long, losenge shaped blades, parallel to the foliation. Plagioclase occurs as 1 to 2 mm wide, equigranular, myrmekitic porphyroblasts growing out of the matrix. Coarse ferroan dolomite grains (0.5-0.8 mm in diameter) occur with quartz and is interpreted to be part of dismembered veins.

Near well defined, 0.5 to 1 cm wide quartz-ferroan dolomite veins the matrix is biotite rich (20%) and plagioclase rich (30%). Biotite increases at the expense of the other sheet silicates and plagioclase porphryoblasts overgrow the matrix. Arsenopyrite may comprise 5% of this rock and is associated with anamalous gold values.

Within proximity to the Quarts Cemented Graphitic Pelite Breccia or Lower Ore Zone the abundance of quartz, ferroan dolomite, calcite and arsenopyrite increases significantly (Plate 7d). Quartz occurs as coarse grained, 0.5 to 1.0 mm wide grains forming 2-3 mm wide elongate patches. Ferroan dolomite or calcite is often intergranular to the quartz or occurs as isolated or composite grains in the matrix. Arsenopyrite is associated with the coarse grained quartz or also occurs as isolated grains, interconnected by single grain trails of quartz and pyrrhotite.

The Chlorite-Sericite-Quartz sub-unit consists of fine grained, 200 to 300 um wide quartz grains (20%), and 300 um long chlorite blades

(30%) and sericite blades (15%), which define a continuous planar foliation. Coarse, brown biotite porphyroblasts (10%), 0.5 to 1.0 mm long, cross-cut the foliation. Chlorite (5%) forms 0.5 mm lozenge-shaped porphyroblasts in the quartz rich matrix. Quartz (10%) and ferroan dolomite (5%) also occur as elongate pods parallel to the foliation which are usually joined by single trails of quartz and are interpreted as deformed veins.

ycm:3.3.3.9 loz

3.3.3.9 Quartz Cemented Graphitic Pelite Breccia (Lower Ore Zone)

The Quartz Cemented Graphitic Pelite Breccia is restricted to the lower part of the Graphitic Pelite. Upper and lower contacts have been arbitrarily defined as the first and last occurrence of greater than 20% massive white quartz veins (Plate 6a). The upper contact is exclusively with Graphitic Pelite while the lower contact is usually with Graphitic Pelite, sometimes it is in contact with Banded Chlorite-Sericite-Garnet Schist. It ranges in thickness from 1-30 m with 10 m the average. Interpretations of diamond drill core data and surface exposures suggest this rock unit forms closely spaced, but discontinuous undulating bodies enveloped by graphitic pelite (Figure 3.2).

The Quartz Cemented Graphitic Pelite Breccia has been divided into three sub-units according to the relative abundance of quartz cement and graphitic pelite:

- i) greater than 80% quartz cement,
- ii) less than 80% and greater than 40% quartz cement,
- iii) less than 40%, and greater than 20% quartz cement.

i. Greater than 80% Quartz

PLATE EIGHT: QUARTZ CEMENTED GRAPHITIC PELITE BRECCIA

8a. Core box sequence of LCZ showing increasing quartz at upper contact with the Graphitic Pelite. (Core width 7cm).

8b. Core sample of LOZ. Light grey, cubic mineral in centre is arsenopyrite. Gold typically at quartz-Graphitic Pelite Margin. (Core width 7cm).

8c. Matrix of LOZ dominated by crenulated sericite. Locally plagioclase porphyroblasts overgrow the matrix. (xpl, Scale Bar = 0.125mm).

8d. Large ferroan dolomite poikilobasts with oligoclase inclusions and densely dusted by carbonaceous material. Sericite matrix with large biotite blades. Opaque to the right is pyrrhotite. (ppl, Scale Bar = 1mm).

8e. Overview of sulphide, chlorite, mica matrix. (xpl, Scale Bar = 1mm).

8f. Backscatter SEM image of sulphides, consisting of pyrrhotite, arsenopyrite and chalcopyrite.

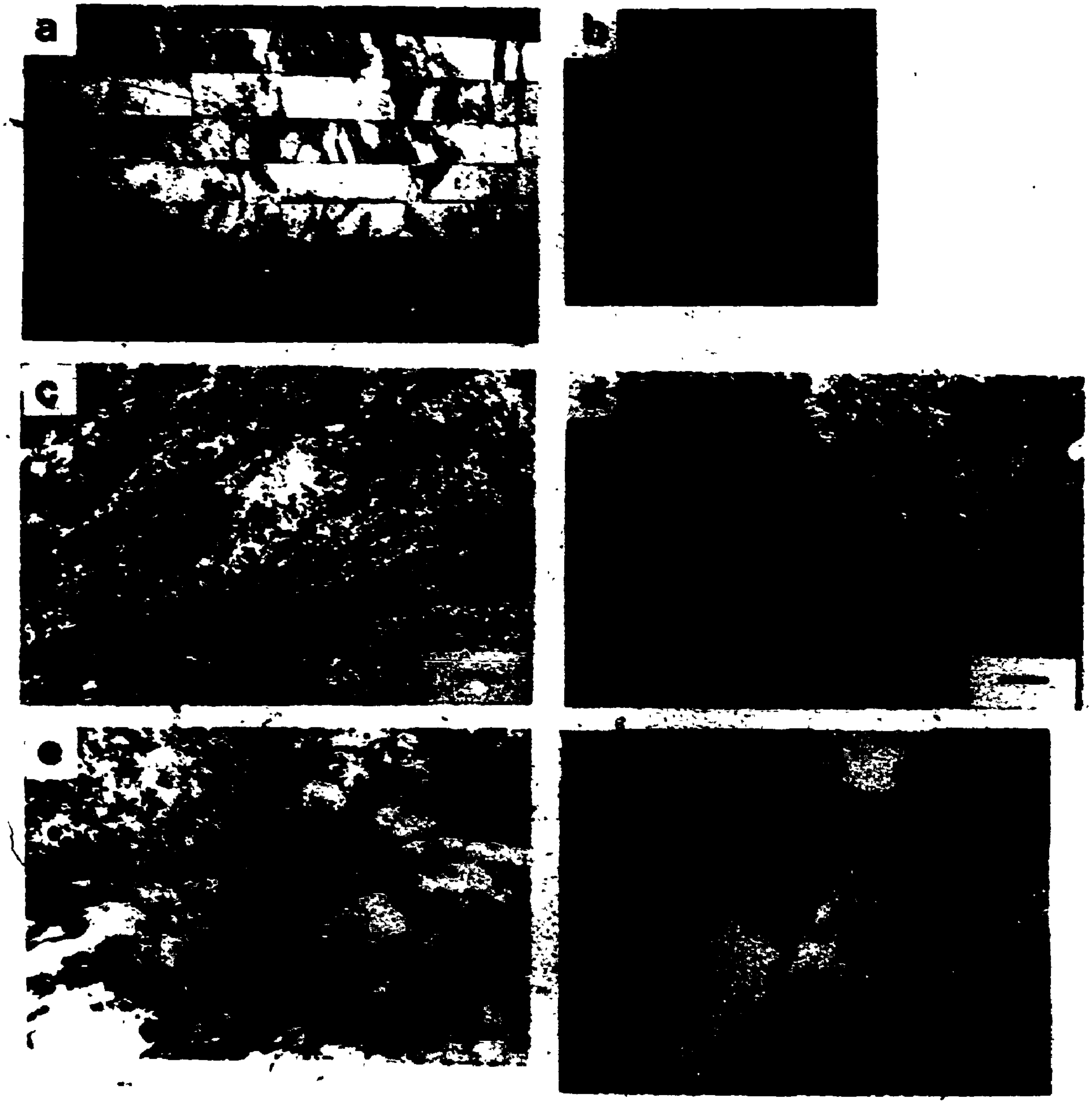
a
b
c

This rock type consists of quartz (80%), sericite (15%) with minor biotite, chlorite, ferroan dolomite and graphite. Quartz occurs as equant to elongated, saccharoidal textured grains (0.5–4 mm long). Wisps of sericite (0.1 mm long) with a dusting of carbonaceous material occur along linear zones where the quartz grains show significant grain size reduction. Minor brown biotite and green chlorite may form epitaxially to sericite. Ferroan dolomite occurs marginal to the sericite and in discontinuous patches (0.3 mm across) intergranular to the quartz. No significant gold concentrations are associated with this sub-unit.

ii. Less Than 80% and Greater Than 40% Quartz Cement

This rock (Plate 8a) consists of quartz (40–80%), sericite (10–50%), ferroan dolomite (2%) and minor pyrrhotite, arsenopyrite. Au concentrations in this unit are significant and represent the ore of the LOZ. Graphitic Pelite fragments consist dominantly of sericite which shows a distinct crenulation cleavage as seen in the Banded Chlorite-Sericite-Garnet Schist (Section 3.3.3.11, Plate 8c). The fragments are disrupted by quartz and ferroan dolomite veins. Pyrrhotite, arsenopyrite and Au occur within and at the margins of the Graphitic Pelite.

iii Less Than 40% and Greater Than 20% Quartz

This rock type is texturally complex and has a varied mineral assemblage. It consists of quartz (20–40%), sericite (20%), biotite (15%), graphite (5%), plagioclase (5%), ferroan dolomite (5%), calcite (5%) with minor arsenopyrite, chalcopyrite, pyrrhotite and anomalous Au. Sericite blades, 200 to 500 um long, again display a crenulation cleavage which is often obscured by graphite. Brown biotite porphyroblasts (1-1.5 mm long) overgrow the sericite blades and frequently contain carbonaceous inclusions which mimic the crenulation cleavage. Plagioclase porphyroblasts (0.3-0.5 mm across) overgrow the sericite in random patches and may replace ferroan dolomite eyes (Plate 8d). The ferroan dolomite, which overgrow the sericite matrix, occurs as rounded, 300 to 500 um in diameter, grains with abundant, very fine inclusions of graphite. This assemblage is disrupted by diffuse veins of quartz (1-2 mm wide), ferroan dolomite, calcite, arsenopyrite, pyrrhotite and chalcopyrite (Plate 8e). The sulphide grains (0.3-0.7 mm wide) are intergranular to quartz and calcite grains. Pyrrhotite is the dominant sulphide mineral but is always acompanied by chalcopyrite. Arsenopyrite occurs as euhedral grains (1-2 mm across), partially or completely rimmed by pyrrhotite (Plate 8f). Visible gold is associated with arsenopyrite and pyrrhotite in these veins but is not included in either phase, occurring at quartz grain boundaries. Although unrepresentative, one 8 cm long sample from this rock type contained 5% disseminated gold.

3.3.3.10 Chlorite-Plagioclase-Quartz-Ferroan Dolomite Schist

The Chlorite-Plagioclase-Quartz-Ferroan Dolomite Schist (CPQFD Schist) is a very distinctive rock type, but represents less than 1% of the subsurface rock volume. It appears to be restricted to the structural lower portions of the geologic profile and is i upper and lower contact to the Graphitic Pelite. It averages less than 1 m wide and is interpreted to be thin, tabular and discontinuous over lengths greater than 50 m.

In hand sample the rock is light grey-green, fine grained, with a homogeneous textured matrix often spotted by 10%, evenly distributed, round to ellipsoid, 1 to 2 mm in diameter, ferroan dolomite eyes. The upper and lower contact boundares are sharp, linear and often are marked by 5mm bleached, fine grained, grey zones.

In thin section the matrix of the CPQFD Schist consists of green chlorite (35%), plagioclase (20%), quartz (20%), biotite (5%), garnet (5%) and ilmenite(5%) and trace pyrrhotite and rutile. Ferroan dolomite poikiloblasts make up 15% of the rock. Chlorite occurs as elongate (200 um long) blades forming an open, anastomosing, foliated mat. Quartz and plagioclase form as interlocking, mosaic textured grains (0.7 mm in diameter) intergranluar to the anastomosing chlorite. Plagioclase also forms as laths with poorly developed albite twinning similar to that seen in the Foliated Amphibolite (Section 3.3.3.1). The laths include chlorite, ilmenite and rutile and show sugrained margins to the matrix. Pleochroic light to medium orange brown biotite occurs as isolated, 300 um long blades, parallel to, and locally cutting the foliation defining chlorite. Irregular, 500 um wide blebs of pyrrhotite are in contact with the biotite. Small, 50 um in diameter, subhedral garnet grains are evenly distributed throughout the rock. They show no particular affiliation with any other mineral. Ilmenite occurs as 100 um long, stubby laths, oriented subparallel to the chlorite.

Rounded to slightly ellipsoidal, 1 to 2 mm in diameter, ferroan dolomite poikiloblasts are evenly distributed throughout. Their grain boundaries are cuspate and irregular. Inclusions make up 20% of the poikiliblasts, giving the grain a "Swiss Cheese" or bubble appearance. The inclusions consist of quartz, ilmenite, chlorite and garnet.

The grey contact zones are composed of a fine grained mosaic textured matrix of quartz (50%) and plagioclase (25%). This is decorated by a bimodal size population of biotite(20%); coarser grained biotite, 0.5 to 1.5 mm long blades, forms a foliated mat which is cut by finer grained biotite (100 um long) blades. Pyrrhotite and trace tourmaline are associated with the coarser biotite. Fine grained (100 um long) ilmenite laths, locally altered to rutile, occur as a dusting throughout the matrix.

3.3.3.11 BANDED CHLORITE-SERICITE-GARNET SCHIST

The Banded Chlorite-Sericite-Garnet Schist (Banded CSG Schist) is a very distinctive and predictable unit occurring at the same structural position within the geologic profile throughout the study area (Figure 3.2). It is invariably in sharp upper contact with Graphitic Pelite or Quartz Cemented Graphitic Pelite Breccia (Lower Ore Zone). It occurs no more than 10 m from the Lower Ore Zone with the average distance approximately 5 m. It is in sharp lower contact with the Banded Quartz-Biotite-Chlorite-Plagioclase Schist. It makes up 15% of the rock volume and ranges in thickness from 4 m to 60 m with 30 m the average. It has a tremendous strike continuity and is interpreted as forming an extensive tabular sheet.

In hand specimen the rock is banded at one to five mm intervals, varying in colour from medium green-grey (50%) to dark grey-green with a distinct sheen (35%) and dark grey-black (15 %). The dark green-grey and medium green-grey bands are fairly regularly spaced at 3 mm

2

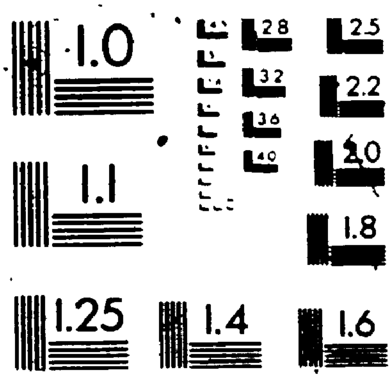

PLATE NINE: BANDED CHLORITE-SERICITE-GARNET SCHIST AND BANDED QUARTZ-BIOTITE-CHLORITE-PLAGIOCLASE SCHIST

9a. Core sample showing well developed colour banding and coarse garnet porphyroblasts. (Core width 7 cm).

9b. Complex inclusion pattern within garnet porphyroblasts. Sigmoidal pattern in core is not continuous to the helicitic rim. (ppl. Scale Bar = 1 mm).

9c. Contact of garnet (upper left) with sericite-chlorite matrix (lower right). Note the helicitic pattern of ilmenite into the garnet from the matrix. (ppl, Scale Bare = 125 um).

9d. Unusual texture now occupied by epidote, possibly pseudomorph of garnet (?). (ppl, Scale Bare = 0.30 mm).

9e. Core sample of Banded Quartz-Biotite-Chlorite-Plagioclase Schist. Bandingis very faint. (Core width = 7 cm).

9f. Overview of matrix showing two attitudes of ilmenite blebs- differing by 20°. (ppl, Scale Bar = 1 mm).


a
b
c

intervals but are not of equal width from band to band or along a single band, varying from 1-2 mm. The dark grey-black bands occur as zones with no particular periodicity. The contact boundaries of the bands also vary, locally appearing smooth and sharp or frayed and interleaved with the contacting band (Plate 9a). In addition, opposite contact boundaries may not show the same sharpness or form, from location to location.

Almandine garnets are characteristic of this unit (Plate 9a). They are pink, sub-idioblastic and vary in size from 1 mm to 2 cm. They tend to occur within, although are not restricted to, the medium green-grey sericite rich bands. Their abundance varies from 0-80%, averaging 30%. The garnets show a distinctive and consistent grain size variation and modal proportion variation with distance from the upper contact. At the upper contact and for 5 m downhole, the garnets may be up to 2 cm in diameter with the average 1 cm. They occur within 5 cm zones at 10 cm intervals and may make up to 80 modal % of the zone. Further downhole (5-20 m) the garnet size gradually decreases to 1 mm, the modal proportion is 5% and the frequency in occurrence is 20 cm intervals. At depths greater than 20 m below the upper contact garnets are not evident in handsample.

Another characteristic feature of this unit is that it is locally calcareous (5%) in the medium portions, 5-20 m below the upper contact. Light green calcite bands locally form 1 m zones alternating with chlorite-sericite bands. These bands parallel the rock schistosity.

The mineralogy of each band is fairly simple consisting of varying proportions of chlorite, sericite, quartz, biotite and garnet as the major minerals. Ilmenite and pyrrhotite are the minor minerals and calcite, plagioclase and chloritiod occur as rare minor minerals in the assemblage. The textural relationships and abundances of minerals vary downhole with distance from the upper contact. In view of this complexity the petrographic descriptions will be subdivided as to their relative depth and band type.

Upper Portion (0-5m below upper contact)

Medium Green-Grey Bands

The medium green-grey bands are dominantly composed of sericite (50-65%), chlorite (15-30%) and quartz (35%) with minor ilmenite (1%) and rare chloritoid and biotite. Colourless to pale green sericite blades are 30-100 um long and define a weakly anastomosing foliation. Locally sericite has distinct 300 um partings, which are bridged by "Z"-shaped sericite. Epitaxial to the sericite are pale green to colourless chlorite blades (30 um). An increase in the abundace of chlorite is at the expense of sericite. Quartz is the matrix to sericite and chlorite, occurring as elongate 1 to 3 grain wide (50-150 um), 5 grain long trails, parallel to the foliation. The quartz shows weak to moderate undulose extinction and the boundaries, for the most part are smooth and regular suggesting recrystallization.

Pale green poikiloblasts of chloritoid, ranging in length from 1-5 mm, are rarely noted and appear to overgrow mixed sericite and chlorite. They generally cross-cut the foliation and include quartz and ilmenite as helicitic trails. Coarse grained chlorite fibres frequently border chloritoid separating the chloritoid from the sericite in the matrix.

Ilmenite is ubiquitous to this band (1%) as 100 um long blebs evenly dispersed and paralleling the cleavage. Trace rutile is also noted with the ilmenite. Pyrrhotite occurs in much the same fashion as the ilmenite. A fine black carbonaceous dusting occurs throughout the band.

Biotite may occur with massive sericite as pleochroic dark orange brown to pale orange brown, 0.5-0.7 mm long porphyroblasts, cross-cutting the sericite defined foliation. Trace pyrrhotite is generaly in contact with the biotite.

Dark Grey Bands

The dark grey-green bands are texturally similar to the medium green-grey bands except that chlorite is the dominant silicate mineral phase. Most often it occurs as a massive chlorite mat with ilmenite blebs paralleling the foliation defined by the chlorite. Biotite porphyroblasts may occur oblique to the foliation but more commonly biotite occurs as coarser (0.5 mm long) grained blades paralleling the foliation. Rare plagioclase porphyroblasts clearly overgrow the chloritic matrix. This type of growth is very similar to that noted in the Chlorite-Magnetite Schist described in section 3.3.3.6.

Dark Grey-Black Bands

Dark grey-black bands are similar to the medium green-grey and dark grey-green bands with the addition of 5% black carbonaceous material believed to be poorly ordered graphite. The fine grained carbonaceous material occurs as linear concentrations along grain boundaries and as localized linear dustings along fine shears throughout the rock. The dusting may locally obscure the other minerals.

Almandine Garnets

Coarse grained (1.5-2.0 cm), colourless to pale pink garnet sub-idioblastic poikiloblasts may occur in all band types but appear to have preferentially nucleated in the more sericite-quartz rich bands. They occur in zones and their abundance ranges from 0-80% with 30% the average. Quartz rich pressure shadow zones are commonly developed.

Inclusions may represent up to 30% of the garnet and are commonly quartz (20%), ilmenite (5%), calcite (5%) and carbonaceous dusting. The inclusions form weakly developed "S" shaped trails through the garnet which generally can be traced into the matrix (Plate 9b, 9c). The fine carbonaceous dusting is also continuous with that noted in the matrix. Polysynthetically twinned chloritiod blades (1-2mm) may be included in garnet. The twin planes of the chloritoid parallel the helicitic fabric of the other inclusions, however, ilmenite inclusions are not oriented parallel the the matrix fabric. Minor sericite is often associated with the chloritoid but it is not clear if this is a separate inclusion type or if it is an alteration product of the chloritoid. Although not modally significant it should be noted that one grain of epidote/clinozoisite was noted as an inclusion within garnet.

The garnets have a well developed 10 um crack system developed perpendicular to the included banding. The cracks are frequently filled with quartz and calcite and more rarely show a faint chlorite green colour along their edge. These cracks may occupy up to 5% of the garnet and cannot be traced into the martrix.

The nature of the boundary of garnet is dependant on the contacting mineral. When in contact with quartz the garnet boundary is a fish-net texture with the quartz clearly being included in the garnet. Where in contact with chlorite or sericite the garnet boundaries are continuous and sharp with few inclusions. Chlorite and sericite blades bend around the edges of the garnet where oblique to foliation. Small (50-100um) plagioclase porphyroblasts occur at the margins of the garnet porphyroblasts, overgrowing the sericite and chlorite matrix. Pyrrhotite is a rare contacting mineral but its texture is noteworthy. It occurs as 1-5 mm blebs intergranular to quartz and brown biotite in a garnet pressure shadow and is clearly included in the garnet.

Medium Portion (5-20 m below upper contact)

The mineralogy of the medium portion of the Banded Chlorite-Sericite-Garnet Schist does not vary from the upper portion except for the presence of epidote(5%) and calcite (5%). The bands of this zone show moderately to strongly developed crenulation cleavage which is asymmetric and incoherent. Linear zones of similarly oriented blades of sericite (0.7-1.0 mm) are abruptly terminated by slightly differently oriented zones, giving an impression of crenulation cleavage along the boundary. In addition, areas rich in sericite may show distinct kinking but with no clear cleavage development (Plates 9b, 9c). In bands with sericite and quartz the crenulation cleavage is more coherent but not traceable over millimetres. "Z" shaped drag folds defined by sericite are developed between cleavage planes (Plate 9b, 9c)).

Epidote/clinozoisite is evenly distributed throughout the rock, occurring as 300-500 um grains which often appear to pseudomorph the crenulation kinks described above. Calcite occurs as fairly coarse (200-500 um wide) grains, forming a one to two grain wide band. The bands are in sharp contact with the boundary bands, and are clearly folded by the crenulation cleavage.

The garnets of the medium portion are poikiloblastic and subidioblastic with spectacular spiral inclusion and mimic textures (Plate 9b, 9c). They range in size from 0.3 to 2.0 mm with 0.5 mm the average size. Quartz, carbonaceous material and ilmenite are the dominant inclusions of garnet with calcite and epidote more rare. One tourmaline grain was noted as an inclusion in garnet. The spiral inclusion textures are developed in garnet cores and best displayed by carbonaceous inclusion trails. The garnet rim inclusions mimic the textures of the bounding matrix crenulation cleavage. (Plate 9c).

The garnets also show a regularly spaced (200-300 mu), consistently oriented 10 um crack set oriented perpendicular to the crenulation cleavage of the rock as noted in the upper portion of Plate 9b). Fine calcite is most often developed along the cracks.

Plate 9d illustrates an unusual texture noted in only one rock. It is 5 mm long, 2 mm wide and looks like three interlocking diamond shaped minerals. It clearly mimics the matrix fabric and is composed of coarse chlorite at the rim and epidote in the core. Its origin remains unclear.

Of particular interest, although not significant in volume (<1%), is the occurrence of Au mineralized sections. Anomalous Au is associated with one metre zones of 1-5 cm wide quartz veins. The veins have 2-4 cm, symmetric haloes of 1%, 1 mm long diamond shaped arsenopyrite grains with pyrrhotite.

Lower Portion (greater than 20 m below upper contact)

The lower portion of the Banded Chlorite-Sericite-Garnet Schist differs from the upper or medium portions in its lack of well defined banding, the rarity of garnets and the increased abundance of epidote porphyroblasts (10%). Quartz (50%) occurs as elongate (300 um long) slightly elipsoid grains intergranular to chlorite (30%) and sericite (20%) defining a continuous, slightly anastomosing foliation. Pleochroic red brown to colourless biotite is rarely noted (<5%) occurring as epitaxial blades parallel to chlorite and sericite. A rare garnet (200 um in diameter) is noted showing a fish-net texture with the matrix quartz. It is locally replaced by chlorite, epidote and calcite. Epidote appears as 0.5 mm wide, ellipsoid poikiloblasts with inclusions of quartz.

3.3.3.12. Banded Quartz-Biotite-Chlorite-Plagioclase Schist

The Banded Quartz-Biotite-Chlorite-Plagioclase Schist (Banded QBCP Schist) does not outcrop within the area of Minas III and is encountered only in drill core. It is a ubiquitous unit, occurring at the same structural position in the geologic profile (Figure 3.2). It represents 5% of the subsurface rock volume but it should be realised that the Banded QBCP Schist marks the "foot of hole" lithology, meaning, that after a maximum of 10m of penetration, drilling was terminated. The true thickness of this unit and nature of the lower contact is unknown. The upper contact is sharp and parallel to the foliation of the Banded Chlorite-Sericite-Garnet Schist.

In hand sample the Banded QBCP Schist is fine grained, colour banded, mid and dark grey-green, with a well developed phylonitic cleavage. The mid grey-green bands make up 80% of the unit and range in thickness from 0.5 to 4 cm and alternate with darker grey-green bands which make up the remaining 10-20% of the rock (Plate 9e). The banding is continuous over centimeters but is often abruptly terminated or laterally displaced by a foliation plane. In several instances this displacement isolates 1-5mm length bands of the dark grey band giving an impression of fragmentation. Close examination of the band contacts in hand sample reveals that they have a sawtooth form (Plate 9e) with each cleavage plane showing minor displacement.

The Banded QBCP Schist consists of dominantly quartz(50%), biotite(40%), chlorite(5%), plagioclase(5%) with tourmaline, epidote, ilmenite, pyrrhotite and graphite as minor minerals and apatite, calcite, garnet and zircon as trace minerals. The banding is a function of mineral grain size, modal proportions and variable textural relationships; therefore, the petrographic descriptions will be divided into the two band types.

Throughout this rock type there is apparent graded bedding in hand sample (Plate 9e). In all cases the grading fines down-hole. This texture is problematical and will be discussed below.

MID GREY-GREEN BANDS

The mid grey green bands are composed of quartz intergranular to anastomosing biotite. The quartz forms 0.5-0.7 mm composite, elipsoid eyes (aspect ratio 3:1) with asymmetric tails and show well developed undulose extinction and subgrains. Locally the quartz may form one grain wide and 3 grain long patches which parallel the rock foliation. More rarely (10%) quartz occurs as coarser grained (0.5-1.0 mm wide), discontinuous, vein-like lenses, oblique to the foliation, interpreted as dismembered veins.

Biotite most commonly (30%) occurs as discontinuous, 100-200 um long blades, defining the dominant foliation. The continuity of the foliation is a function of the degree of flattening. Where the quartz forms elipsoid eyes the foliation is discontinuous, whereas where the quartz occurs as elongate patches, the foliation is continuous and well defined. The degree of flattening is variable even within a single band, occuring in zones which die out over centimetres. Biotite(5%) also occurs as 200-500 um long porphyroblasts in those rocks where the quartz forms 500-700 um elipsoid eyes. Sigmoidal graphitic trails are included in the cores, paralleling the (001) cleavage which is perpendicular to the foliation direction. In the more flattened rocks, porhyroblasts do not occur. Biotite(5%) occurs at the margins of the coarse grained quartz lenses, interpreted to be veins as coarse grained 0.7-1.2 mm long blades lined up parallel to the vein margin or partially included within the vein quartz. Zircons are frequently included in this type of biotite.

Chlorite is relatively uncommon, occuring as very ight green, 100-200 um long blades epitaxial to biotite. It does not appear to overgrow or be overgrown by the matrix biotite. It also occurs as elongate 0.5 mm long blades paralleling the coarse grained quartz.

Tourmaline is equally distributed throughout the band. The grains are idioblastic, 50-100 um in diameter and colour zoned from blue cores to green rims.

Ilmenite occurs as rounded, 70 um in diameter, composite blebs, elongate parallel to the foliation. The blebs may partially include both quartz and biotite, with the grain bounary taking on the shape of the included mineral.

Plagioclase porphyroblasts are identifed in the less flattened portions. They are associated with the coarse grained quartz and are equigranular with good asymmetric quartz pressure shadow tails. Albite twinning rarely occurs. Myrmekite has been noted in the cores and the rims of a few porphryoblasts. In the more flattened portions of this band type it is not clear what protion of the quartz matrix is in fact feldspar due to the complete lack of distinguishing features from quartz. It is therefore assumed that the same abundace of plagioclase does exist in the band but cannot be optically distinguished from quartz.

Clinozoisite is noted to occur most often as xenoblastic, rounded, 100 um in diameter grains in quartz and in contact with biotite and feldspar. No obvious preferred association could be noted.

Pyrrhotite occurs as 0.5-1.0 mm blebs at the grain boundaries of the coarse grained quartz of the deformed quartz veins. Often associated with the pyrrhotite are sub-idioblastic to anhedral, 30-300 um grains of garnet. Trace clinozoisite is evident along cracks in the garnet.

Apatite euhra as well as calcite are the rarest minerals. Apatite is evenly distributed while carbonate is noted only at the margins of the coarse grained quartz veins.

DARK GREY BANDS

The dark grey bands consist dominantly of fine grained 30-50 um in diameter quartz grains which are intergranular to pleochroic mid brown to colourless, 10 to 50 um long biotite blades. Biotite defines a tightly spaced (150-200 um), weakly anastomosing, discontinuous, asymmetric crenulation or strain-slip cleavage. Neoblasts of biotite (5%), are oblique to and overgrow the crenulation cleavage plane. They may form asymmetric tails and contain cores with linear trails of a graphitic dustings, Inter-cleavage biotite (10%) is fine grained (30 um long) and occurs as 2-5 blade bundles and define the angular or curved herring bone texture cleavage.

Colour zoned, blue core to olive green rim, sub to euhedral tourmaline grains are equally distributed throughout the band. They appear not to be directly associated with any one mineral species and contact bondaries are sharp.

A fine grained, graphitic dusting occurs throughout the band. It is most dense along the crenulation cleavage, as well as at the boundary of the band. In several instances, more graphite is associated with one bounary of the band fading out toward the other boundary. It is this gradational change which may account for the apparent graded bedding seen in hand sample and noted above.

Calcite occurs as 0.5mm patches apparently overgrowing and including the matrix.

Locally two foliations are developed-- one defined by the closely spaced penetrative cleavage of fine grained matrix biotite and the second is a non-prenetrative and zonal crenulation cleavage that is most evident through the allignment of ilmenite trails and a weak to moderate re-orientation of biotite flakes apparent in crossed nicols (Plate 9f). The penetrative cleavage locally exhibits small asymmetric "Z" kinks which have an axial planar cleavage parallel to the non-penetrative cleavage. The boundaries of this type of textural band are parallel to the penetrative cleavage.

Table 3.1. Summary of mineral assemblages of Minas III rock types.

Mineral	qt	pl	mh	th	ep	cl	fd	ch	se	bt	gt	ct	gn	tr	gr	il	mt	rt	po	cp	as	Au
Regional Amphibolite		X	X		X	X					X					X	X		X	X		
Foliated Amphibolite		X		X		X		X		X						X			X	X		
FDCBQ Schist	X					X	X	X	X	X						X			X	X	+	+
v FDCSBQ Schist	X	X					X	X	X	X						X			X	X	+	<
Massive FD							X	X	X	X				X		X		X	X	X	+	<
Ser-Chl Schist		X					X	X	X	X	X	X		X		X			X	X	X	>
Chl-Mag Schist		X					X	X	X	X	X	X	X	X	+	X	X		X	X	X	>
Silicified Dolomite	X	+					X	+	X	+				+	X	+		+	+			
Graphitic Pelite	X	+				+	X	X	X	X	X			+	X	X			X	X	+	<
LOZ	X	X				X	X	X	X	X					X	X			X	X	X	>
CRQFD Schist	X	X					X	X	X	X	X			X		X		+	+			
Banded Chl-Ser-Gnt Schist	X	X			X	X	X	X	X	X	X	X		X	X	X			X	X	X	<
Banded QBCP Schist	X	X			X	X	X	X	X	X				X	X	X			X	X		

qt=quartz;pl=plagioclase;mh=magnesio hornblend;th=tsermakitic hornblend;
ep=epidote;cl=calcite;fd=ferroan dolomite;ch=chlorite;se=sericite;bt=biotite;
bt=biotite;gt=garnet;ct=chloritoid;gn=grunerite;tr=tourmaline;gr=graphite;
il=ilmenite;mt magnetite;rt=rutile;po=pyrrhotite;cp=chalcopyrite;
as=arsenopyrite;Au=gold.
X=>1 modal %;+=trace,<1 modal %
>= >2 g Au/tonne;<=< 2 g Au/tonne

CHAPTER FOUR

Rock Geochemistry

4.1. Introduction

The rock geochemistry of the twelve rock types distinguished in Chapter 3, are presented in this chapter. The data is used to confirm the valididy of the petrographic distinctions of Chapter 3 and to establish the relative relationships of the units to one another.

A total of 120 samples representative of the twelve rock units were analysed for major, minor and trace elements. The raw analysis and details of the analytical procedures are presented and discussed in Appendix III. The averages of the major and minor oxides and trace elements, with one standard deviation (1o) are presented in Table 4.1. The data used for the plots presented below are recalculated on a LOI and CO_2 free basis unless otherwise stated.

The coefficient of variation (V) is also presented in Table 4.1. It equals one standard dev -ion (1o) divided by the mean (x), multiplied by 100. This value allows for the discussion of the relative variation within and between the oxide and elemental groups.

4.2 Rock Types

4.2.1 Foliated Amphibolite

Examination of the co-effiecint of variation for the major oxide values of the Foliated Amphibolite (Table 4.1) indicates that the chemistry is relatively uniform. SiO_2 shows the smallest variation at 7% with TiO_2, Al_2O_3; FeO (Fe_2O_3 converted to FeO), MnO, MgO, K_2O, and P_2O_5 varying from 19 to 25%. CaO and Na_2O has the next to largest variation at 40 and 41% repectively. K_2O has the largest variation at

TABLE 4.1. Average Values of Whole Rock Analysis

	Foliated Amphibolite (n=4)			FDCBQ Schist (n=6)			Veined FDCSB Schist (n=7)		
	$\bar{x}$	1σ	v	$\bar{x}$	1σ	v	$\bar{x}$	1σ	v
SiO_2	48.65	3.78	7	37.23	7.30	20	41.39	5.20	13
TiO_2	1.32	0.32	24	0.80	0.26	32	0.94	0.25	27
Al_2O_3	13.26	2.60	21	9.14	3.32	36	12.40	3.43	28
FeO	14.03	2.66	19	11.54	4.94	43	10.06	2.64	26
MnO	0.21	0.05	23	00.25	0.16	65	0.16	0.05	31
MgO	6.49	1.63	25	7.13	4.51	63	7.34	1.50	20
CaO	8.46	3.36	40	13.44	9.16	68	10.58	4.50	33
Na_2O	2.31	0.93	41	1.36	1.34	99	1.48	1.30	88
K_2O	0.04	0.09	183	0.69	0.58	84	1.54	0.77	50
P_2O_5	0.12	0.03	23	0.24	0.31	129	0.09	0.05	61
LOI/CO_2	5.00	5.57	111	15.61	5.05	32	14.99	5.03	34
Nb	10.60	9.27	87	30.43	41.21	135	17.71	9.26	52
Zr	88.60	15.59	18	78.84	49.90	63	67.96	15.62	23
Y	19.95	9.34	47	33.54	40.13	119	17.34	7.98	46
Sr	140.52	86.55	61	137.77	53.07	39	146.02	28.10	19
Rb	26.43	12.85	200	32.64	23.97	73	47.70	20.09	42
As	19.75	8.34	42	461.54	718.39	155	395.91	405.44	102
Zn	103.05	11.43	11	123.24	119.02	97	86.47	57.11	66
Cu	28.78	10.02	35	21.40	11.66	54	27.07	21.84	81
Ni	29.68	13.47	45	28.13	17.08	61	22.14	11.67	53
Cr	62.15	16.03	10	75.21	25.17	33	64.24	24.96	39
Ba	37.10	19.98	54	463.11	503.80	108	719.14	495.05	69
V	221.18	63.46	29	160.28	105.40	66	148.06	44.02	30
S	318.55	326.76	103	421.69	684.07	162	462.03	523.19	113

	Massive Ferroan Dolomite (n=8)			Sericite-Chlorite Schist (n=9)			Chlorite-Magnetite Schist (n=7)		
	$\bar{x}$	1σ	v	$\bar{x}$	1σ	v	$\bar{x}$	1σ	v
SiO_2	20.16	6.04	30	41.10	7.56	18	31.92	11.76	37
TiO_2	0.35	0.15	44	1.64	0.59	36	1.80	1.03	57
Al_2O_3	5.45	3.00	55	20.60	7.99	39	12.78	5.63	44
FeO	14.74	13.73	93	15.07	6.40	42	37.53	14.80	39
MnO	0.34	0.14	42	0.09	0.06	63	0.17	0.08	49
MgO	10.49	4.00	38	6.47	3.70	57	4.90	2.73	55
CaO	19.84	3.37	17	3.50	4.15	118	3.89	3.98	102
Na_2O	0.29	0.33	117	0.42	0.41	98	0.54	0.96	176
K_2O	0.71	0.87	122	3.25	2.36	73	1.04	1.05	101
P_2O_5	0.15	0.78	52	0.09	0.04	49	0.25	0.21	83
LOI/CO_2	30.73	4.73	15	8.85	4.82	54	4.12	2.59	63
Nb	14.91	22.24	149	14.30	8.76	61	7.90	7.39	93
Zr	37.04	18.35	50	96.21	39.84	41	44.30	34.40	78
Y	15.24	12.61	83	-29.26	41.44	142	12.53	10.56	83
Sr	37.83	68.01	50	60.66	50.37	83	30.56	43.63	143
Rb	28.96	24.05	83	72.47	53.08	73	25.98	26.03	100
As	811.56	1747.19	215	25.78	852.09	136	5821.90	7965.70	136
Zn	72.36	57.70	80	143.69	57.15	40	205.54	154.52	26
Cu	12.55	4.61	37	15.29	8.40	55	130.70	127.67	98
Ni	10.66	5.80	54	35.36	18.53	52	33.06	18.84	57
Rb	47.01	24.71	53	105.87	39.59	37	134.33	67.23	50
Ba	471.46	650.30	137	2654.02	1985.63	75	372.37	369.81	99
V	110.91	72.99	66	309.17	147.23	48	457.07	246.16	54
S	125.65	176.08	140	317.80	443.70	139	4218.31	3106.17	74

TABLE 4.1. continued

x	Sil Dol 7 (n=19) 1σ	v	x	Graph Pelite 8 (n=12) 1σ	v	x	LOZ 9 (n=3) 1σ	v
SiO_2	23.76	18.13	72	55.35	10.59	19	45.89	4.12	9
TiO_2	0.07	0.06	77	0.67	0.20	31	1.31	0.52	39
Al_2O_3	1.18	0.79	67	13.58	4.24	31	21.05	6.39	30
FeO	2.89	1.67	58	6.97	1.88	26	14.92	6.77	45
MnO	0.25	0.15	58	0.17	0.09	56	0.17	0.04	20
MgO	14.03	3.79	27	4.40	3.34	77	3.62	1.87	52
CaO	22.40	5.31	23	5.03	5.38	107	4.559	1.54	134
Na_2O	0.04	0.04	120	1.33	0.72	54	0.59	0.48	82
K_2O	0.30	0.25	183	2.40	0.81	34	3.81	2.34	61
P_2O_5	0.81	0.86	106	0.18	0.08	42	0.08	0.09	100
LOI/CO_2	33.03	8.18	25	9.00	7.80	87	6.99	1.53	22
Nb	14.85	11.57	78	15.30	5.11	33	33.40	43.35	129
Zr	26.94	10.98	41	127.62	41.64	32	131.53	75.26	57
Y	15.07	18.76	124	25.30	13.70	154	43.47	62.35	143
Sr	141.90	50.10	35	127.50	52.77	42	118.03	72.63	162
Rb	34.99	46.13	1	74.26	24.31	34	98.80	67.36	68
As	122.94	286.18	232	257.96	533.07	206	15787.40	26835.16	170
Zn	32.26	13.70	42	101.88	58.67	58	143.20	53.56	37
Cu	14.56	23.77	163	20.15	7.10	35	151.60	38.63	75
Ni	8.19	8.24	101	17.65	8.25	47	19.27	2.71	14
Rb	27.89	18.76	76	54.84	18.14	33	118.87	60.11	51
Ba	244.70	185.01	76	1201.08	1646.41	54	1741.98	637.49	21
V	21.29	13.22	57	380.94	31.20	39	175.23	50.20	29
S	54.42	150.26	92	1241.82	981.29	80	3195.77	3411.81	106

	CPQFD Schist 10 (n=2)			Banded C-S-G Schist 11 (n=3)			Banded QBCP Schist 12 (n=3)		
	x	1σ	v	x	1σ	v	x	1σ	v
SiO_2	47.83	0.62	13	56.19	6.85	[illegible]	55.16	8.04	10
TiO_2	2.42	0.23	9	1.18	0.32	27	0.83	0.30	36
Al_2O_3	15.77	0.03	1	16.76	1.77	11	16.01	2.17	14
FeO	0.27	0.59	1	13.42	5.80	43	9.34	2.64	28
MnO	6.27	0.04	1	0.12	0.05	44	0.15	0.13	89
MgO	9.123	0.04	1	3.26	0.99	31	4.93	2.13	43
CaO	1.53	0.11	1	1.37	0.54	139	3.47	3.09	89
Na_2O	0.26	0.45	29	0.02	0.78	86	1.32	0.97	73
K_2O	0.40	0.20	76	2.49	0.42	17	2.90	1.03	35
P_2O_5	0.81	0.04	10	0.11	0.05	142	0.13	0.05	39
LOI/CO_2	8.74	0.40	1	3.38	1.19	35	3.57	1.18	33
Nb	72.10	37.62	52	36.80	37.90	103	36.23	34.93	96
Zr	191.94	42.64	22	132.13	135.30	102	171.80	101.79	59
Y	43.45	18.17	42	67.07	50.06	106	40.87	39.25	196
Sr	321.25	61.88	19	140.80	173.95	124	136.20	137.64	88
Rb	95.55	53.65	56	94.15	62.61	66	85.87	58.12	68
As	98.15	2.62	20	54.58	39.01	72	47.77	35.08	73
Zn	188.85	0.35	1	159.93	64.84	41	177.93	96.61	54
Cu	16.10	3.68	22	24.30	20.03	82	14.03	3.58	26
Ni	46.90	7.21	15	30.17	13.83	46	25.37	7.16	28
Rb	73.55	5.16	7	108.98	27.45	25	117.73	20.68	17
Ba	78.25	109.12	139	767.38	202.90	26	897.97	25.97	28
V	90.15	24.96	27	214.30	146.93	69	137.27	113.55	82
S	569.75	541.29	5	636.83	741.32	116	278.33	376.87	135

183% but given the low mean value of 0.048 the variation is considered insignificant. The same tight clustering of elements occurs with the trace elements. The coefficient of variation for Zr, Zn, Cu, Cr and V ranges from 11 to 35%; Y, As, Ni, Ba and Sr range from 42 to 61%. Nb and S have the largest coefficients of variation at 87 and 103% respectively.

The geochemistry of the Foliated Amphibolite compares well with the average tholeiitic basalt presented by Hyndman (1985,pg 205;Table 4.2,#6). The FeO value of the Foliated Amphibolite is at the high end of the range for Hyndman's tholeiitic basalt, whereas the P_2O_5 value is at the low end of the range.

Figure 4.1 is a typical alkali-silica variation diagram and illustrates the tholeiitic affiliation of the Foliated Amphibolite as well as the variability in the abundances of alkali oxides. Plotted on a Pierce and Cann (1973) diagram the samples fall into the fields of ocean floor basalts and within plate basalts (Figure 4.2). On a Ti versus Zr plot the samples all fall within the ocean floor basalt field (Figure 4.3).

In this study no analyses were completed of the regional mafic rocks ; however, de Saboia (1981) and Kuyumjian(1981) provide analyses of regional mafic rocks as well as ultramafic rocks for comparison. In Figures 4.1 and 4.2 the regional mafic rocks plot within the tholeiite basalt field and the low potassium tholeiite field, respectively. Figure 4.4 is adapted from Viljeon et al. (1982) and empirically illustrates the divisions between the various mafic and ultramafic fields. The Minas III Foliated Amphibolite plots

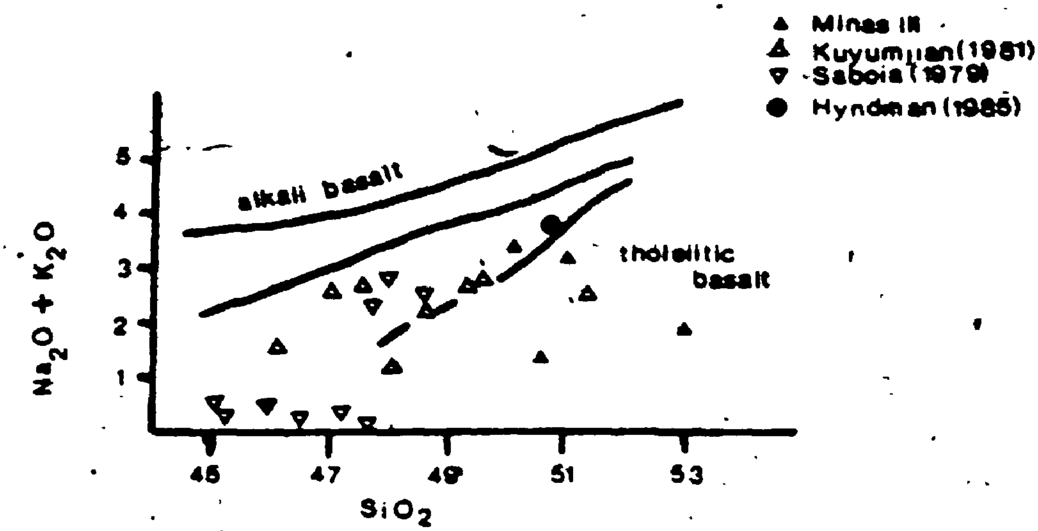

Figure 4.1. $Na_2O + K_2O$ versus SiO_2 of Regional and Minas III mafic rock types.

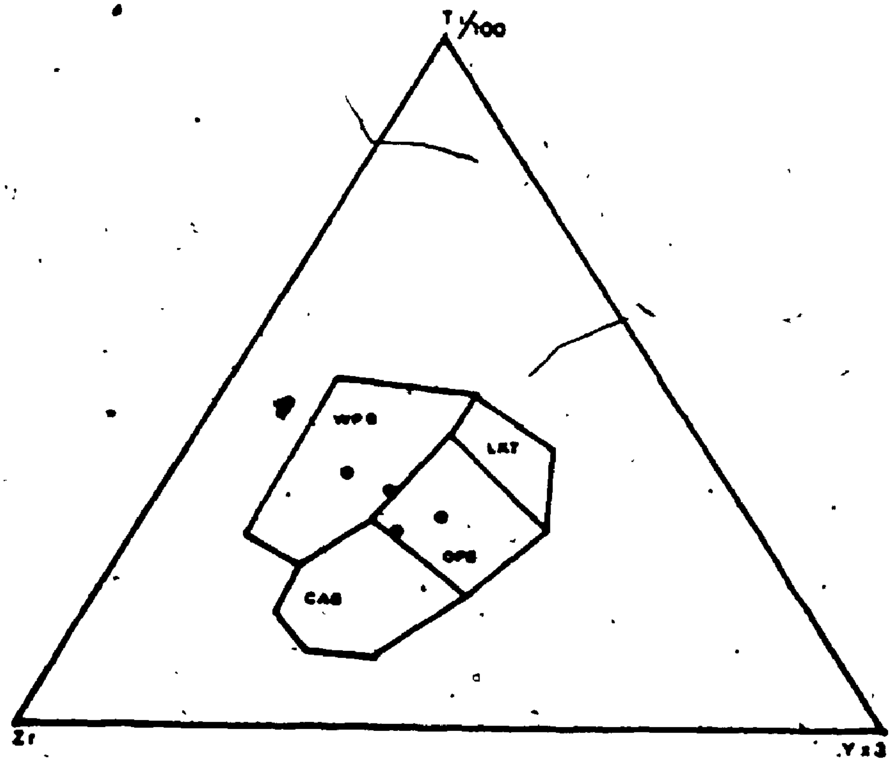

Figure 4.2. Ternary Ti/100:Zr:Yx2 of Foliated Amphibolite Samples. WPB = Within Plate Basalt; LKT = Low Potassium Tholeiite; OFB = Ocean Floor Basalt; CAB = Continental Alkaline Basalt. (after Pearce and Cann, 1973)

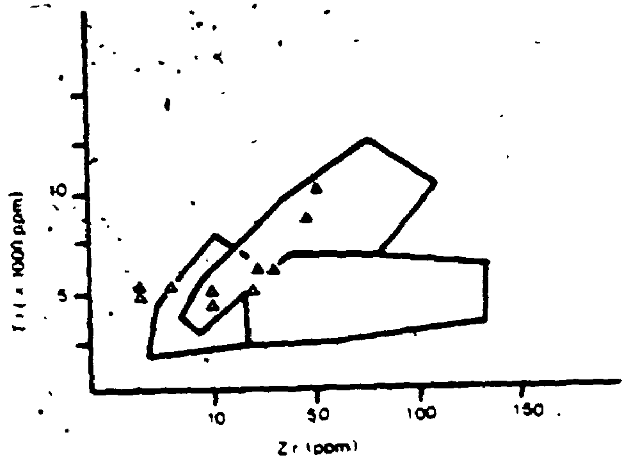

Figure 4.3. Ti versus Zr of Minas III Foliated Amphibolite and Regional Amphibolite. Boundaries after Pearce and Cann, 1973. Symbols as in Figure 4.1.

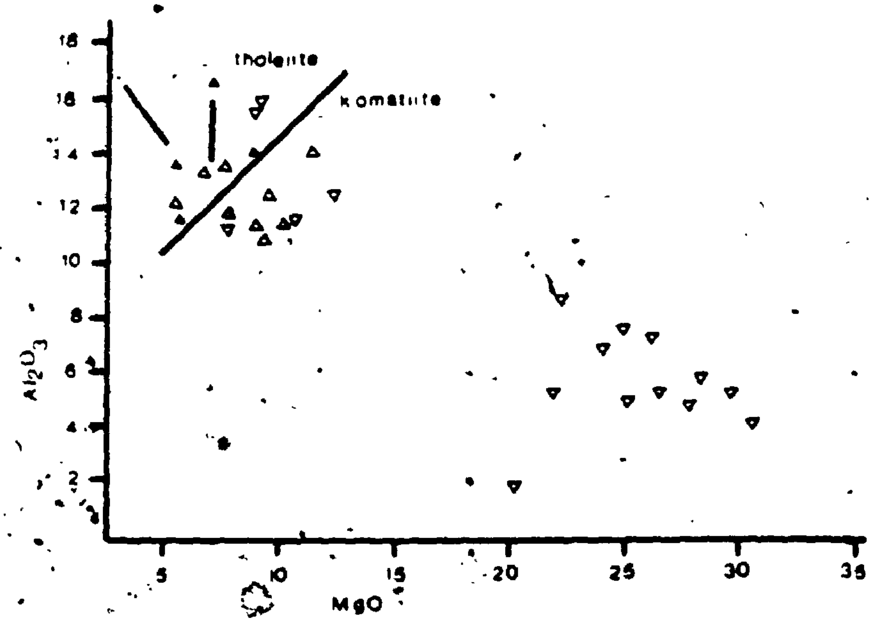

Figure 4.4. Al_2O_3 versus MgO for Regional and Minas III mafic rock types. (after Viljeon et. al., 1982). Symbols as in Figure 4.1

within the tholeiite field. The regional mafic rocks show moderate variability, plotting within both the tholeiite and komatiite fields, although, the komatiitic basalts are distinct from the high MgO, true komatiite rock analysis provided by de Saboia (1981). Figure 4.5, of $TiO_2:P_2O_5$, shows a consistent 10:1 ratio for the Minas III and regional rock.

4.2.1.1 Discussion

The geochemistry of the Foliated Amphibolite of Minas III and the regional mafic rocks is comparable to typical tholeiitic basalts, suggesting that, although metamorphosed (Section 6.2) the primary chemistry is not significantly altered. The minor shifts in alkali elements is consistent with spillitization (Fyfe et al., 1978).

4.2.2 Ferroan Dolomite Chlorite Biotite Quartz Schist

The Ferroan Dolomite-Chlorite-Biotite-Quartz Schist shows moderate variation in its major element chemistry. The co-efficient of variation for SiO_2, TiO_2, Al_2O_3, FeO and CO_2 ranges from 20 to 43%; MnO, CaO, MgO, K_2O and Na_2O varies from 63 to 99%. The large variation in P_2O_5 is due to anomalous values in samples 159-36 and 156-2 respectively. If eliminated the average of P_2O_5 is 0.10% +/_ 0.03 (1σ) with a co-efficient of variation of 30%.

The variability in the trace element abundances is similar to that of the major oxides: those elements which have a narrow range and those elements which have a wide range. The first group includes Zr, Y, Rb, Sr, Zn, Cu, Ni, Cr, and V which have coefficents of variation ranging from 33 to 97%. The second group includes Nb, Y, As, Ba, and S with a coefficient of variation ranging from 108 to

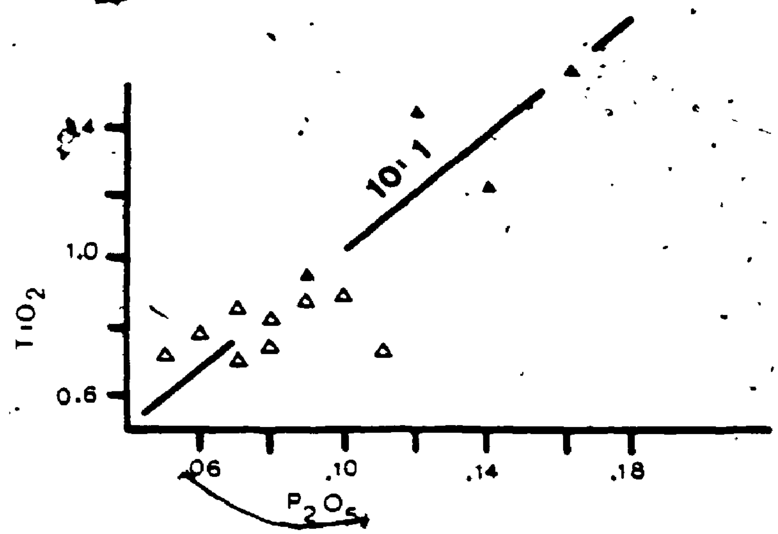

Figure 4.5. TiO_2 versus P_2O_5 for mafic rock types after Floydd and Winchester (1977). Symbols as in Figure 4.1.

162%.

In a series of plots (Figures 4.6 to 4.13) of TiO_2 versus various oxides, a range of TiO_2 values are evident. Higher TiO_2 values cluster closer to the Foliated Amphibolite samples and lower TiO_2 values cluster close to the Massive Ferroan Dolomite samples. In comparison to the Foliated Amphibolite, the first group shows a relative increase in K_2O, CO_2, MgO (Figures 4.6a,7,8a), As, Ba, S (Table 4.1) and a decrease in FeO (Figure 9a) and Al_2O_3 (Table 4.1). The second group shows a relative increase in CO_2 (Figure 4.7) and a decrease in V (Figure 4.10a), K_2O (Figure 4.6a) and Na_2O (Figure 4.11a) relative to the higher TiO_2 group. Figure 4.12 is a plot of TiO_2 versus P_2O_5. The higher TiO_2 values plot close to the 10:1 ratio of the Foliated Amphibolite illustrated in Figure 4.5, whereas the lower TiO_2 values define an approximate ratio of 5:1. In the ternary plot of Ti:Y:Zr (Figure 13a) the FDCBQ Schist samples plot with a similar Ti:Zr ratio as the Foliated Amphibolite with the Y values varying.

4.2.2.1 Discussion

The evidence presented above strongly suggests that the FDCBQ Schist is geochemically affiliated with the Foliated Amphibolite. The consistent Ti:Zr ratio of the FDCBQ Schist and the Foliated Amphibolite supports the generally held believe that it is immobile under most geologic conditions (Pierce and Cann, 1973). Although the significance of the consistent TiO_2:P_2O_5 ratio of 10:1 is unclear, it is considered to be significant. The apparent decrease in TiO_2 and apparent gains in CO_2 associated with decreases in K_2O, FeO and Na_2O

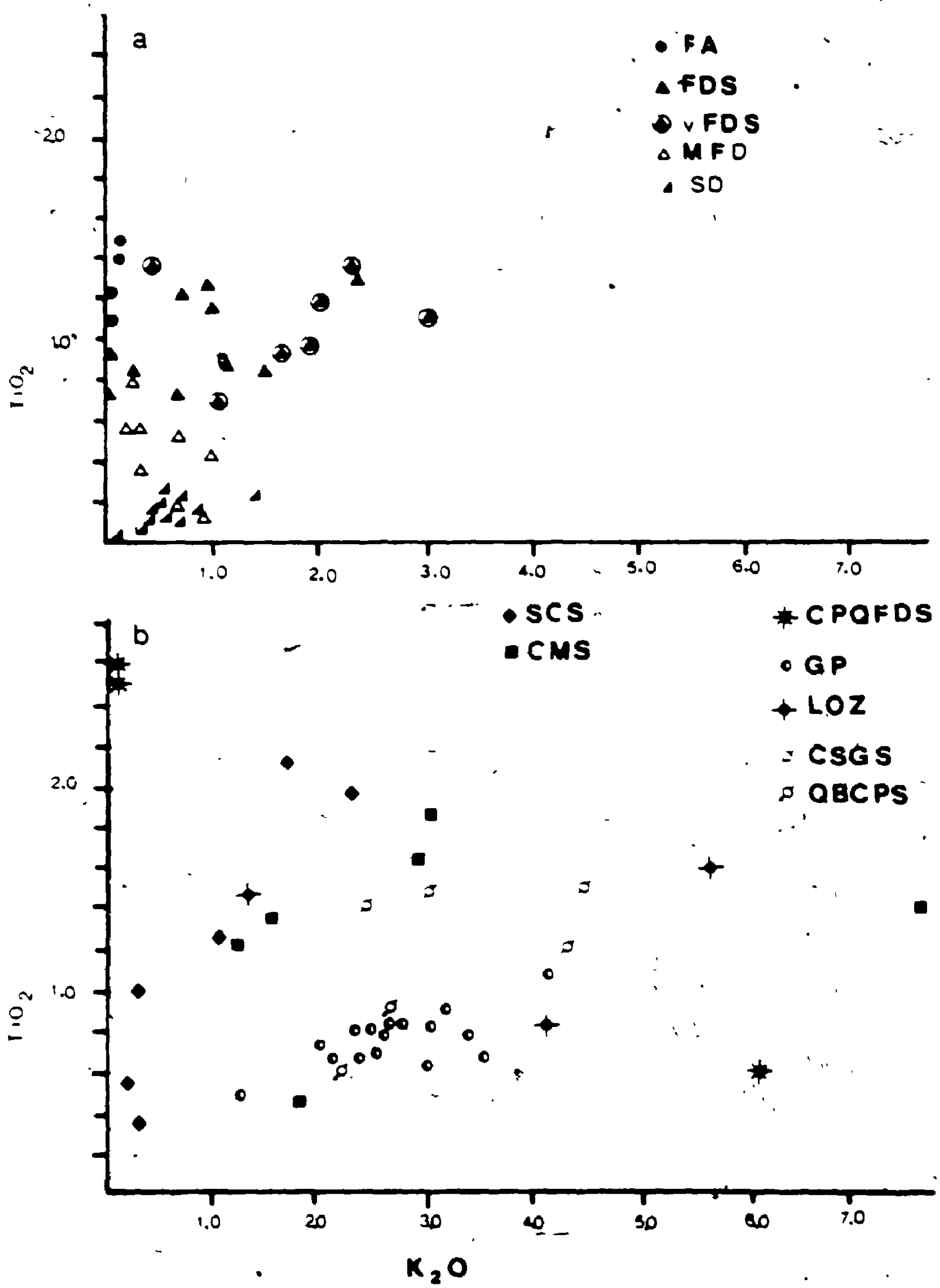

Figure 4.6 a & b. TiO_2 versus K_2O of rock types of Minas III. FA=Foliated Amphibolite; FDS=Ferroan Dolomite Schist; vFDS=veined Ferroan Dolomite Schist; MFD=Massive Ferroan Dolomite; SD=Silicified Dolomite; SCS=Sericite-Chlorite Schist; CMS=Chlorite-Magnetite Schist; CPQFDS=Chlorite-Plagioclase-Quartz-Ferroan Dolomite Schist; GP=Graphitic Pelite; LOZ=Lower Ore Zone; CSGS=Chlorite-Sericite-Garnet Schist; QBCPS=Quartz-Biotite-Chlorite-Plagioclase Schist.

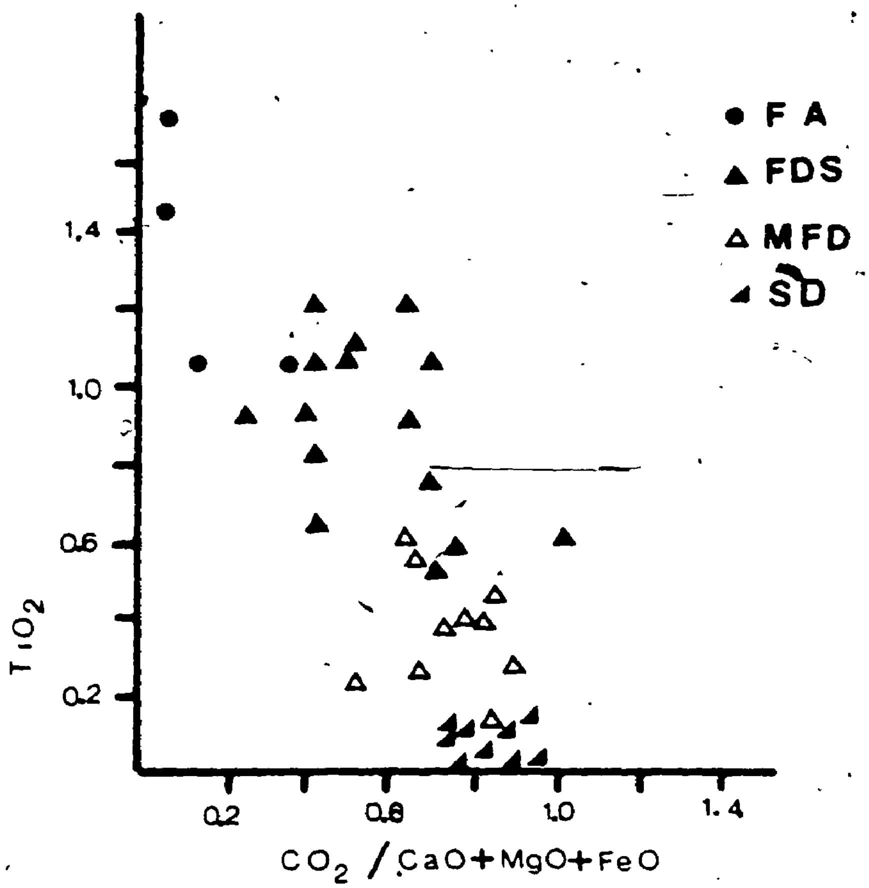

Figure 4.7. TiO_2 versus $CO_2/(CaO+MgO+FeO)$ for carbonate rich rock types. Symbols as in Figure 4.6 except for now FDS = Ferroan Dolomite Schists which is a combination of FDCBQ Schist and veined FDCSBQ Schist.

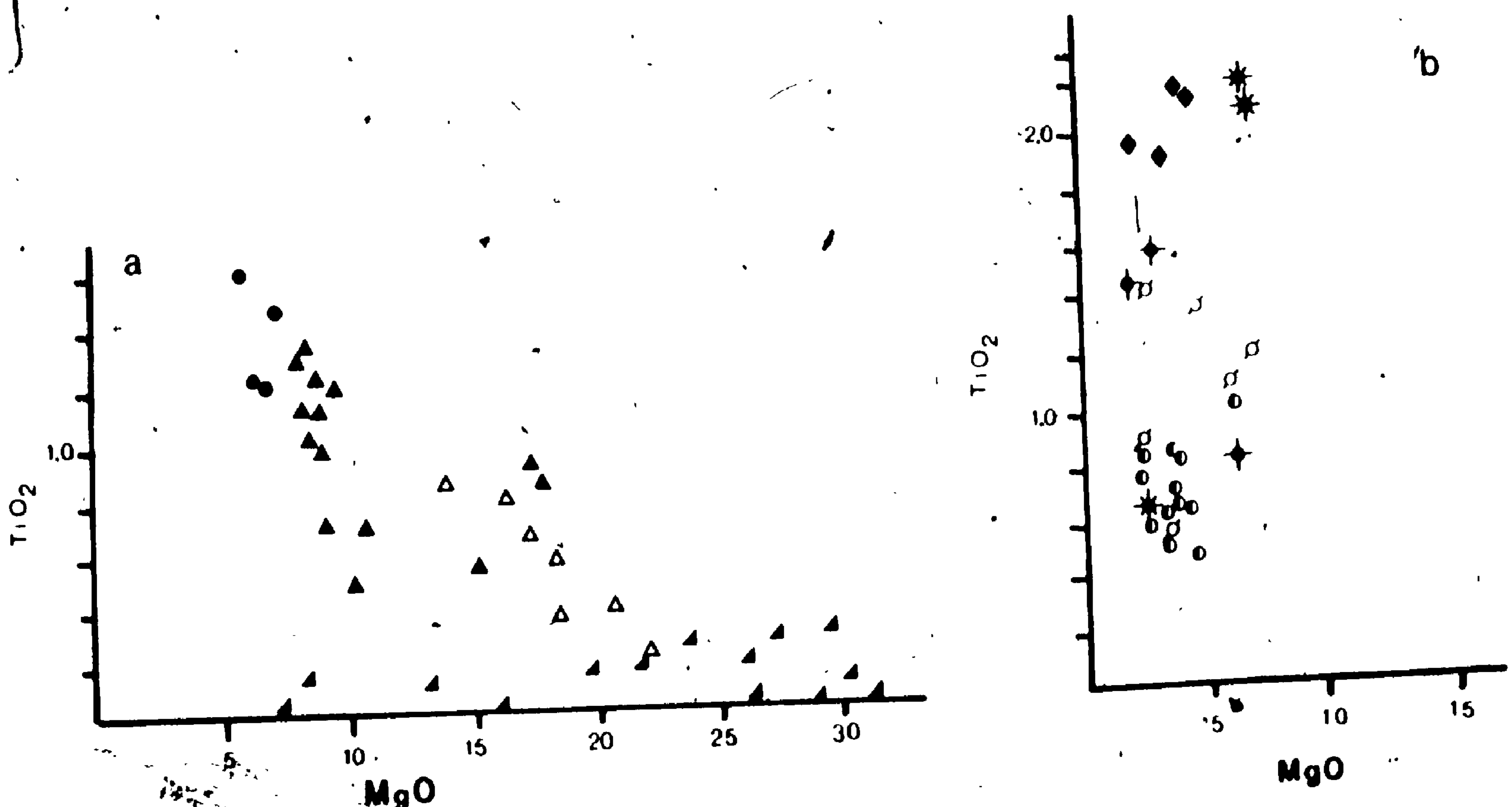

Figure 4.8 a & b: TiO_2 versus MgO for all rock types. Symbols as in Figure 4.6.

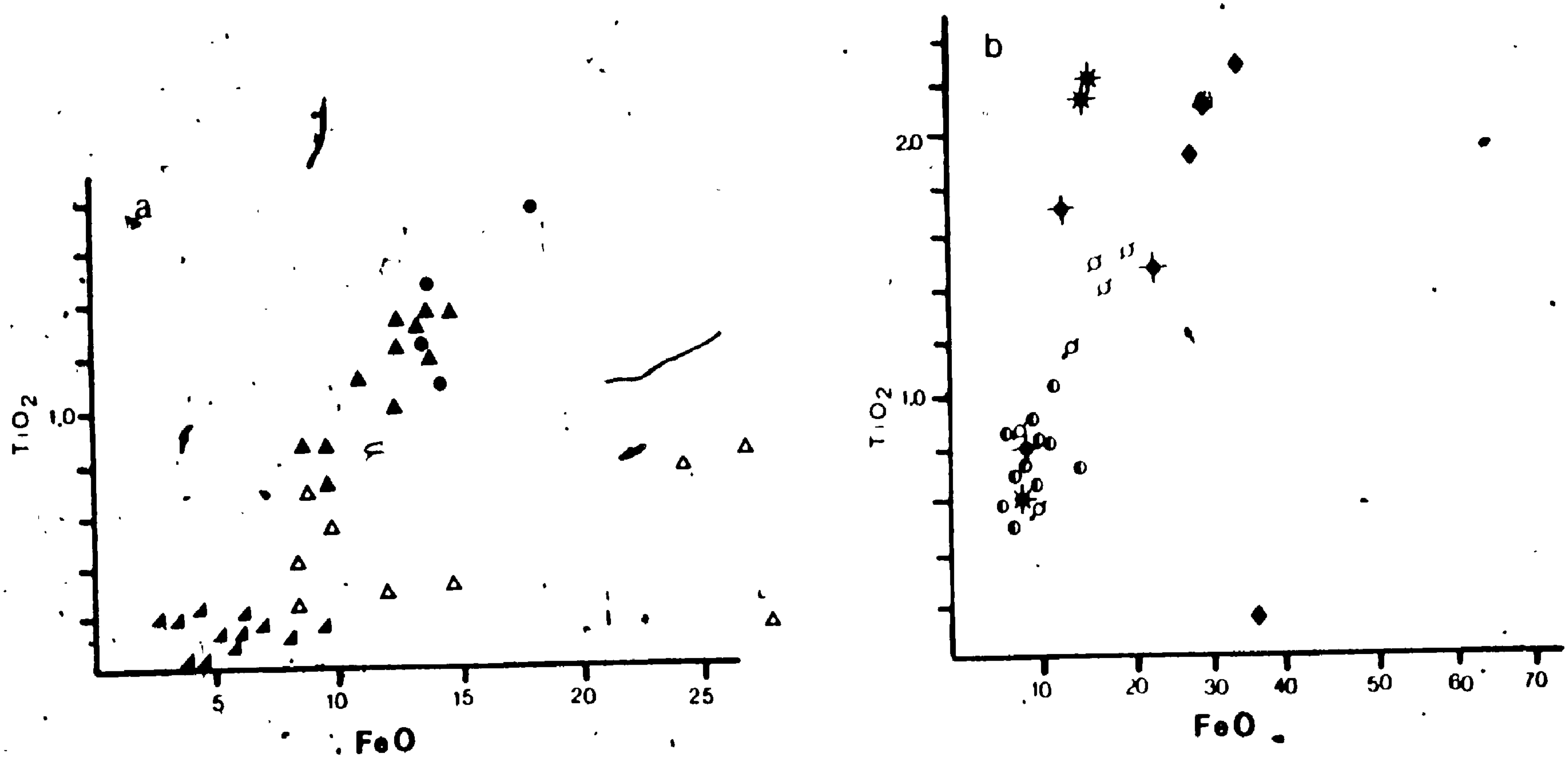

Figure 4.9 a & b. TiO_2 versus FeO for all rock types. Symbols as in Figure 4.6.

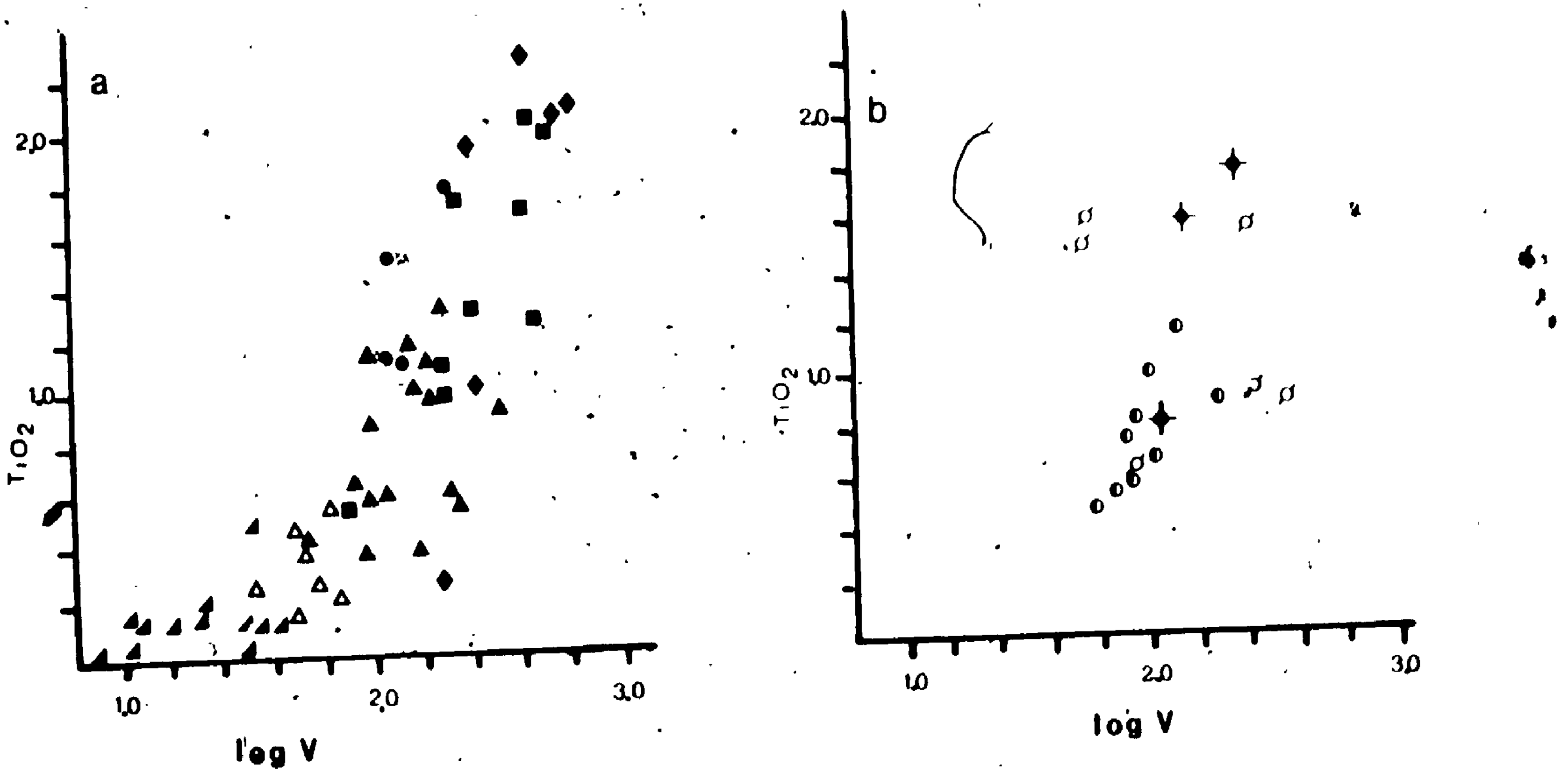

Figure 4.10 a & b. TiO_2 versus log V for all rock types. Symbols as in Figure 4.6.

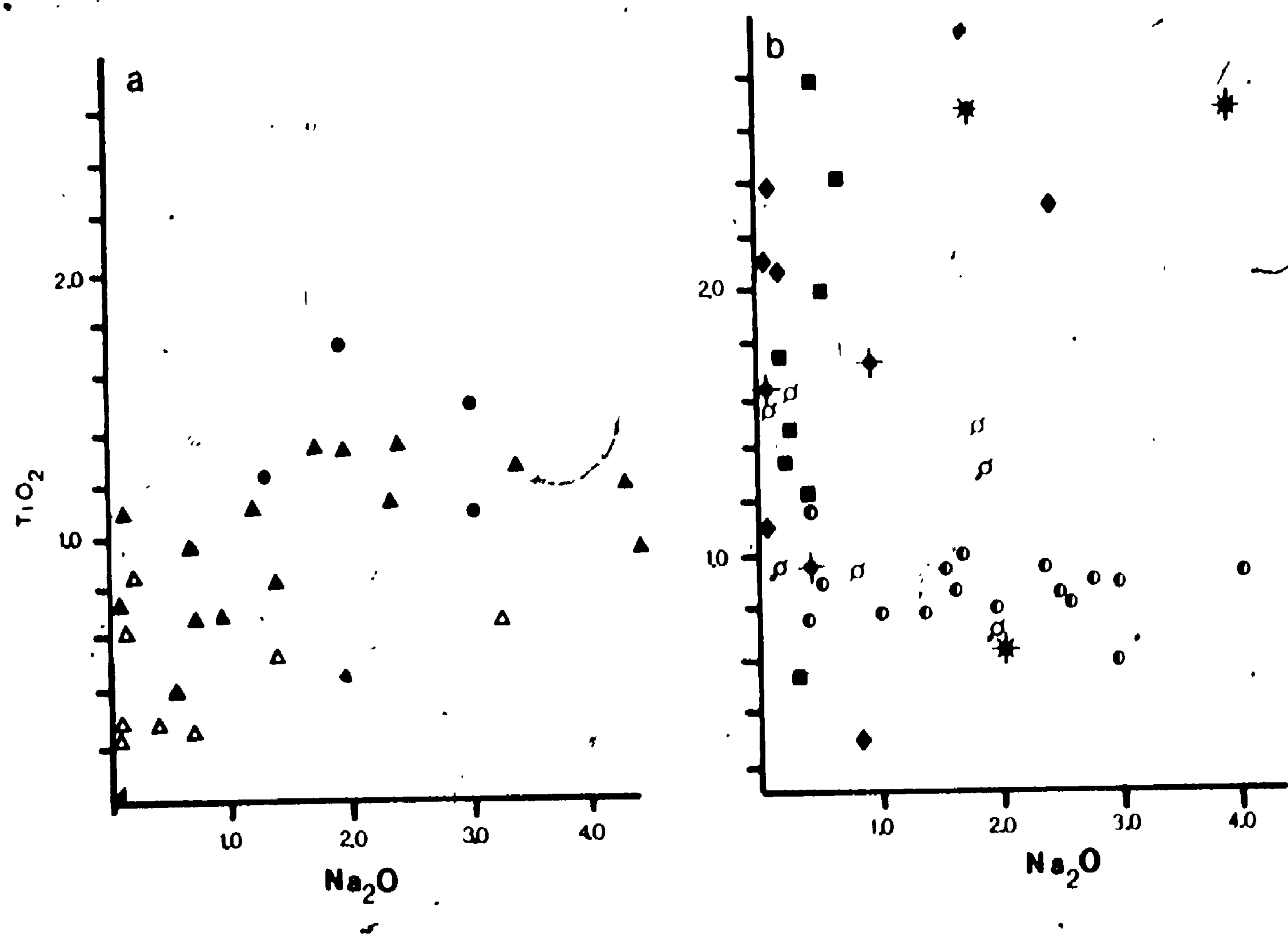

Figure 4.11 a & b. TiO_2 versus Na_2O for all rock types. Symbols as in Figure 4.6. Note Silicified Dolomite values restricted to zero Na_2O value.

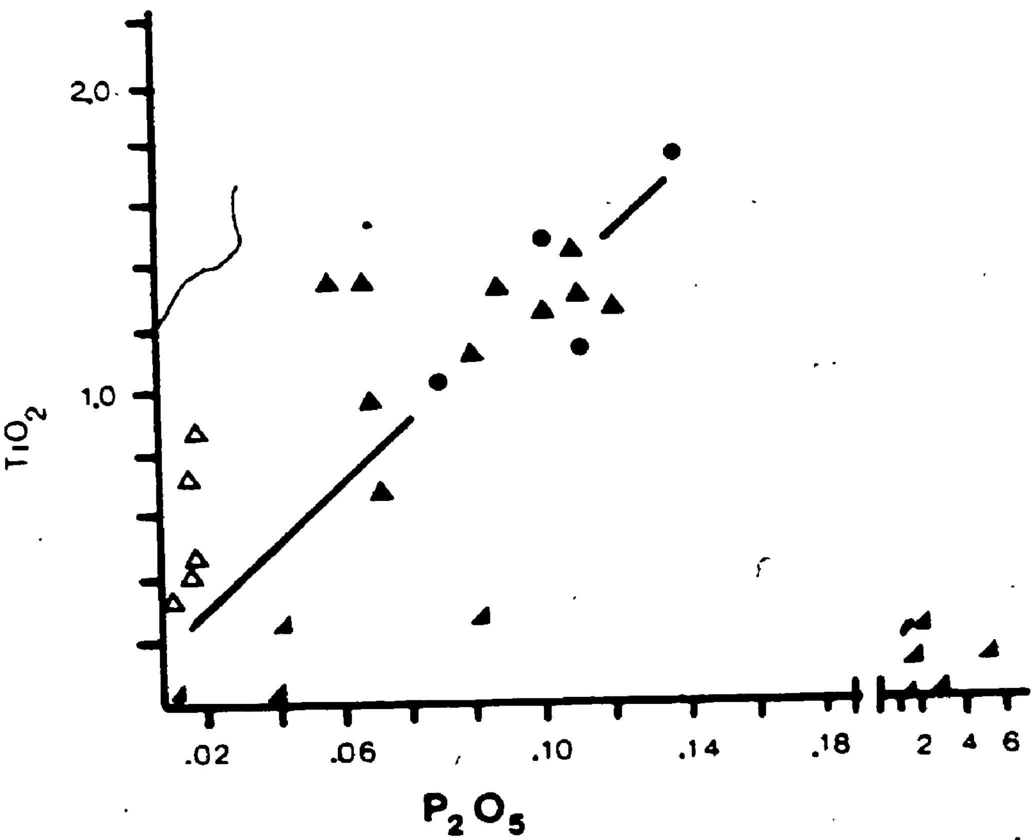

Figure 4.12. TiO_2 versus P_2O_5 for carbonate rich rock types. Symbols as in Figure 4.6.

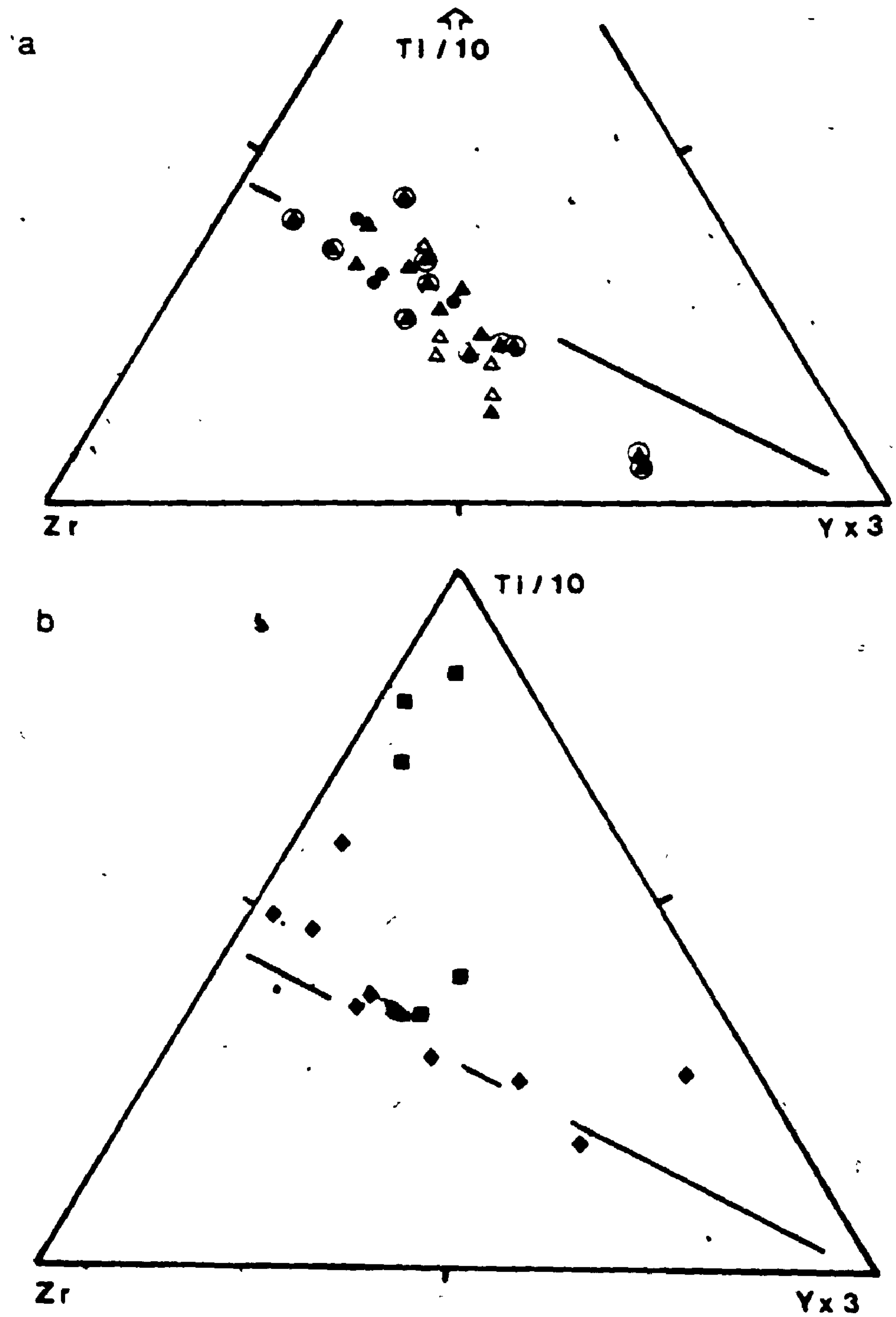

Figure 4.13 a & b. Ternary Ti/100:Zr:Yx3 for carbonate rich rock types (a) and Sericite-Chlorite Schist and Chlorite-Magneitie Schist (b). Lines represent general trend.

are interpreted to represent a process of carbonatization. This corresponds with the progressive formation of ferroan dolomite. This will be more fully discussed in Section 4.3.

4.2.3. Veined Ferroan Dolomite-Chlorite-Sericite-Biotite-Quartz Schist

The variation of the geochemisty of the veined FDCSBQ Schist is much the same as that of the FDCBQ Schist described in Section 4.2.2. Silica shows the least variation with a coefficient of variation of 13%. The coefficient of variation for TiO_2, Al_2O_3, FeO, MnO, MgO, CaO and CO_2 ranges from 20 to 33%. K_2O and Na_2O vary to the largest extent, with coefficients of variation of 50 to 88%. Again P_2O_5 shows a large variation (61%), due to one anomalous anlaysis. If removed from the calculation the coefficient of variation is reduced to 33%. The coefficient of variation for Nb, Zr, Y, Ni, Cr and V ranges from 23 to 53%; Zn, Cu, Ba range from 66 to 81%. As and S have the largest coefficient of variation at 102 and 113% .

The veined FDCSBQ Schist shows larger ranges in composition than seen in the FDCBQ Schist (Figures 4.6 to 4.13). TiO_2 values of the veined FDCSBQ Schist range between the Foliated Amphibolite and Massive Ferroan Dolomite (for example Figure 4.6a). In comparison to the FDCBQ Schist it is relatively enriched in K_2O (Figure 4.6a), CaO and Ba (Table 4.1). The Ti:Zr is consistent with that of FDCBQ Schist and Foliated Amphibolite as illustrated in Figure 4.13. Similarly the TiO_2:P_2O_5 ratio is 10:1 as that of the Foliated Amphibolite and FDCBQ Schist (Figure 4.12).

4.2.3.1 Di scussion

The similar Ti:Zr (Figure 4.13) and the TiO_2:P_2O_5-(Figure 4.2) ratios strongly suggest that the geochemistry of the veined FDCSBQ Schist is genetically linked to the FDCBQ Schist and therefore to the Foliated Amphibolite. The relative increase in CO_2 (Figure 4.7) suggests carbonatization and accounts for the increase in CaO and MgO and the decrease in TiO_2, FeO and Na_2O; however, it does not account for the marked increase in K_2O and Ba. Sericitization is considered a significant process of alteration in the development of the veined FDCSBQ Schist. Sample 156-7 is of particular interest in that it shows a marked increase in Na_2O relative to the other samples (Figure 4.11a). This sample is an example of the plagioclase-ferroan dolomite vein type described in Section 3.3.3.3.

The range in As and S are attributed to an increase in the abundance of arsenopyrite and pyrrhotite. A more complete discussion of the relative gains and losses due to alteration will be discussed in Section 4.4 with reference to mass balance calculations. The mineral reactions will be presented in the metamorphic section 6.3.

4.2.4 Massive Ferroan Dolomite

The Massive Ferroan Dolomite shows fairly consistant SiO_2, TiO_2, Al_2O_3, FeO, MnO, MgO,CaO and CO_2 values with the coefficient of variation ranging from 13 to 33%. P_2O_5 has a coefficient of variation of 61% and the coefficient of variation for K_2O and Na_2O is 50 and 88% respectively. The trace element chemistry shows more variation than for those rocks described in Sections 4.2.2 and 4.2.3. Nb, Zr, Y, Sr, Ni, Cr and V have coefficients of variation which range from 19 to

52%; Zn, Cu, Ba range from 66 to 81% and As and S are 102 and 113% respectively.

In Figures 4.6 to 4.13 inclusive, it is evident the Massive Ferroan Dolomite shows a range in TiO_2 values between FDCBQ Schist the Silicified Dolomite. For instance, the CO_2 values of the Massive Ferroan Dolomite is less than that of FDCBQ Schist and veined FDCSBQ Schist but is distinctly elevated relative to the Silicified Dolomite (Figure 4.7). Similarily the FeO and MgO fields of the Massive Ferroan Dolomite are transitional between the FDCBQ Schist and viened FDCSBQ Schist and the Silicified Dolomite (Figures 4.8a, 4.9a). It is interesting to note the two trends evident in the K_2O and Na_2O fields (Figures 4.6a, 4.11a). The higher TiO_2 samples are generally lower in Na_2O and K_2O and show a restricted range, while the lower TiO_2 samples show a higher and wider range in Na_2O and K_2O. The Ba values of massive Ferroan Dolomite show little difference from those of the Ferroan Dolomite Schists (Table 4.1) . The Ti:Zr ratio (Figure 4.13a) is slightly smaller than that of the Ferroan Dolomite Schists and the Foliated Amphibolite and shows a variation in the Y values. The $TiO_2:P_2O_5$ ratio (Figure 4.12) appears to be unrelated to the 10:1 ratio seen in the Ferroan Dolomite Schists and Foliated Amphibolite.

4.2.4.1. Discussion

The geochemical evidence suggests a geochemical affiliation of the Massive Ferroan Dolomite to the Ferroan Dolomite Schists and therefore to the Foliated Amphibolite. The Ti:Zr ratio is consistent, although the $TiO_2:P_2O_5$ ratio departs from the 10:1 ratio. The similarity in the trends of a decrease in TiO_2, K_2O, FeO associated with CO_2 and MgO again suggests carbonatization as seen for the FDCBQ Schist and veined FDCSBQ Schist. The limited increase in Na_2O and K_2O with lower TiO_2 values may be related to the sericite-chlorite partings common to this rock type.

4.2.5. Sericite-Chlorite Schist

The major oxide chemistry of the Sericite-Chlorite Schist shows similar groupings as seen above. The coefficient of variation of SiO_2, TiO_2, Al_2O_3, FeO, CO_2 and P_2O_5 vary from 18 to 54%; MnO, MgO, K_2O range from 57 to 73% and CaO and Na_2O are 118% and 98% respectively (Table 4.1). This differs from those rocks discussed above where K_2O and Na_2O show distinct, large coefficients of variation. coefficients of variation for Nb, Zr, Zn, Cu, Ni, Cr, V and Ba range from 37 to 61% and the largest degree of variation occurs for Y, Sr, As and S ranging from 83 to 142%.

The most distinctive geochemical character of this rock is the relatively elevated values of Al_2O_3, TiO_2, K_2O, Ba and V compared to the rocks described above (Table 4.1, Figure 4.6b, 4.10a). The Na_2O is depleted relative to the Foliated Amphibolite and Ferroan Dolomite Schists and Massive Ferroan Dolomite and more similar to the Silicified Dolomite (Figure 4.11b). The FeO is distinctly elevated and plots in a similar range as Massive Ferroan Dolomite samples (Figure 4.9b). MgO shows a bimodal distribution: those samples with less than 5% and those samples with more than 10% MgO on a dry weight basis (Figure 4.8b). K_2O values increase with increasing TiO_2 (Figure 4.6b). The Ti:Zr ratio (Figure 4.13b) is similar to that of the Ferroan Dolomite Schists and Foliated Amphibolite, except for the sample which deviates toward higher Ti and lower Zr. Y shows a large variation. The $TiO_2:P_2O_5$ ratio is low, and shows no variation, similar to that of the Massive Ferroan Dolomite and Silicified Dolomite.

4.2.5.1. Discussion

The aluminous and potassic nature of this rock type distinguishes it from other rock types (Table 4.1, Figure 4.6b). The similarity in Ti:Zr (Figure 4.13b) and TiO_2:V ratios (Figure 4.10a) with the Foliated Amphibolite, Ferroan Dolomite Schists and the Massive Ferroan Dolomite is significant. It suggests a similar parentage, assuming immobility of these elements. In contrast to the Ferroan Dolomite Schists and Massive Ferroan Dolomite , where shifts in chemistry can be attributed to carbonatization, the increase in TiO_2 seen in the Sericite-Chlorite Schist is attributed to sericitization. Muscovite substitutes significant K_2O, Ba and V values (see Table 5.3, Appendix III for sericite analysis). The bimodal MgO distribution is due to the variability in chlorite content of the rock, commonly seen as the characteristic "tiger striping" of sericite and chlorite.

The modal abundance of arsenopyrite and to a lesser extent pyrrhotite accounts for the variation in As and S.

4.2.6. **Chlorite-Magnetite Schist**

The analysis of the Chlorite-Magnetite Schist proved to be fairly difficult, due to its high iron and sulphide nature. The data presented are commonly normalized to 100% and are, therefore, not as reliable as those of other rock types. The major oxide chemistry of the Chlorite-Magnetite Schist clusters into three groups. SiO_2 and

FeO have a coefficients of variation of 37 and 39% respectively; TiO_2, Al_2O_3, MnO and MgO vary from 44-57%. The coefficient of variation of K_2O, P_2O_5 and CaO ranges from 85 to 106%. The coefficient of variation for Na_2O is 176% due to the anomalous value associated with sample 60-9-3. If the sample is eliminated from the calculation the mean becomes 0.24 +/- 0.21 which results in a coefficient of variation of 87% which is within the range of the third group. The trace elements show more variation than the rock types described above. The coefficient of variation for Zn, Ni, Cr, and V ranges from 26 to 54%; Zr, Y, Cu, Ba and S ranges from 74 to 99% and Sr and As are the most variable at 143% and 136% respectively.

Several geochemical parameters distinguish the Chlorite-Magnetite Schist from the other rock types. The high FeO (Figure 4.9b), As, Cu, Zn and S values (Table 4.1) are most notable. TiO_2 and V are elevated similar to the Sericite-Chlorite Schist (Figure 4.10a). K_2O is intermediate in comparison to the other rock types (Figure 4.6b). Ba is depleted in comparison to the Sericite-Chlorite Schist and is comparable to the other rock types (Table 4.1). Na_2O is depleted with respect to Foliated Amphibolite, Ferroan Dolomite Schists and Massive Ferroan Dolomite but is similar to the Sericite-Chlorite Schist (Figure 4.11b). The Ti:Zr:Y ratio is not consistent within the suite (Figure 4.13b). Several samples show the same Ti:Zr ratio as that of the Foliated Amphibolite with depleted Y; whereas other samples show a shift towards higher Ti and lower Zr, significantly displaced from the Foliated Amphibolite trend. The $TiO_2:P_2O_5$ ratio is low, showing no variation.

4.2.6.1. Discussion

The Chlorite-Magnetite Schist represents the core of the Upper Ore Zone and its geochemistry is clearly distinctive. The high iron values and base metal values make it different from the other rock types, but some similarities to the other rock types are important. The high K_2O, TiO_2 and V values and the shift in the Ti:Zr ratio are similar to that seen in the Sericite-Chlorite Schist. The consistent Ti:Zr ratio and the textural evidence that the Chlorite-Magnetite Schist is transitional to the Sericite-Chlorite Schist strongly suggests a genetic link between the two rock types, and therefore may be related to the Foliated Amphibolite.

The high iron content and distinctive mineral assemblage of chlorite and magnetite, may lead to the alternative suggestion that these rocks represent a primary chemical precipitate, in particular, an iron formation. Deformation has obliterated any primary textures, thus eliminating it as a tool for distinguish the original nature of the rock type. Geochemistry may therefore be the only method available to approximate its original character. Table 4.2 is a listing of the average oxide values of Minas III Chlorite-Magnetite Schist, metamorphosed Labrador Iron Formation (Gole and Klein,1981) and other silicate and sulphide facies Iron Formations (Maynard, 1983; Stanton, 1972). Also presented in the same table is the range of values for tholeiitic basalts presented by Hyndman (1985, Table 6.9). Selected data are plotted in Figure 4.14 and illustrate the range in chemistry of the different rock types. The range in FeO values of the metamorphosed Labrador Iron Formation completely

TABLE 4.2. Representative Analysis of Silicate and Sulphide Iron Formation and Oceanic Tholeiite

	1	2	3	4	5	6
SiO_2	31.92	59.00	42.50	51.18	21.50-68.30	42.80-52.56
TiO_2	1.80	-	-	0.51	0.00- 0.18	0.35- 3.69
Al_2O_3	12.78	2.41	6.23	11.95	0.01- 3.51	7.30-22.30
Fe_2O_3	*	8.70	15.10	8.09	1.70-37.60	0.69- 7.90
FeO	37.53	16.30	14.60	12.15	14.40-66.60	2.87-13.58
MnO	0.17	-	-	2.71	0.04- 2.76	0.09- 0.44
MgO	4.90	2.73	2.31	2.42	1.00- 9.63	4.59-26.00
CaO	3.89	-	-	1.12	0.32- 7.61	6.69-14.10
Na_2O	0.54	0.20	0.91	2.12	0.02- 0.57	0.90- 4.45
K_2O	1.04	0.63	0.73	1.86	0.00- 0.61	0.04- 0.70
P_2O_5	0.25	0.10	0.17	0.54	0.02- 0.45	0.06- 0.56
LOI/CO_2	4.12	2.50	3.00	5.96	**	-

1) average of Chlorite-Magnetite Schist, Minas III.
   * all Fe_2O_3 recalculated to FeO
2) average of Lake Superior Type Silicate Facies Iron Formation (Maynard, 1983, table 2.5, after Gross, 1980)
3) average of Algoma Type Sulphide Facies Iron Formation (Maynard, 1983, table 2.5, after Gross, 1980)
4) silicate iron formation, Iron River district, Michigan (Stanton, 1972, Table 13-11, pg.441, after James, 1954, pg.271)
5) range of compositon for Labrador Trough Metamorphosed Banded Iron Formation, (Gole & Klein, 1981)
   ** recalculated to 100% on a H_2O and CO_2 free basis
6) range of composition for oceanic tholeiites (Hyndman, 1985, Table 6.9, pg. 205).

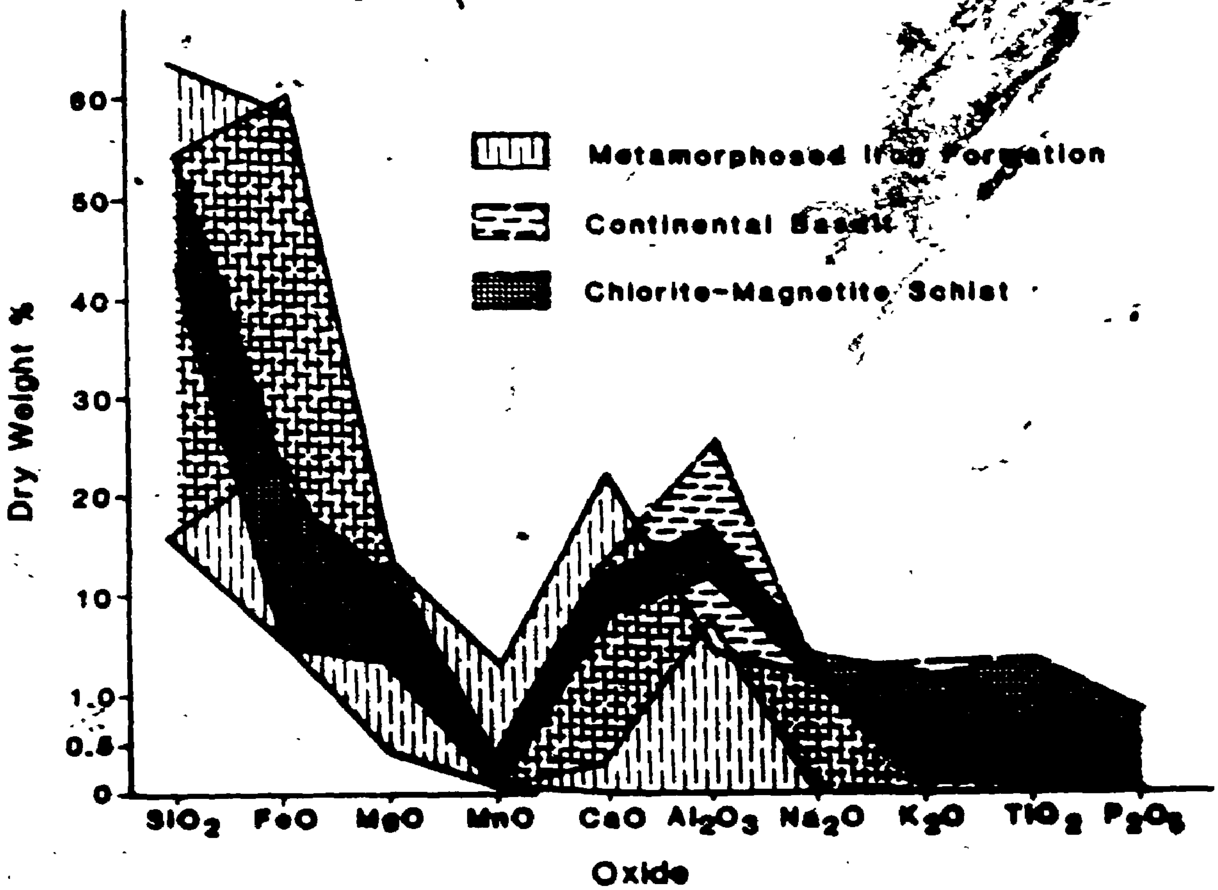

Figure 4.14. Weight % of various oxides of BIF (Gole and Klein,1981), Tholeiite (Hydman, 1985) and Chlorite-Magnetite Schist of Minas III.

encompasses those of the Chlorite-Magnetite Schist and basalt and does not discriminate between rock types. Al_2O_3 and TiO_2 are the only oxides which separate the different groups. In both instances the Al_2O_3 and TiO_2 values of the metamorphosed Labrador Iron Formation are well below that of the overlapping fields of the Chlorite-Magnetite Schist and basalt. The point to be made is that the Chorite-Magnetite Schist is iron rich but it is also elevated in Al_2O_3 and TiO_2 values with respect to the Labrador Iron Formation and is therefore most similar to the average basalt. Although the comparison is not definitive, it does indicate that the major oxide geochemistry of the Chorite-Magnetite Schist is not readily comparable to a typical Archean Iron Formation but is, rather, more comparable to a tholeiitic basalt.

4.2.7. Silicified Dolomite

The Silicified Dolomite is a chemically uniform rock type. CaO and MgO show the least variability with coefficients of variation of 23 and 27% respectively. SiO_2, TiO_2, Al_2O_3, FeO, MnO and K_2O have a slightly larger variability with the coefficient of variation ranging from 58 to 83%, P_2O_5 and Na_2O are the most variable at 106 and 120% respectively. The coefficients of variation for Zr, Sr, Zn and V range from 25 to 57%; Nb, Cr, Ba and S range from 67 to 92% and Y, As, Cu, Ni range from 101 to 232%.

It is evident in Figures 4.6 through to 4.13 that the Silicified Dolomite defines a unique geochemical group. This distinction is illstrated by low TiO_2, V (Figure 4.10a), FeO (Figure 4.9a) and Na_2O (Figure 4.11a) values and high, very tightly clustered CO_2 values

(Figure 4.7). MgO shows the widest spread in values (Figure 4.8a). K_2O (Figure 4.6a) has a bimodal population: those samples with no or minor K_2O and those with greater than 0.20% K_2O. The elevated K_2O values show a positive correlation with TiO_2 values. The P_2O_5 of the Silicified Dolomite defines two groups (Figure 12): those samples with a P_2O_5 range from 0.02% to 0.10% and those samples with a P_2O_5 range from 1% to 5%.

The trace element chemisty of the Silicified Dolomite is generally depleted in comparison to the other rock types described. Sr, As, Ba, and S (Table 4.1) are particularly depleted with respect to the Foliated Amphiolite, Ferroan Dolomite Schists and Massive Ferroan Dolomite.

In comparing the composition of the Minas III Silicified Dolomite against the Archean and Proterozoic samples presented by Holland (1984; Table 4.3) it is evident that the rocks are more similar than dissimilar. Table 4.3 shows the average major oxides of the Silicified Dolomite recalculated to 15% SiO_2. The most marked difference is the lower CaO values, differing by 6-8%.

4.2.7.1. Discussion

Veiser (1984) points out that the bulk rock chemistry of sedimentary carbonate rocks is controlled primarily by the non-carbonate component. The variability and abundace of SiO_2 can be directly attributed to quartz veining (Plate 6a). The variability in K_2O and Na_2O may be associated with sericite and plagioclase, often noted overgrowing sericite. It is suggested that the relative encrichment of Ba, As and S are due to the introduction of these elements associated with muscovite and sulphides.

The similarity of the geochemistry of the Silicified Dolomite to the dolomites presented in Table 4.3 and the dissimilarity to Massive Ferroan Dolomite strongly suggest a different paragenesis for the two. The Silicified Dolomite is considered to be a sedimentary rock which has undergone metamorphism and limited alteration.

4.2.8. Graphitic Pelite

The geochemical variation within the Graphitic Pelite suite is less pronounced than in the other rock types described above. The coefficient of variation for SiO_2, TiO_2, Al_2O_3, FeO and K_2O varies from 19 to 34%; MnO, P_2O_5 and Na_2O varies from 42 to 56% and MgO, CaO and LOI varies from 77 to 107[illegible] The large variability apparent in the trace elements is due to two samples, 159-37 and 67-14. These are enriched in Nb, Zr, Sr, Zn, Cu, Ni, Ba and V and have a coefficient of variation ranging from 33 to 58%. Y, As, S vary from 80 to 206%.

The chemistry of the Graphitic Pelite is distinctive, bearing little similarity to the other rock types described. This is well illustrated in Figures 4.6 to 4.13. The geochemical parameters of the Graphitic Pelite consistently cluster together, apart from the other rock types. It tends to be relatively depleted in most oxides and trace elements (Table 4.1). The exceptions are As, Ba and S which are similar in range to the Ferroan Dolomite Schists and Sericite-Chlorite Schist (Table 4.1).

One of the most distinctive characteristic of the Graphitic Pelite is its black colour, thought to be due to the presence of carbonaceous material. In order to determine its nature, it was floated off and several powdered samples were run for an XRD pattern. The results were not definitive. While no amorphous "hump" is evident on the scan, no characteristic graphite peaks were evident either. One of the difficulties is that of the 100% intensity of graphite is at the same 100% peak intensity of the (001) reflection of chlorite. Chlorite consistantly floated off with the graphite and could not be easily separted. According to Dr. J. P. Golightly, 1-2% graphite is reported by the INCO Research Staff (personal communication, 1985). It is therefore assumed that the black carbonaceous material is graphite, although the degree of ordering is unknown.

Table 4.3 contains Archean pelite analyses from the Pilbara Block, Australia (McLennan and Taylor, 1984) and a muscovite-chlorite pelite from Connemara, Ireland (Yardley, 1980). The Minas III Graphitic Pelite is depleted in Al_2O_3 aand K_2O and enriched in MgO, CaO and Na_2O with respect to both the Australian and Irish pelites. It is most similar to the Australian sample with respect to TiO_2 and P_2O_5. The trace elements of Sr, Cu, Ni, Cr, and V for Minas III Graphitic Pelite are distinctly lower than the Pilbara Pelite with Nb and Ba comparable.

Figure 4.15 represents a modified diagram presented by Garrels and McKenzie (1971, Figure 9.2, pg. 229) showing the chemistry of pelite or lutites throughout gelogic time and different geographic locations. Included in Figure 4.15 is the curve describing a weathering path based on Na_2O and K_2O variations after Kronberg & Nesbitt (1981). Initial chemical weathering follows a path of Na_2O depletion with relatively no K_2O depletion represented by the formation of illite

TABLE 4.3. Representative Rock Analysis from the Literature

	MacLennan & Taylor, 1983.	Yardley et. al, 1980.	Shaw, 1956[a]	Clarke, 1924[b].	Ronov & Migdisov, 1970[c].		Minas III Silicified Dolomite
	1	2	3	4	5	6	7
SiO_2	55.07	50.82	63.51	61.90	13.76	18.27	15.00
TiO_2	0.61	1.09	0.79	-	0.02	0.18	0.97
Al_2O_3	25.50	24.46	17.35	16.90	2.16	3.00	2.08
Fe_2O_3	-	-	2.00	4.20	1.99	0.29	-
FeO	5.17	9.53	-	3.00	0.50	1.62	3.79
MnO	0.01	1.69	4.71	-	-	0.04	1.15
MgO	3.32	2.74	2.31	2.40	15.65	10.15	14.93
CaO	0.01	1.59	1.24	1.49	28.51	30.73	23.30
Na_2O	0.37	0.19	1.96	1.07	0.31	0.32	0.94
K_2O	4.67	3.75	3.35	3.70	0.28	0.67	1.12
P_2O_5	-	0.23	-	-	0.37	0.10	1.71
LOI/CO_2	5.27	3.36	2.64	5.44	34.97	32.99	33.93
Nb	12.7	-	-	-	-	-	14.9
Zr	120.0	-	-	-	-	-	26.9
Y	-	-	-	-	-	-	15.1
Sr	41.4	-	-	-	-	-	141.9
Rb	-	-	-	-	-	-	35.0
As	-	-	-	-	-	-	122.9
Zn	79.0	-	-	-	-	-	32.26
Cu	333.0	-	-	-	-	-	14.6
Ni	615.0	-	-	-	-	-	8.1
Cr	1114.0	-	-	-	-	-	-
Ba	153.0	-	-	-	-	-	244.7
V	-	-	-	-	-	-	21.7
S	-	-	-	-	-	-	54.4

1) Shale, Pilbara Block, Australia
2) Shale, Connemara, Ireland
3) average shale
4) average high grade pelite
5) Dolomite, Russian Platform
6) Dolomite, North American Platform
7) average Minas III Silicified Dolomite recalculated to 15% SiO_2.

a) In: Garrels & Mackenzie, 1971. Figure 8.2, pg.209
b) In: Garrels & Mackenzie, 1971. Table 9.1.
c) In: Holland, 1984.

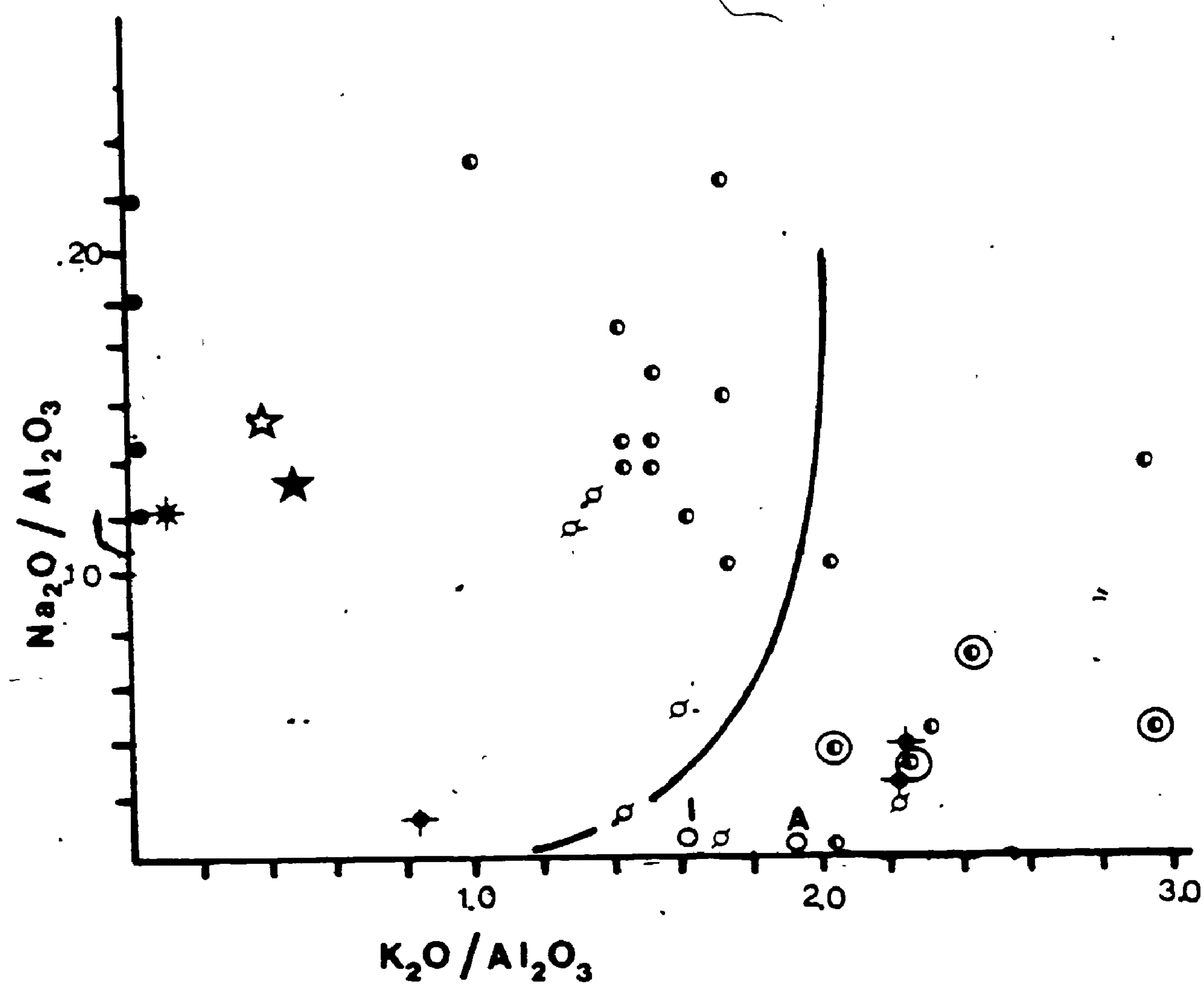

Figure 4.15. Na_2O/Al_2O_3 versus K_2O/Al_2O_3 after Garrels and McKenzie (1971). Line represents weathering trends. Open and closed stars composition of average tholeiite (Hyndman, 1985). I = Irish, Connemara, Ireland (Yardley et al, 1980); A = Australian, Pilbara Block Shale (MacLennan & Taylor, 1984). Graphitic Pelite with anomalous Au values marked by circled half circles. Symbols as in Figure 4.6.

until all the Na_2O is removed. At this point K_2O is removed and the rock becomes progressively more aluminous, with kaolinite the product. A trend toward K_2O enrichment, that is, a shift to the right of the diagram is representative of K_2O introduction or metasomatism and not a natural weathering process. The Graphitic Pelite from Minas III appears to be divided into two groups: one with relatively elevated Na_2O values; and another with depleted Na_2O and relatively enriched K_2O. Importantly, those samples enriched in K_2O are quartz veined or in close proximity to the Quartz Cemented Graphitic Pelite or Lower Ore Zone. Also plotted on this diagram are the pelite compositions from Maclennan and Taylor (1984) and Yardley et al. (1980). They are very low in Na_2O and show only minor variation in K_2O from the Minas III Graphitic Pelite.

4.2.8.1. Discussion

The tight clustering of the composition of the Graphitic Pelite suggests that this rock type has undergone little geochemical alteration to perturb its original geochemical signature. The Graphitic Pelite is therefore designated as a primary rock type, as are the Foliated Amphibolite (4.2.1.1) and Silicified Dolomite (4.2.3.1).

Figure 4.15 reveals two points of discussion. Firstly, it is evident that the Graphitic Pelite samples are the product of intermediate weathering processes characteristic of illite formation (Kronberg & Nesbitt, 1981). This is in comparison to those samples from the Pilbara Block and Ireland which are significantly lower in Na_2O, indicative of more advanced weathering with the formation of kaolinite.

Secondly, a second group of samples exhibit substantially higher K_2O values. As noted above, an increase in K_2O must represent a metasomatic potassium addition, if Al_2O_3 is considered to be immobile (Kronberg & Nesbitt, 1981). This is significant in view of the fact that those samples which are enriched in K_2O are invariably associated with either quartz veining or proximal to the Lower Ore Zone and contain anomalous gold values. This point will be more fully discussed in Section 6.6.

The low Ni and Cr values of the Minas III Graphitic Pelite suggest that ultramafic rocks were not a weathering source. The Graphitic Pelites from the Pilbara Bock have considerably elevated Cr and Ni values, strongly suggesting an ultramafic source rock. H.W. Nesbitt(1986, personal communication) reports that selected pelite samples from the Canadian Abitibi also show elevated Cr and Ni values. There are several implications to consider. Given the present distribution of the ultramafic rocks within the Crixas Greenstone Belt (Figure 2.2) it is possible that the ultramafic rocks of the greenstone belt were buried and therefore were not available as a source rock for the Graphitic Pelite; or the rocks have been juxtaposed into their present positions, and therefore the ultramafic rocks were too distal to provide a source for the Graphitic Pelite. No answer is possible with the limited amount of data.

4.2.9. Quartz Cemented Graphitic Pelite Breccia

The Quartz Cemented Graphitic Pelite Breccia is the Lower Ore Zone. The three samples analysed consist of less than 50% quartz cement in order to assess the chemistry of the intervening matrix. The coefficient of variation for SiO_2 is 9%; TiO_2, Al_2O_3, FeO, MnO, MgO ranges from 20 to 52%; K_2O and Na_2O are 61 and 100% respectively. P_2O_5 shows a large range due to a null value for sample 159-61. The coefficient of variation for Zr, Zn, Ni and Cr ranges from 14 to 57%; Y, Sr, As, Cu and S range from 62 to 106%.

Compared to the Graphitic Pelite the Quartz Cemented Graphitic Pelite Breccia is relatively elevated in most oxides and trace elements (Table 4.1). It defines a bimodal group with respect to TiO_2.: one comparable to the Graphitic Pelite and the other comparable to the Banded Chlorite-Sericite-Garnet Schist (i.e. Figure 4.6b). K_2O values are elevated and are more comparable in range to those of the Sericite-Chlorite Schist (Figure 4.6b). The Na_2O values are generally low (Figure 4.11b). Increased FeO values (Figure 4.9b) are related to higher TiO_2. MgO values (Figure 4.8b) are within the range of the Graphitic Pelite. Al_2O_3 is elevated relative to the Graphitic Pelite (Table 4.1).

The trace elements As, V and S of the Quartz Cemented Graphitic Pelite Breccia are, as a group slightly elevated (Table 4.1, Figure 4.10b) in comparison to the Graphitic Pelite. It is interesting to note that Ba has approximately the same value as in the Sericite-Chlorite Schist (Table 4.1). The large variations in Nb, Y, and Sr, due to sample 74-12, make a comparison to Graphitic Pelite for these elements difficult. The remaining elements of Zn, Ni and Cr are not consistent within the group with only sample 60-24 near the values of the Graphitic Pelite suite (Table 4.1).

4.2.9.1. Discussion

The few samples make a full discussion of the geochemistry limited but some comments are warranted. There is little doubt that the Quartz Cemented Graphitic Pelite Breccia is a silicified equivalent of the Graphitic Pelite. It is generally enriched in K_2O, depleted in Na_2O, which is comparable to those samples of Graphitic Pelite anomalously enriched in Au. TiO_2, As, V, Sr, Cu and S are all elevated with respect to the Graphitic Pelite. As previously suggested, elevated TiO_2 and K_2O and V values appear to be related to muscovite. Similarily the elevated As and Cu are believed to be related to sulphides.

4.2.10. Chlorite-Plagioclase-Quartz-Ferroan Dolomite Schist

The major oxide and trace element geochemistry of the Chlorite-Plagioclase-Quartz-Ferroan Dolomite Schist shows very little variation. The coefficient of variation for SiO_2, TiO_2, Al_2O_3, FeO, MnO, MgO, CaO, P_2O_5 and LOI are less than or equal to 13%. Na_2O and K_2O are the most variable with a coefficient of variation of 29 and 76% respectively. Zr, Sr, As, Zn, Cu, Ni, Cr and V are the least variable of the trace elements with the coefficients of variation ranging from 7 to 22%; Nb, Y, Ba and S are the most variable with the coefficient of variation ranging from 42 to 139%.

The high TiO_2 values isolate several samples as a unique geochemical group similar in range to that of the Foliated Amphibolite (ie. Figure 4.6b). The FeO and MgO values are intermediate in range (Figures 4.8b, 4.9b). The Na_2O values are relatively elevated (Figure 4.11b). The Ti:Zr ratios are similar to those of the Foliated

Amphibolite.

4.2.10.1 Discussion

The very limited rock geochemistry suggests that there is an affiliation of the CPQFD Schist to the Foliated Amphibolite. However, the data does not allow for unequivocable conclusions. The most attractive interpretation is that the CPQFD Schist is a mafic rock which has been metamorphosed, deformed and altered. The evidence of possible chill margins may suggest that it is a deformed sill or dyke.

4.2.11. Banded Chlorite-Sericite-Garnet Schist

The Banded Chlorite-Sericite-Garnet Schist is geochemically uniform. The major oxides except for Na_2O have a coefficient of variation ranging from 11 to 43%. Na_2O has a coefficient of variation of 86% which can be attributed to the anomalously high Na_2O value in sample 159-71. The coefficient of variation of the trace elements As, Zn, Cu, Ni, Cr, Ba and V range from 25 to 82%; Nb, Zr, Y, Sr and S range from 102 to 116%. Sample 159-71 is anomalously high in Nb, Zr, Y and Sr accounting for the large range in their coefficients of variation.

The TiO_2 values are very uniform at approximately 1.3, with the exception of a single sample having a TiO_2 value of 0.6 (i.e. Figure 4.6b). The unit is relatively elevated in FeO (Figure 4.9b), K_2O (Figure 4.6b) and depleted in Na_2O (Figure 4.11b) except for a single sample which is enriched in Na_2O. The average Nb, Zr, Y and Sr values (Table 4.1) and V (Figure 4.10b) are within the range of Graphitic Pelite.

Plotted in Figure 4.15, the Banded Chlorite-Sericite-Garnet Schist samples show a consistent loss of Na_2O comparable to the pelites of Connemara and Pilbara. Minor K_2O variation occurs, except for a single sample which is elevated in K_2O and comparable to the auriferous Graphitic Pelite and LOZ.

4.2.11.1. Discussion

The few samples analysed of Banded Chlorite-Sericite-Garnet Schist makes it difficult to propose definitive statements. There appears to be a geochemical affiliation between the Banded Chlorite-Sericite-Garnet Schist and Graphitic Pelite. The shift in chemistry from the Graphitic Pelite to Banded Chlorite-Sericite-Garnet Schist can be attributed to gains in K_2O, FeO and losses in Na_2O which is consistant with those trends seen in the other rock types. It is therefore tentatively suggested that the Banded Chlorite-Sericite-Garnet Schist is a product of alteration of a Graphitic Pelite. Alternatively, the rock may represent a more weathered rock type than the Graphitic Pelite, which subsequently underwent metasomatic shifts in chemisty similar to those auriferous samples of Graphitic Pelite. Additional work is needed to solve this problem.

4.2.12. Banded Quartz-Biotite-Chlorite-Plagioclase Schist

The geochemistry of the Banded Quartz-Biotite-Chlorite-Plagioclase Schist shows little variation. The coefficient of variation for SiO_2, TiO_2, Al_2O_3, FeO, MgO, K_2O and P_2O_5 ranges from 14 to 43% and coefficnets for MnO, CaO and Na_2O ranges from 73 to 89%. The trace element chemistry tightly clusters with the coefficient of variation for Zr, Zn, Cu, Cr and Ba ranging from 17 to 59%; and coefficients for Nb, Y, Sr, As and V ranging from 73 to 96% and S showing the greatest variation at 135%.

The major oxide chemistry is most similar to that of the Graphitic Pelite. The TiO_2, K_2O, Na_2O, FeO and MgO values are within the range of Graphitic Pelite. In Figure 4.15 the samples show a decrease in Na_2O relative to K_2O, within the range of Graphitic Pelite.

Although not analysed, the presence of tourmaline would suggest a high boron content.

4.2.12.1. Discussion

The geochemical evidence suggests that the Banded QBCP Schist is chemically similar to the Graphitic Pelite. The relatively depleted values of Na_2O suggest that the Banded QBCP Schist is perhaps the product of more advanced weathering than the Graphitic Pelite.

The high boron content suggested by tourmaline is consistent with a clay rich precursor. Boron is commonly adsorbed to clay surfaces in a sedimentary enviranment (Wedepohl, 1969)

4.3. Factor Analysis of Whole Rock Geochemistry

4.3.1. Introduction

Factor analysis is concerned with interpreting the structure of the variance-covariance matrix obtained from a collection of multivariate observations (Davis, 1973,p.476). The calculations result in the distinction of factors which have not been specified *a priori*. In geochemical terms, these factors are the grouping of elements which may or may not be related. A positive relationship may reflect any number of things; for instance, the original rock paragenesis or the association of elements in rock forming minerals. It is only through an understanding of the geochemical associations such as seen in Section 4.2 in this study, that factor analysis can be used to an advantage.

The Factor Analysis for this study was conducted using the Statistical Package for Social Sciences (SPSS) on the Cyber 35. A Kaiser varimax rotation of single rock types and all rock types combined was employed to determine the Factors. Table 4.4 shows the coefficients of correlation for the six factors distinguished for all the rock types combined. A value approaching +1 indicates a positive relationship to the factor whereas a value -1 indicates a negative relationship to the factor. Coefficient of correlation approaching zero indicate no relationship to the factor.

4.3.2 Factors for individual rock types.

Table 4.5 indicates the element clusterings which have been distinguished as factors for the individual rock types . Those elements which show coefficients of correlation greater than or less than +/-0.7 and those elements with values less than or greater than +/- 0.7 but which are significantly higher than the remaining values are presented. The maximum number of factors calculated is six and the minimum is two.

Three factors are indicated for the Foliated Amphibolite. Factor 1 can be subdivided into four subfactors. TiO_2 and V are probably related to ilmenite; Zr and P_2O_5 may be related to apatite and zircon respectively, although these mineral were not noted in thin sections. Zn and S are probably related to the sulphide component of the rock.

Table 4.4. Coefficient Correlation Values for all Rock Types

	Factor 1	Factor 2	Factor 3	Factor 4	Factor 5	Factor 6
SiO_2	-.08216	.94196	.15393	.09652	-.07329	-.19028
TiO_2	.78430	.36615	.07410	.19494	-.04222	.12675
Al_2O_3	.27135	.38462	.04796	.43033	.03879	.57023
FeO	.81939	.06664	-.07547	.07837	.27577	.34988
MnO	-.08487	-.36664	.08717	-.34488	.02215	-.05318
MgO	-.28172	-.72367	-.11638	-.23323	.00005	-.16988
CaO	-.36789	-.82607	-.06804	-.26306	-.05362	.03066
Na_2O	-.00688	.52723	.15534	-.10872	-.01843	.18649
K_2O	.18689	.34189	.09103	.85011	-.00070	.02126
P_2O_5	-.14205	-.36321	-.00379	-.09716	-.08128	-.07223
LOI	-.45663	-.77026	-.10421	-.14326	-.09647	.11627
Nb	.01290	-.01539	.96765	-.01456	.08181	-.04347
Zr	.05201	.27112	.93976	.13692	.00896	-.00454
Y	.11163	.07731	.46185	.17644	-.12685	-.05290
Sr	-.27783	-.00658	.78763	-.13370	-.02752	.26704
As	.03100	.01946	-.09256	.04260	.77807	.01076
Zn	.43860	.13462	.73250	.00325	.19535	-.06062
Cu	.17997	.08214	.21820	-.06263	.93616	-.02580
Ni	.68751	.20012	.43093	.09201	-.07167	-.03166
Cr	.83038	.24661	.02191	.23556	.02949	-.13374
Ba	.20035	.13960	.25183	.89379	-.05035	-.01789
V	.92081	.10082	-.01464	.18683	.14038	.00678
S	.00940	-.01142	-.02734	.12766	.11033	.03299

	Eigen Value	% of Variance
Factor 1	7.367	32.0
Factor 2	3.192	13.9
Factor 3	2.330	10.1
Factor 4	1.538	6.7
Factor 5	1.222	5.3
Factor 6	0.654	2.8

Table 4.5. Factor groupings for rock types.

	Factor 1	Factor 2	Factor 3	Factor 4	Factor 5	Factor 6
Foliated Amphibolite	Ti,V Zr,P Zn,S Ba	Mg,Cr,Ni Na,Si	Nb,Y K,Sr As			
FDCBQ Schist	V,Ni,Cr Nb,Zr,Y Fe,Zn Ba	As,S	K,Al,Ti	Na Ti Cu	Mg,Fe (V)	Sr (Ba,LOI)
veined FDCSBQ Schist	Ti,V,Ni,Cr Nb,Zr,Y Fe,Zn	Mg,Na,Mn LOI	As,S	P	K,Ba,Sr	
Massive Ferroan Dolomite	Si, Cu,S Ba,K	Nb,Zr,Y Sr	Al,Fe	Ti,V Mn Zn	(Ti,V,Ni, Cr,Y)	(Ca,LOI As,Cu V,Ni,Cr Y)
Sericite-Chlorite Schist	Ti,V, Zr Al,Ba	Fe,Zr (As)	Na,Sr	Ni,Cr, S	P(Zr)	Cu (Si)
Chlorite-Magnetite Schist	Ti,V,Ni,Cr, K,P	Ca,Mg,Sr Cu	Si Zr,Y	Al,Ba (K)	Mn (Zr,Ni)	
Silicified Dolomite	Ca,Mg,LOI	Ti,Al,K	V As,Cu,S	Nb,Zr	P,Y	(Fe,Na)
Graphitic Pelite /	Ti,V K,P	Nb,Y Cr Zn	Si,Na	S (Fe,As,Cu Sr)		
LOZ	V Na,Ca,Al As,Cu,S	Ni Fe,Mn Y,Sr				
Banded Chlorite-Sericite-Garnet Schist	Nb,Zr,Y Mg,LOI Na,Ba,Sr	Ti,Ni Fe,Mn,Al Zn				
Banded QBCP Schist	Ca,Mg,Sr Nb,Y,Zr As,S Ni K	Ba Cu				

The relationship of Ba is not clear. The second factor is subdivided into two subfactors. MgO, Cr and Ni are related to the mafic component of the rock possibly derived from an olivine or pyroxene precursor. Na_2O and SiO_2 may be related to plagioclase. Factor 3 has three subfactors. Nb and Y are refractory components and are probably related to the mafic component of the rock and K_2O and Sr may relate to biotite which occurs in 159-4. As is related to the increase in sulphides often accompanning biotite.

Six factors are distinguished for the FDCBQ Schist. Factor 1 is made up of three subfactors. V, Ni, Cr, Nb, Y and Zr are similar to Factors 1, 2, and 3 of the Foliated Amphibolite, considered to be mafic indicators. FeO and Zn may be associated with a sulphide component and Ba with biotite. Factor 2, As and S, is a sulphide association. Factor 3, K_2O, Al_2O_3 and TiO_2, reflects the association of biotite and ilmenite. The significance of Factor 4 is unclear. Factor 5, MgO, FeO and V, is a ferro-magnesium association probably representing chlorite altering from hornblende. Factor 6 of Sr and to a lesser extent Ba and LOI is possibly a mixed association of mica and carbonate

Five factors are distinguished for the veined FDCSBQ Schist. Factor 1 is the same as Factor 1 for the FDCBQ Schist and reflects a mafic component to the rock. Factor 2 is a carbonate factor. Factor 3 is a sulphide factor. The significance of Factor 4 (P_2O_5) is unclear. It may represent apatite which is noted in thin section. K_2O, Ba and Sr, Factor 5, reflects the sericite and to a lesser extent biotite.

Six factors are distinguished for the Massive Ferroan Dolomite. Factor 1 is divided into 3 subfactors: SiO_2 is associated with quartz, Cu and S with chalcopyrite and Ba and K_2O to sericite. Factor 2 is difficult to interpret . It appears to relate to Factor 3 of the Foliated Amphibolite and Factor 4 of the Silicified Dolomite. Factor 3, Al_2O_3 and FeO, is associated with chlorite of the chlorite-sericite partings common to this rock type. TiO_2 and V of Factor 4 may represent ilmenite. Factor 5 is a mafic rock association and Factor 6 is a combination of carbonate, sulphide and mafic rock associations.

Six factors are determined for the Sericite-Chlorite Schist. Factor 1 has three subfactors: TiO_2 and V are associated with ilmenite, Al_2O_3 and Ba are associated with sericite and Zr may reflect rare zircon inclusions within the sericite. Factor 2 is difficult to interpret. The weak association of FeO and As probably reflects the occurrence of arsenopyrite, but the FeO and Zr association is not obvious. Factor 3 of Na_2O and Sr may be a plagioclase association, as plagioclase porphryoblasts are common. Factor 3 of Ni, Cr and S may reflect a mafic component as may Factor 5 as indicated by Factor 1 of the Foliated Amphibolite. Factor 6 is a sulphide association.

Five factors are determined for the Chlorite-Magnetite Schist. Factor 1 has two subfactors: TiO_2, V, Ni, Cr are interpreted to reflect a mafic component whereas the association of K_2O and P_2O_5 is unclear. Factor 2 is a carbonate association . Zr and Y (Factor 3) reflects an immobile component. Factor 4 is related to sericite and Factor 5 may be related to ilmenite or carbonate.

Five factors are determined for the Silicified Dolomite. Factor 1 is a carbonate association. Factor 2 is related to sericite with associated rutile. Factor 3 is a sulphide component. Factor 4 is reflects an immobile component as does Factor 5 which may be zircon and apatite.

Four factors are determined for the Graphitic Pelite. Ti_2 and V of Factor 1 is related to ilmenite, but the association of K_2O and P_2O_5 is unclear. Factor 2 reflects a refractory component of possible mafic origin as seen in Factor 3 of the Foliated Amphibolite. Factor 3, of SiO_2 and Na_2O may be plagioclase, commonly developed as porphyroblasts. Factor 4 is a sulphide component made up of pyrrhotite, chalcopyrite and arsenopyrite.

Two complex factors are related to the Quartz Cemented Graphitic Pelite Breccia. Factor 1 can be divided into three subfactors. Na_2O, CaO and Al_2O_3 may relate to plagioclase and carbonate. As, Cu and S clearly relates to sulphides of arsenopyrite and chalcopyrite. V may relate to ilmenite. Factor 2 can be divided into three subfactors. Fe and Mn may relate to carbonate. Y and Ni are refractory components possibly reflecting a mafic origin of the Graphitic Pelite host. The association of Sr is unclear.

Two complex factors are calculated for the Banded Chlorite–Sericite–Garnet Schist. Factor 1 is subdivided into three subfactors. Nb, Zr, and Y are immobile components. Mg and LOI reflects a carbonate component and Na_2O, Ba and Sr may reflect sericite and plagioclase. Factor 2 is also divided into three subfactors. TiO_2 and Ni are related to a mafic component. FeO, MnO and Al_2O_3 can be associated with spessartine rich almandine garnet. The association of Zn is unclear.

Two complex factors are determined for the Banded QBCP Schist. Factor 1 can be subdivided into five possible subfactors. CaO, MgO and Sr may be related to carbonate. Nb, Y, and Zr are immobile components. As and S are a sulphide factor, probably arsenopyrite. Ni may reflect a mafic component. K_2O may be associated with biotite. Factor 2 components of Ba and Cu associations are not clear.

4.3.3. Factor analysis for all rock types combined

Six factors are distinguished in considering all the rock types. Factor 1 is made up of FeO, TiO_2, Ni, Cr, and V which is interpreted to represent a strong mafic contribution to the rocks. Factor 2 is SiO_2; however, it also shows strong negative correlation with MgO, CaO and LOI, the carbonate factor. Factor 3 is the association of Nb, Zr, Sr and Zn. Nb and Zr are immobile components of possible mafic contribution. The association of Sr and Zn is unclear but Zn is often associated with Nb and Zr. Factor 4 is K_2O and Ba which is dominatly sericite with minor biotite. Factor 5 shows the association of FeO, As and Cu and to a lesser extent V and S. This is the sulphide association. Factor 6 is a weak association of Al_2O_3 and FeO. This may well reflect the development of such minerals as chloritoid.

4.4.4. Discussion

The mafic association of V, Ni, and Cr in the FDCBQ and veined FDCSBQ Schists, Massive Ferroan Dolomite, Sericite-Chlorite Schist and Chlorite-Magnetite Schist furthur supports the suggestion that these rocks were originally basaltic in composition.

The negative correlation of the carbonate factor to the silicate factor suggests that the process of carbonatization as occurs in the FDCBQ Schist, veined FDCSBQ Schists and Massive Ferroan Dolomite, replaces the silicate fraction of the rocks. This is consistent with the process of carbonatization (See Section 6.3)

The K_2O and Ba factor is one of sericitization. K_2O and Ba are elevated in the Sericite-Chlorite Schist and to a lesser extent Chlorite-Magnetite Schist (Figures 4.6a); however, as seen in Table 4.5 the association is also common to the veined EDCBSQ Schist and MasSive Ferroan Dolomite suggesting a Similar process.

The association of FeO, As and V, is a sulphide factor, but should also be considered a mineralization factor. Gold is invariably related to the presence of arsenopyrite. It appears, therefore, that FeO is the only major oxide which can be related to gold mineralization. This will be further discussed in Section 6.8 on gold solubility.

Nb and Zr consistently group together as a factor interpreted to represent a consistent behavior as a refractory component. This consistent behavior is taken to indicate element immobility and is used in deciding on the immobile components in the mass balance calculations (Section 4.4.)

4.4. Mass Balance Calculations for Upper 90 m of Borehole 159

4.4.1 Introduction

It is suggested that the alteration of Foliated Amphibolite occurs through carbonatization, sericitization and sulphidization. The upper 90 m of Borehole 159, as illustrated in Figure 4.16a

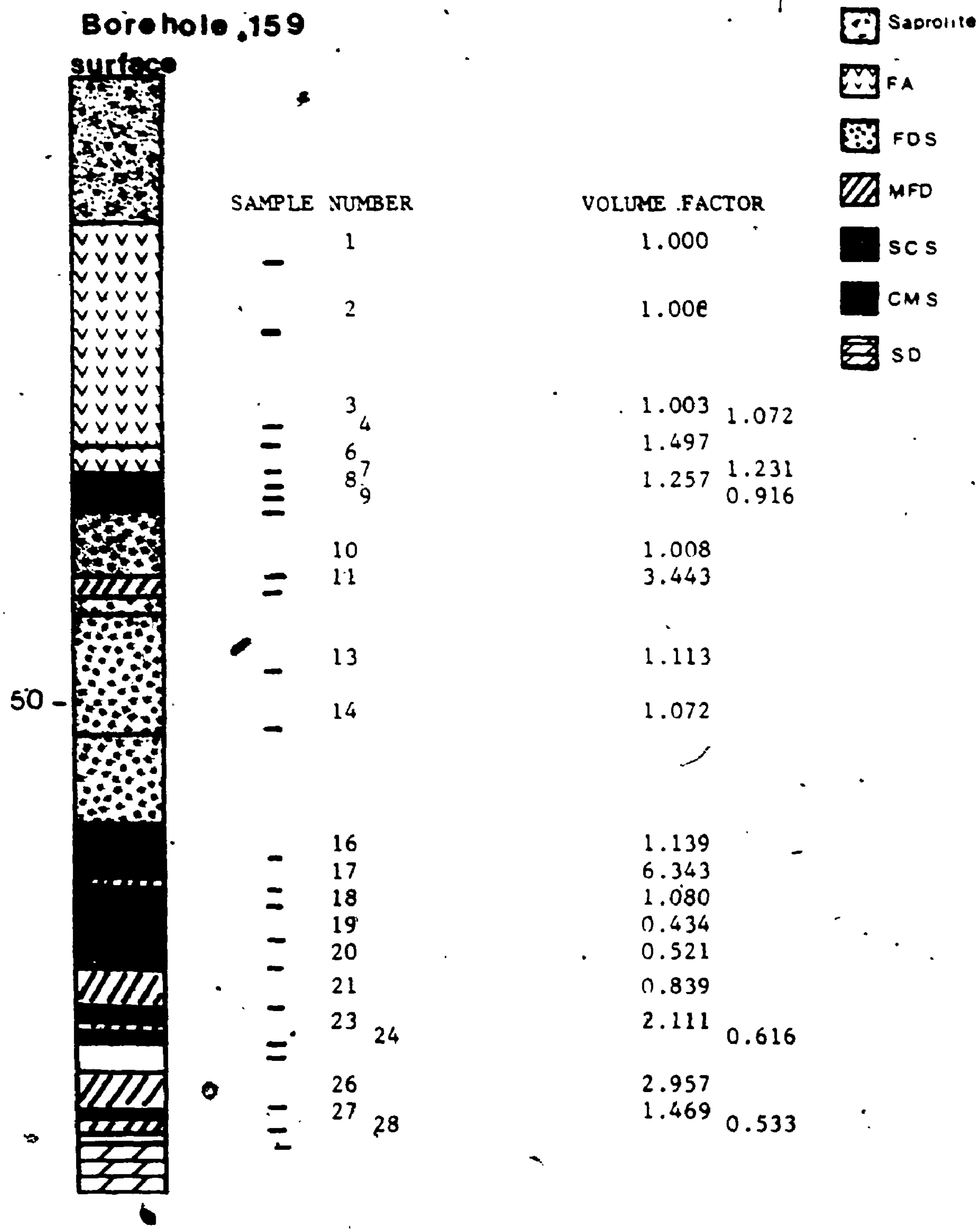

Figure 4.16 a. Detailed geology of the first 90 metres of Borehole 159. Samples from this hole used in Mass Balance calclutions. Also included are volume factors relative of Sample 159-1 a Foliated Amphibolite.

provides a detailed downhole section which includes Foliated Amphibolite, FDCBQ Schist, veined FDCSBQ Schist, Massive Ferroan Dolomite, Sericite-Chlorite Schist and Chlorite-Magnetite Schist. These samples are used in the mass balance and volume calculations presented below. It is the aim of this procedure to see if the chemical gains and losses as well as the volumes gains and losses are consistent with the alteration processes suggested.

Gresens (1967) presents a method of quantifying the relationship between composition and volume changes that accompany a metasomatic or hydrothermal alteration of a parent rock to a daughter rock. The change in a chemical component n is expressed as x_n, where,

$$x_n = a(f_v(pB/p_A)c_nB-c_nA) \quad (1)$$

and:

a = amount of parent rock in grams (usually considered to be 100 for convience)

f_v = volume factor
p_A = specific gravity of parent rock
p_B = specific gravity of daughter rock
c_nA = weight fraction of component n in parent rock
c_nB = weight fraction of component n in daughter rock

To solve equation (1) it is necessary to know either the volume change or the geochemical behavior of one or several components. As shown by Weerasoyria and Larson (1987,in preparation) if one considers a single element or group of elements immobile, x_n is solved through simple ratioing:

$$x_n = a\,(c_iA/c_iB)c_nB-c_nA \quad (2)$$

In calculating the volume changes associated with the alteration, specific gravities of the parent and daughter rocks must be known and the change in component i is zero thus deriving the relationship:

$$f_v = (pA/_{pB})*(c_iA/_{c_i}B)$$

or

$$= {}^{v}B/_{v_A}$$

The immobile elements used in the mass factor calculation are TiO_2, Al_2O_3, Zr. In most cases the mass factor is an average of these three elements; however where they differ significantly, TiO_2 and Al_2O_3 are preferentially used. When these two elements differ significantly, TiO_2 is used in the mass factor calculations. This is based on the geochemical evidence that TiO_2 tends to become encriched (Figure 4.13b).

The percent gains and losses of volume relative to the Foliated Amphibolite are also presented. One hundred grams of the Foliated Amphibolite with a volume of 33.56 cm^3 based on a determined specific gravity of 2.98 for Sample 159-1.

Sample 159-1 is considered the parent rock. The whole rock analyses of Sample 159-1 and other samples are presented in Appendix I. Null values are converted to 0.001 weight percent and 0.001 ppm in the mass balance calculation.

4.4.2.1 Percentage Mass Gains and Losses of Elements and Volume.

Figures 4.16 b to m inclusive, show the log of the percent mass gains and losses of various components. These include: SiO_2, TiO_2, Al_2O_3, FeO, MnO, MgO, CaO, Na_2O, K_2O, Ba, As, S. Figures 4.16n and 4.16o present the log of the percentage gains and losses in LOI (includes CO_2) and volume. The behavior of the various elements can be divided into several groups:

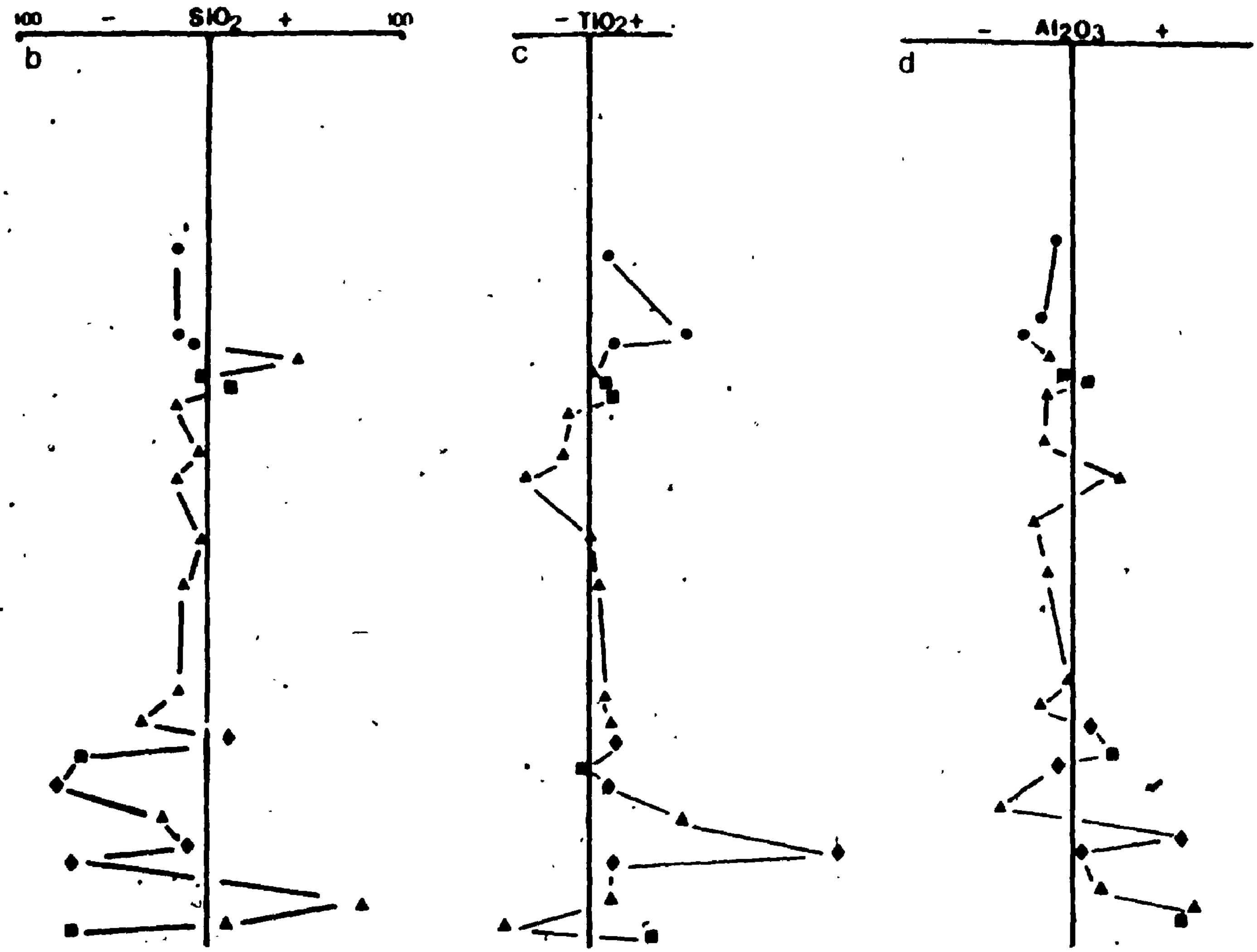

Figure 4.16b+c+d. Mass balance log % gains and losses of SiO_2, TiO_2 and Al_2O_3. Symbols for Figures 4.16 b to p: circle, Foliated Amphibolite; triangle, Sericite-Chlorite Schist; square, Chlorite-Magnetite Schist; diamond, Massive Ferroan Dolomite.

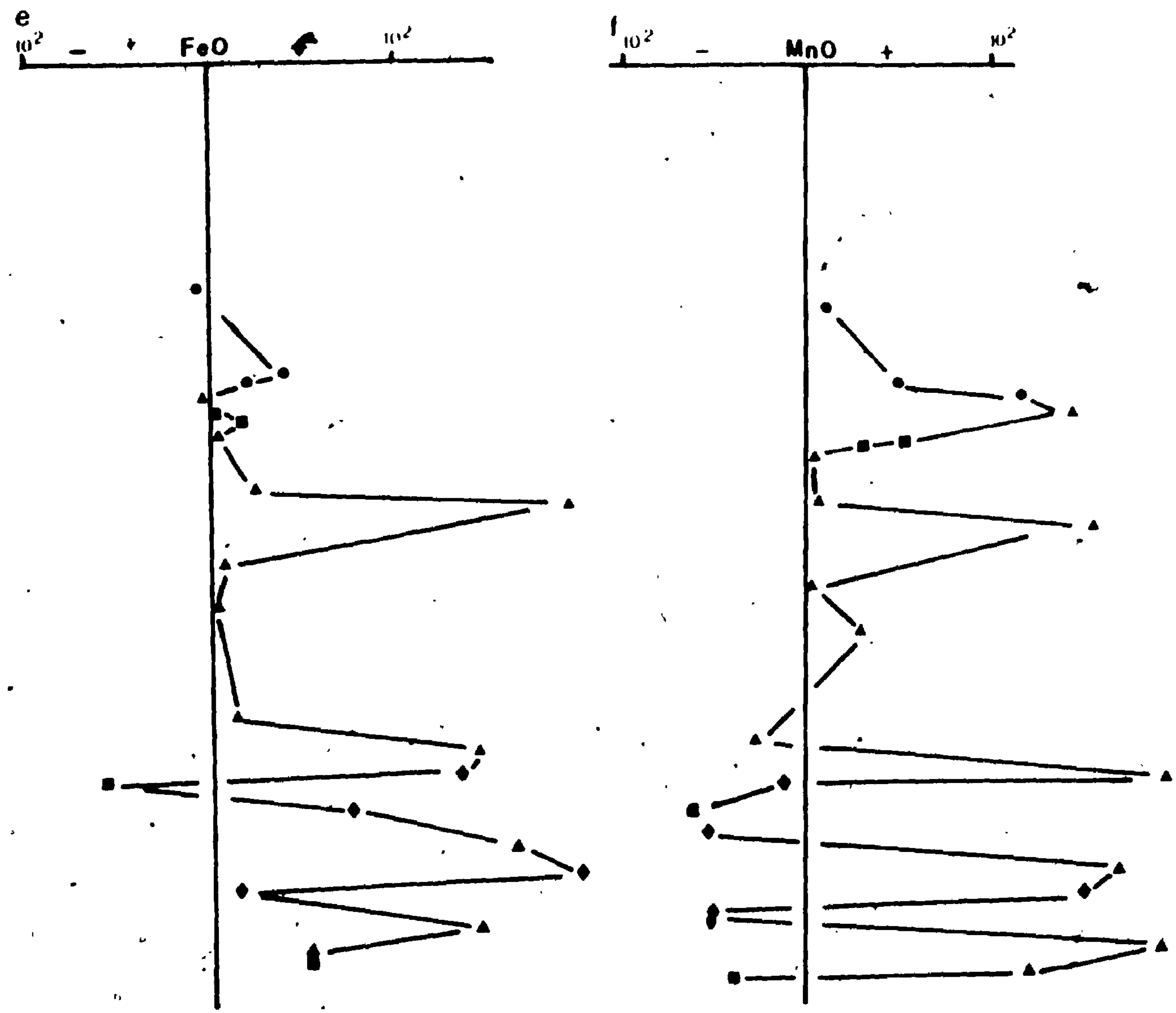

Figure 4.16 e & f. Percent gains and losses of FeO and MnO. (log scale).

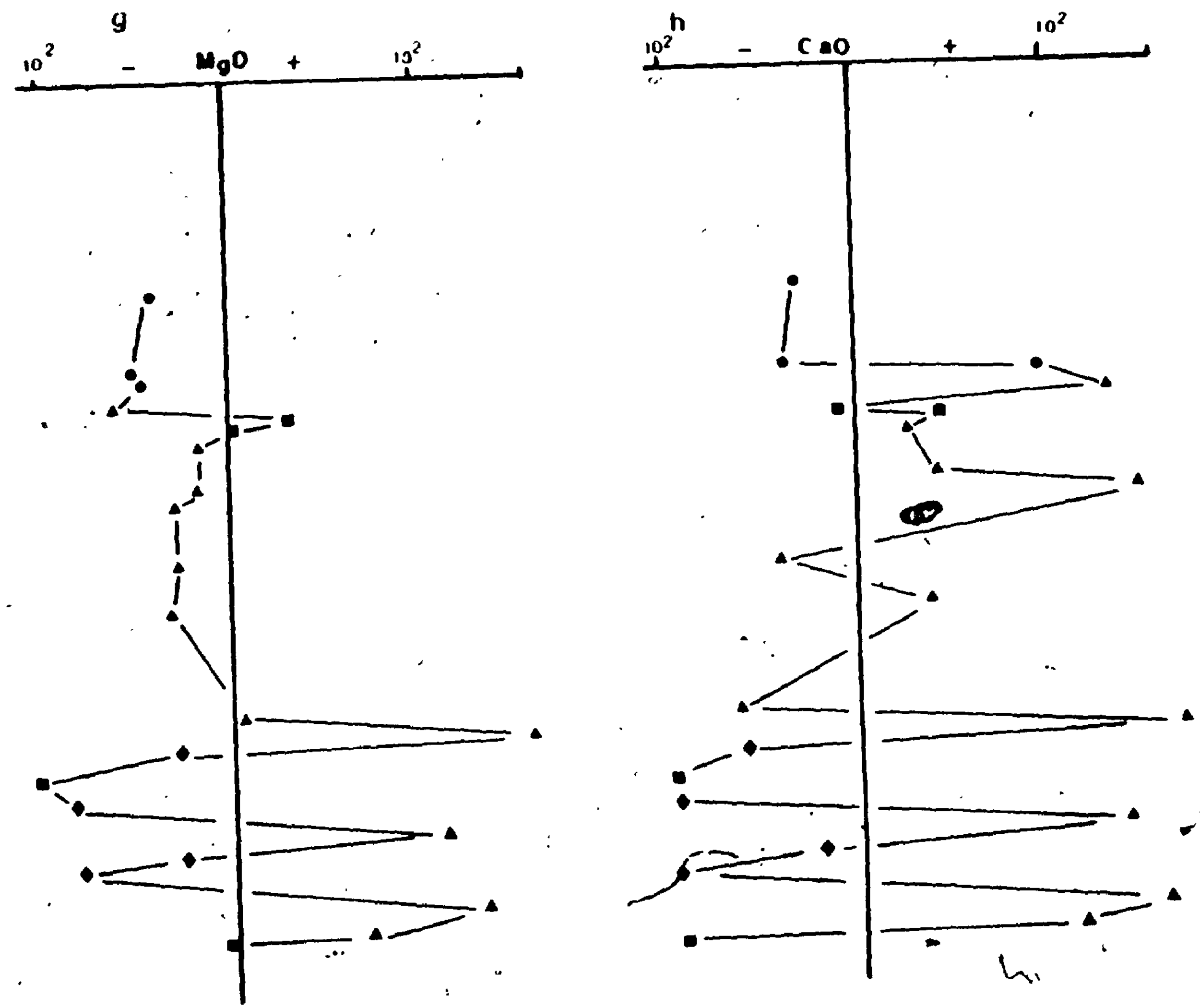

Figure 4.16 g & h. Percent gains and losses of MgO and CaO. (log scale).

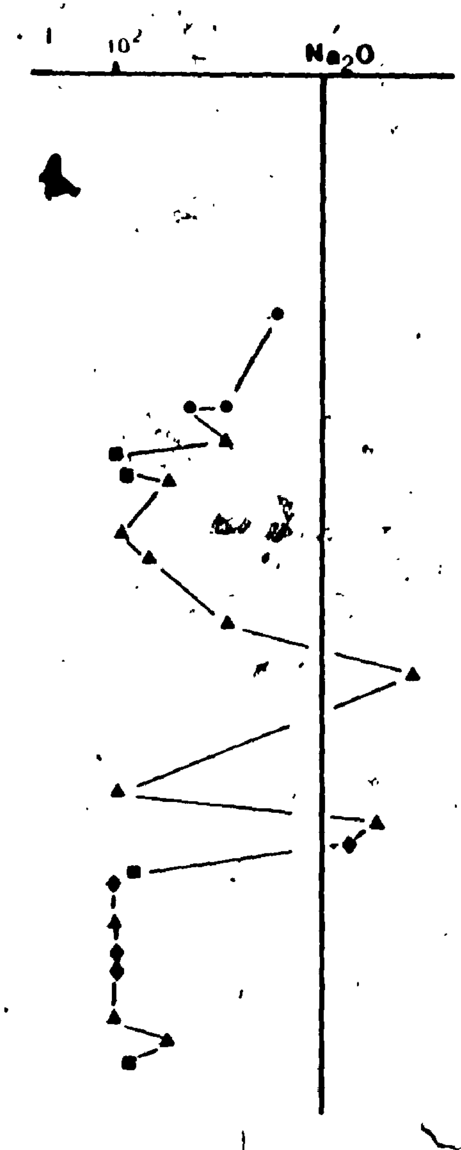

Figure 4.16 i. Percent gains and losses of Na_2O. (log scale).

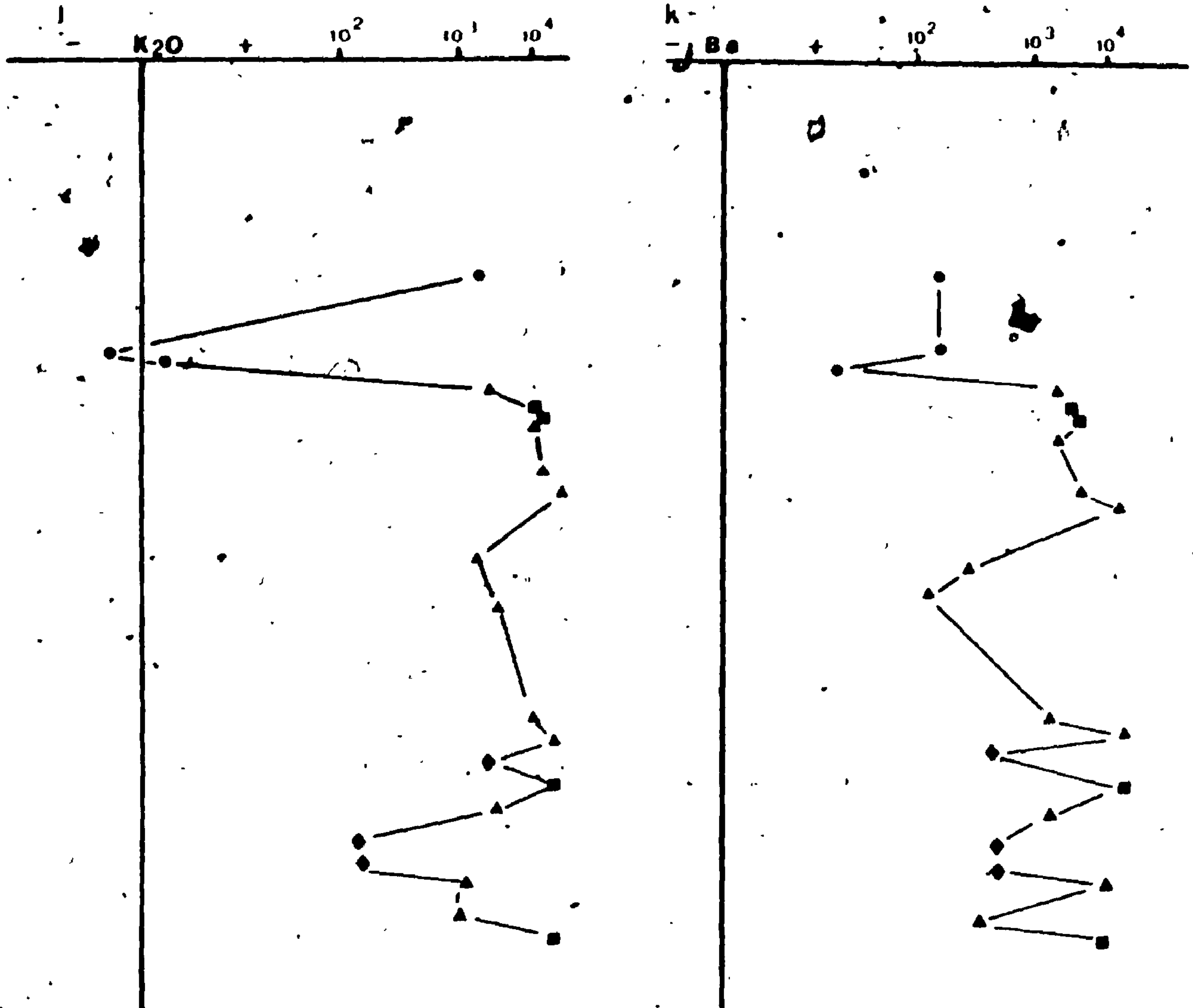

Figure 4.16 j & k. Percent gains and losses of K_2O and Ba. (log scale).

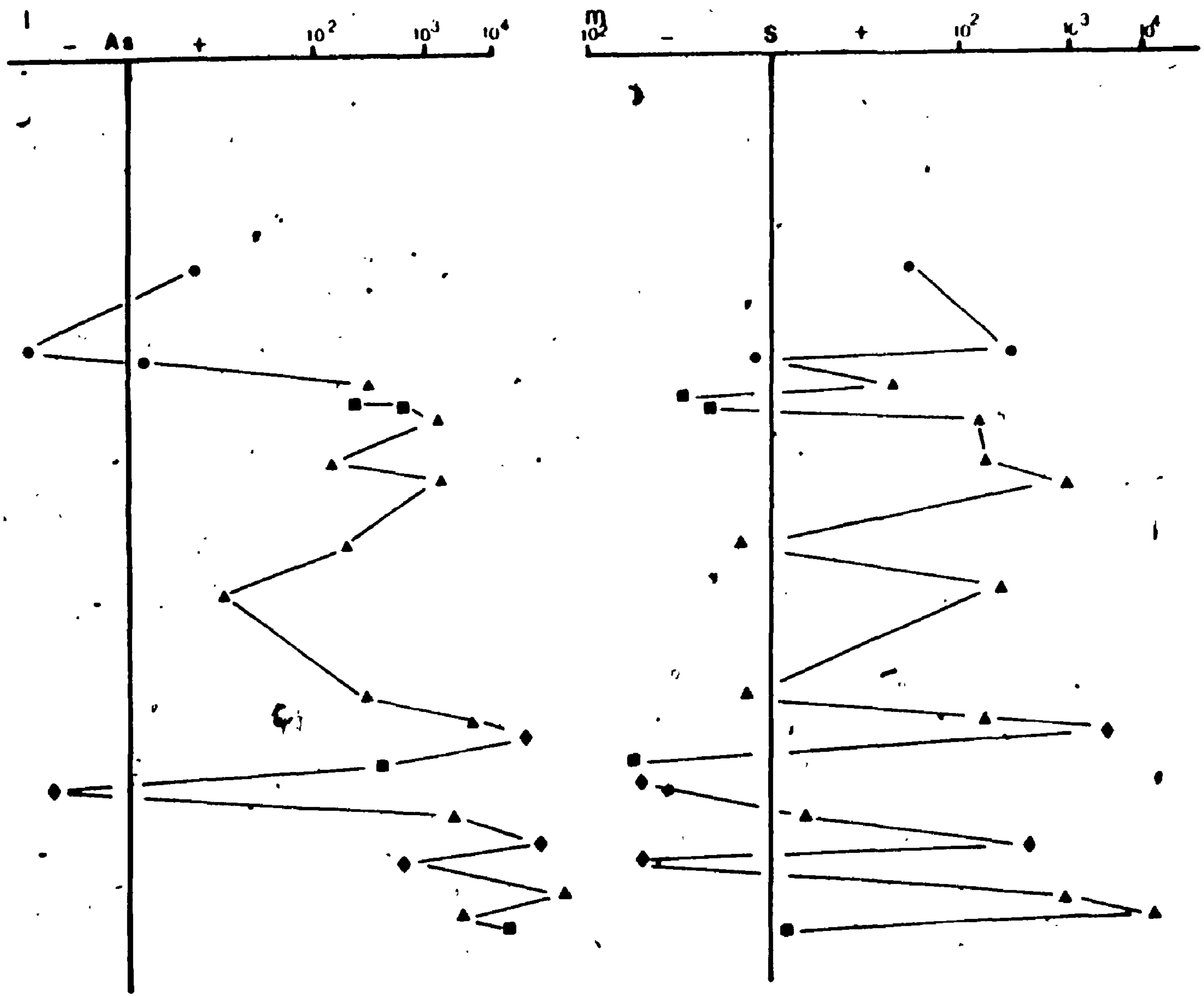

Figure 4.16 l & m. Percent gains and losses of As and S. (log scale).

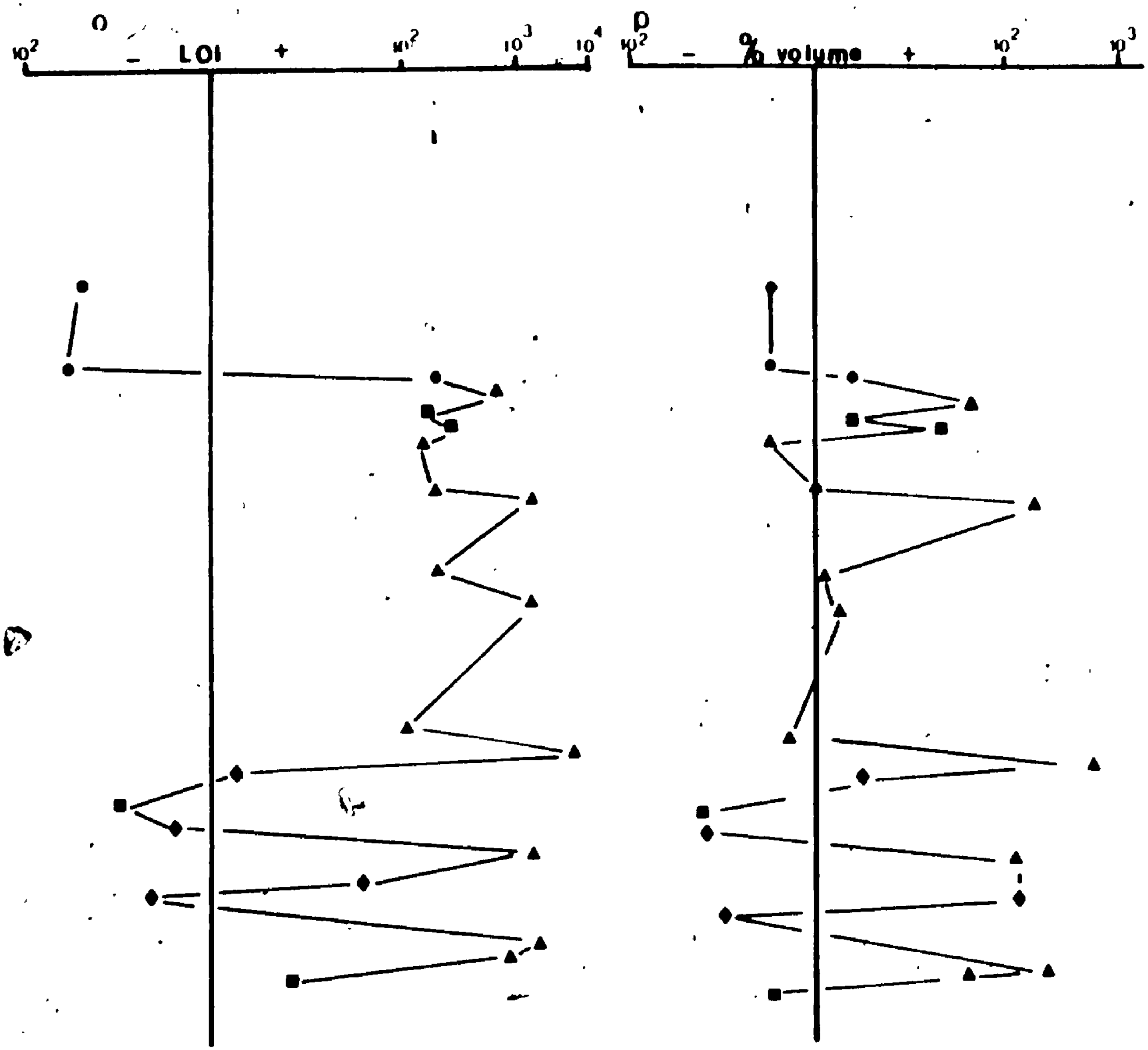

Figure 4.16 o & p. Percent gains and losses of LOI and volume. (log scale).

Group 1: TiO_2 and Al_2O_3
Group 2: FeO, MnO, MgO, CaO LOI and volume
Group 3: K_2O and Ba
Group 4: As and S
Group 5: SiO_2
Group 6: Na_2O

In addition to element groupings the behavior of the elements vary consistently according to the rock type. Samples 159-1, 159-2, 159-3, 159-4 are Foliated Amphibolites. Group 1 elements show minor gains and losses, whereas Group 2 elements show losses in Samples 159-2, 159-3 and gains in Sample 159-4 (Figures 4.16 c and d). K_2O of Group 3 shows a large gain in Sample 159-3, whereas Sample 159-4 shows a small loss (Figure 4.16 j). Ba also shows large gains in Samples 159-2, 159-3 and to a lesser extent Sample 159-4 (Figure 4.16 k). Group 4 components do not behave consistently. Sample 159-2 shows an increases in As and S, Sample 159-3 shows a decrease in As and an increase in S and Sample 159-4 shows an increase in As and decrease in S (Figures 4.16 l and m). SiO_2 and Na_2O both show decreases in mass (Figures 4.16 b and i).

Samples 159-6, 159-14 and 159-16 are FDCBQ Schist. Group 1 components show very minor mass gains and losses from the Foliated Amphibolite parent. Group 2 components behave consistently within each sample but not between samples. Sample 159-6 shows gains, Sample 159-16 shows losses in all Group 2 components. Sample 159-14 shows gains in CaO and volume and losses in FeO, MnO and MgO. The Group 3 components show percentage mass gains. Group 4 components are not consistent in mass gains and losses from sample to sample. In Samples 159-6 and 159-16 As and S are gained but in Sample 159-14, As and S are gained relative to 159-1 but As breaks the trend with S showing a relatively small gain. SiO_2 (Group 5) is generally lost while Na_2O shows gains in 159-14 and 159-16 and a loss in 159-6.

Samples 159-9,159-10 and 159-13 are veined FDCSBQ Schists. Group 1 components show slight losses. Group 2 components behave consistently within and between samples. Small losses are associated with FeO, MnO, MgO and small gains are associated with CaO and volume. K_2O and Ba (Group 3) shows large gains which are larger than that of the FDCBQ Schist but slightly lesss than the Sericite-Chlorite Schist. Arsenic shows mass percentage gains within the same range for the three samples. Mass gains of S occur in Samples 159-9 and 159-10 whereas there is a small loss in Sample 159-13. Both SiO_2 and Na_2O show small mass losses, but there is an increase in the trend for Na_2O.

Samples 159-11, 159-17, 159-21, 159-26 and 159-27 are Massive Ferroan Dolomite. Group 1 components show slight gains and losses with the exception of Al_2O_3 in Sample 159-11 which shows large percentage mass gains. The Group 2 components are very consistent in their relative behavior with all showing large percentage gains. These gains are often the largest seen for all rock types shown in the geologic profile. Similar trends in large gains are seen in the components of Group 3 and 4. SiO_2 shows small gains while Na_2O generally shows large losses with the exception of Sample 159-17 which shows a large gain.

Samples 159-7, 159-8, 159-19, 159-24 and, 159-28 are Sericite-Chlorite Schist. Group 1 components show minor percentage mass gains and losses. Group 2 components generally show slight to large losses. Group 3 components show large gains as do Group 4 components; however, S is closely correlative with As. SiO_2 and Na_2O generally show large losses with the expection in Samples 159-7 and 159-8 where SiO_2 shows small losses and gains respectively.

Samples 159-18, 159-20 and 159-23 are Chlorite-Magnetite Schists. The Group 1 components show small gains and losses in Samples 159-18 and 159-20 but large gains in Sample 159-23. The Group 2 components do not behave consistently. MnO, MgO and CaO show small to large percentage mass losses and FeO shows small to large gains in all samples. The LOI and volume of Samples 159-18 and 159-23 show small to large gains whereas in Sample 159-20 these components show small to large losses. The Group 3 components show percentage mass gains relative to sample 159-1 but are relatively the smallest gains. The Group 4 components behave much as LOI and volume, showing large gains in Samples 159-18 and 159-23 but large losses in Sample 159-18. SiO_2 and Na_2O show small relative increases in 159-18 and large decreases in Samples 159-20 and 23.

4.4.3 Discussion

Mass gains or losses of rock forming elements must be reflected in a change of mineralogy. It is not surprising, therefore, that five of the six groups distinguished are mineral forming components:

Group 1 components of TiO_2 and Al_2O_3 are artifacts of choosing them as immobile for the mass factor calculations.

Group 2 components of FeO, MnO, MgO CaO, LOI and volume, in general, represent carbonate mineralogy; however as shown above there is not always a strict correlation. For instance, in the FDCBQ Schist, gains are related to CaO, LOI and volume and losses are related to FeO, MnO and MgO. It is suggested that FeO, MnO and MgO remain partially related to chlorite, biotite and ilmenite, reflecting the vestiges of the parent rock mineral chemistry.

Group 3 components, K_2O and Ba, reflect the presence of sericite and to a lesser extent biotite in the assemblage.

Group 4 components, of As and S indicate the gains and losses of the sulphides, arsenopyrite, pyrrhotite and chalcopyrite. The local lack of direct correlation of As to S is believed to result from the association of S with pyrrhotite and chalcopyrite without significant arsenopyrite.

Group 5 is represented by SiO_2. It shows small to moderate percentage mass losses. This appears to be contradictory to the occurence of quartz veins in the veined FDCSBQ Schist. However; carbonatization results in desilicification with the best example of this process being serpentization (Hyndman, 1985, pg. 556).

Group 6, Na_2O, is related to plagioclase. It shows a general percentage mass loss. The exceptions to this are Samples 159-14, 159-17 and 159-18 which show Na_2O gains. This may reflect the presence of plagioclase porphryoblasts.

The calculation of the percentage volume gains and losses provides valuable information regarding the nature of behavior of the elements choosen as immobile components in the mass factor calculation. TiO_2 is taken as immobile in these calculations. In Figure 4.10a FDCBQ Schist, veined FDCSBQ Schist and Massive Ferroan

Dolomite show TiO_2 loss and large carbonate group component gain (Figure 4.16g, h, n). Sericite-Chlorite Schist and Chlorite-Magnetite Scist show TiO_2 gain and large sericite group component gains (Figures 4.16j, k, n). This is not fortuitous, and is related to the volume changes associated with alteration. Rocks with TiO_2 loss show volume gains reflecting dilution of the immobile element, due to carbonatization. Rocks with TiO_2 gain show volume losses reflecting concentration of the immobile element, due to sericitization.

4.5. Summary

Geochemistry of the Minas III rock suite supports the distinction of the twelve rock types presented in Chapter III. It also distinguishes the difference between altered and unaltered lithologies and the nature of that alteration. Table 4.6 summarizes the findings of Chapter 4.

Table 4.6. Summary of the geochemistry.

	Lithology	Process
Foliated Amphibolite	Parent	tholeiitic basalt
FDCBQ Schist*	Daughter	Carbonatization
veined FDCSBQ Schist*	Daughter	Carbonatization
Sericite-Chlorite Schist*	Daughter	Sericitization
Chlorite-Magnetite Schist*	Daughter	Sericitization Sulphidization
Silicified Dolomite	Parent	sediment
Graphitic Pelite	Parent	sediment
LOZ**	Daughter	Silicification
CPQFD Schist	Parent/Daughter?	dyke/sill? carbonatized
Banded Chlorite-Sericite-Garnet Schist**	Parent/Daughter?	Sericitization? sediment?
QBCP Schist	Parent	sediment

* - daughter of Foliated Amphibolite

** - daughter of Graphitic Pelite

CHAPTER FIVE

Mineral Chemistry

5.1. Introduction

The chemistry of minerals and the modification of the chemistry of minerals is governed by numerous parameters such as pressure, temperature, fluid composition (f_{O2}, f_{CO2}, f_{H2O}) and bulk rock chemistry. Careful analysis of the mineral chemistry of assemblages provides the basis for any investigation into the nature of the controlling parameters. In the following section the mineral chemistry of the silicate phases - amphibole, chlorite, biotite, sericite, plagioclase and chloritoid and the carbonate phases - calcite, dolomite and ferroan dolomite are presented.

The term ferroan dolomite is used in this study and is preferred to ankerite because of limited iron substitution in the dolomite structure. Reeder (1983) points out, "Where there are no readily adhered to rules, there does seem to be a preference to the term ankerite when referring to more Fe-rich phases along this limited join, and ferroan dolomite for those less Fe-rich" (Reeder,1983,p26).

Comprehensive mineral analyses are presented in Appendix II. The structural mineral formulae are calculated according to Deer et al., (1971). No attempt was made to charge balance the formulae to account for possible ferric iron substitution.

In the discussions below FDCBQ Schist and veined FDCSBQ Schist are grouped together and labelled Ferroan Dolomite Schist.

5.2.1. Foliated Amphibolite

5.2.1.1. Amphibole

The amphiboles of the Foliated Amphibolite are hornblendic (classification after Hawthorne, 1980). They range in composition from magnesio-hornblende to ferro-tschermakite (Figure 5.1). Included in Figure 5.1 are amphiboles from two regional amphibolites. Sample Cr-39 is taken from a relatively undeformed pillow lava locality while Sample Cr-52 is taken from a highly deformed rodded amphibolite locality. The amphibole compositions are magnesio-hornblende and ferro-tschermakite respectively. Samples 159-1 and K2-7 bear magnesio-hornblende whereas the amphibole of Sample K4-2 is ferro-tschermakite. The amphiboles of Sample K4-2 are poikiloblastic and cross-cut the fabric.

Variations in composition of calcic amphiboles are a function of A-site, octahedral and tetrahedral site substitutions. The most common of these substitutions are:

$$Al^{iv}Al^{vi} = Al^{iv}(Na+K) \quad (1)$$

$$Al^{vi} = Ti^{vi} \quad (2)$$

$$(Mg,Fe)2Si = Al^{vi}Al^{vi} \quad (3)$$

These substitutions are illustrated in Figure 5.2. Increases in Na+K is matched by an increase in Al^{iv} (Figure 5.2a, Substitution 1). Sample Cr-39 is the least hornblendic; 159-1, K2-7 and Cr-52 show a range and K4-2 is the most hornblendic. The same trend is seen in Figure 5.2b where increasing Ti content is matched by increasing Al^{iv} contents. A combination of substitutions 1 and 2 (Figures 5.2a,b) is illustrated in Figure 5.2c. Raase, 1974 has suggested that coupled Al^{iv} and Al^{vi} substitution represents increases in metamorphic

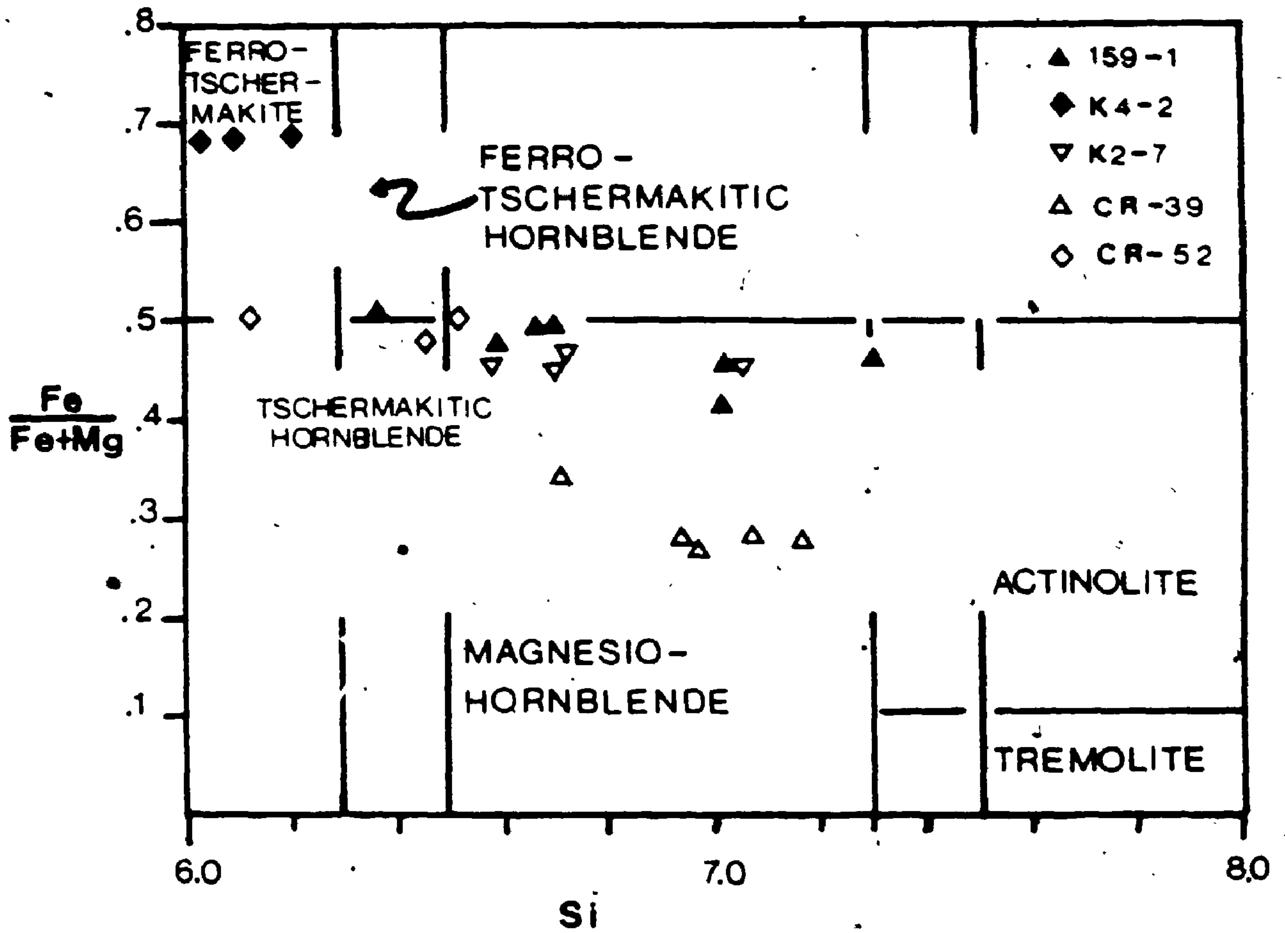

Figure 5.1. Amphibole classification diagram after Hawthorne (1983).

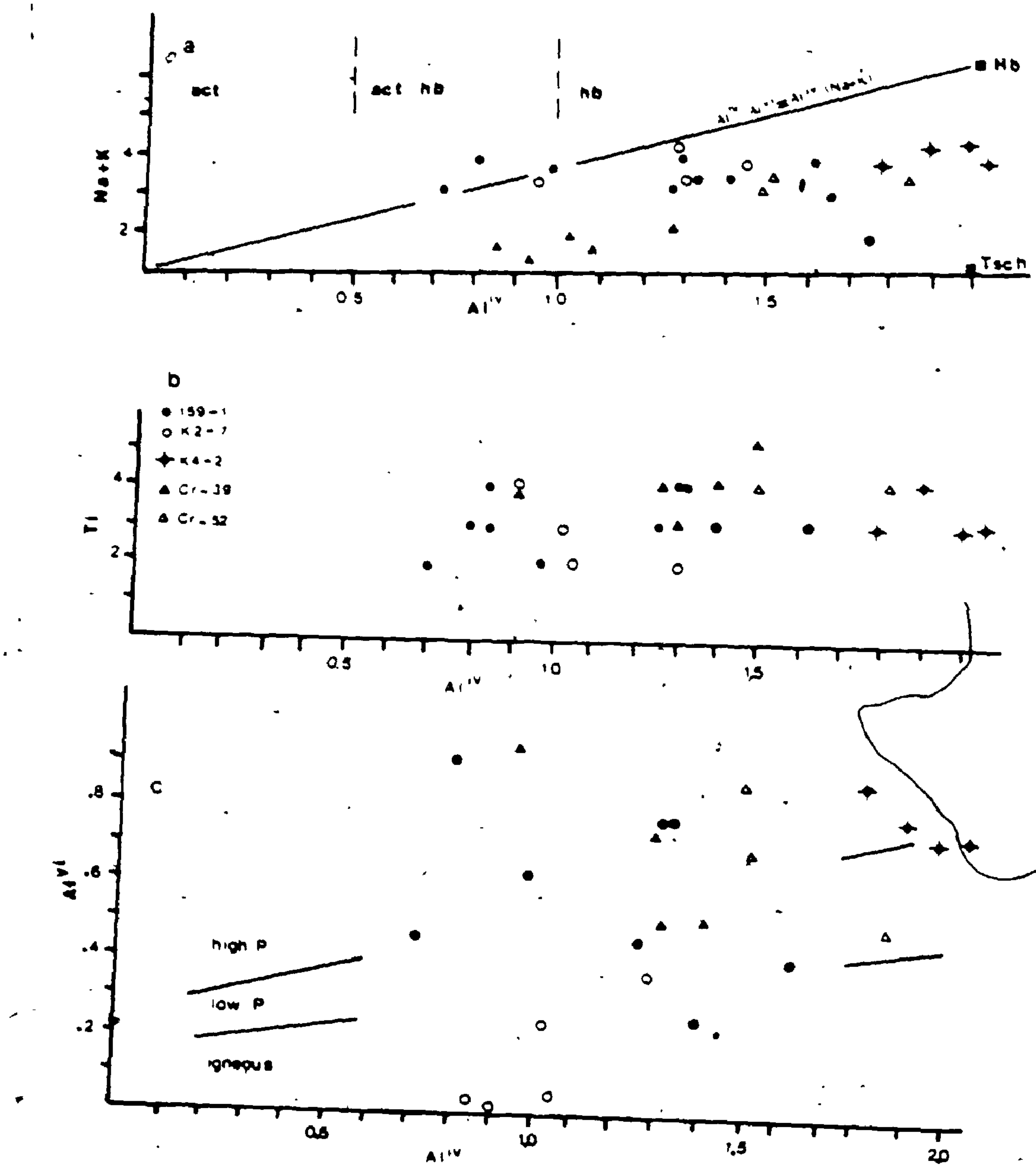

Figure 5.2. a) A-site (Na+K) versus Al^{iv} for Foliated Amphibolite and Regional Amphibolite. b) Ti versus Al^{iv} as in a. c) Al^{vi} versus Al^{iv} as for a. (after Raase, 1974).

pressure. Sample Cr-39, the pillow lava basalt, plots within the igneous field; Samples 159-1, K2-7 and Cr-52 plot dominantly in the low pressure region of less than 5 Kb, but several analyses plot in the high pressure region of greater than 5 Kb. Sample K4-2 plots dominantly in the high pressure region.

5.2.1.2 Chlorite

Chlorite of the Foliated Amphibolite shows an increase in Fe/(Fe+Mg) from Sample 159-1 to Samples 159-4 and 159-6 which are calcite bearing (Figure 5.3). As well, there is a progressive decrease in Si with increasing Fe. The decrease in Si is the result of Al substitution into the tetrahedral site, possibly representing the third (3) substitution presented above for the amphiboles. No textural changes are apparent with the shift in mineral chemistry.

5.2.1.3 Biotite

Biotite is restricted to Samples 159-4 and 159-6. Sample 159-6 is a calcite-chlorite-biotite-quartz schist and is best considered transitional between Foliated Amphibolite and FDCBQ Schist. The biotite compositions are intermediate between annite and phlogipite compositions based on Fe/(Fe+Mg) ratios (Figure 5.4a). They also show a range in Al_{vi} values with the lower values associated with a slight increase in Fe/(Fe+Mg) (Figure 5.4a). No consistent variation in Ti is associated with increases in Al^{iv} (Figure 5.5a).

5.2.1.4. Plagioclase

Albite is the characteristic plagioclase of Foliated Amphibolite samples (Table 5.1). The composition range is narrow, from $An_{0.8}$ to $An_{2.6}$, with two anomalous analyses from Sample 159-4 at $An_{8.4}$. Samples 159-4 and K2-7 show a slight core to rim variation of lower

Table 5.1. Plagioclase Feldspar Compositons

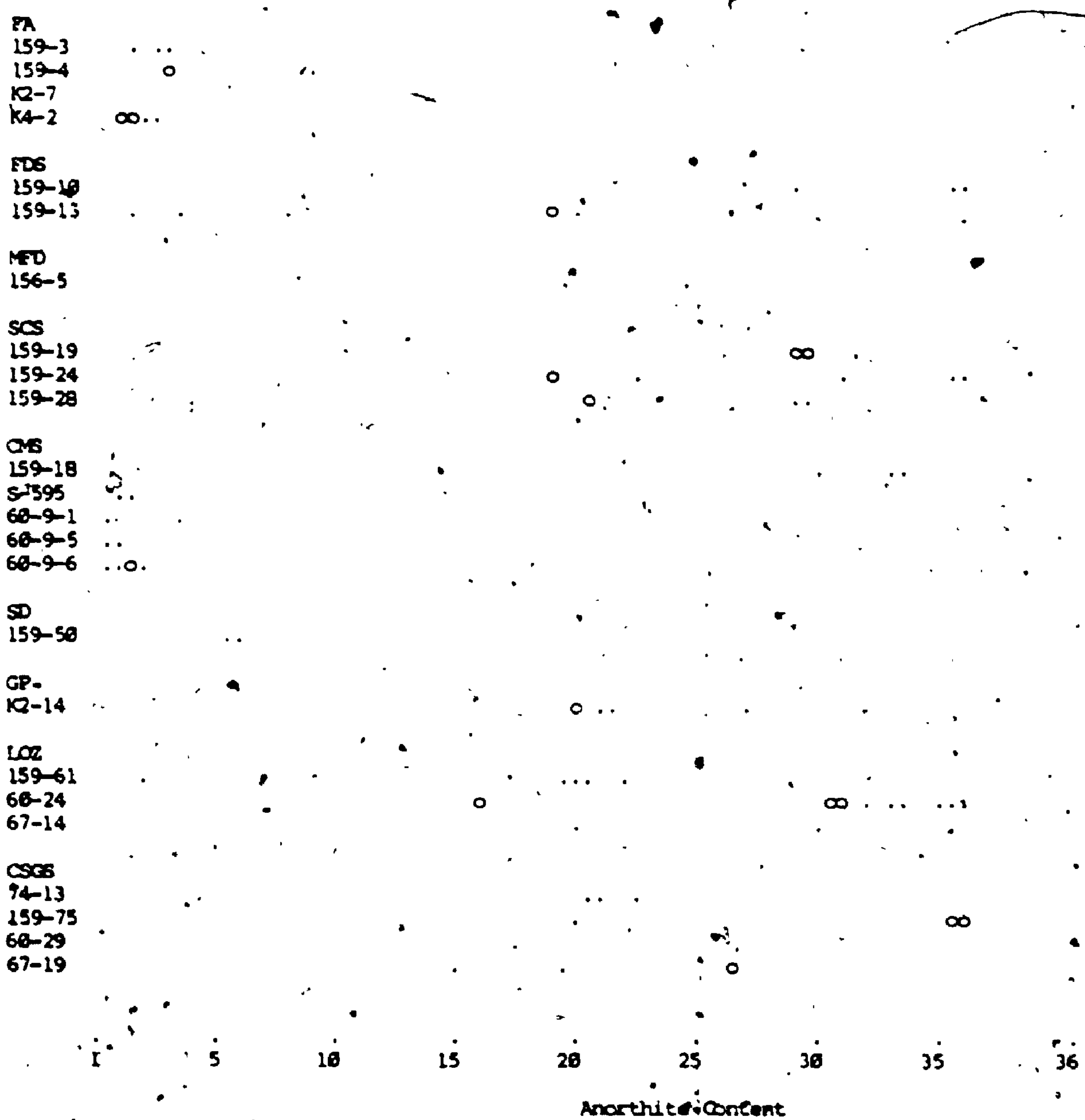

. core value
o rim value

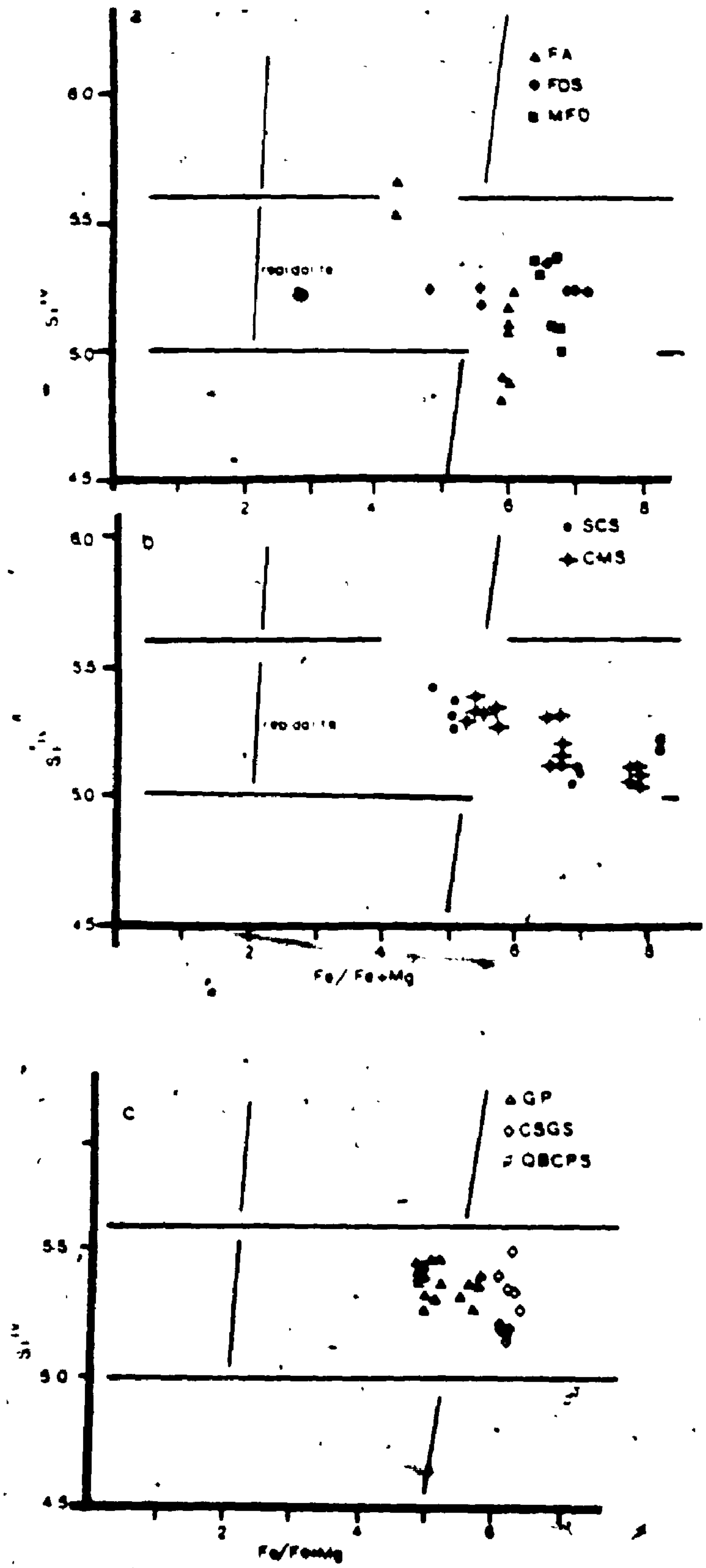

Figure 5.3 a - c. Chlorite classification diagram of all rock types.

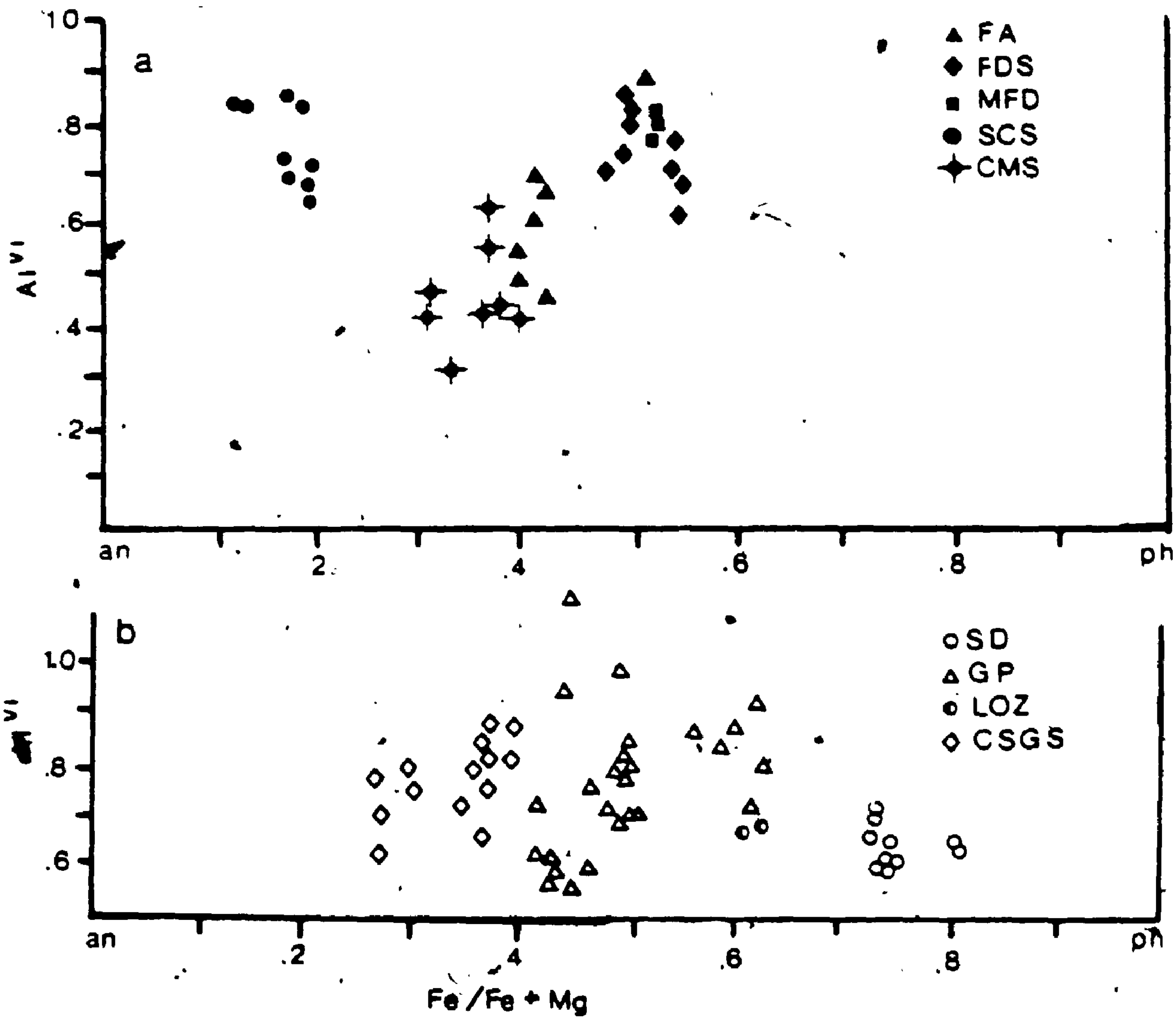

Figure 5.4 a & b. Biotite classification diagram. An = annite, ph = phlogopite.

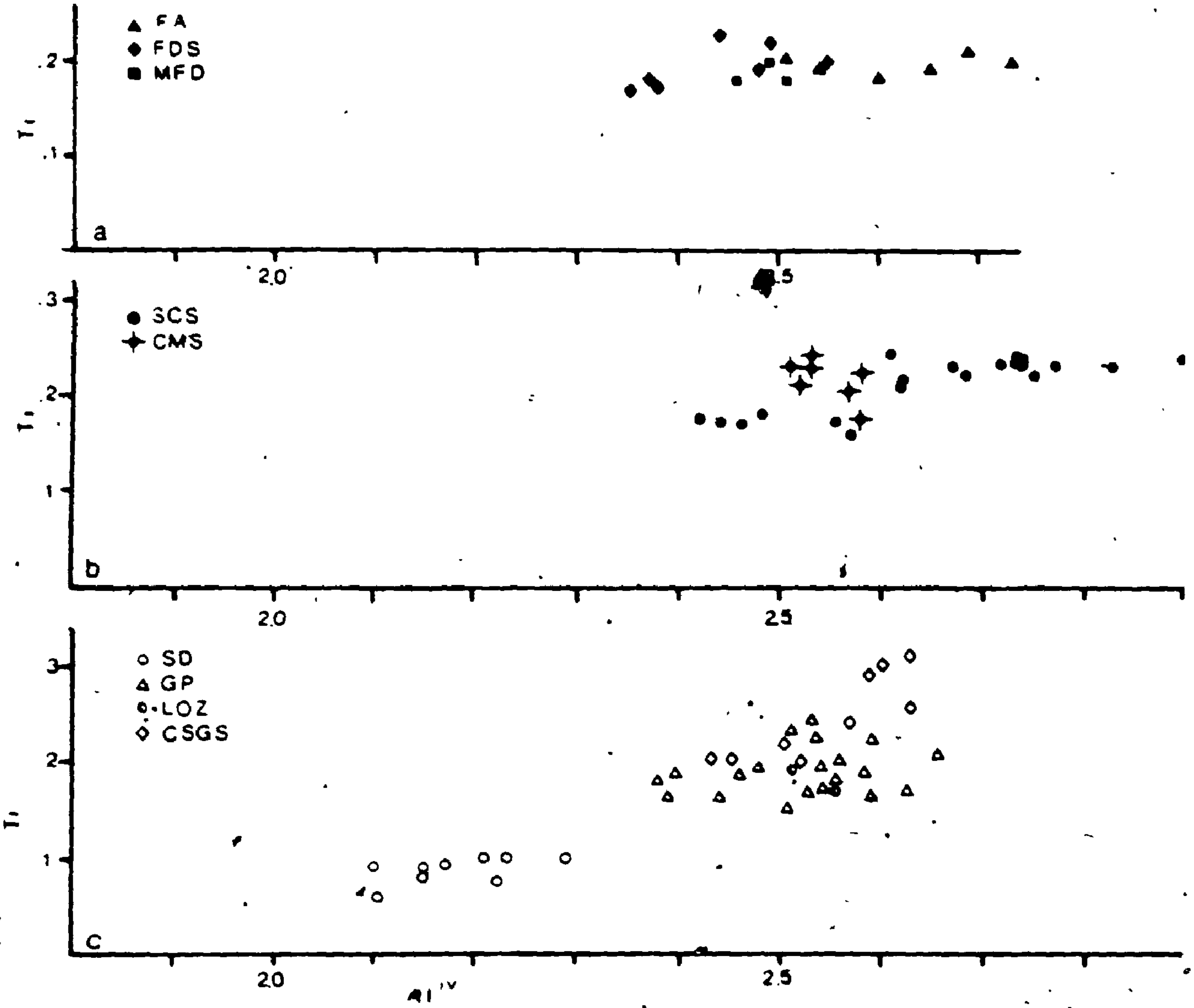

Figure 5.5 a - c. Al^{iv} versus Ti for biotite representing the substitution: $Mg^{vi}2Si^{iv} = Ti^{vi}2Al^{iv}$.

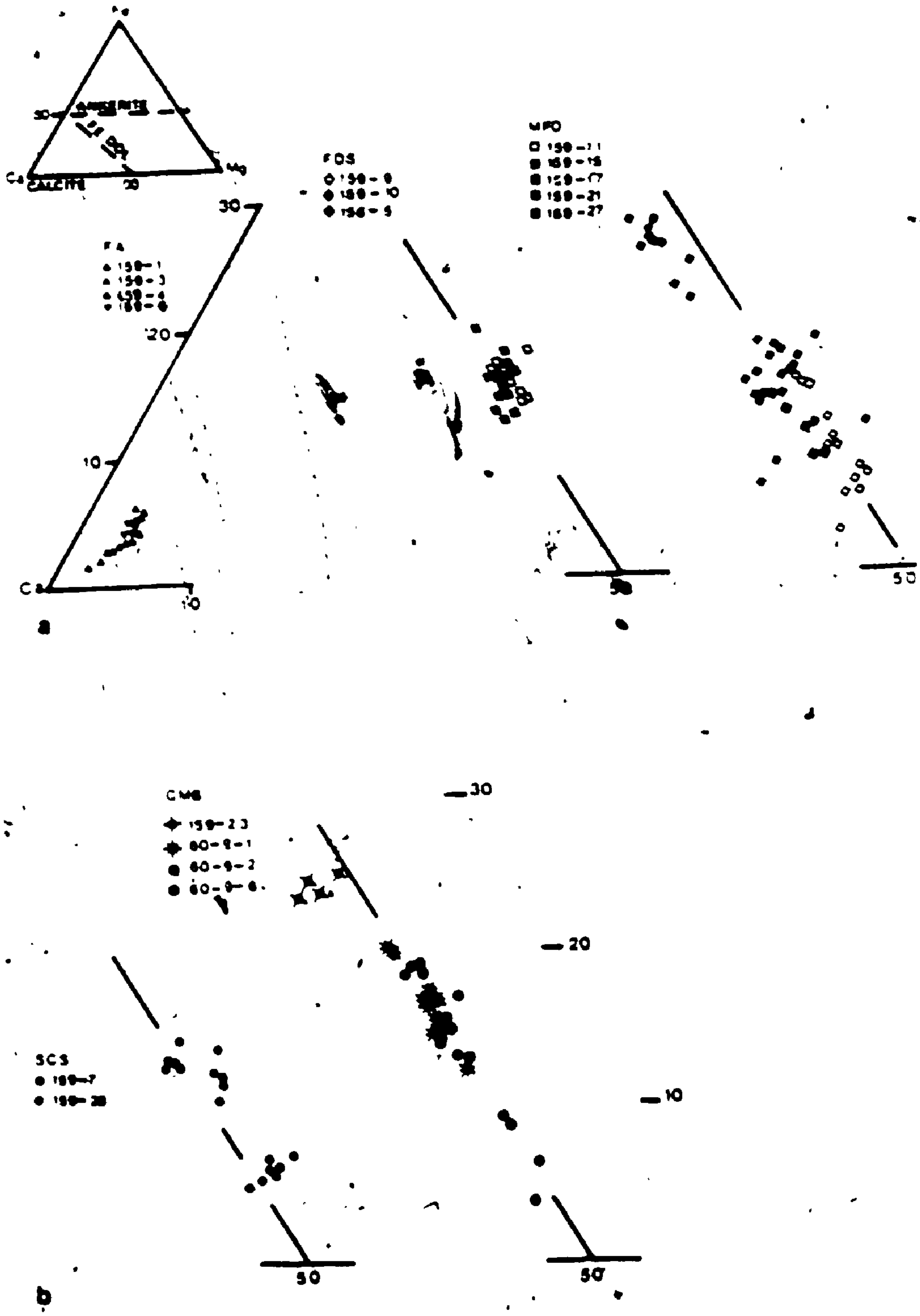

Figure 5.6 a & b. Carbonate ternary Ca-Fe-Mg classification

anorthite content.

5.2.1.5. Carbonate

Calcite is the sole carbonate of the Foliated Amphibolite. The calcite of Samples 159-1 and 159-3 show a 3% Fe and Mg substitution (Figure 5.6a). Samples 159-4 and 159-6, transitional chlorite-calcite schists, contains 6% Fe and Mg substitution. The MnO values (Table 5.2) are relatively high in comparison to the Ferroan Dolomite Schists, Massive Ferroan Dolomite and comparable to the remaining rock types.

5.2.2. Ferroan Dolomite Schists

The mineral chemistry of the FDCBQ Schist and veined FDCSBQ Schist will be presented undet the heading of Ferroan Dolomite Schists.

5.2.2.1. Carbonate

Ferroan dolomite is the characteristic carbonate of the Ferroan Dolomite Schists (Figure 5.6a). The Ca:Mg or dolomite ratio is fairly constant, with Fe also varying little from 12% to 19%. The MnO values are relatively depleted with respect to the Foliated Amphibolite (Table 5.2).

5.2.2.2. Chlorite

Chlorite of the Ferroan Dolomite Schists is repidolite, and shows a tight clustering in composition (Figure 5.3a). The Fe/(Fe+Mg) ratio is similar to and slightly elevated relative to the Foliated Amphibolite. The Si values are intermediate and within the range of the Foliated Amphibolite samples.

5.2.2.3. Biotite

The biotite compositions of the Ferroan Dolomite Schists are

Table 5.2. MnO contents of Carbonate from various rock types.

	MnO carbonate	1σ	MnO whole rock
Foliated Amphibolite			
159-1 (calcite)	0.81	0.08	0.17
159-3 "	1.00	0.00	0.21
159-4 "	0.57	0.07	0.27
Ferroan Dolomite Schists			
159-6 (calcite)	0.31	0.04	0.21
159-9	0.50	0.14	0.16
159-10	0.38	0.07	0.13
156-5	0.56	0.34	0.15
Massive Ferroan Dolomite			
159-11	0.23	0.15	0.25
159-15	0.73	0.33	0.25
159-17	0.79	0.29	0.32
159-21	0.69	0.18	0.38
Sericite-Chlorite Schist			
159-7	0.81	0.11	0.18
159-28	0.65	0.10	0.07
Chlorite-Magnetite Schist			
159-23	1.13	0.57	0.17
60-9-1	1.27	0.17	n/a
60-9-2	1.32	0.15	0.11
60-9-6	0.62	0.26	n/a
Silicified Dolomite			
159-29	0.84	0.49	0.30
159-39	1.27	0.72	0.41
159-48	0.18	0.08	0.17
159-53a	0.45	0.03	n/a
159-50	0.23	0.19	0.25
159-54	0.26	0.14	0.19
159-56	0.35	0.12	0.75
159-57a	0.27	0.16	0.30
Graphitic Pelite			
159-36	1.43	0.69	0.47
159-37	3.01	0.61	0.17
60-12	3.49	1.23	0.17
60-15	2.88	0.65	0.26
67-10 (dolomite)	1.53	0.00	0.12
(calcite)	2.12	0.00	0.12
Quartz Cemented Graphitic Pelite Breccia (LOZ)			
159-61 (dolomite)	0.91	0.32	0.15
(calcite)	1.26	0.09	
Banded Chlorite-Sericite Garnet Schist			
4-13	0.36	0.01	0.06
67-19 (dolomite)	2.12	0.00	n/a
(calcite)	1.53	0.00	n/a

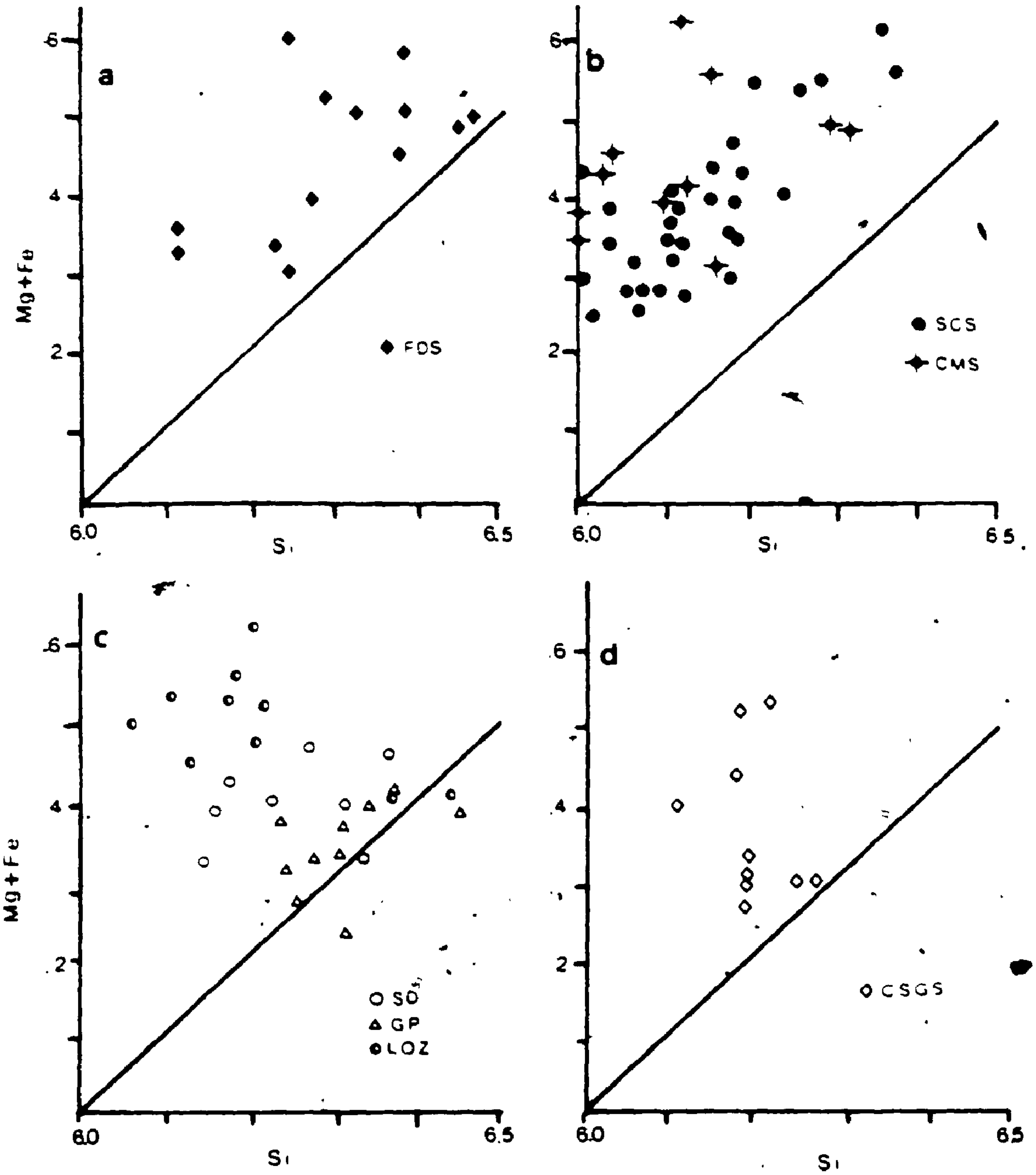

Figure 5.7 a - d) Muscovite Fe+Mg versus Si plot.

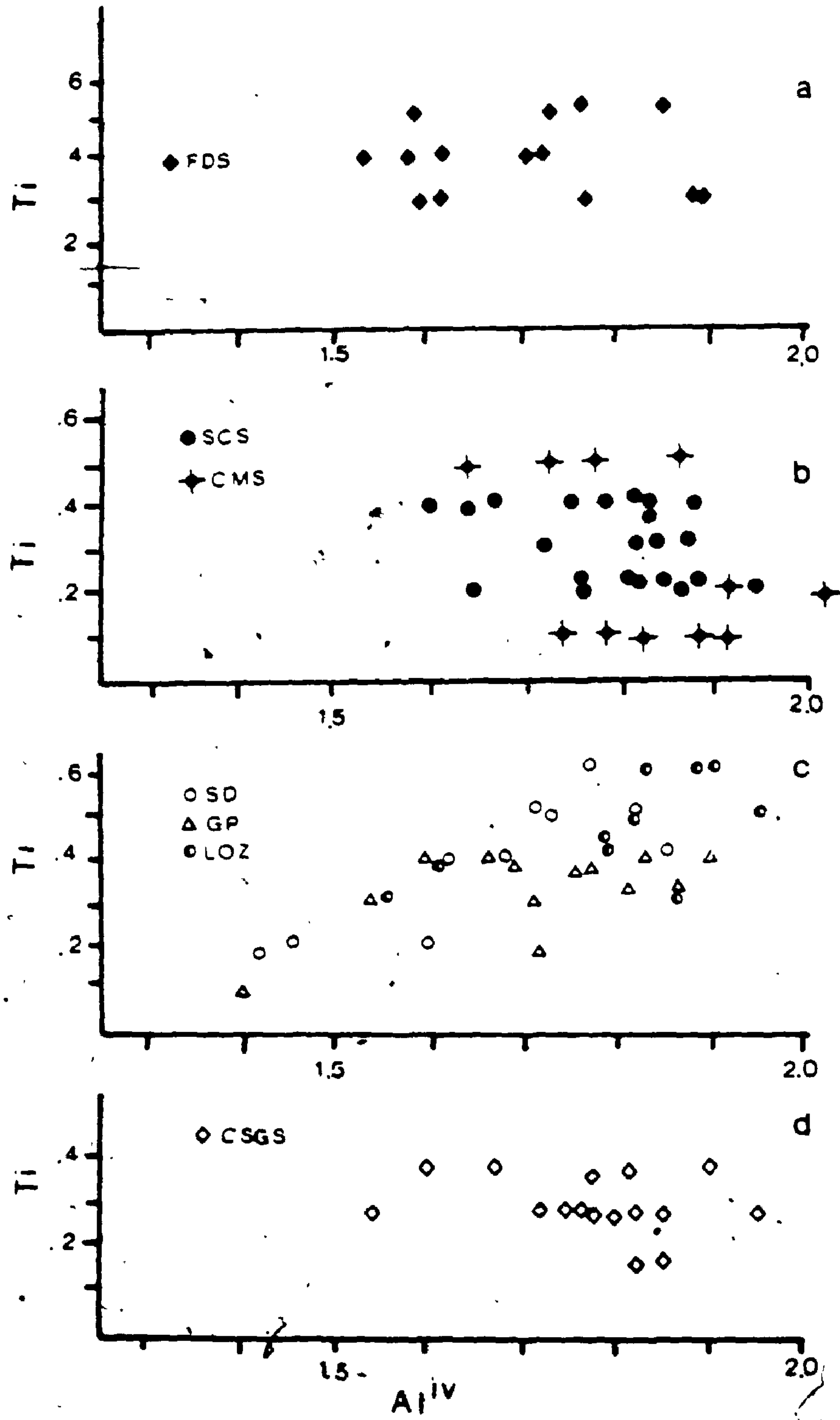

Figure 5.8 a - d. Al^{iv} versus Ti for muscovite representing the substitution: $Mg^{vi}2Si^{iv} = Ti^{vi}2Al^{iv}$.

Table 5.3. K/(K+Na) of White Mica

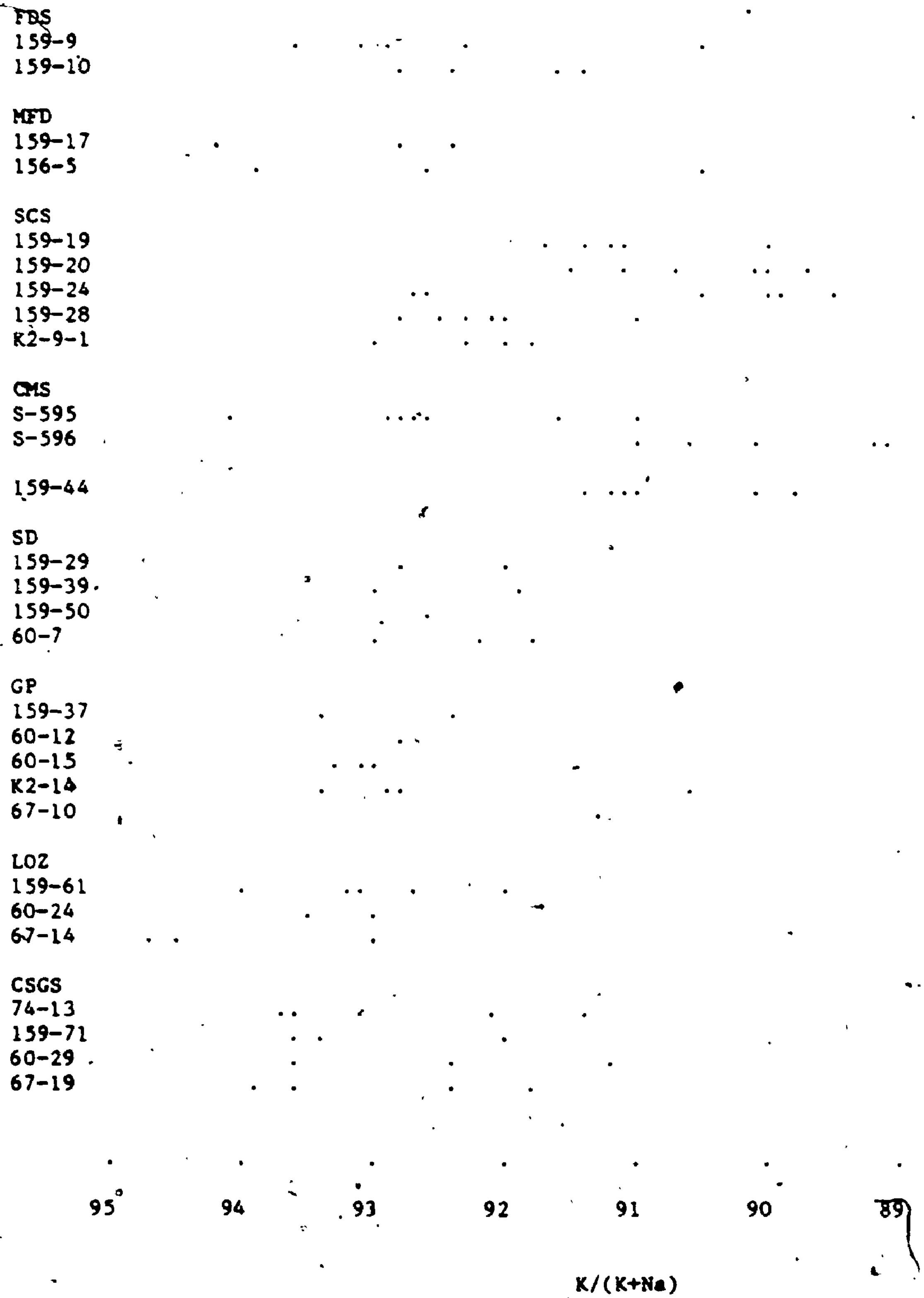

Table 5.4. Ba of Muscovite and Whole Rock

	Structural Ba	1σ	Average	1σ	Whole Rock Ba (ppm)
FDS			.42	0.15	
159-9	0.40	0.13			805
159-10	0.45	0.07			1315
MFD			.67	0.23	
159-17	0.63	0.07			NA
156-5	0.71	0.03			487
SCS			0.88	0.22	
159-19	0.63	0.16			6195
159-20	0.86	0.18			NA
159-24	0.74	0.21			3339
159-28	0.99	0.23			4139
K2-9-1	1.18	0.38			NA
CMS			0.80	0.10	
S-595	0.74	0.22			NA
S-596	0.75	0.12			NA
159-44	0.92	0.25			NA
SD			0.48	0.13	
159-29	0.47	0.05			430
159-39	0.63	0.02			110
159-50	0.32				120
60-7	0.50	0.03			344
GP			0.58	0.10	
159-37	0.59	0.02			3152
60-12	0.41				466
60-15	0.67	0.21			1279
K2-14	0.60	0.20			NA
67-10	0.65				1298
LOZ			0.47	0.05	
159-61	0.49	0.07			2329
60-24	0.41				1833
67-14	0.51	0.18			NA
CSGS			0.35	0.08	
74-13	0.45	0.02			666
159-71	0.35				1001
60-29	0.28	0.07			635
67-19	0.30	0.01			964

presented in Figures 5.4a and 5.5a. The Fe/(Fe+Mg) ratio and Al^{vi} are distinctly elevated with repsect to the Foliated Amphibolite (Figure 5.4a). The Fe/(Fe+Mg) ratios are relatively constant within the rock group, whereas Al^{vi} shows a range. The Al^{iv} values are significantly lower than those for the Foliated Amphibolite (Figure 5.5a). There is a slight Ti decrease with the Al^{iv} decrease. The increase in Fe, Al^{vi} and decrease in Ti, Al^{iv} may reflect the substitution:

$$(Mg,Fe)2Si = Ti^{vi}Al^{iv}$$

5.2.2.4. Sericite

Sericite is restricted to veined FDCSBQ Schist. No Ca content was observed in the analyses of the white micas. The K/(K+Na) ratio ranges from 0.89 to 0.95 thus classifying them as muscovite (Table 5.3).

White micas commonly show substituitions similar to that seen amphiboles (Section 5.2.1.1):

$$(Mg,Fe)\ Si^{iv} = Al^{vi}Al^{iv} \quad (1)$$

this substitution is referred to as a phengite, celadonite or tschermakite substitution. The values show a range in both Mg+Fe and Si and generally subparallel the ideal celadonite substitution (Figure 5.6a).

Figure 5.7a represents the substitution:

$$Mg2Si = Ti^{iv}2Al^{iv} \quad (2).$$

It is apparent that the variation in Al^{iv} is not related to increases in Ti.

The Ba substitution in the muscovite of the Ferroan Dolomite Schists is slightly elevated relative to several other rock types. This is reflected in the whole rock Ba values as well (Table 5.4). The Ba substitutes for K and Na in the muscovite structure as represented by the substitution:

$$Ba^{xii},Al^{iv} = (K,Na)^{xii}Si^{iv}$$

5.2.2.5. Plagioclase

Two compositions of plagioclase occur in the Ferroan Dolomite Schist (Table 5.1). Sample 159-13 plagioclase composition is albite and ranges from An_1 to An_8. These compositions are similar to those of the Foliated Amphibolite. The plagioclase values of Sample 159-10 range from An_{32} to An_{35} which is andesine. This composition range is similar to that seen for the Sericite-Chlorite Schist, Quartz Cemented Graphitic Pelite (LOZ) and the Chlorite-Sericite-Garnet Schist. A single core to rim variation of decreasing Ca content was noted in Sample 159-13.

5.2.3. Massive Ferroan Dolomite

5.2.3.1. Carbonate

The carbonate of the Massive Ferroan Dolomite is ferroan dolomite. Its composition is illustrated in Figure 5.6a. The Ca:Mg is approximately 50:50; however, it is less constrained than that of the FD Schist. The Fe varies from 6 to 31% and shows a trimodal distribution. The lower Fe samples are similar in range to the Silicified Dolomite; the intermediate Fe samples are comparable to the FD Schists and the high Fe values (Sample 159-21) defines its own group. The MnO of the carbonate is relatively elevated in comparison to the FD Schists (Table 5.2), with the exception of Sample 159-11 which also showed the least Fe enrichment (Figure 5.6a).

5.2.3.2. **Chlorite**

Chlorite of the Massive Ferroan Dolomite is repidolite (Figure 5.3a). The Fe/(Fe+Mg) ratio is comparable to the FD Schists. There is a relatively large range in Si and a slight increase in Fe with increasing Si. This may represent the substitution:

$$2Mg^{vi}Si^{iv} = 2Al^{iv}Fe^{vi}$$

5.2.3.3. **Sericite**

The white mica of the Massive Ferroan Dolomite is muscovite showing a relatively wide spread in K/(K+Na) ratio similar to that of the Ferroan Dolomite Schists (Table 5.3). The samples generally follow a celandonite substitution (Figure 5.7a), but are more aluminous than the ideal substitution would suggest. There is no clear relationship of Ti to Al^{iv} in Figure 5.8a. Figure 5.8a also indicates that the sericite of the Massive Ferroan Dolomite is more enriched in Al^{iv} than those of the FD Schists. This suggests the substitution:

$$Mg^{vi}Si^{iv} = Al^{iv}Al^{vi}$$

Ba is elevated in comparison to the FD Schist but is comparable to the Sericite-Chlorite Schist and Chlorite-Magnetite Schist (Table 5.4).

5.2.3.4. **Biotite**

The biotite composition of the Massive Ferroan Dolomite is comparable to the FD Schist but is distinctley elevated in comparison to the Foliated Amphibolite (Figure 5.4a). There is no direct relationship of Ti to Al^{iv} (Figure 5.5a) and the Al_{iv} values are

3

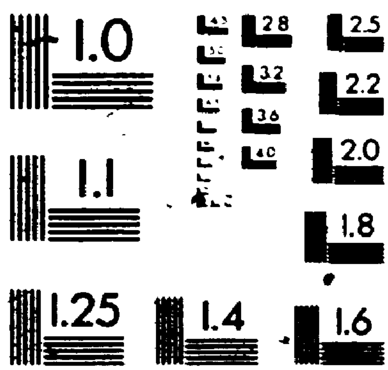

within the range of the FD Schist.

5.2.3.5. **Plagioclase**

Plagioclase is represented by the single sample 156-5. The composition is oligoclase (Table 5.1) which is comparable to FD Schist.

5.2.3.6. **Summary**

Relative to the FD Schist carbonate the Massive Ferroan Dolomite shows an Fe and Mn increase. Chlorite also shows an Fe increase with a decrease in Si, and therefore increase in Al. The sericite shows an increase in Al without an increase in Ti. Ba is also elevated. Plagioclase is comparable.

5.2.4. **Sericite-Chlorite Schist**

5.2.4.1. **Sericite**

The composition of sericite of the Sericite-Chlorite Schist is relatively paragonitic (Na end-member) in comparison to the other rock types with the exception of the Chlorite-Magnetite Schist (Table 5.3). The K/(K+Na) ranges from 0.914 to 0.848. The compositions show a large range of celandonite substitution (Figure 5.7b) with a significant increase in Al^{iv} in comparison to the FD Schist and Massive Ferroan Dolomite. There is no direct relationship of Ti to the increases in Al^{iv} (Figure 5.8b). The Ba values of the muscovite is the highest of all the rock types (Table 5.4). This is matched by elevated whole rock Ba levels (Table 5.4).

5.2.4.2. **Chlorite**

Chlorite is repidolite in composition (Figure 5.3b). The Fe/(Fe+Mg) ratio shows a trimodal distribution. The low Fe/(Fe+Mg) of 0.50 is at the low range of the FD Schist and Massive Ferroan

Dolomite; the intermediate Fe/Fe+Mg of 0.70 is at the high range of the FD Schist and Massive Ferroan Dolomite and the high Fe/(Fe+Mg) of 0.80 defines its own group, most comparable to the Chlorite-Magnetite Schist. The increase in Fe is reflected by a distinct decrease in Si and therefore an increase in Al^{iv}.

5.2.4.3. Biotite

The biotite of the Sericite-Chlorite Schist defines a fairly unique group (Figure 5.4a) The Fe/(Fe+Mg) ratio is the largest of all rock types with the Al^{iv} content comparable to the FD Schist and Massive Ferroan Dolomite. The Ti values (Figure 5.5b)are also elevated in comparison to the other rock types and show a minor correlation to increasing Al^{iv} suggesting the substitution:

$$Mg^{vi}2Si^{iv} = Ti^{vi}2Al^{vi}$$

5.2.4.4. Garnet

The garnets of the Sericite-Chlorite Schist are almandine rich with the almandine component ranging from 85 to 93%. The pyrope component is restricted to 0.2% to 0.6%. The garnets show normal zoning of MnO, with the range of spessartine component 1.23 to 1.52%. (Appendix II).

5.2.4.5. Plagioclase

The plagioclase composition for the Sericite-Chlorite Schist ranges from An_{37} cores to An_{19} rims (Table 5.1). A compositional gap occurs between An_{20} to An_{26}. A single grain in Sample 159-28 has an anomalous composition of An_5.

5.2.4.6. Chloritoid

The chloritoid composition corresponds to the Fe end member with the Fe/(Fe+Mg) ratio restricted to 0.96 $^+/_-$ 0.01 (Appendix II). No compositional zoning is noted.

5.2.4.7. Carbonate

Carbonate in the Sericite-Chlorite Schist is fairly rare. The Ca:Mg ratio tends towards a more Mg rich dolomite and the Fe component shows a bimodal distribution of less than 10% and 15 to 20% (Figure 5.6b). This is comparable to that seen for the Massive Ferroan Dolomite (Figure 5.6a). The MnO values are elevated in comparison to the FD Schists and the Massive Ferroan Dolomite (Table 5.2).

5.2.4.8. Summary

The sericite, biotite, chlorite garnet and chloritoid of the Sericite-Chlorite Schist is elevated in either Fe or Al or both. Where Ti is not related to Al substitution in the sericite it is related to Al substitution in biotite. MnO values are elevated in the carbonate, but are not in the garnet. The plagioclase is zoned towards decreasing Ca.

5.2.5. Chlorite-Magnetite Schist

5.2.5.1. Chlorite

Chlorite of the Chlorite-Magnetite Schist groups into three populations similar to the Sericite-Chlorite Schist (Figure 5.3b). The three Fe/(Fe+Mg) groups are 0.55, 0.70 and 0.80. It is interesting to note that the mineralogy of the low and intermediate Fe/(Fe+Mg) ratio samples is relatively simple, consisting of dominantly chlorite and magnetite with minor biotite. The mineralogy of the high Fe/(Fe+Mg) ratio chlorite bearing samples is more complex, consisting of varying proportions of chlorite, magnetite, garnet, grunerite, chloritoid, arsenopyrite, pyrrhotite, pyrite and gold. An increase in Si is associated with the increase in Fe. No increases in

Ti are associated to increases in Al^{vi} (Figure 5.5b).

5.2.5.2. Garnet

Almandine garnet is characteristic of the Chlorite-Magnetite Schist. The almandine component ranges from 76% to 94%. The garnets are normally zoned with more spessartine rich cores (5.14%) decreasing to spessartine poor rims (0.73%).

5.2.5.3. Amphibole

Grunerite is the sole amphibole type which occurs within the Chlorite-Magnetite Schist. It is near end member composition with the Fe/(Fe+Mg) ratio clustering around 0.75. No significant Al substitution is noted in the tetrahedral site, infact, the analysed Si contents are higher than the tetrahedral site can accommodate. This is attributed to high oxide totals (See Appendix II).

5.2.5.4. Biotite

Biotite is generally restricted to assemblages of the Chlorite-Magnetite Schist where sulphides are a very minor component of the assemblage. Samples 60-9-1 and 60-9-3 are representative. The Fe/(Fe+Mg) ratio is intermediate between the Sericite-Chlorite Schist and FD Schists, whereas the Al^{vi} is significantly depleted with respect to the other rock types (Figure 5.4a). Ti values are at the low range of those for the Sericite-Chlorite Schist and show no relationship to Al^{iv} content.

5.2.5.5. Sericite

Sericite is not a common mineral within the Chlorite-Magnetite Schist and is restricted to the transitional contacts with the Sericite-Chlorite Schist. This rock type has the largest range in K/(K+Na) ratio (0.94 to 0.88) and the highest paragonite content

(Table 5.3) It also has the highest Mg+Fe and the highest Al^{iv} contents (Figure 5.7b). The Ti values show a bimodal range of very low (0.1) and very high (0.5) values. The Ba values are elevated and comparable to those of the Sericite-Chlorite Schist (Table 5.4).

5.2.5.6. Plagioclase

Albite is the characteristic plagioclase of the Chlorite-Magnetite Schist with the exception of Sample 159-18 which is andesine (Table 5.1). The albite is restricted compositional range from $An_{0.1}$ to $An_{2.2}$. A minor core to rim decrease in Ca is noted in Sample 60-9-6 but in general there is no core to rim variation.

5.2.5.7. Carbonate

The carbonate of the Chlorite-Magnetite Shcist is ferroan dolomite (Figure 5.6b). It shows a wide range in Fe varying from less than 10% up to 33%. It is significantly enriched in MnO (Table 5.2) in comparision to the relatively low whole rock values.

5.2.5.8. Summary

The mineral compositions of the Chlorite-Magnetite Schist are most comparable to those of the Sericite-Chlorite Schist. The chlorite, biotite and garnet are enriched in Fe. The sericite is relatively depleted in Al^{iv}. The carbonate is enriched in Fe and Mn and the plagioclase is albite.

5.2.6. Silicified Dolomite

5.2.6.1. Carbonate

The carbonate of the Silicified Dolomite is dolomite to ferroan dolomite (Figure 5.6c). The composition is constrained to a Ca:Mg ratio of 50:50. A trimodal Fe distribution is apparent (Figure 5.6c). The lower Fe group ranges from 0.0 to 4.0% Fe (Samples 159-29, 159-39, 159-48, 159-53a, 159-54, 159-56), the intermediate Fe group ranges from 5.0 to 5.3% Fe (Sample 159-50), and the higher Fe group ranges from 8.5 to 16.5% Fe (Samples 159-29, 159-39, 159-53a, 159-57a). The higher Fe group is related to those samples which have anomalous Au values and which are in contact with either Massive Ferroan Dolomite or LOZ. The MnO values of the Silicified Dolomite, group into two groups-- those samples with MnO values less than 0.36 (Samples 159-48, 159-50, 159-54, 159-56, 159-57a) and those samples with MnO values greater than 0.36 (Samples 159-29, 159-39, 159-53a) which correspond to those samples with anomalous Au.

Samples 159-50 and 159-54 are examples of the spotted dolomite texture described in Section 3.3.3.7 (iv). Analysis of the complex grains show that the cores of the grains are more Fe and Mn rich than the radiating grains making up the rims (Appendix 2).

5.2.6.2. Sericite

The sericite of the Silicified Dolomite shows an intermediate range in K/(K+Na) (Table 5.3). There is a wide range in Mg+Fe and Al^{iv} substitution (Figure 5.7c) with a weak trend toward ideal celadonite substitution. The Ti values (Figure 5.8c) shows a direct association with Al^{iv} suggesting the substitution:

$$Mg^{vi}2Si^{vi} = Ti^{vi}2Al^{iv}$$

The Ba values are at the low range of the other rock types (Table 5.4) which is consistant with the low whole rock Ba values.

5.2.6.2. Biotite

Biotite is rare in the Silicified Dolimite and is restricted to thin, linear zones associated with sericite. It defines a unique group in comparison to biotite of the other rock types. It is

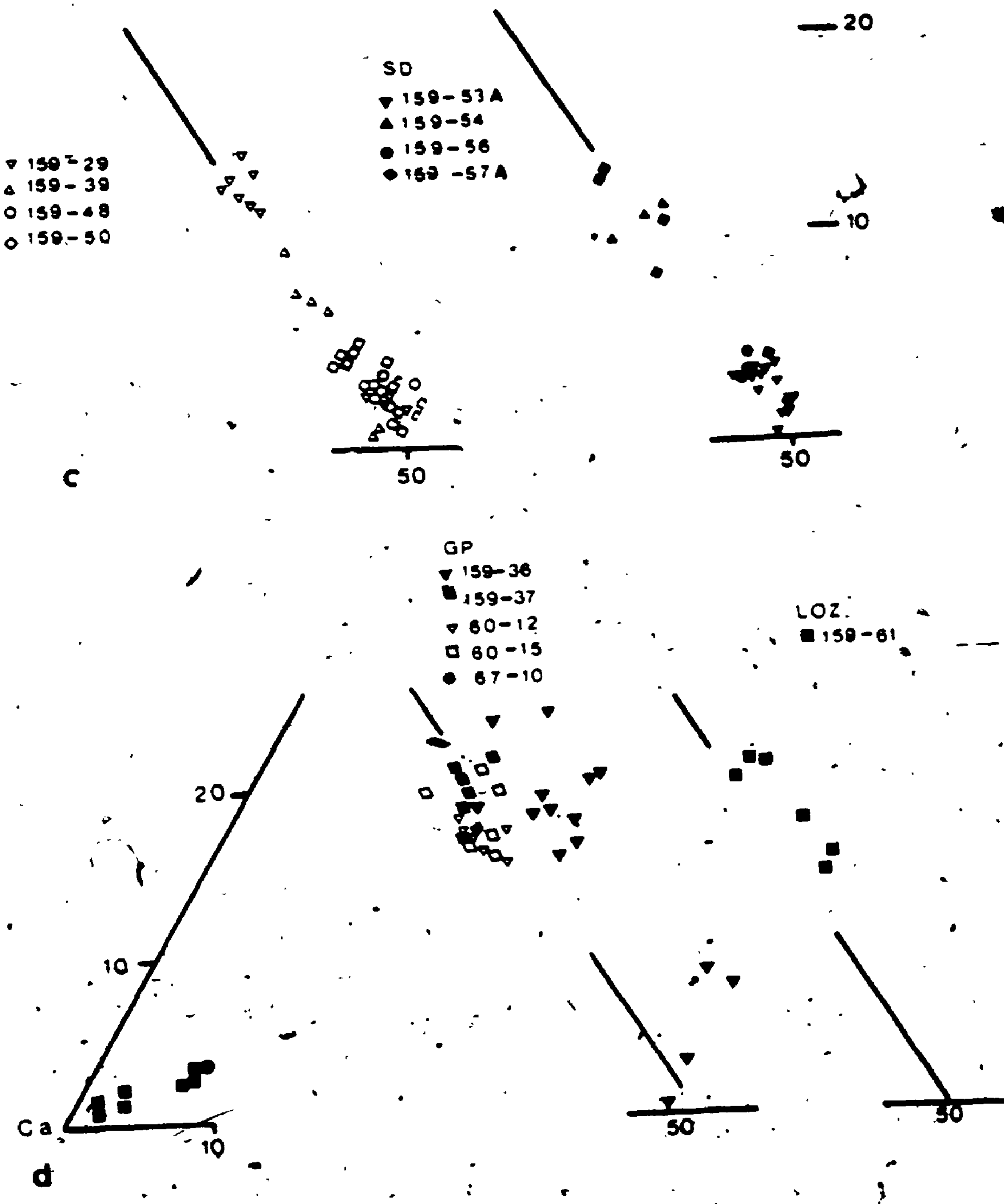

Figure 5.6 c & d. Carbonate ternary Ca-Fe-Mg classification

distinctly more phlogopitic with the Fe/(Fe+Mg) ratio ranging from 0.22 to 0.19 (Figure 5.4b). It is also depleted in Ti and Al^{iv} with respect to the other rock types (Figure 5.5b). This inverse relationship of Ti to Mg/(Mg+Fe) is consistant with that noted by Guiodotti (1983).

5.2.6.4. Plagioclase

Albite is the plagioclase of the Silicified Dolomite if Sample 159-50 is representative. The composition appears to be bimodal with $An_{0.8}$ representative of the first group and the range $An_{6.0}$ to $An_{8.0}$ representative of the second group. This range is consistent with that seen in Sample 159-13 of the Ferroan Dolomite Schist.

5.2.6.5. Summary

The minerals of the Silicified Dolomite define their own compositional groups. The biotite is phlogopitic, the carbonate is dolomite with limited Fe substitution with the exception of those samples associated with anomalous Au and which show increased Fe substitution. Plagioclase is albite. Ti shows a positive correlation to Al^{iv} in biotite.

5.2.7. Graphitic Pelite

5.2.7.1. Sericite

Sericite of the Graphitic Pelite shows a narrow, intermediate range toward a high K/(K+Na) ratio (Table 5.3). The Mg+Fe and Si variation approaches most closely the ideal tschermakite substitution (Figure 5.7c). The Ti values are at the low end of the range of all the rock types and show minor increase with increasing Al^{iv} (Figure 5.8c). Ba is intermediate in range for all the rock types, reflecting the intermediate to slightly elevated whole rock Ba levels (Table

5.4).

5.2.7.2. **Biotite**

The biotite of the Graphitic Pelite define a fairly unique compositional group (Figure 5.4b). The Fe/(Fe+Mg) ratio clusters between 0.45 and 0.59 and the Al^{vi} ranges from 0.61 to 1.14 and defines a positive slope suggesting the substitution:

$$Mg^{vi}Si^{iv} = Al^{iv}Al^{vi}.$$

A second substitution is suggested in Figure 5.5c where increasing Ti is matched by increasing Al^{iv}. The substitution is:

$$Mg^{vi}2Si^{vi} = Ti^{vi}2Al^{iv}$$

5.2.7.3. **Chlorite**

The chlorite of the Graphitic Pelite defines a fairly unique compostional group as illustrated in Figure 5.3c. The Fe/(Fe+Mg) ratio varies slightly, ranging from 0.49 to 0.53. No variation is associated with the bladed and porphyroblastic textural styles.

5.2.7.4. **Garnet**

The garnet of the Graphitic Pelite is almandine rich with the almandine component ranging from 59% to 74% (Appendix II). The spessartine component is elevated in comparison to garnets from other garnet bearing rock types and ranges from 10 to 21%. The pyrope component is also elevated in comparison to the other rock types and ranges from 4% to 6%. No significant core to rim zoning occurs in the garnets as illustrated in Table 5.5.

5.2.7.5. **Carbonate**

Ferroan dolomite, dolomite and calcite are represented within the carbonate assemblage of the Graphitic Pelite (Figure 5.6d). The Ca:Mg ratio of the ferroan dolomite and dolomite shows a fairly tight range with the exception of Sample 159-36 which shows a trend toward increasing Mg. The Fe content of the ferroan dolomite (Figurtre 5.6d) is intermediate to slightly elevated in comparison to carbonate of the other rock types. The MnO values are distinctly elevated (Table 5.2) in comparison to the other rock types, although the whole rock MnO is not consistently elevated.

Calcite within the Graphitic Pelite is represented by a single analysis from Sample 67-10 (Figure 5.6d). The Fe content is elevated and comparable to that seen in the Foliated Amphibolite. The MnO values are also elevated. (Table 5.2).

5.2.7.6. Plagioclase

Plagioclase is restricted in its occurrence within the Graphitic Pelite as porphyroblasts marginal to quartz-ferroan dolomite veins associated with arsenopyrite and anomalous Au values. Sample K2-14 is representative showing a bimodal core to rim distribution (Table 5.1). The core has a composition of An_{27} and the rim a composition of An_{19} and the gap occurs between An_{21} and An_{26}. This decrease in Ca from core to rim is consistant with that seen in the FD Schist and Sericite-Chlorite Schist described above (Table 5.1).

5.2.8. Quartz Cemented Graphitic Pelite Breccia (LOZ)

5.2.8.1. Sericite

The sericite of the LOZ is K rich and falls within the same K/(K+Na) range as the FD Schist (Table 5.3). It is significantly elevated in Mg+Fe and Al^{iv} in comparison to the Graphitic Pelite, approximating the range of the Sericite-Chlorite Schist (Figure 5.7c) The increase of Ti in association with Al^{iv} suggests the substitution:

$$Mg^{vi}2Si^{iv} = Ti^{vi}2Al^{iv}$$

Ba values (Table 5.4) are intermediate in range, although the whole rock Ba is slightly elevated.

5.2.8.2. Biotite

Biotite of the LOZ is represented by analysis from a single sample, Sample 159-61. The Fe/(Fe+Mg) ratio, Al^{vi} and Ti values are similar to the low range of the biotite of the Graphitic Pelite (Figure 5.4b and 5.5c).

5.2.8.3. Plagioclase

The plagioclase composition of the LOZ ranges from $An_{19.2}$ to $An_{31.8}$ with a single analysis of $An_{2.5}$ in Sample 159-61 (Table 5.1). The grains show distinct core to rim variations of decreasing Ca content which is comparable to that seen in the rock types decribed above. The core to rim compositions are not consistent from grain to grain. In Sample 60-24 one grain has a core composition of $An_{29.9}$ rimmed by compositions of $An_{28.2}$ and $An_{24.2}$. In another grain the core compoiton of $An_{31.8}$ is rimmed by $An_{28.4}$ (Table 5.1).

5.2.8.4. Carbonate

Ferroan dolomite and calcite are representative of the LOZ (Figure 5.6d). The Fe values of the ferroan dolomite ranges from 9.26 to 14.25 which is comparable to that the Graphitic Pelite. The MnO values (Table 5.2) are elevated relative to most rock types, except for the Graphitic Pelite.

Calcite also shows a range in Fe and Mg values (Figure 5.6d) which are comparable to the Foliated Amphibolite (Figure 5.6a). The MnO values are relatively elevated (Table 5.2).

5.2.8.5. Summary

The LOZ is distinguished from the Graphitic Pelite by sericite with high Fe+Mg and Al^{iv} and the presence of calcite. Biotite is comparable in composition to the biotite of the Graphitic Pelite. Plagioclase is also comparable in composition to the plagioclase of the Graphitic Pelite with the exception of two albite analysis. The plagioclase shows decreasing Ca content from core to rim.

5.2.9. Chlorite Sericite Garnet Schist

5.2.9.1. Chlorite

Chlorite of the Chlorite-Sericite-Garnet Schist is repidolite and defines a unique group based on Fe/(Fe+Mg) ratio (Figure 5.3c). The Si shows a range from 4.14 to 5.62 without a significant shift in Fe/(Fe+Mg). It is more Fe rich than the chlorite of the Graphitic Pelite.

5.2.9.2. Sericite

Sericite of the Chlorite-Sericite-Garnet Schist shows a relatively narrow range of K/(K+Na) (Table 5.3). This ratio is comparable to the sericite of the Graphitic Pelite. Mg+Fe and Al^{iv} are not related to celadonite substitution. There is a range in Mg+Fe without significant variation in Si (Figure 5.7d). In addition increases in Al^{iv} do not vary with increases in Ti (Figure 5.5c). The Ba values are the lowest of all the rock types studied, which is consistent with low whole rock Ba levels (Figure 5.4).

5.2.9.3. Garnet

The garnet poikiloblasts display a spectacular spriral inclusion texture (Plate 9b). They are almandine garnets with the almandine component ranging from 72 to 76% and are normally zoned with the spessartine component decreasing from 5% in the cores to 0.25% at the rims (Appendix II). The pyrope component ranges from 2% at the core to 4% at the rim.

5.2.9.4. Biotite

The biotite of the Chlorite-Sericite-Garnet Schist are enriched in Fe/(Fe+Mg) with respect to the biotite of the Graphitic Pelite (Figure 5.4b). There is a minor variation of increasing Al^{vi} with decreasing Fe/(Fe+Mg) suggesting the substitution:

$$Mg^{vi}Si^{iv} = Al^{iv}Al^{vi}.$$

The Ti values increase with increasing Al^{iv} (Figure 5.5c) suggesting the substitution:

$$Mg^{vi}2Si^{vi} = Ti^{vi}2Al^{vi}.$$

5.2.9.5. Chloritoid

Chloritoid is rarely noted within the Chlorite-Sericite-Garnet Schist. Its composition is similar to that seen in the Sericite-Chlorite Schist (Appendix II). The Fe/(Fe+Mg) ratio is 0.96.

5.2.9.6. Plagioclase

The plagioclase shows a large compositonal variation, ranging from $An_{20.2}$ to $An_{36.6}$. There is an increasin in Ca from core to rim (Table 5.1). This is the complete oppositie to those rocks structurally above the Chlorite-Sericite-Garnet Schist, where Ca decreases from core to rim. The core compositions range from $An_{20.2}$ to $An_{24.6}$ while rim compositions range from $An_{33.8}$ to $An_{36.6}$.

5.2.9.7. Carbonate

Calcite and ferroan dolomite are both present in the Banded Chlorite-Sericite-Garnet ~~Schist. The~~ ferroan dolomite is comparable to that of the LOZ and the calcite shows minor Fe substitution (Appendix II).

5.2.9.8. Summary

The most distinguishing feature of the Chlorite-Sericite-Garnet Schist is the reverse zoning in the plagioclase toward more Ca rich rims, the elevated Fe/(Fe+Mg) ratio of the biotite and the lack of association between Ti and Al^{iv} of the sericite.

5.3. Garnet-Biotite Geothermometry

5.3.1. Introduction

Co-existing garnet and biotite occur in Sericite-Chlorite Schist, Graphitic Pelite and Chlorite-Sericite-Garnet Schist. The garnets were analysed for core to rim variations (Table 5.5 and Appendix II). Biotite blades in contact with garnet were preferentially analysed and used in the calculations; however, where not available, matrix biotite grains were analysed and used in the calculations. There is a small (3%) difference in the Fe/(Fe+Mg) ratio of the two biotite groups. As a first approximation this is considered a small enough difference to consider the analysis of biotite not in contact with garnet to be representative of a biotite in contact with garnet.

Table 5.5 illustrates the metamorphic temperatures calculated for the calibration equations presented by various authors. Accompaning the calculated temperatures are the K_d values of the Fe and Mg exchange between the garnet-biotite pairs and the garnet MnO values. Temperatures derived from the calibrations of Ferry & Spear(1978), Thompson (1978), Hall (1980) and Perchuk (1977) result in different temperatures associated with the same K_d values. The spread in temperatures is generally within the 50°C error, with the Ferry & Spear (1978) calibration commonly the most disparate. The temperatures quoted in the following discussion are calculated from

Table 5.5. Garnet-Biotite Geothermometric Temperatures of Various Authors. Temperatures given in °C.

Sample	Ferry & Spear(1978)	Thompson (1978)	Hall (1981)	Perchuck (1980)	log K_d	MnO
Sericite Chlorite Schist						
K2-9-1-1r	317	367	410	425	2.79	0.32
K2-9-1-2	390	430	457	477	2.40	0.48
3	516	531	533	557	1.89	0.75
4	562	566	561	583	1.75	0.87
5c	631	617	601	620	1.55	1.08
6	502	520	525	549	1.94	0.74
7r	341	387	426	442	2.65	0.16
K2-9-2-1*	348	393	430	447	2.62	0.10
2*	442	472	489	511	2.17	0.14
3*	468	493	504	527	2.07	0.05
4*	437	468	486	507	2.19	0.07
5c	529	541	541	564	1.85	0.15
6c	494	514	520	543	1.97	0.17
7r	471	496	506	529	2.05	0.04
159-44*	436	467	484	493	2.19	0.83
Graphitic Pelite						
60-12* (80m)	398	436	461	467	2.38	9.48
60-15c (60m)	389	429	456	461	2.40	9.18
r	405	442	466	486	2.33	8.42
159-37-1*	376	418	448	467	2.48	9.30
2*	365	408	440	459	2.53	8.76
K2-13-1c	385	424	453	473	2.42	6.39
r	416	451	473	494	2.28	5.61
2c	404	441	465	486	2.33	7.21
r	623	611	597	616	1.57	5.43
K2-14-1c (50m)	402	439	464	485	2.34	8.13
r	648	630	611	630	1.51	7.29
2*	379	420	450	469	2.45	8.17
3*	394	432	459	479	2.38	8.11
4*	376	417	447	467	2.47	8.87
5c	374	416	447	466	2.47	8.75
r	359	403	437	455	2.55	8.79
67-10-1c (30m)	442	472	489	511	2.17	5.50
r	428	462	481	502	2.22	4.64
2c	382	423	452	471	2.44	6.91
r	446	475	491	513	2.15	4.94

* - random analysis
a - above Graphitic Pelite Quartz Breccia (LOZ)

Table 5.5 con't. Garnet-Biotite geothermometric temperatures of various authors.

Temperatures given in °C.

Sample	Ferry & Spear(1978)	Thompson (1978)	Hall (1981)	Perchuck (1980)	log K_d	MnO
Chlorite-Sericite-Garnet Schist						
74-3-1-1r (5m[b])	360	404	438	456	2.55	0.40
	359	403	437	455	2.55	0.23
c	357	401	436	454	2.56	0.11
67-19-1-1c (14m)	328	377	417	433	2.73	3.26
2	324	373	415	430	2.75	2.96
3	330	378	418	434	2.72	2.06
4	343	390	427	443	2.64	0.52
5r	405	442	466	487	2.33	0.07
67-19-2-1c	333	381	421	436	2.70	2.02
2	301	353	400	413	2.89	2.96
3	325	374	416	431	2.74	1.86
4r	369	412	444	462	2.50	0.13
60-29-1-1c (50m)	348	394	430	447	2.61	0.13
2	376	418	447	467	2.47	0.06
3	388	427	455	475	2.41	0.09
4r	442	472	488	511	2.17	0.00
60-29-2-1c	248	305	365	371	3.27	2.41
2	260	316	372	380	3.18	1.20
3r	330	378	419	434	2.71	0.11

b -below Quartz Cemented Graphitic Pelite Breccia (LOZ) the calibration of Thompson (1978).

5.3.2 Calculated Temperatures

5.3.2.1 Sericite-Chlorite Schist

Garnet porphyroblasts of the Sericite-Chlorite Schist are large, 0.5 to 1.0 cm in diameter, sub- to euhedral and show no optical zoning. The variation of the absolute metamorphic temperatures range from a high temperature of $620^{\circ}C$ in the core to a lower temperature of $370^{\circ}C$ at the rim in Sample K2-9-1. The calcuated temperature of Sample K2-9-2 (Table 5.5) varies form $393^{\circ}C$ in the core to $541^{\circ}C$ at the rim (Table 5.5). In addition, Sample K2-9-1 appears to have a distinctly lower temperature rim with a temperature spread from inner garnet to rim of $130^{\circ}C$. Sample 159-44 was not analysed for a core to rim variation and has a calculated metamorphic temperature of $467^{\circ}C$.

5.3.2.2 Graphitic Pelite

The garnets of the Graphitic Pelite are small, 1.0 to 5.0 mm, sub- to euhedral. The absolute metamorphic temperature associated with the garnet cores are generally consistent from sample to sample with an average temperature of $420^{\circ}C$ (Table 5.5). The rim temperatures appear to fall into two groups-- $470^{\circ}C$ (Sample 67-10) and $600^{\circ}C$ (Samples K2-13 and K2-14). The change in metamorphic temperature from core to rim is opposite to that noted for the Sericite-Chlorite Schist.

5.3.2.3 Banded Chlorite-Sericite-Garnet Schist

These garnets are large, 0.5 to 1.0 cm, anhedral, showing complex spiral textures (Plate 9b) and have a distinct static rim. The absolute metamorphic temperature differs from sample to sample. Sample 74-13 has a temperature of $400^{\circ}C$ with no varation from core to rim evident. Samples 67-19 and 60-29 show increases in temperature from core to rim but Sample 67-19 shows a wider spread. A dramatic increase in temperature is associated with the rim of Sample 67-19. The core temperatures of 350°C and 390°C for Samples 67-19 and 60-29 respectively are lower than the core temperatures calculated for the Graphitic Pelite. The rim temperatures are more similar to the core temperatures of the Graphitic Pelite.

5.3.3 Discussion

Garnet and biotite geothermometry is based on the exchange reaction represented by:

$$KMg_3Si_3Al_{10}(OH)_2 + Fe_3Al_2Si_3O_{12} =$$
$$KFe_3SiAl_{10}(OH)_2 + Mg_3Al_2Si_3O_{12}$$

It assumes that as temperature of metamorphism increases the equilibrium distribution of Fe and Mg or the K_d between the biotite and garnet is predictably shifted. This relationship is quantified through the following equations:

lnK_d = 0.2109(10*4/T(°K)-0.782 (Ferry & Spear, 1978)

lnKd = 0.02825(10*4/T(°K)-1.623 (Thompson ,1978)

lnKd = 0.3650 (10*4/T(°K)-2.57 (Perchuck, 1977)

lnKd = 1.49 (10*6/T*2)-0.40 (Hall ,1980)

The distribution of Fe and Mg between garnet and biotite is a significant component in the calibration but the influence of Mn and Ca in garnet and the Ti and Al^{vi} in biotite on the calibration must be considered. As Winkler (1975, pg 214) points out the presence of Mn in garnet lowers the stability field of the garnet, thus allowing it to nucleate at a lower metamorphic temperature. Temperature has a direct influence on the garnet-biotite geothermometry. Thompson

(1976) and Perchuck (1977) base their calibrations on field observations and therefore empirically include Mn and Ca substitutions in garnet and Ti and Al^{vi} substitutions in biotite. Hall's (1980) calibration is based on a recalculation of the oxygen isotope data presented by Goldman & Albee (1977). Ferry & Spear's calibration (1978) is based on experimental work. Both Goldman & Albee's (1977) and Ferry & Spear's (1978) calibrations are restricted to limited Mn, Ca, Al^{vi} and Ti substitutions. Ferry & Spear (1978) suggest that their geothermometer be applied only to those systems where (Ca+Mn)/(Ca+Mn+Fe+Mg) garnet ratio is less than 0.2 and the (Al^{vi}+Ti)/(Al^{vi}+Ti+Fe+Mg) biotite ratio of less than 0.15. All authors present a margin of error for their temperatures of +/-50°C.

The question of the reliability of the calculated metamorphic temperatures must be addressed. As with any modelling technique certain assumptions are made. The first assumption is that the calibration equation is precise. It is certainly beyond the scope of this study to debate the current thinking on garnet-biotite geothermometry (see [illegible]ene, 1982). It is therefore assumed that the calibration equations, within their published limitations of +/-50°C, are accurate.

The second assumption is that the garnet and biotite pairs are in equilibrium. The textural evidence of garnet in contact with biotite is considered good evidence that the minerals are in equilibrium (Hyndman,1985). The presence of zoning within the garnets does however, suggest disequilibrium between the garnet cores and the biotite at the garnet rims. This is not accounted for in the calculations presented in Table 5.5. The calculations assume that the core and rim compositions of the garnet are in equilibrium with the biotite, but as will be illustrated below this assumption is incorrect but does provide a starting point..

The third assumption is that the substitution of Mn and Ca in garnet and Ti and Al^{vi} in the biotite are not sufficient to deviate the calibrations and therefore, has a direct bearing on the accuracy of the calibration. This becomes an issue for the Graphitic Pelite and to a lesser extent Chlorite-Sericite-Garnet Schist. For instance, Sample 60-15 has a garnet Mn value of 0.89 and Ca value of 1.15 and the biotite has a Ti value of 0.89 and Al^{vi} value of 0.19 which based on the limitations presented by Ferry & Spear (1978) is above the upper limits of their calibration [ie. $(Ca+Mn)/(Ca+Mn+Fe+Mg) = 0.34$ and $(Al^{iv}+Ti/(Al^{iv}+Ti+Fe+Mg) = 0.19)$]

A discussion of the garnet-biotite geothermometric calculations for the three lithologies can be divided into two: 1) the variation in the temperatures within the rock group and 2) between the rock groups.

5.3.3.1 Sericite-Chlorite Schist

The rim temperature of 387°C as compared to the core temperature of 620°C in Sample K2-9-1 suggests the rim is retrograde. This is not only inconsistent with the metamorphic assemblage of chlorite and chloritoid believed to be the precusor assemblage to the prograde biotite-garnet assemblage (see Section 6.4) but also with the normal zoning in the garnet (Essene,1982). This inconsistency can be explained by considering the assumption of equilibrium made above. In the geothermometric calculation equilibrium is assumed between the garnet core and the biotite at the rim of the garnet. This maybe an invalid assumption. It is possible instead to assume that the temperature of metamorphism remained fairly constant while either the Fe/Mg ratio of the biotite or the bulk rock composition changed. The hypothetical Fe/Mg ratio of the biotite in equilibrium with the garnet core at 387°C would have a Fe/Mg ratio of 0.71. A comparison with the Fe/Mg ratio of 4.25 for the biotite in equilibrium at the rim of the garnet suggests a six-fold increase of the Fe/Mg ratio of biotite from the time of garnet nucleation. Sample 159-9, of the same rock type, is considered to represent an early stage of the alteration (see Chapter 6). The Fe/Mg ratio of the biotite in this rock is 0.86 which compares well with the calculated Fe/Mg ratio in equilibrium with the garnet core.

5.3.3.2 Graphitic Pelite

The garnet-biotite metamorphic temperatures of 400°C to 440°C associated with the core to rim compositional variation is within the +/- 50 degree significance is consistent with upper greenschist facies or low amphibolite facies metamorphic grade as suggested by the metamorphic assemblage of biotite, garnet, muscovite, quartz and plagioclase. The exception to this occurs within single garnet analyses from Samples K2-13 and K2-14. In both these cases the rim temperature is approximately 610°C. The difference between the Samples K2-13 and K2-14 and the other Graphitic Pelite samples is that the K2 samples represent Graphitic Pelite samples which are cut by quartz-ferroan dolomite veins with associated arsenopyrite and gold. Here, the garnet is not in contact with biotite and therefore the matrix biotite composition used in the calculation is not in equilibrium with the rim of the garnet. Similar to the argument presented for the Sericite-Chlorite Schist it is assumed that the garnet rim temperature is not representative of the conditions of metamorphism but is in fact a product of changing equilibrium conditions. It is furthur suggested that the matrix biotite which is probably in equilibrium with the core of the garnet precedes and predates the veining and is not in equilibrium with the rim composition of the garnet which may be coeval with veining. The calculated Fe/Mg ratio of the hypothetical biotite in equilibrium with the rim of the garnet for Samples K2-13 and K2-14 is 2.40 and 2.15 respectively. This indicates a two-fold increase in Fe/Mg ratio from 0.996 in Sample K2-14 and 0.959 in Sample K2-13. This is consistent with Fe gains seen elsewhere in the other rock types.

5.3.3.3. Banded Chlorite-Sericite-Garnet Schist

The temperature of metamorphism for the Banded Chlorite-Sericite-Garnet Schist samples appear to vary according to sample distance from the Quartz Cemented Graphitic Pelite Breccia or Lower Ore Zone. Samples 74-13, 67-19 and 60-29 are 5, 14 and 50 m respectively below the Lower Ore Zone. Sample 74-13 shows minor and continuous zoning from core to rim and Samples 67-19 and 60-29 show discontinuous zoning in temperature from core to rim (able 5.5). Discontinuous zoning is often attributed to polymetamorphism (Rumble & Finnerty, 1974) but in this study polymetamorphism is not texturally supported. Static rimming occurs only within the Banded Chlorite-Sericite-Garnet Schist and is restricted to a distance of 50 m below the Lower Ore Zone. Thompson et al.,(1977) suggest that a break in garnet zoning might represent a single metamorphic episode if two garnet producing reactions occur. The first reaction consumes the reactants, then as the temperature increases a second garnet forming reaction occurs using different reactions from the first reaction. The higher temperature associated with the static rim and the distinctly lower MnO values of the rims does suggest a hiatus in growth. It is proposed that at the lower temperature the formation of the core was stabilized by partitioning MnO into the core of the garnet. Once all the MnO was consumed garnet growth terminated. Nucleation of the static rim is thought to represent an increase in temperature and therefore the re-stabilization of garnet, regardless of available MnO. The source of the heat for the increase in temperature to form the static rim is interpreted to be from "above" associated with the formation of the LOZ. This will be furthur discussed in Chapter 7.

The ~~constant~~ metamorphic temperatures of Samples 74-13 and 67-19 within the inner-garnet contrasts with the temerature zoning within the inner-garnet of Sample 60-29 (Table 5.5). This can be explained by considering diffusion kinetics and their proximity to the Lower Ore Zone and therefore their proximity to the proposed heat source. Diffusion can be quantified by the following equation:

$$D_t = D_o \exp(-Q/RT)$$

where Dt is the coefficient of diffusion at the temperature of interest T, Do is the diffusion coefficient where 1/T approaches zero, Q is the activation enery of diffusion, R is the universal gas constant and T is the temperature of interest (Fyfe et al., 1977). From this equation it can be seen that the variables that affect diffusion are temperature and activation energy of diffusion. With increasing temperature diffusion increases. In the ideal case of garnet growth, at a constant high temperature of metamorphism (ie.

$650^{\circ}C$) diffusion is significant and compositional zoning would not be maintained due to continuous equilibration resulting in homogenization (Tracy et al.,1976). Within the Banded Chlorite-Sericite-Garnet Schist there is no evidence for metamorphic temperatures as high as $650^{\circ}C$ but rather metamorphic temperatures of approximately $420^{\circ}C$. The homogeneity of garnet compositions are attributed to high diffusion rates associated with temperature, modification of chemical activity gradients (Hyndman,1985,pg463; Nicolas & Poirier,1976,pg.62) and permeability along grain boundaries and within mineral lattices. The presence of a fluid also influences the rates of diffusion. In a dry system diffusion is much slower than that in a wet system.

Garnet growth within proximity to the LOZ is considered to have been greatly influenced by the presence of a high fluid flow associated with the LOZ and therefore, a high activity gradient between the attendant fluid and host rock. Deformation is also associated with the LOZ (see Section 3.3.3.9). Nicolas & Poirier (1976) point out that stresses set up a vacancy or defect gradient in a mineral lattice and the motion of the vacancies in the lattice are analagous to Brownian motion and allow the continuous diffusion of constituents through the lattice. Although not rigorously constrained, it is suggested that the homogenity of the garnet composition is due to enhanced diffusion as the result of a high chemical activity gradient in concert with deformation.

If the enhanced diffusion rate accounts for the homogeneous composition of the garnets within Sample 74-13 and 67-19, a reduced diffusion rate accounts for the zoned nature of the garent within Sample 60-29. With distance from the LOZ and away from the high fluid flow and deformation the diffusion was no longer enhanced. This resulted in the preservation of the changing Fe/Mg distribution in the garnet and similar core to rim calculated temperatures.

5.3.4 Summary

The average temperature of metamorphism for the Sericite-Chlorite Schist, Graphitic Pelite and Banded Chlorite-Sericite-Garnet Schist is $486^{\circ}C$ +/- $50^{\circ}C$, $452^{\circ}C$ and $388^{\circ}C$ respectively. The core to rim variations of the Sericite-Chlorite Schist and Graphitic Pelite garnets are interpreted to represent a shift in Fe/Mg ratio due to either coupled mineral reactions involving Fe and Mg or whole rock shifts in Fe and Mg.

The lack of compositional zoning in the garnet of the upper portions of the Banded Chlorite-Sericite-Garnet Schist in comparison to lower portions of the Banded Chlorite-Sericite-Garnet Schist, is considered to be due to temperature increase and enchanced fluid flow at the top of the unit. The heat and fluid source is associated with the LOZ.

CHAPTER SIX

METAMORPHISM AND METASOMATISM

6.1 Introduction

The distinction between metamorphism and metasomatism in what follows is critical. Metamorphism refers to changes in a rock due to complex, interdependant variations in temperature, pressure and composition (T-P-X) (Winkler, 1974) under conditions of low water:rock ratios. Variations in composition may include gains and losses of components, changes in relative proportions of fluids and gases such as H_2O, CO_2, O_2 and S_2. In this study, regional dynamothermal metamorphism describes a regional geothermal gradient which dictates the temperature and pressure. Variations in composition are small, due to a minor amount of fluid and rock interaction. Metasomatism refers to an allochemical process where bulk chemical changes occur within a rock and is governed by high water:rock ratios.

Parent rock types and metasomatic daughters are recognized within the rock assemblage of Minas III. This distinction is based on spatial distribution of the rocks types, clearly developed textures of replacement, mineral assemblages and rock geochemistry described in Chapters 3, 4 and 5. The parent rock types are:

Foliated Amphibolite,
Silicified Dolomite and
Graphitic Pelite.

The metasomatic daughter products of the Foliated Amphibolite are:

Ferroan Dolomite-Chlorite-Biotite-Quartz Schist,
veined Ferroan Dolomite-Chlorite-Sericite-Biotite-Quartz Schist,
Massive Ferroan Dolomite,
Sericite-Chlorite Schist,
Chlorite-Magnetite Schist.

The metasomatic daughter product of the Graphitic Pelite is:

Pelite Quartz Cemented Graphitic Pelite Breccia

and possibly,

Banded Chlorite-Sericite-Garnet Schist.

It is the intent of this chapter to discuss the conditions of metamorphism of the parent rock types and their metasomatism resulting in the formation of the daughter rock types.

No attempt will be made to dicuss the metamorphism or metasomatism of the Chlorite-Plagioclase-Quartz-Ferroan Dolomite Schist and Banded Quartz-Biotite-Chlorite-Plagioclase Schist.

A listing of the mineral name short forms and expansions are given in Appendix II.

6.2. Foliated Amphibolite

The metamorphic transition from Greenschist to Amphibolite Facies of metamorphism of mafic rocks proceeds through an intermediate facies termed Epidote-Amphibolite Facies (Laird & Albee 1981; Moody et al., 1983 and Thomson et al., 1985). A common Greenschist assemblage consists of:

act + chl + ab + qtz (Laird & Albee, 1981).

The common transitional Epidote Amphibolite Facies assemblage consists of:

act + ab + ep,

where chlorite has reacted to form epidote. (In this discussion epidote refers to the Epidote Group minerals, often referring specifically to zoisite or clinozoisite). The Amphibolite Facies is reached when the assemblage consists of:

hb + olg+ qtz.

The amphibole is more aluminous and sodium rich through tschermakite and edenite substitutions:

$(Mg,Fe)Si = Al^{iv}Al^{vi}$ tschermakite

$(\square)Si = NaAl^{iv}$ edenite

Coupled with the shift in composition of amphibole is a shift in plagioclase composition marked by a decrease in sodium and aluminum contents, thereby "jumping" the peristerite gap of An_7 to An_{17} (Grapes and Graham, 1978). Epidote reacts to form hornblende.

Under normal geothermal gradients the temperature of metamorphism for the Epidote-Amphibolite Facies is between 450° and 500° C (Figure 6.I, Fyfe et al., 1978). The additional sensitivity of these reactions to the prevailing P,X conditions cannot be discounted. Apted and Liou (1983) show that at P>3Kb, chlorite of a Greenschist Facies assemblage will disappear before the breakdown of epidote resulting in the transitional assemblage of hornblende+epidote+albite. Elevated pressures of 5Kb may also result in the nucleation of almandine garnet at Amphibolite Facies conditions (Winkler, 1974), although, as Miyashiro (1973) points out, the bulk composition of the rock (Fe/Fe+Mg) is an important factor in garnet nucleation.

Factors such as f_{O2} also influence mineral stability. For instance, increased f_{O2} will stabilize epidote and destabilize chlorite, again resulting in the assemblage hornblende+epidote+ albite (Apted and Liou,1983).

An understanding of metamorphism of the Minas III Foliated Amphibolite assemblage can be gained by first looking at the Regional Amphibolites. The Regional Amphibolite assemblage consists of:

hb+ab+zo+qtz+il

This assemblage is consistent with an Epidote Amphibolite Facies at pressures of metamorphism at greater than 3 Kb (Lou & Apted, 1983) assemblage. In contrast, Kuyumjian (1981) reports a Greenshist Facies assemblage for the Regional Amphibolites of:

act+zo+chl+ab+qtz+carb+il.

which supports de Saboia (1979). This variation in regional metamorphism might be attributed to the nodal development of isograds, as described by James (1955) for the Michipicoten Area.

The mineral assemblages of the Foliated Amphibolite of Minas III can be divided into two groups:

hb+ab+zo+qtz (Ia)

hb+ab+zo+bi+gnt+qtz+po,cpy (Ib)

hb+ab+zo+qtz+chl+bi+cc (II)

Assemblage Ia is the same as that of the Regional Amphibolite and indicates an Epidote Amphibolite Facies metamorphism at intermediate pressures. Assemblage lb is uncommon. The presence of almandine garnet (no analysis available) supports an intermediate pressure of metamorphism of 5 Kb (Winkler, 1974); however, the high Fe/Fe+Mg of the tschermakitic-hornblende (Figure 5.1) might suggest elevated Fe/Fe+Mg values which could stabilize garnet growth at lower pressures (Miyashiro, 1973, pg 259). The pressure of metamorphism is therefore constrained at > 3kb and < 5Kb.

The second assemblage, II, is marked by the addition of chlorite and calcite occuring as fine, 0.5 mm wide veinlets and as 1 to 10 mm wide zones and patches within Asseblage I. The presence of chlorite and calcite as veinlets might suggest the retrograde, Mg-endmember reaction (Hashimoto, 1972):

$$3chl + 10cc + 21qtz = 3act + 2zo + 10\ CO_2 + 8H_2O, \quad (1);$$

however, the presence of Chlorite-Biotite-Calcite Schist (Assemblage II) patches completely altering the Epidote-Amphibolite Facies Assemblage Ia points to CO_2-H_2O fluid ingress driving the Reaction (1) to the left.

The presence of biotite with chlorite and calcite is interpreted as the introduction of K with CO_2-H_2O fluid. This is supported by the Mass Balance calculations (Section 4.4, Figure 4.16). It is suggested that Fe and Mg of the Mg-hornblende are redistributed between chlorite and biotite with the chlorite becoming more Fe rich as the alteration proceeds (Figure 5.3a). Similarly, the presence of ilmenite is interpreted to be the result of the redistribution of Fe and Ti from the Mg-hornblende. Biotite shows no increase in Ti with increase in alteration

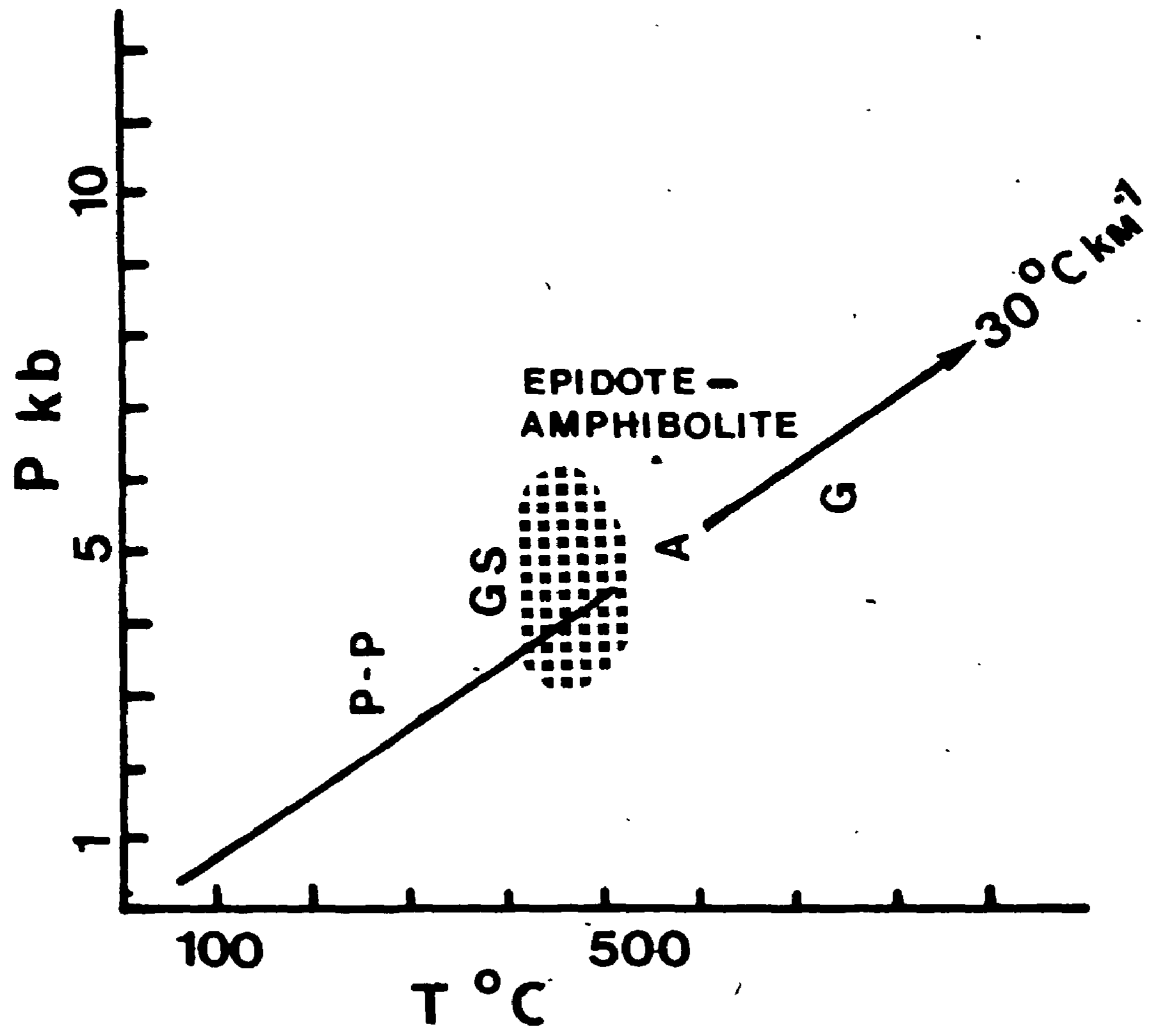

Figure 6.1. Metamorphic facies variation in Temperature versus Pressure space. Line represents regional geothermal gradient of 30 degree per kilometer depth. P-P = Prehnite-Pumpellyite Facies; GS = Greenschist Facies; A = Amphibolite Facies; G = Granulite Facies. (After Fyfe et al., 1978).

(Figure 5.5a) suggesting that ilmenite buffers the Ti contents of the rock.

In summary, the Foliated Amphibolite is metamorphosed to Epidote Amphibolite Facies metamorphism and shows incipient H_2O-CO_2 metasomatism in the form of patches and zones of calcite and chlorite. The temperature of metamorphism ranged between 450–500°C and the pressure of metamorphism ranged between 3 to 5 Kb (Figure 6.1).

6.3 FDCBQ Schist, veined FDCSBQ Schist and Massive Ferroan Dolomite

The FDCBQ Schist, veined FDCSBQ Schist and Massive Ferroan Dolomite are considered to be the metasomatic daughter products of the Foliated Amphibolite.

FDCBQ Schist is represented by the assemblage:

chl+bi+ab+ol+cc+FD+qtz+il+po,cpy (III);

veined FDCSBQ Schist represented by the assemblage:

chl+bi+mu+ol+FD+qtz+il+po,cpy+aspy,Au (IV);

and the Massive Ferroan Dolomite is represented by the assemblage:

FD+chl+mu+qtz+il/rt+po,cpy,aspy,Au (V)

Assemblage III is transitional between Assemblage II of the Foliated Amphibolite (Section 6.2) and Assemblage IV. It is marked by co-existing albite and oligoclase as well as calcite and ferroan dolomite as separate grains not showing compositional zoning (Table 5.1, Figure 5.6a). The appearance of ferrroan dolomite is attributed to the destabilization of the MgO components of the silicate assemblage under increasing X-CO_2. Chlorite (Figure 5.3a) and biotite (Figure 5.4a) are generally more Fe rich suggesting that the increase in FeO in the silicates is due to relative loss of MgO consummed a ferroan dolomite producing reaction. The reaction might be:

$$CaCO_3 + MgO + CO_2 = CaMg(CO_3)_2 \quad (2)$$

The appearance of oligoclase in this assemblage is attributed to the liberation of CaO from calcite to form dolomite:

$$2CaCO_3 + MgO = CaMg(CO_3)_2 + CaO \quad (3).$$

Oligoclase may also have been stabilized over albite by the net loss of Na_2O as suggested by the mass balance calculations (Section 4.4.2.1, Figure 4.16).

Assemblage IV is marked by the complete disappearance of calcite and albite and the appearance of muscovite. This is attributed to Reactions (2) and (3) which are driven to completion by increasing X-CO_2.

Muscovite first occurs as fine blades intergrown with chlorite. Ferry (1976) considers the growth of muscovite as a carbonatization reaction. Presented as Mg-endmembers the reaction is:

$$bt + chl + 8cc + 8CO_2 = mu + 8dol + 3qtz + 4H_2O \quad (4)$$

The most striking aspect of Reaction (4) is the complete redistribution of MgO into dolomite and Al_2O_3 into muscovite. If taken to completion the products of this reaction represents the Massive Ferroan Dolomite assemblage. Excess MgO, FeO and Al_2O_3

are thought to form chlorite which as seen in Figure 5.3a is Fe rich and Si depleted.

Rutile occurs most commonly associated with the sericite rich zones and appears to buffer the Ti of the assemblage as there is no Ti variation in the muscovite (Figure 5.8a). Rutile is interpreted as an alteration product, possibly of ilmenite:

$$FeTiO_3 = TiO_2 + FeO \quad (5)$$

where the FeO is incoporated into the host ferroan dolomite. It is also possible that rutile may be a direct alteration product from the Foliated Amphibolite amphibole, due to complete partioning of Fe into ferroan dolomite.

Figure 6.2 is taken form Clark et al., (1986) and is after Carmichael (1984). It shows T-X_{CO2} equilibrium curves at 3 Kb in the system SiO_2-Al_2O_3-MgO-CaO-Na_2O-K_2O-H_2O-CO_2. The activities of the endmembers of tremolite, paragonite, muscovite, clinozoisite, annite, clinochlore, quartz, calcite, dolomite were used in the calculations for the common co-existing minerals of metablalts. Figure 6.2 illustrates that under increasing X_{CO2} the common Greenschist Facies assemblage of actinolite + zoisite will be carbonatized to chlorite + calcite (Reaction (1)) and ultimately to oligoclase + dolomite (Reaction (4)).. These types of reactions lend strong support to the proposed carbonatization reaction of the Foliated Amphibolite to form the FDCBQ Schist, veined FDCSBQ Schist and Massive Ferroan Dolomite.

In summary, the mineral assemblages and mineral chemistries of the FDCBQ Schist, veined FDCSBQ Schist and the Massive Ferroan

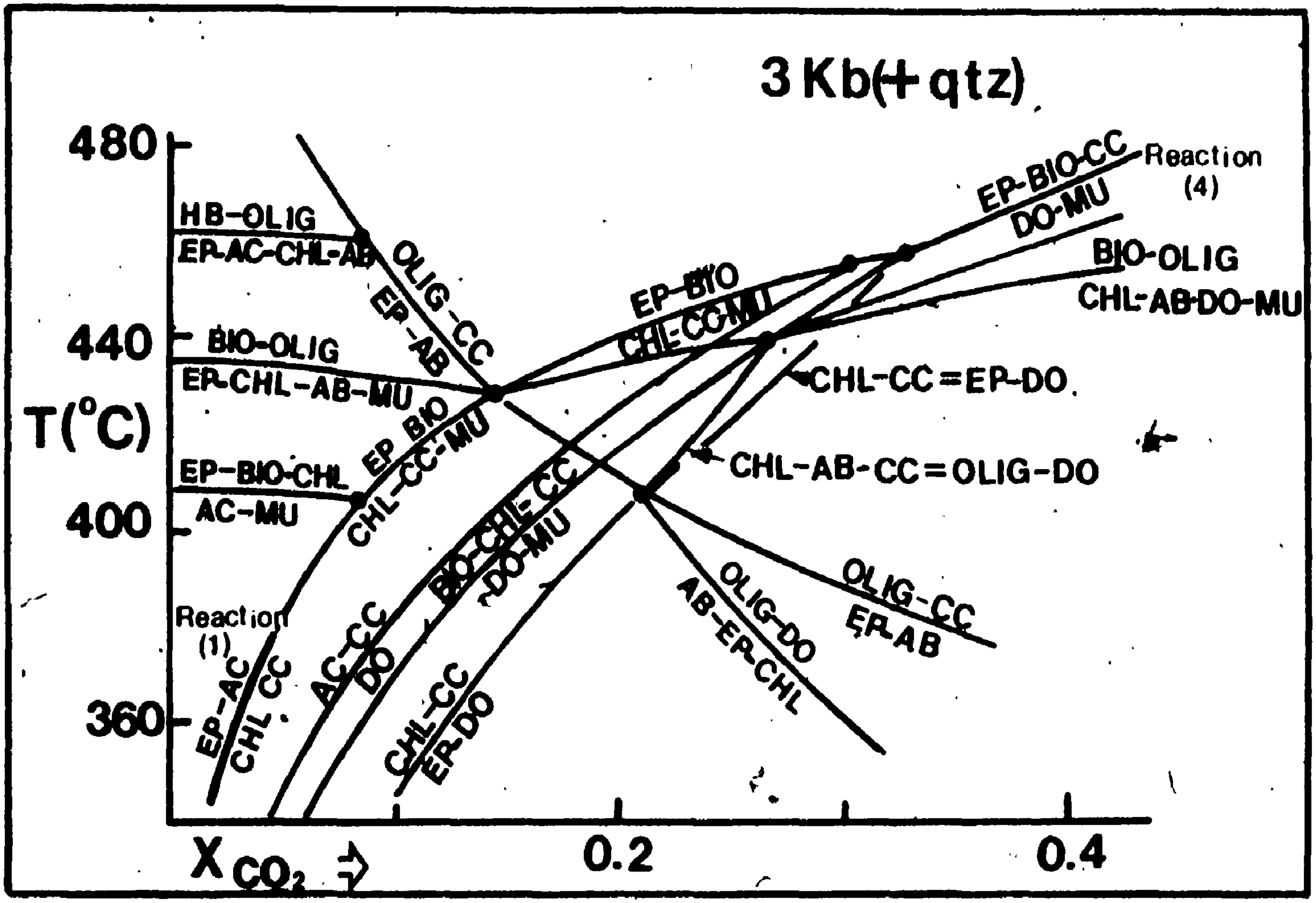

Figure 6.2. X_{CO_2} versus Temperature in the mafic system SiO_2-Al_2O_3-MgO-CaO-Na_2O-K_2O-H_2O-CO_2 using MgO endmembers to calculate curves. Reaction (1) and Reaction (4) in text. (Clark et al, 1986).

Dolomite can be explained by progressive carbonatization of the parent Foliated Amphibolite. Carbonatization represents a progressive increase in Fe of the silicate phases. Ti is immediately partioned into an oxide phase of either ilmenite or rutile and buffers the Ti in the silicate phases.

6.4. Sericite-Chlorite Schist and Chlorite-Magnetite Schist

6.4.1. Introduction

Unlike the clear parent and daughter textural relationship between the Foliated Amphibolite and the Ferroan Dolomite Schists and Massive Ferroan Dolomite the parent and daughter relationship of the Foliated Amphibolite and the Sericite-Chlorite Schist and Chlorite-Magnetite Schists are not texturally seen and this relationship has been documented geochemically in Chapter 4. Based on the mass balance calculations (Section 4.4.2) the metasomatic alteration involves gains in FeO, K_2O, BaO, As and losses in MnO, MgO, CaO, Na_2O relative to the Foliated Amphibolite. This alteration pattern is interpreted to represent sericitization resulting in leaching of components which are lost. No attempt is made to work out the systematics of the initial alteration of the Foliated Amphibolite assemblage to the Sericite-Chlorite Schist. It is speculated that the progressive loss in CO_2 related to the carbonatization of the Foliated Amphibolite might well have decreased the pH of the fluid thus promoting the sericitization reactions.

Sericite-Chlorite Schist and Chlorite-Magnetite Schist do show a texturally transitional contact, represented by the increase in chlorite and the appearance of magnetite. In the following section, Section 6.4.2 and 6.4.3, mineral reactions are proposed to account for the development of the paragenetic sequence in each rock unit. Section 6.5 will present the proposed reactions which account for the transitional relationship of the two rock types.

6.4.2 Sericite-Chlorite Schist

The mineralogy of the Sericite-Chlorite Schist is represented by the silicate phases sericite, chlorite, biotite, chloritoid, almandine garnet, plagioclase, quartz, the oxide phases ilmenite and rutile, with rare sulphides of pyrrhotite, arsenopyrite and chalcopyrite, galena and the precious metals Au and Ag. Several mineral associations occur and are best discussed separately. These are:

1) sericite-chlorite-oligoclase (most common)
2) sericite-chlorite-chloritoid +/- oligoclase (most common)
3) sericite-chlorite-chloritoid-biotite-garnet (less common)

Ilmenite or rutile is present in all these assemblages, although quartz may or may not be present.

1) Sericite-Chlorite-Oligoclase

The association of sericite, chlorite and plagioclase is not an unfamiliar one in the rock types of the deposit. In the Sericite-Chlorite Schist oligoclase is seen as rounded, up to 1 mm in diameter, porphyroblasts showing a decreasing anorthite content from core to rim (Table 5.1. The porphryoblasts often overgrow a chlorite mat with sericite blades in close association (Plate 3e). One possible partial reaction might be (Chimmer, 1967):

$$musc + 6SiO_2 + 3Na^+ = 2albite + 2H + K^+ \quad (6)$$

The analysis of the sericite from Samples 159-20 and 159-24 show significant paragonite substitution in the muscovite structure (Table 5.3), thus providing an internal source for the Na^+. This does not, however, account for the intimate association of chlorite. The details of this reaction might be represented by the unbalanced reaction:

$$(Na,K)\ musc + Ca^{2+} + (Fe\ poor, Al\ rich)\ chl =$$
$$(K)\ musc + (Fe\ rich, Al\ poor) chl + (Na,Ca)\ plag \quad (7)$$

This accounts for the wide variation in Al^{iv} in chlorite as seen in Figure 5.3b. It is also consistent with increasing Fe.

The decreasing anorthite content from core to rim of the plagioclase in Sample 159-24 may indicate a continuous reaction in response to Reaction (7). Ca could either have been removed by the attendant fluids or exhausted by the reaction and not replenished by the fluids. The mass balance suggests that Ca is lost to the system which supports the former.

2) Sericite-Chlorite-Chloritoid +/- Oligoclase

The relationship of chloritoid with sericite and chlorite is not always obvious in a single thin section. Reviewing several thin sections allows for the establishment of the paragenetic sequence. The orientation of ilmenite blebs as inclusions in chloritoid porphyroblasts and in the sericite-chlorite matrix are most commonly parallel suggesting that the chloritoid may have overgrown the sericite-chlorite matrix. There is, however, conflicting evidence supporting an early growth of chloritoid, pre-dating the sericite-chlorite matrix. Plate 3f shows ilmenite inclusions in a chloritoid porphyroblast oriented obliquely to the ilmenite of the sericite-chlorite matrix. As well, ilmenite may be randomly oriented, short and stubby within chloritoid and oriented, elongate and needle like in the sericite-chlorite matrix. Chloritoid, may also include coarse grained sericite in close association with plagioclase. Additional evidence of the sericite-chlorite matrix post-dating the chloritoid is the cuspate boundaries of chloritoid in contact with coarse grained chlorite. The coarse grained chlorite is sheath-like and forms a rectangular shape consistent with the shape of the larger chloritoid porphyroblasts, suggesting psuedomorphic replacement. Marginal to the rectangular shape of coarse-grained chlorite, the grain size of the chlorite blades are transitional to the finer grain size of the sericite-chlorite matrix (Plate 3c). Plagioclase may occur associated with the coarse grained chlorite. The paragenetic sequences is considered to be:

i) early growth of chloritoid from a sericite-ilmenite bearing assemblage

ii) alteration of chloritoid to chlorite and sericite (+/-plagioclase)

iii) alteration of ii to finer grained sericite-chlorite matrix.

The reaction accounting for the growth of chloritoid from an early sericite-chlorite matrix is suggested by Zen (1960) and

Frey (1978):

$6pa + 2chl + 4qz = 9chtd + 6ab + 5H_2O$ (8)

in the subsystem $Na_2O-CaO-Al_2O_3-FeO(KAl_3O_5-Si_2O-H_2O-CO_2)$.

The breakdown of chloritoid to sericite is presented by Atherton and Smith (1979, after Carmichael, 1969)

$2chtd + 2K^+ + 4H^+ + 3SiO_2 = 2musc + 3(Fe,Mg) + 3H_2O$ (9)

In this case, the K^+ is introduced, as suggested by the mass balance calculations (Figure 4.16j). The product (Fe,Mg) is incorporated to form chlorite with the needed Al coming from co-existing silicate phases.

Sample S80-595 shows a wide range in K/K+Na with the low ratio values as inclusions within the chloritoid and higher ratio values associated with muscovite of marginal to the chloritoid porphyroblasts. This suggests the combination of Reactions 8 and 9 where the inclusion sericite is representative of Reaction (8) and the matrix muscovite represents Reaction (9).

3) **Sericite-Chlorite-Chloritoid-Biotite-Garnet**

The assemblage sericite-chlorite-chloritoid-biotite-garnet is represented in Plate 3d and by Samples K2-9-1 and K2-9-2. Chloritoid poikiloblasts include biotite. The contact is sharp and is interpreted to be an equilibrium contact. Plagioclase blebs, 200 um in diameter, are most often associated with both sericite and biotite or occur as isolated grains within the chloritoid. The cuspate boundaries of both chloritoid and biotite with chlorite of the sericite-chlorite matrix suggests that both are being consumed by chlorite. Similarly, the contact of the chloritoid and biotite with garnet appears to be one of garnet overgrowing the chloritoid and biotite. These overgrowth boundaries are interpreted to represent disequilibrium. In contrast, however, the contact of the garnet the chlorite -dominated sericite-chlorite matrix is sharp and is interpreted as an equilibrium contact (Plate 3d).

These textures suggest the following sequence of mineral growth:

1) biotite with sericite
2) chloritoid including biotite and sericite replaces by chlorite
3) chlorite possibly coeval with garnet
4) garnet

Hyndman (1985, pg 585) suggests the reaction:

$$3musc + 5chl = 3\ biot + 4\ Al\ chl +/- 7qtz + 4H_2O \quad (10)$$

which accounts for the presence of biotite overgrowing a sericite-chlorite matrix. The chloritoid forming reaction may follow that of Reaction (8) involving the product chlorite and unreacted muscovite of Reaction (10). A garnet forming reaction involving biotite might be:

$$2chtd + annite + 5FeO + 4SiO_2 + 2O_2 = alm + 1\ chl + K_2O \quad (11)$$

(Hydnman, 1985)

The phases chlorite, garnet, chloritoid and biotite are presented in A'FM space (after Thompson, 1957) in Figure 6.3. It can be seen the phases chloritoid-garnet-biotite can co-exist, that is , do not represent crossing tie lines; however, the petrographic evidence suggests that chlorite and garnet are in equilibrium as are chloritoid and biotite. The two assembages of chlorite-garnet and chloritoid-biotite are thus represented in Figure 6.3 as crossing tie lines. The crossing tie lines are interpreted as shifts in mineral stability due to changing compositional differences. These are progressive increase in Fe, transfer of Al and loss of most other consituents.

In summary the mineral paragenesis is interpreted as:

Time →			
sericite	------------	------	------
ilmenite	------------	------	------
chlorite	---------		-------
biotite		-------	
oligoclase		------	
chloritoid			----
garnet			------

6.4.3 Chlorite-Magnetite Schist

The mineralogy of the Chlorite-Magnetite Schist is represented by the silicate phases chlorite, sericite, biotite, chloritoid, almandine garnet, albite, and quartz; oxide phases magnetite and ilmenite; sulphide phases of pyrrhotite, arsenopyrite, chalcopyrite and galena. Gold and silver occur in association with the sulphide assemblage. Several mineral associations occur and are best discussed separately. These are:

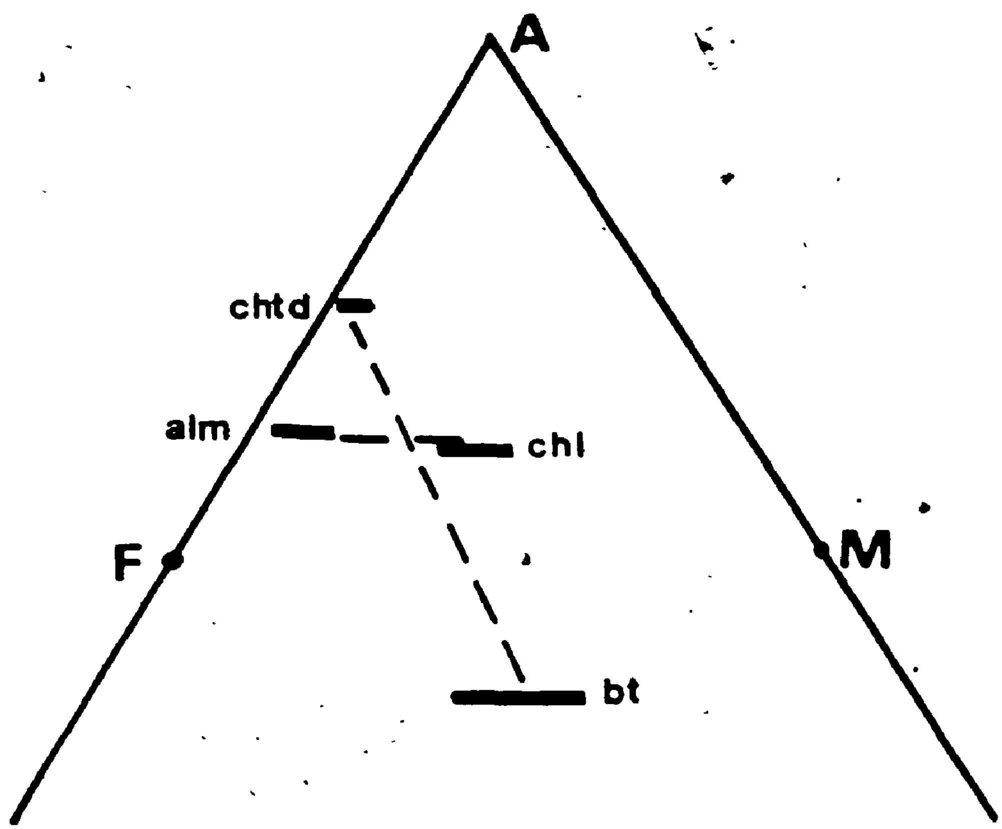

Figure 6.3. AFM Diagram showing the relationship of chloritoid (chtd), almandine garnet (alm), chlorite (chl) and biotite (bt). (After Thompson, 1957)

1) chlorite-magnetite-garnet-quartz +/- biotite +/- grunerite (most common)
2) chlorite-garnet-chloritoid +/- biotite (common)
3) chlorite-sericite-albite (common)
4) grunerite-chlorite-garnet +/- ferroan dolomite (rare)
5) pyrrhotite-arsenopyrite-chalcopyrite-pyrite-galena (common)

Ilmenite is present in all these assemblages with the addition of rutile in chlorite-magnetite-garnet-quartz +/- biotite. Quartz may or may not be present. INCO Metals reports the presence of graphite within the Chlorite-Magnetite Schist (J.P Golightly, 1986, personal communication)

1) Chlorite-Magnetite-Garnet-Quartz +/- Biotite +/- Grunerite

This assemblage is the most common and represents the transitional assemblage from the Sericite-Chlorite Schist. It is frequently associated with massive sulphide which can make up to 90 percent of the rock volume.

Dark green chlorite forms a mat like matrix to the remaining minerals. Quartz occurs as pressure shadow zones to magnetite, separating it from chlorite (Plate 4c). Magnetite porphyroblasts may include muscovite, tourmaline, chlorite and grunerite. Garnet includes magnetite and is in sharp contact with magnetite. Rare biotite occurs as blades intergrown with chlorite.

The presence of magnetite suggests an increase in oxygen fugacity where a portion of ferrous iron is oxidized to ferric

The possible reaction oxidizing chlorite might be:

$$3Fe_5Al_2Si_3O_{10}(OH)_2 + 7O_2 = 5Fe_3O_4 + 9SiO_2 + Al_2O_3 + 3H_2O; \quad (12)$$

where the quartz rims and the magnetite and the excess Al_2O_3 is consumed in other reactions such as forming a more aluminous chlorite (i.e. Sample 60-9-3, Figure 5.3b). Alternatively the excess Al_2O_3 and H_2O and introduced K^+ may be consumed in a biotite forming reaction.

The f_{O2} range represented by this assemblage at 500°C and 5 Kb may be constrained. Figure 6.4 is taken from Hall (1980) illustrating the fields of stability in the Fe-Ti-O-S-C system. The boundary for the oxidation of graphite to CO_2 (Gfmax) is coincident with the faylite-magnetite-quartz buffer (QFM). The equilibrium f_{O2} for this assemblage is constrained to below the magnetite-heamatite buffer (f_{O2}= 10^{-19}) the graphite-CO_2 buffer (f_{O2}=10^{-22}) and above or at the rutile-ilmenite equilibrium curve. (f_{O2}=$^{-36}$).

2) Chlorite-Garnet-Chloritoid +/- Biotite

This assemblage is comparable to the Sericite-Chlorite Schist, assemblage 3 (Section 6.4). Garnet is seen to overgrow and include chloritoid and is in sharp contact with chlorite. Chlorite also appears to overgrow chloritoid although does not include it. Reaction (11) of chloritoid+annite reacting to almandine+chlorite is considered to be the most representative of this assemblage. It involves the components FeO, SiO_2 and O_2 which is conistent with the high iron bulk rock chemistry and the presence of magnetite in assemblage 1.

3) Chlorite-Sericite-Albite

This assemblage is comparable to Assemblage 2 of the Sericite-Chlorite Schist (Section 6.4) differing by the absence of chloritoid and albite rather than oligoclase as the porphyroblast.

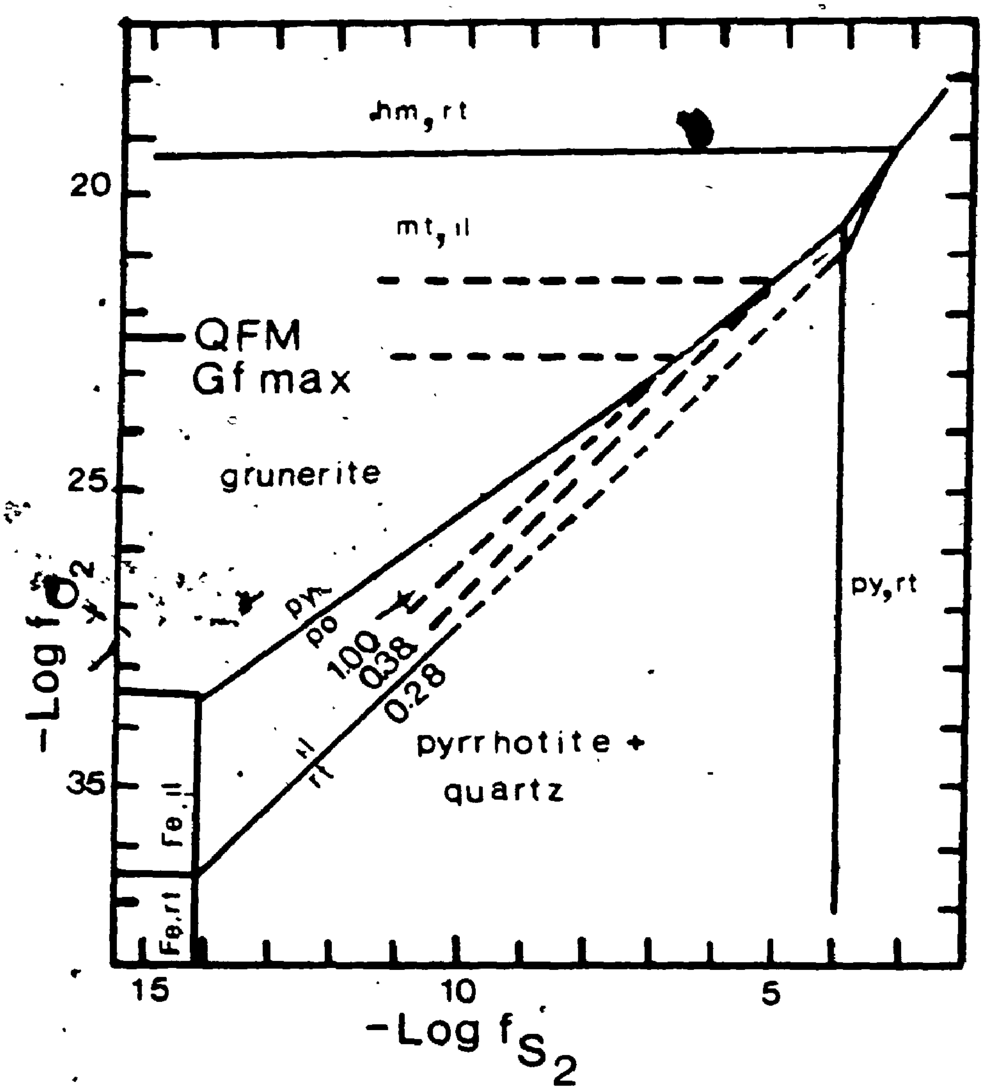

Figure 6.4. -Log f_{O_2} versus -Log f_{S_2} in the system Fe-Ti-S-O-C at 500°C and 5Kb. Grunerite (Fe/Fe+Mg) contured on diagram. (After Hall, 1980, Froese, 1972).

Albite porphyroblasts occur within mats of chlorite in contact with sericite blades. The partial rection:

(Na+K) musc = albite + K musc (similar to Reaction 6)

does not include chlorite which probably is involved by providing Al_2O_3 to form albite. The lack of Ca in the reaction is interpreted to indicate the loss of Ca to the system due to alteration.

4) Grunerite—Chlorite—Garnet +/- Ferroan Dolomite

Although this assemblage is quite rare it occurs solely within the Chlorite-Magnetite Schist. Both garnet and chlorite appear to overgrow grunerite; however, in several instances grunerite is apparently overgrowing a chlorite matrix (Plates 4d, 4e). The possible reaction might be:

$$7Fe_5Al_2Si_3O_10(OH)_2+19SiO_2 = 5Fe_7Si_8O_{22}(OH)_2+2H_2O+7Al_2O_3 \quad 6. (13)$$

The excess Al_2O_3 may be consumed in a subsequent reaction involving the formation of garnet from grunerite:

$$2Fe_5Al_2Si_3O_{10}(OH)_2 + 4Al_2O_3 = 3Fe_3Al_2Si_3O_12+ Fe_5Al_2Si_3O_{10}(OH)_2 +SiO_2 + 2H_2O \quad (14)$$

thus, representing a continuous reaction from Reaction (13). This is consistent with the reaction involving the formation of chloritoid from a chlorite matrix and the alteration of chloritoid by chlorite as seen in the Sericite-Chlorite Schist.

Ferroan dolomite occurs as isolated patches at the margin of grunerite blades. It is interpreted to represent carbonatization of grunerite through the possible reaction:

$$Fe_7Si_8O_{22}(OH)_2 + 7CaO + 7Mg_O + 14CO_2 =$$

$Ca(Fe,Mg)(CO_3)_2 + 8SiO_2 + H_2O$, (15)

5) **Pyrrhotite-Arsenopyrite-Chalcopyrite-Pyrite-Galena**

The sulphide assemblage is restricted to the Chlorite-Magnetite Schist. It may make up to 90% of the rock and as little as 1%, averaging 5%. Plate 5a shows the intimate intergrowth of the sulphides which is interpreted to represent coeval, equilibrium assemblage.

As magnetite and graphite are used to indicate the prevailing oxygen fugacity during metasomatism, sulphides can be used to indicate the sulphur fugacity. Co-existing pyrite and pyrrhotite constrain the f_{S2} to the univariant curve illustrated in Figure 6.4.

6.4.4 Interdependence of Silicate, Oxide and Sulphide Assemblages.

Iron is common to the silicate, oxide and sulphide assemblages of the Chlorite-Magnetite Schist and as indicated above its stability and phase preference is sensitive to f_{O2} and f_{S2}. Recent studies by Hall (1980) and Nesbitt (1982, 1986a,b) of sulphide rich silicate mineral schists indicate that complex interaction occur between silicates, oxides and sulphides during metamorphism.

An important distinction must be made between those studies by Hall (1980) and Nesbitt (1986) and this study. The former studies deal with the reaction between silicates, oxides and sulphides of a pre-exising massive sulphide occurrences or deposits and host rocks and assumes a relatively closed geochemical system. In this study, however, it has been shown that the assemblages seen in the Chlorite-Magnetite Schist are the product of continuous metasomatism of an essentially sulphide free host rock (Foliated Amphibolite) resulting in the formation of a Fe-silicate+Fe-oxide+Fe-sulphide assemblage.

Froese (1972) shows how the oxidation and sulphidization of grunerite will result in the formation of magnetite and pyrite.:

$$Fe_7Si_8O_{22}(OH)_2 + 7/6\ O_2 = 7/3Fe_3O_4 + 8SiO_2 + H_2O \quad (16)$$

$$Fe_7Si_8O_{22}(OH)_2 + 7/2\ S_2 = 7/3FeS_2 + 8SiO_2 + 7/2O_2 \quad (17)$$

Figure 6.4 shows the contour lines of varying Fe/Fe+Mg of grunerite with the value for this study of 1.00. It is apparent from these types of reactions, that the Fe-silicate phase can be consumed to form oxides or sulphides depending on the availability of O_2 or S_2.

Where the sulphide assemblage makes up greater than 50% of the rock, the included silicates are rarely Fe-silicates, consisting most often of albite and muscovite. This is considered to be good evidence that the Fe-silicate assemblage is consumed in a sulphidization reaction similar to Reaction (17). Iron for the sulphides is supplied by the Fe-silicates whereas the As, Cu, Pb and S are supplied by the metasomatic fluid.

6.5 Relationship of Chlorite-Magnetite Schist with Sericite-Chlorite Schist

The possible paragenetic sequence of minerals is:

```
            Time   ------->

chlorite    ---------    ---------
chloritoid    ------
grunerite       -----
magnetite          -----------
albite                   ------
garnet                 -----------
sulphides                    ------
Au and Ag                    ------
```

This clearly represents the progressive relative increase in Fe, f_{O2}, and f_{S2} and the relative decrease of other cations with time and therefore duration of alteration. It is suggested that these variations are the direct cause of the transition from Sericite-Chlorite Schist to Chlorite-Magnetite Schist. Increases in Fe, f_{O2}, f_{S2} are interdependant. For instance, without high bulk rock Fe values, subtle change in either f_{O2} or f_{S2} would not have been reflected in the silicate, oxide or sulphide assemblage.

6.6 Silicified Dolomite

The evidence of the metamorphism of a silicious dolomite is limited to high temperatures due to the restricted bulk rock chemistry of the rock. The most distinctive mineral reaction of a silicified dolomite is (Figure 6.5):

$$3dol+4qt+1H_2O = 1talc+3cal+3CO_2 \quad (18)$$

This reaction occurs at temperatures greater than 450° C and at pressures of 1Kb; however, at the estimated pressures of metamorphism for the Minas III rocks of 3 to 5 Kb (Section 6.2)

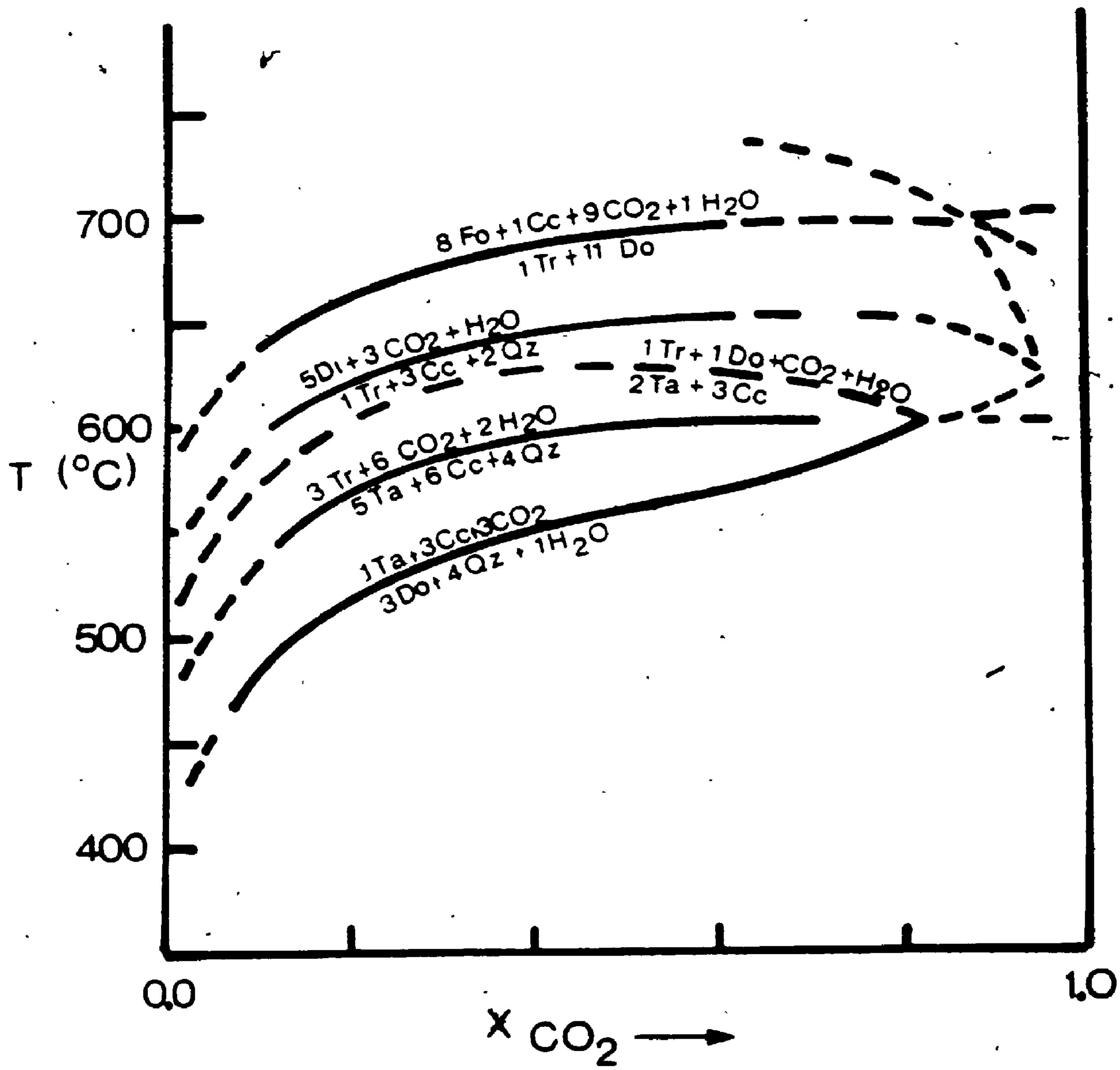

Figure 6.5. X_{CO2} versus Temperture diagram of a dolomite system. (After Winkler, 1976).

the temperature range of the reaction increases to 550° C and 600° C respectively. Again, if the estimated temperatures of metamorphism of the Minas III rocks of 400 and 500° C is applicable (Section 5.3), this reaction would not be expected to occur. This is confirmed by the absence of talc and only minor calcite in later veins.

The silicates present in the Silicified Dolomite are chlorite, biotite and muscovite, rare plagioclase and trace tourmaline. The sheet silicates occur as anastomosing blades along what appear to be micro-shear planes. As Vieser (1983) points out the non-carbonate components in a sedimentary carbonate rock are the result of contamination by terrestrial sources, with clays being the most common contaminant. This accounts for the abundance of Al_2O_3 in the the form of sericite. It does not, however, account for the association of biotite, chlorite, ferroan dolomite, feldspar and tourmaline with sericite. This is more likely due to metasomatic alteration resulting in the idealized reaction:

dol+musc+Fe+Na+B = biot/chl+olg+FD+tour (19)

The rare occurrence of buff-orange sericite and rutile patches is noteworthy. It is suggested that the reaction may be:

$FeTiO_3+CO_2 = TiO_2+FD$ (20)

where the Fe migrates to the edges of the sericite-rutile mat to locally react with the dolomite forming ferroan dolomite. Ilmenite is suggested to have the precursor to rutile, although it is not seen elsewhere in the unit.

In summary, consistent with the indicated temperature and pressure of metamorphism for the Foliated Amphibolite (Section 6.2) the Silicified Dolomite shows no metamorphic mineral reactions. The presence of sericite is probably the result of the metamorphism of clay within the primary carbonate sediment (Vieser, 1983). The presence of biotite, chlorite, feldspar, tourmaline and rutile are the result of the introduction of Fe, Na and B. The nature of this metasomatism is consistant with that seen for the other rock types within the deposit.

6.7 Graphitic Pelite

The metamorphism of pelitic rocks has been very well documented by such workers as Thompson (1957), Thompson (1976) and Ferry (1981). Isograds are marked by the appearance and disappearance of marker minerals. For instance the appearance of biotite through the reaction:

$$\text{phengite+chlorite} = \text{biotite+quartz+}H_2O \quad (21)$$

is the transition from very low to low grade metamorphism (Winkler,1976). The appearance of almandine garnet in a pelite marks the transition from low to mid-grade metamorphism through the reaction:

$$\text{chlorite + quartz} = \text{garnet} + H_2O \quad (22)$$

The complete consumption of chlorite in the presence of biotite marks the end of the transition and the beginning of mid-grade metamorphism

Bulk rock chemistry does, however, govern the presence or absence of mineral assemblages. For instance, chloritoid will only occur in aluminous rocks and stilpmonelane will only occur in those rock which are iron rich (LaTour, 1981, Winkler, 1975).

The Graphitic Pelite of Minas III is characterized by the assemblage:

bt+musc+qtz+chl+graph+FD+po +/- gnt+plag+tour.

This assemblage can be partially represented on an AFM diagram (Figure 6.6) projected through muscovite after Thompson (1957). The tie lines of chlorite-garnet-biotite do not cross, indicating an equilibrium assemblage. The compositions of garnet, chlorite, and biotite conform to the heirachy of Fe partitioning presented by Thompson (1976, Table 2) of Fe-gnt>Fe-chl>Fe-biot. In Figure 6.6 the almandine garnet and chlorite compositions cluster, whereas, the biotite compositions shows a wide spread in both Fe/Mg and Al. The composition of muscovite is also fairly consistant (Figure 5.7d) with the largest shift in chemistry in the Fe/Fe+Mg ratio.

The local appearance of almandine garnet suggests upper low-grade metamorphism. Caution must be used here, in light of the high MnO present in the garnet (4-9%). Manganese will greatly reduce the temperature necessary for nucleation. Within these constraints the Graphitic Pelite is interpreted to be metamorphosed to biotite grade metamorphism or upper low-grade metamorphic conditions. The temperature of metamorphism between 420 and 470°C (Section 5.3.2.2). The pressure cannot be constrained.

Samples K2-13 and K2-14 are noteworthy. They represent examples of altered Graphitic Pelite which are enriched in ferroan dolomite, plagioclase, arsenopyrite and anomalous in Au. Ferry (1984) investigated the metamorphism of carbonate rich rocks intercalated with pelitic rocks. He designated the biotite isograde as the reaction:

$$chl + FD + H_2O = bt + cc + CO_2 \quad (23)$$

In the Minas III Graphitic Pelites calcite is fairly rare with ferroan dolomite far more common. The ferroan dolomite occurs as poikiloblasts and as dismembered veinlets. It is suggested that the FD is a product of carbonatization due to increasing $X\text{-}CO_2$ as seen for the Foliated Amphibolite.

Plagioclase poikiloblasts are noted to occur with abundant ferroan dolomite in several samples. The plagioclase is oligoclase with a core composition of An_{27} and a rim composition of An_{19}. This composition is consistent with garnet-biotite grade metamorphism in a pelitic rock (Thompson, 1957). The occurence of oligoclase poikiloblasts in association with ferroan dolomite strongly suggest that it too, is a product of carbonatization of a previously metamorphosed Graphitic Pelite. The reaction might be:

$$bt + cc + Na + CO_2 = olg + FD \quad (24)$$

where the Al_2O_3 and FeO for the plagioclase and ferroan dolomite respectively comes from biotite, thus accounting for the loss in these two elemets as seen in Figures 5.4b and 5.5c.

In summary, the Graphitic Pelite is metamorphosed to at least biotite grade metamorphism and possibly to garnet-biotite grade

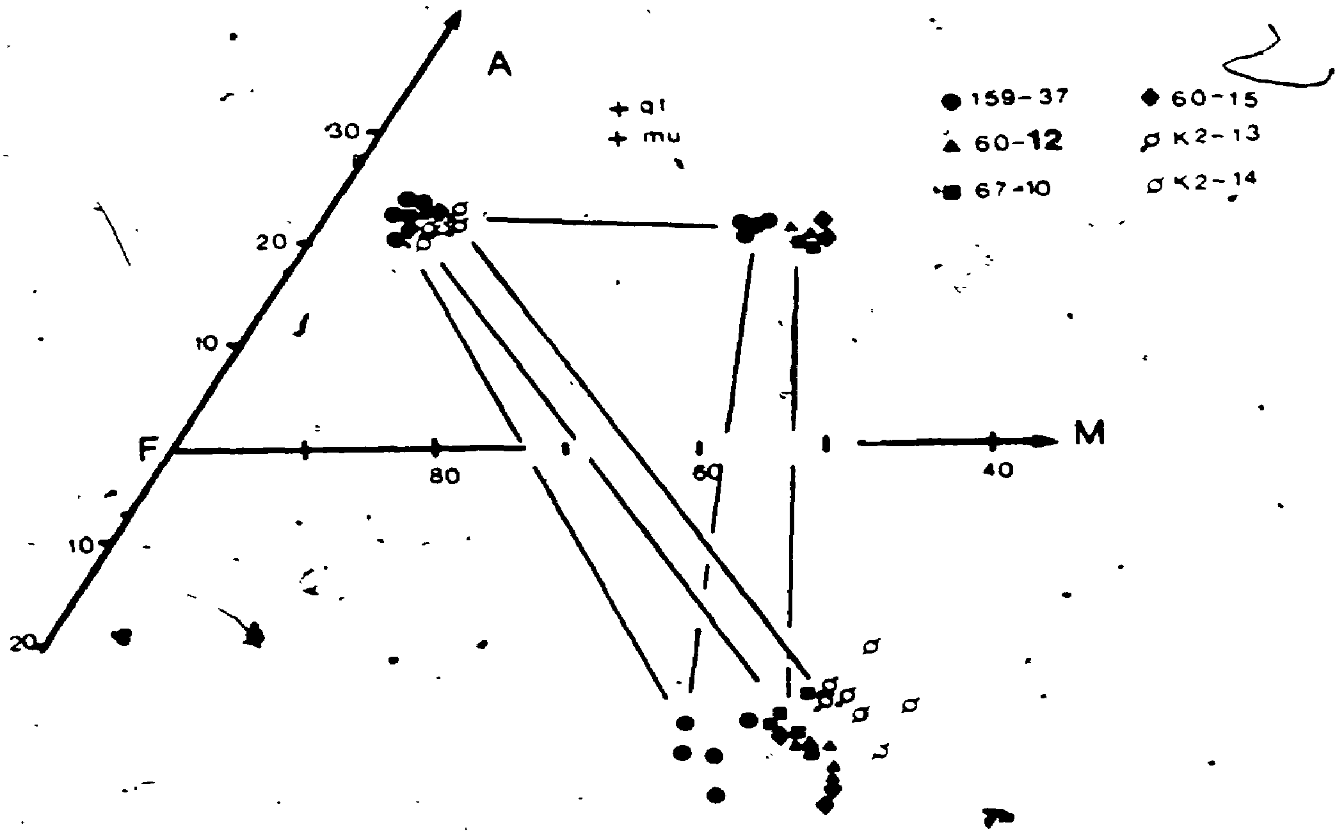

Figure 6.6. AFM digram for Graphitic Pelite (after Thompson, 1957). Samples K2-13 and K2-14 represent altered Graphitic Pelite with anomalous Au.

metamorphism. The temperature of metamorphism is constrained to 420 to 470°C but the pressure of metamorphism cannot be constrained. Latter carbonatization resulted in the formation of ferroan dolomite and oligoclase poikiloblasts and is closely associated with occurrence of anomalous Au. This is consistent with that seen for the Ferroan Dolomite Schist and the Massive Ferroan Dolomite.

6.8 Quartz Cemented Graphitic Pelite Breccia

The mineral assemblages of the Lower Ore Zone are:

i) sericite-oligoclase-ferroan dolomite

ii) brown biotite-sulphides

iii) quartz-ferroan dolomite-calcite veins

Oligoclase porphyroblasts helicitically overgrow a crenulated sericite matrix. The white mica is K rich suggesting that the paragonite component has been consumed to produce the oligoclase. This can be represented by Reaction (6). Ferroan dolomite inturn overgrows the oligoclase porphyroblasts (Plate 8d). This indicates a carbonatization reaction such as:

(Na,Ca) plagioclase + CO_2 + Fe^{2+}+Mg^{2+} = FD + Na^+ + excess Al_2O_3 (25)

Large blades of brown biotite are often in contact with the sulphides of the LOZ and are folded or cross cut the crenulation fabric common to the sericite. The Fe/Mg value of the biotite is compatable to the biotite of the altered Graphitic Pelite but depleted in comparision to the unaltered Graphitic Pelite. This is interpreted to indicate a preferential partioning of Fe to the sulphides.

The precipitation of quartz and carbonate as veins is interpreted to be due to cooling of the fluid (Fyfe et al., 1978). With decreasing temperature and continued wall rock interactions the X_{CO2} also decreased thus precipitating calcite rather than ferroan dolomite.

The proposed paragenetic sequence of the Lower Ore Zone assemblage is:

```
                 Time  ------->

quartz    ----------------------------------------
sericite       ------------
oligoclase          -------------
ferroan dolomite        -------------
biotite                       ----------
sulphides                     ----------
Au                                    -----
calcite                                     -------
```

This sequence is completely compatible with that proposed for the Chlorite-Magnetite Schist (Section 6.5.2) and Graphitic Pelite (Section 6.7). Most significantly it suggests the processes of sericitization, carbonatization and sulphidization.

6.9 Banded Chlorite-Sericite-Garnet Schist

The contact of the Banded Chlorite-Sericite-Garnet Schist to either Graphitic Pelite or Quartz Cemented Graphitic Pelite Breccia is sharp. The geochemistry of this rock type also appears to be fairly unique with only a slight affiliation to that of the Graphitic Pelite (Chapter 4). This unit will therefore not be discussed as a metasomatic daughter product.

Several variations in mineralogy occur from the upper contact to the lower contact of the BCSG Schist. These are:

1) the occurrence of chloritoid as inclusions in garnet and overgrowing the chlorite matrix at the upper contact in the assemblage;

2) the occurrence of plagioclase at the margin of the garnet in association with sericite and chlorite;

3) the increasing occurrence of epidote and decreasing occurence of garnet with depth from the upper contact.

4) reverse zoning of more sodic cores than rims in plagioclase porphyroblasts.

5) the presence of calcite bands

Both assemblages 1) and 2) have been noted in other rock types, most notably as Assemblages 2 and 3 of the Sericite-Chlorite Schist. A combination of Reactions 7,8 and 11 account for the formation of chloritoid, plagioclase and garnet from a sericite-chlorite matrix. This mineral assemblage in the Sericite-Chlorite Schist is interpreted to be an alteration product of a parent lithology. The restricted occurrence of it at the upper contact of the BCSG Schist might also indicate that it too is an alteration assemblage, probably related to the development of the LOZ.

Winkler (1976) indicates that the assemblage "zoisite/clinozoisite + chlorite + muscovite is diagnostic for the complete temperature range of low-grade metamorphism" (pg 81). This contrasts with the garnet-biotite assemblage present at the upper contact which is at the high end of low-grade metamorphism ($420^{\circ}C$, Table 5.5). In support of the geothermometric calculations suggesting an inverse geothermal gradient within the BCSG Schist the occurrence of epidote and absence of garnet with depth can be attributed to a decrease in temperature with depth.

The reverse zoning of sodic cores to more calcic rim of the plagioclase porphyroblasts is attributed to higher temperature at the upper contact which dissipate to lower temperatures with depth.

The bands of calcite common to this rock type are attributed to decreasing X_{CO2} possibly related to decreasing temperature. The calcite bands do not occur at the upper contact where, as proposed, the X_{CO2} would have been elevated.

In summary, the BCSG Schist is metamorphosed to upper low-grade (biotite-garnet) metamorphism at its upper contact and low grade (epitode) metamorphism at its lower contact. This stronly suggests a inverse geothermal gradient. Metasomatic alteration as seen in the Sericite-Chlorite Schist appears to be restricited to the upper contact and is attributed to alteration associated with the LOZ.

6.10 Summary and Conclusions

The parent rock types for Minas III are defined to be Foliated Amphibolite, Silicified Dolomite and Graphitic Pelite. The Banded Chlorite-Sericite-Garnet Schist may or may not be a parent rock type. The Foliated Ampibolite is metamorphosed to Epidote Amphibolite Facies metamorphism (400-500$^{\circ}C$) at an intermediate pressure of 3-5Kb. There are no diagnostic mineral assemblages within the Silicified Dolomite indicating metamorphism below the dolomite+quartz = talc+calcite isograd. The Graphitic Pelite is metamorphosed to biotite-garnet grade metamorphism which is upper low-grade metamorphism and which is equivalent to the Epidote Amphibolite Facies metamorphism of the Foliated Amphibolite.

The assemblage of biotite-garnet occurs within the upper portions of the Banded Chlorite-Sericite-Garnet Schist while at the lower portions epidote is the diagnostic mineral and garnet does not occur. This is interpreted to represent a down temperature metamorphic gradient and is consistent with the geothermometric data presented in Chapter 5.

The metasomatic daughter products of the Foliated Amphibolite are the Ferroan Dolomite Schists, Massive Ferroan Dolomite, Sericite-Chlorite Schist and Chlorite-Magnetite Schist. The Ferroan Dolomite Schists and Massive Ferroan Dolomite are interpreted to be the result of progressive carbonatization (increasing $X\text{-}CO_2$) of the Foliated Amphibolite where Fe and Mg are partitioned in carbonate, Ti in ilmenite and Al into muscovite.

The Sericite-Chlorite and Chlorite-Magnetite Schists cannot texturally be shown to be alteration products of the Foliated Amphibolite; however, there is good geochemical evidence of a genetic link (Chapter 4). The initial stage of alteration appears to be sericitization or cation leaching. The driving force for this style of alteration may well have been the decrease on $X\text{-}CO_2$

due to the carbonatization of the Foliated Amphibolite thus raising the pH of the altering fluid. The development of chloritoid, biotite and oligoclase and ultimately grunerite, albite and garnet overgrowing the sericite-chlorite matrix indicate the continued partioning of Fe, Na and Al into endmember compositions, thus reducing the number of components in the system. Magnetite is seen to be the result of the high Fe bulk-rock chemistry of the Chlorite-Magnetite and not a shift in f_{O2}.

The sulphide assemblage, commonly as massive sulphide in the Chlorite-Magnetite, is interpreted to be the result of sulphidization of the high Fe bulk-rock assemblage. This is supported by the reduction of the Fe-silicates in direct proportion to the increase in sulphides.

The Quartz Cemented Graphitic Pelite Breccia shows a similar alteration assemblage as seen in the Sericite-Chlorite Schist, consisting of sericite, oligoclase and biotite, but differing in the presence of ferroan dolomite apparently replacing oligoclase. Sulphides post-date the sericite alteration and are inturn partially post-dated by silicification.

CHAPTER SEVEN

Model for Gold Deposition

7.1 Gold Solubility and Gold Deposition

Gold solubility in experimental and natural conditions has been the subject of several studies (Helgeson & Garrels, 1968; Henley, 1973; Seward 1973; Fyfe & Kerrich, 1984). Much of the research effort has been to distinguish the transporting ligand for gold and the conditions of optimal solubility and precipitation. Cl, S, As, Te, Sb, Br, and I have been suggested as possible Au transporters (Kishida, 1984); however, as Romberger (1986) points out limited experimental work limits comment to Cl, S and to a lesser extent As. Based on Henley's work (1973) Au is soluble if complexed with a chloride species in acidic and oxidizing solutions at 300 to 500°C (Figure 7.1). Alternatively, Seward (1973) indicates that Au is soluable if complexed with a bisulphide species under reducing conditions and near neutral pH (Figure 7.1). Thioarsenide is suggested by Grigoryeva and Sukneva (1981) as a third significant complexing species for Au, although this is not well constrained through experimentation.

Studies of the precipitation of gold have often involved the simplistic model of non-interaction of the gold-bearing fluid with the host wall rocks (Helgeson & Garrels, 1968). In these models cooling of the fluid can result in the precipitation of gold; however, decreasing temperature is not considered to be an effective method of gold precipitation except for chloride solutions between 450 and 400°C (Seward, 1973). In addition, in most lode gold deposits there is little geothermometric evidence

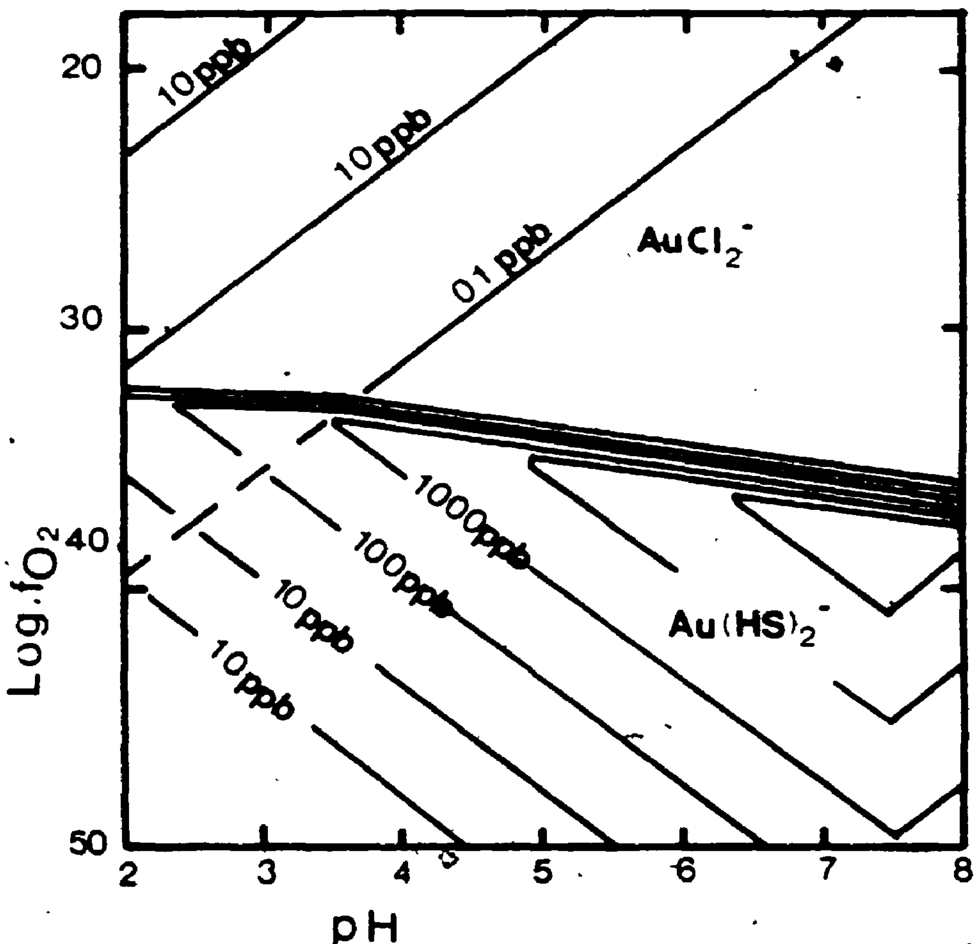

Figure 7.1. -Log f_{O2} versus pH for the system Au-NaCl-S-H_2O at 250°C. (after Romberger, 1986).

that there is a significant variation in temperature during a single mineralizing episode. (Romberger, 1986). It is assumed, therefore, that temperature is not a significant variable during gold extraction.

Those variables which are considered significant are:

f_{O2}, f_{S2}, f_{CO2},

as they influence the stability of the transporting ligand by controlling such parameters as pH. For instance 90% of $AuCl_2^-$ will be precipitated by an increase in pH by two units or a decrease in f_{O2} by 10 units (Figure 7.1). Similarly, 90% of gold can be precipitated from a saturated $Au(HS)_2^-$ solution at near neutral conditions upon a drop of 1 pH unit or a decrease in f_{O2}(Figure 7.1). Under more basic conditions, the solubility of gold as the ligand $Au(HS)_2^-$ will decrease with an increase in pH or decrease in f_{O2}(Figure 7.1). Romberger (1986, pg. 175) suggests that oxidation and increase in pH of a thioarsenide, $AuAsS_2^o$, bearing solution will result in the precipitiation of Au.

The distinction of the participating ligand is important to interpret the conditions of transport and deposition of gold. At 300°C gold bearing hydrothermal solutions are low-salinity and are therefore undersaturated in $AuCl_2^-$; whereas, at this temperature hydrothermal fluids are enriched in sulphur and therefore saturated in $Au(HS)_2^-$ (Cathles, 1986). Cautiously, extrapolating to 500°C it is assumed therefore, that the hydrothermal fluid resulting in the formation of Minas III, was low-salinity and enriched in sulphur with $Au(HS)_2^-$ as the gold complex.

The available gold solubility data is limited to a maximum temperature of 300°C, thus making it uncertain to extrapolate to the intepreted mineralizing temperature of 420-470°C of Minas III. The relative shapes of the phase boundaries for the magnetite-heamatite buffer and the pyrite-pyrrhotite buffer at 250°C and 500°C (Figure 7.2) are the same. The solubility curves of Au are also assumed to retain the same relative configuration, and are shown, along with the stability field of the phases in the system Fe-As-S-O in Figure 7.2.

Two scenerios for the depostion of Au within Minas III are possible given either $Au(HS)^{-}2$ or $AuAsS_2^{\circ}$ as the gold transporting ligands. These are:

1) increase in f_{O2} and decrease in f_{S2};
2) decrease in f_{O2} and decrease in f_{S2},

respectively.

7.2 Mechanism for Au Deposition with Minas III

The paragenetic mineral sequences of the Upper Ore Zone consisting of the Ferroan Dolomite Schist, Massive Ferroan Dolomite, Sericite-Chlorite Schist and Chlorite-Magnetite Schist and that of the Lower Ore Zone or the Quartz Cemented Graphitic Pelite Breccia are similar. They are marked by early carbonatization and sericitization and late sulphidization with Au mineralization associated with the sulphides. It is suggested that the interactions and variations of whole rock chemistry, f_{O2}, f_{S2} and f_{CO2} throughout the paragenetic sequence are critical in creating the appropriate geochemical enviroment for gold deposition.

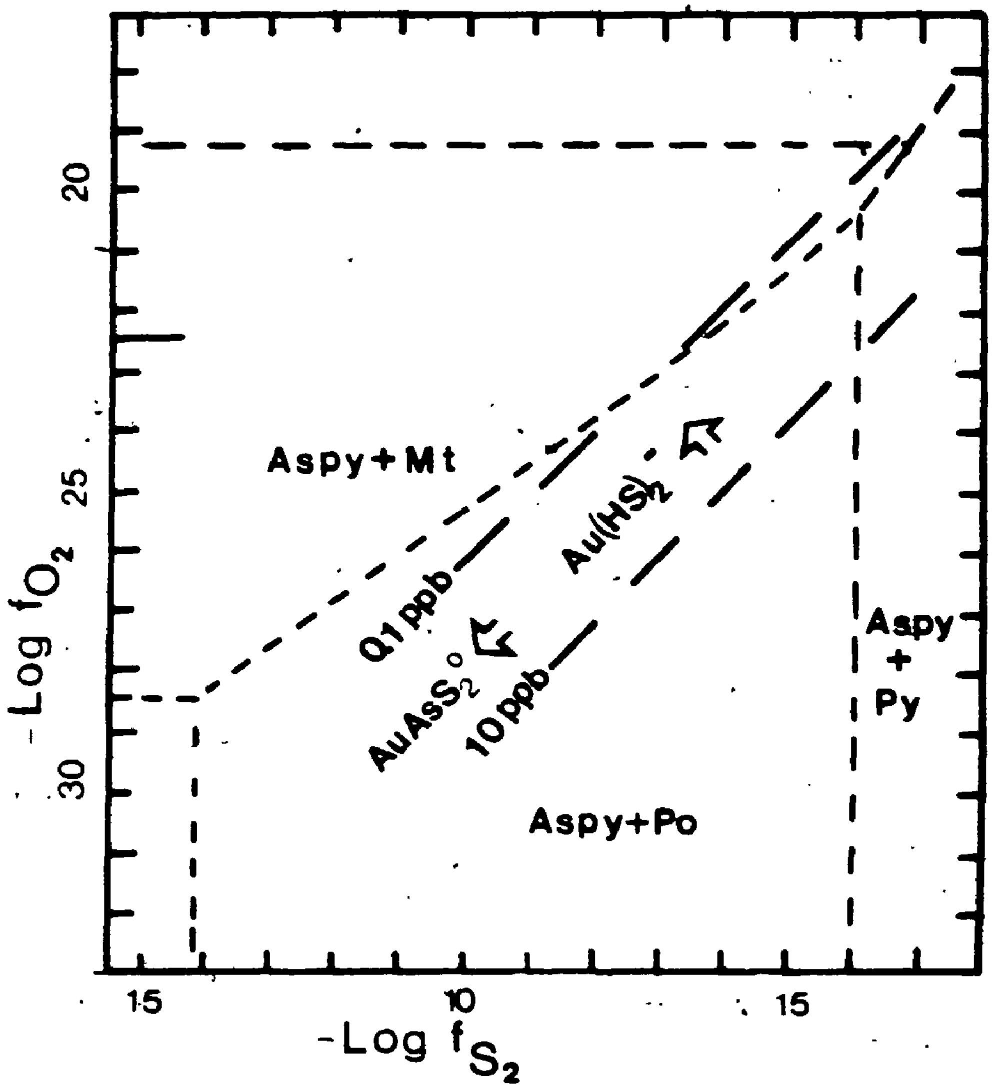

Figure 7.2. -Log f_{O2} versus $-Logf_{S2}$ in the system Au-As-Fe-S-H_2O. Phase boundaries and solubility curves of $Au(HS)_2$, $AuAsS_2$ and arsenopyrite extrapolated to 500°C, 5 Kb from 250°C. (after Romberger, 1986 and Hall, 1980).

Turning to the Upper Ore Zone it can be shown (Figure 7.3) that the reaction:

ph+an+cc+CO2 = mu+do+qtz

partially represented by Reaction (4) and shown in Figure 7.3 results in the formation of the Massive Ferroan Dolomite assemblage from the Foliated Amphibolite parent. Importantly, increases in f_{CO2} drives the reaction and, effectively increase f_{O2}. This type of reaction would also increase the pH of the system through continued loss of CO_2 to the wall rocks.

The textural and geochemical evidence suggests that the deposition of the sulphides was at the expense of a high Fe silicate assemblage. It is proposed that the f_{S2} is dramatically reduced through reactions such as Reaction (17) (Section 6.5.1, Froese, 1972) where grunerite is sulphidized to pyrite with quartz and O_2 as reaction products. This type of reaction meets the requirements for the reduced solubility of $Au(HS)_2^-$ of increased f_{O2} and decreased f_{S2}.

The mineral reactions of the Lower Ore Zone appear to be less complex than those seen for the Upper Ore Zone. Perhaps a critical difference between the two ore zones is the presence of carbonaceous material in the Lower Ore Zone which would act as a tremendous oxygen buffer and may well have decreased the f_{O2}. Again the development of sulphides appear to be linked to the decrease of Fe in the system. For instance, biotite shows a marked Fe/Fe+Mg decrease where associated with sulphides.

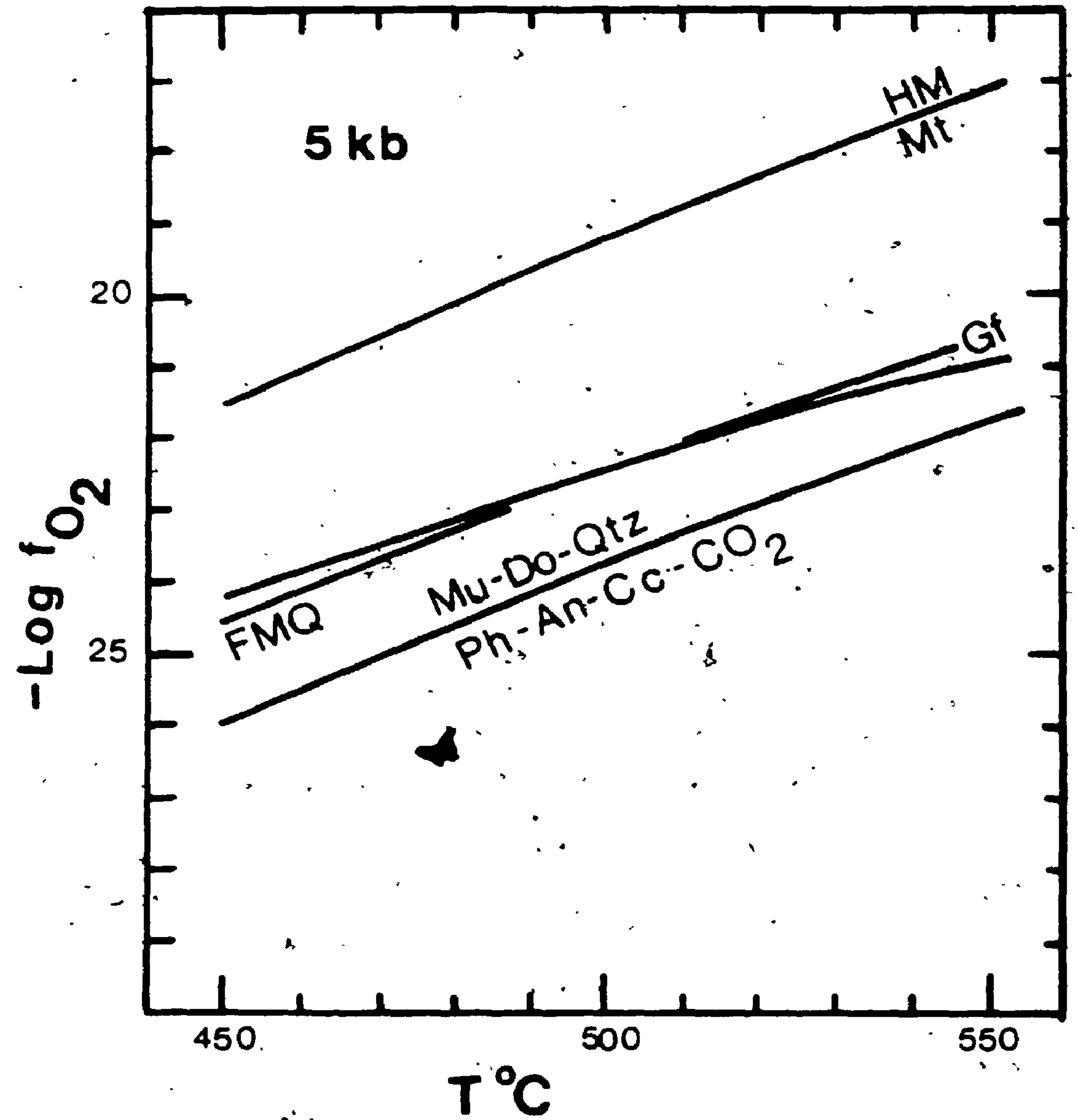

Figure 7.3. -Log f_{O_2} versus temperature. The carbonatization Reaction (4) partially represented (after Hall, 1980).

In this situation of decreasing f_{O2} and f_{S2} it appears that the ligand $AuAsS2^{o}$ may have been the gold carrier. The textural evidence suggests that arsenopyrite is coeval with pyrrhotite and chalcopyrite. Although, as gold does not necessarily occur in contact the sulphides its paragenetic relationship to arsenopyrite remains speculative.

If stated in the simplest of terms the most important factor in the deposition of gold in the Upper and Lower Ore Zones appears to have been the availability of Fe to allow for the development of sulphides. The combining of Fe with the available S to form the sulphides lowered the f_{S2} thus reducing the solubility of the gold-bearing ligand.

CHAPTER EIGHT

Structural Interpretation of Minas III

8.1 Introduction

A systematic, rigorous structural interpretation of Minas III is certainly beyond the scope of the available structural data base. There are, however, some data which should be presented.

8.2 Regional Data

Kuyumjian and de Araujo Filho (1984) present structural data and a structural geologic history of the Crixas Greenstone Belt. They divide the map region into six domains and interpret five phases of deformation. These are:

D_1 - semi-recumbent, isoclinal folds, subparallel to bedding at N10-15S, as parasitic folding on a large synclinorium

D_2 - large scale cross-folds, vertical E-W axial plane, deformation due to ascent of granitic domes

D_3 - type 3 interference folds (Ramsay, 1967), subhorizontal E-W axial plane

D_4 - crenulation cleavage, folding on metre scale at N-S and N40W with vertical axial plane

D_5 - large open folds on the km scale at N-S and N30W with a vertical axial plane.

This author is in general agreement with the work of Kuyumjian and de Araujo Filho (1984) with the one notable additon of thrust faulting. Kuyumjian and de Araujo Filho (1984) recognize a fault within the vicinity of the town of Crixas. It is an inverse fault at N60W which juxtaposes the basal ultramafic unit (CAF) and metasediments (RAF) against the metasediments of the Araxa Group. They suggest that the fault is possibly Mid-Proterzoic in age. The attitude of this fault, as mentioned in Section 2.4, is subhorizontal, plunging at 10-15° to the SE and is interpreted by O. J. Marini (1987, personal communication) as a thrust contact. It is here suggested that not only is the Archean-Araxa Group contact a thrust contact, but so too are the contacts of the Archean units of Corrego Alagadinho Formation, Rio Vermelho Formation and Ribeirao das Antas Formation making thrusting a major component of the structure of the Crixas Greenstone Belt.

The most compelling megascopic evidence for thrusting within the Crixas Greenstone Belt is the presence of a well developed mineral lineation within the rocks of Minas III. The lineation shows an attitude of E-W to WSW plunging at 10-15° which is consistent with that seen at the Araxa Group contact to the underlying Archean rocks. The Sericite-Chlorite Schist and Chlorite-Magnetite Schist of the Upper Ore Zone is boudinaged along this trend (Figure 8.1). The quartz bodies of the Lower Ore Zone are rodded parallel to the trend (Figure 7.1) showing a striking ribbing at the margins of the quartz to the host Graphitic Pelite.

8.3 Significance of Garnet Inclusion Textures within the Graphitic Pelite and Banded Chlorite-Sericite-Garnet Schist

According to Spry (1969) the development of inclusions within minerals may occur syn- and post-deformation. Where syn-deformational the inclusions are often S-shaped and are interpreted to be due to growth of the garent within a shear plane. Post-deformation inclusion trails are helicitic, having passively overgrown the surrounding matrix, thus including the matrix texture. Post-deformation garnets are distinguished from the syn-deformation garnets by idioblastic forms, without pressure shadow zones. The idea that S-shaped, snowball or spiral inclusions are due to rotation of the garnet has been widely

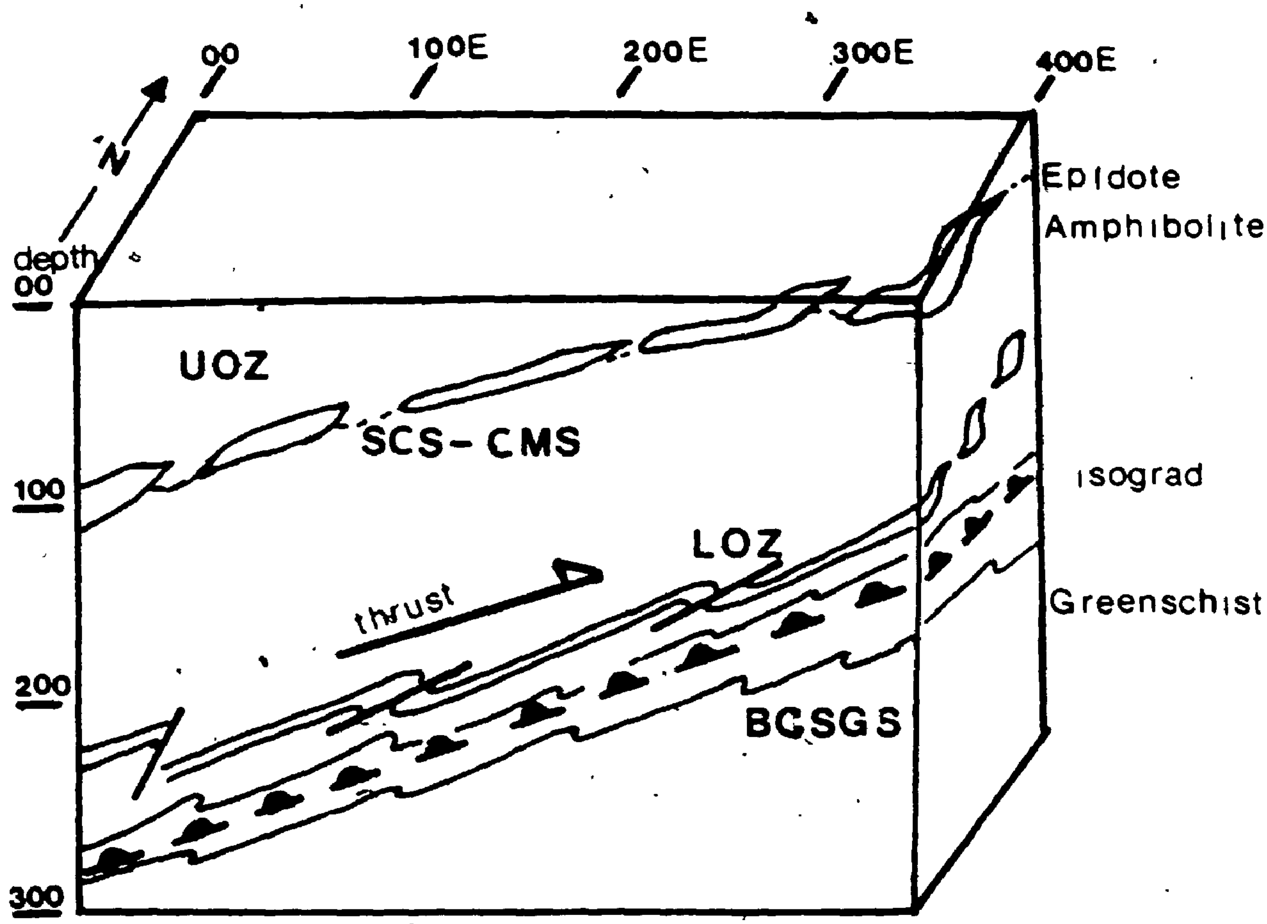

Figure 8.1. Block diagram of Minas III as in Figure 3.3 showing the Epidote Amphibolite-Greenschist isograd. Thrust direction determined from attitude of mineral lineation. UOZ, Upper Ore Zone; SCS-CMS, Sericite-Chlorite Schist-Chlorite-Magnetite Schist; LOZ, Lower OreZone; BCSGS, Banded Chlorite-Sericite-Garnet Schist.

held for a number of years; however, Bell (1985) has recently presented an alternative explanation to the spiral texture. He and his co-workers suggest that porphyroblasts do not rotate due to shear stress and that non-coaxial deformation is taken up within the matrix surrounding the garnet. The inclusions are therefore interpreted to represent the preservation of previous fabrics now obliterated by subsequent re-orientations of the stress elipsoid.

The garnets of the Graphitic Pelite are sub- to euhedral, 0.1 to 1 mm in diameter and are relatively inclusion free (Plate 7c). The matrix of sericite and chlorite wrap slightly around the garnets. The garnets are therefore interpreted to have formed post-deformational or at the late stages of deformation of the Graphitic Pelite.

The inclusion patterns noted within the garnets of the Banded Chlorite-Sericite-Garnet Schist vary with distance from the Quartz Cemented Graphitic Pelite Breccia, giving a clue to the deformation history of this rock. At the upper contact (Samples 74-13, 159-75) the garnets are sieve-textured and poikiloblastic. Quartz is most commonly included within the garnet, but chloritoid, tourmaline and pyrrhotite are also noted. The quartz inclusion patterns show a preferred attitude, paralleling that of the matrix. The elongate direction of the chloritoid blades do not show a preferred orientation within the garnet, nor do the ilmenite inclusions within the chloritoid. The matrix, consisting of chlorite and sericite, wraps around the garnet and is locally re-oriented between garnet poikiloblasts.

The presence of non-oriented ilmenite inclusions within the chloritoid would suggest that prior to nucleation of the chloritoid there was no preferred fabric to the rock. Similarly the lack of orientation of chloritoid within the garnet suggests the chloritoid did not nucleate under directional stress. The garnet, however, appears to have nucleated during deformation as suggested by the rounded shape and abundance of inclusions.

At 20 m below the Quartz Cemented Graphitic Pelite Breccia the garnets display complex inclusion patterns in both core and rim. The core inclusion patterns resemble crenulation cleavage patterns found in the matrix (Plate 9c) although the orientation are not the same. This pattern is interpreted to represent the overgrowth of a previous fabric, which has undergone reorientation. The rim inclusion patterns are clear overgrowths of the matrix foliation pattern suggesting syn-deformational growth (Plate 9c). In the context of Bell's (1985) interpretation of inclusion patterns, it might be suggested that deformation was not co-axial, and dramatically changed in orientation during garnet core and rim growth.

At depths of greater than 40 m below the Quartz Cemented Graphitic Pelite Breccia the inclusions patterns in the garnet porphyroblasts are simple. They are sub-parallel to a co-planar matrix fabric as at the upper contact and are interpreted to be syntectonic.

What do these textures suggest concerning the nature of deformation of the Banded Chlorite-Sericite-Garnet Schist? There can be little doubt that the inclusion patterns within the intermediate depth garnets are the result of non-coaxial deformation or shearing. The deformation during garnet growth at the upper contact and toward the base of the rock unit appear to have either remained essentially co-axial during continuous deformation or, alternatively, the garnet growth preserved a single co-axial event. The former is not favoured, given the evidence of significant re-orientation of the fabric and therefore non-coaxial deformation at intermediate depths in the unit. The most likely model to explain the rapid shift in deformation style between the Graphitic Pelite and the Banded Chlorite-Sericite-Garnet Schist and within the Banded Chlorite-Sericite-Garnet Schist is thrusting.

8.4 Thrusting and the LOZ

A thrust zone is considered a shear zone which represents a zone of large ductile shear strain (Hobbs et al., 1976, pg266). Shear zones may be further classified into brittle, brittle-ductile and ductile. The transition from ductile to brittle deformation or vice versa is a function of hydrostatic pressure, temperature and strain rate. The lower the temperature and hydrostatic pressure the more likely a rock is to deform in a brittle manner by fracturing. Conversely, the higher the temperature and the hydrostic pressure and the lower the strain rate the more likely a rock is to deform in ductile manner through crystal lattice slip (ibid). Under normal geothermal gradients this transition occurs at approximately 400-500°C (Hyndman,1985) which is the Greenschist and Amphibolite Facies transition. Ramsay (1980, pg 83) points out, "In brittle-ductile shear zones it is quite possible that the ductile part of the deformation history formed at a different time from that of the fault discontinuity", indicating that a single shear zone may show a continum of textures reflecting the changes in the conditions of deformation.

Figure 8.1 is a schematic structural interpretation of Minas III. Above the Lower Ore Zone at Amphibolite Facies temerperatures (420-470°C) the style of deformation is dominantly ductile. At the

Lower Ore Zone and within the BCSG Schist at transitional temperatures to Greenshcist Facies (350-400°C) the style of deformation is ductile in the form of crenulation cleavage within the LOZ and the BCSG Schist, S-shaped inclusion textures within garnets in the BCSG Schist and brittle in the form of quartz cement within the LOZ.respectively. Sibson (1977, pg. 199) states that fault zones arise through the local concentration of deformation thus partially explaining why the zone consisting of the Lower Ore Zone and the BCSG Schist concentrated the brittle deformation of the LOZ.

Just as the Lower Ore Zone marks a zone of concentration of deformation, so too does it represent the concentration of fluid flow as indicated by the large quartz vein network (Fyfe et al., 1978). These two phenomena appear to be inseparable in terms of the deposition of Au. That is, without fluid flow, deformation would not have occurred, and without the fluid the Au would not have been depositied. It would therefore appear that gold mineralization at Minas III is related to the development of shear deformation related to thrusting.

8.5 Timing of Thrusting and Mineralization

No systematic age dating has been done to determine the age of deformation of Minas III, making the following discussion highly speculative. There is, however, indirect evidence from the Quadriatero Ferrifero (QF), Minas Gerais. de Oliveira (1986) suggests that large scale thrust faults occur within the QF and that Au mineralization is related to these thrust faults. The age of faulting is believed to be 550-450 Ma and is part of the Braziliano Cycle or Pan-African tectonic event.

It is therefore suggested that the thrusting seen in the Crixas

Greenstone Belt and is Braziliano Cycle in age. Further, it is suggested that the Au mineralization of Minas III, although hosted by Archean age rocks, is Braziliano Cycle in age.

CHAPTER NINE

CONCLUSIONS

1. Twelve unique lithologies are distinguished based on petrographic, lithogeochemical and mineralogical bases within the Crixas Gold Deposit. These rock types from structural top to bottom are:

    i. Foliated Amphibolite
    ii. Ferroan Dolomite-Chlorite-Biotite-Quartz Schist,
    iii. veined Ferroan Dolomite-Chlorite-Sericite-Biotite-Quartz Schist,
    iv. Massive Ferroan Dolomite,
    v. Sericite-Chlorite Schist,
    vi. Chlorite-Magnetite Schist,
    vii. Silicified Dolomite
    viii. Graphitic Pelite,
    ix. Quartz Cemented Graphitic Pelite Breccia,
    x. Chlorite-Plagioclase-Quartz-Ferroan Dolomite Schist,
    xi. Banded Chlorite-Sericite-Garnet Schist.
    xii. Banded Quartz-Biotite-Chlorite-Plagioclase Schist.

2. The twelve lithologies can be divided into two groups: parent rock types which are metamorphosed but essentially unmetsomatised and daughter rock types which are both metamorphosed and metasomatised. The parent rock types are:

Foliated Amphibolite which is metamorphosed tholeiitic basalt. Conditions of metamorphism were Epidote-Amphibolite, approximately 450°C at an estimated pressure of 3 to 5Kb.

Silicified Dolomite which is a metamorphosed primary carbonate sediment. Talc does not occur within this unit suggesting a metamorphic temperature of below 600°C at 3 to 5 Kb.

Graphitic Pelite is metamorphosed primary aluminous sediment. Conditions of metamorphism reached Biotite-Garnet grade which is consistent with Epidote-Amphibolite facies.

Chlorite-Plagioclase-Quartz-Ferroan Dolomite Schist is an enigma but may possibly represent a metamorphosed mafic dyke.

Banded Quartz-Biotite-Chlorite-Plagioclase Schist is a Greenschist Facies metasediment probably best described as a greywacke.

The daughter rocks are the products of four styles of metasomatism: carbonatization, sericitization, Fe-metasomatism and sulphidization.

Ferroan Dolomite-Chlorite-Biotite-Quartz Schist is carbonatized daughter product of Foliated Amphibolite.

veined Ferroan Dolomite-Chlorite-Sericite-Biotite-Quartz Schist is carbonatized daughter product of Foliated Amphibolite.

Massive Ferroan Dolomite is a carbonatized daughter product of Foliated Amphibolite.

Sericite-Chlorite Schist is a sericitization and Fe-metasomatism product of Foliated Amphibolite

Chlorite-Magnetite Schist is Fe-metasomatism and sulphidization product of Sericite-Chlorite Schist and probably Foliated Amphibolite.

Quartz Cemented Graphitic Pelite Breccia is a sericitization, Fe-metasomatism and sulphidization product of Graphitic Pelite. The quartz cement is late in the alteration history and appears to seal brecciation and does not silicify the silicate assemblage.

Banded Chlorite-Sericite-Garnet Schist is sericitized and Fe-metasomatised within 25 m of its upper contact with Graphitic Pelite. It is considered to be a metasomatized daughter product of either Graphitic Pelite or a previously metamorphosed aluminous sediment.

3. Parent rock metasomatism post-dates peak upper low-grade or Epidote-Amphibolite Facies metamorphism (420° to 470°C). The sequence of metasomatism is interpreted as:

   Carbonatization
   Sericitization
   Fe-metasomatism
   Sulphidization

   Metsomatic fluids enriched in CO_2, K_2O, Ba, S and metals such as As, Cu, Pb, Au and Ag drove carbonate, silicate and sulphide mineral reactions. The apparent lack of buffering of the fluid by the parent rock types in the core of the alteration zones suggest that the conditions were that of high fluid flow.

4. Mass balance calculations indicate carbonatization and sericitization resulted in volume increase and volume decrease repectively. This is significant to the interpretation of the apparent gains and losses of the immobile elements such as Al and Ti. In carbonatization Al and Ti values are diluted by volume increase, whereas, in seritization Al and Ti are concentrated by volume decrease. This reconciles the obviously different compositions of the Ferroan Dolomite Schists and Massive Ferroan Dolomite, and the Sericite-Chlorite Schist and Chlorite-Magnetite Schist of the Upper Ore Zone.

5. Gold mineralization is associated with metasomatism and post-dates peak metamorphism. It is related to the reduction of f_{S2} during sulphidization at near neutral conditions. Gold is probably carried as a $Au(HS)_2^-$ ligand.

6. Garnet-biotite geothermometry for the Graphitic Pelite and

Banded Chlorite-Sericite-Garnet Schist suggest a decrease in metamorphic temperature with depth. Calculated temperatures for the Graphitic Pelite range from 455° to 513°C whereas those for the Banded Chlorite-Sericite-Garnet Schist range from 365° to 478°C. This is consistent with an interpreted inverse geothermal gradient located at the Lower Ore Zone.

7. Garnet inclusion textures within Graphitic Pelite and Banded Chlorite-Sericite-Garnet Schist suggest a major structural discontinuity exist between the two units. The garnets of the Graphitic Pelite are 0.5 to 1.0mm in diameter, sub- to euhedral and are contain few inclusions. The garnets of the Banded Chlorite-Sericite-Garnet Schist show a variation from the upper contact to the lower contact of the unit. At the upper contact they are large 0.5 to 1.0 cm, rounded and show a complex inclusion texture and make up to 20% of the rock. Near the low contact the garnets are small 0.5 to 1.0 mm, anhedral and show no inclusions and are very rare.

8. Metamorphic mineral assemblages of the Graphitic Pelite suggest an upper low grade metamorphism, whereas, those of the Banded Chlorite-Sericite-Garnet Schist decrease from upper low grade metamorphism to low grade metamorphism. This is interpreted as further evidence for an inverse geothermal gradient.

9. The geothermometric data, garnet inclusion textures and metamorphic assemblages point to the region of the Lower Ore Zone or the Quartz Cemented Graphitic Pelite to be a major structural and thermal discontinuity. The most appropriate intertpreation is that the Lower Ore Zone is a shear zone

related to a low angle thrust. This model also accounts for the Upper Ore Zone by providing a mechanism for massive fluid flow through ductile shearing.

10. The age of the thrusting is not known. It is speculated that it may be related to the Brasiliano Cycle or Pan-African event (570 Ma).

APPENDIX I

GEOCHEMICAL TECHNIQUES

I-1 WHOLE ROCK GEOCHEMICAL ANALYSIS

Samples of diamond drill core were used exclusively for whole rock geochemistry. They were carefully selected from the complete core sample section to represent a homogeneous unit, especially in the case of the veined samples. The samples were powdered in new tungsten-carbide pots to avoid contamination, at the INCO gold assaying facilities, Copper Cliff, Ontario. X-ray Fluorescence Spectrometry was completed using a Philips PW-1450. A Rh tube were used for major, minor and trace element.

The major element analysis were obtained using glass discs. The fusion charge was made up of 2.0000 g of flux composed of lithium borate, lithium carbonate and lanthanum oxide, 0.0267 g of sodium nitrate and 0.3733 g of baked sample. Prolonged melting time in excess of 40 minutes was required for the very iron rich samples.

Internal standards consisted of UWO-1, MGR-1, BCR-1 and G16. Several duplicates were run to test for accuracy. The duplicate values were found to be precise to plus or minus 5% of the amount present.

Na_2O and S values were determined using a calibration line defined by international standards G-2 and DTS-1.

Trace elements were analysed using pressed powder pellets with reference to international standards. Data was reduced using interference and matrix correction through the computor program Tr[illegible] develped at U.W.O.

Problems arose in analysing samples with arsenopyrite as the dominant sulphide and galena as a minor one. The L line of As is similar to the M line of Pb resulting in a significant overlap. The values presented therefore, for As are in fact a combination of As and Pb and are denoted by a "+" symbol.

I-2 LOI AND CO_2 DETERMINATIONS

LOI or loss on ignition represents a fairly sample procedure. Approximately 10.0 g if the sample is placed in a ceramic crucible of a known weight and baked in a furnace at 1000°C for two hours. The difference in weight from before and after baking is taken as the volitile loss. The volitiles include H_2O, CO_2 and S.

The CO_2 values were determined using the Chittick Apparatus after the procedure described by Dreimanis (1962). The method involes using 0.85 grams of powdered sample which is placed in a small flask. Approximately 20 ml of 20% HCl is poured in to a small vile which is placed in the flask, being careful not to spill any onto the sample. The flask is sealed with a rubber stopper and tubing which leads to a calibrated column of water. Once sealed the HCl is poured on the sample and stirred using a magnet. The evolved CO_2 displaces the column of water. The amount of displacement is recalculated to percentage CO_2 using room temperature and barometric pressure for corrections. The accuracy of the procedure was tested using international standard of dolomite and argillaceous limestone and was found to be precise to within 2% of the published values.

Whole Rock Analysis

Foliated Amphibolite

	159-1	159-2	159-3	159-4
SiO_2	49.49	49.04	52.57	43.48
TiO_2	1.06	1.44	1.72	1.06
Al_2O_3	13.51	16.24	13.39	9.91
FeO	13.61	13.05	17.65	10.35
MnO	0.17	0.17	0.21	0.27
MgO	8.43	7.18	5.51	4.84
CaO	7.33	7.24	5.86	13.40
Na_2O	3.02	3.13	1.92	1.17
K_2O	0.00	0.08	0.00	0.00
P_2O_5	0.19	0.12	0.16	0.12
total	100.83	99.34	100.46	99.32
LOI/CO_2*	4.02	1.46*	1.36	13.14*
Nb	12.4	22.2	0.1	7.8
Zr	72.0	97.9	105.3	79.2
Y	16.5	33.8	13.4	16.1
Sr	106.1	228.8	35.9	191.7
Rb	0.0	25.7	0.0	0.0
As^+	18.5	31.1	11.0	18.4
Zn	98.1	110.3	114.4	89.3
Cu	35.2	26.7	37.7	15.5
Ni	48.2	30.6	17.6	22.3
Co	23.7	21.3	20.7	16.9
Cr	78.0	73.9	49.0	47.7
Ba	17.1	48.0	59.5	23.8
V	182.5	184.3	315.4	202.5
S	117.6	258.9	797.0	100.7

Whole Rock Analysis

Ferroan Dolomite-Chlorite-Sericite Schist

	159-6	159-14	159-36	156-4	156-6	156-8	156-16	156-10	67-7-1
SiO_2	31.56	43.22	37.96	43.32	36.91	40.12	40.02	41.66	21.14
TiO_2	0.64	1.05	0.39	0.94	1.08	1.08	0.57	0.60	0.34
Al_2O_3	7.53	11.91	5.86	13.62	12.02	12.32	7.72	6.71	6.05
FeO	5.69	9.70	9.59	10.12	9.10	10.79	11.52	5.88	5.82
MnO	0.21	0.16	0.47	0.13	0.16	0.20	0.16	0.20	0.24
MgO	2.35	6.01	11.11	7.04	5.99	7.63	7.65	9.59	11.37
CaO	26.62	9.29	13.81	4.85	12.40	9.13	11.67	12.75	19.73
Na_2O	1.07	3.80	0.05	2.02	1.43	2.96	0.72	0.07	0.83
K_2O	0.29	0.58	0.22	0.77	1.96	0.82	0.52	1.02	1.13
P_2O_5	0.11	0.11	0.34	0.11	0.11	0.10	0.01	0.09	0.05
total	98.87	98.82	100.00	99.46	98.40	99.48	99.35	99.64	97.01
LOI/CO_2*	22.82*	10.78*	20.20	7.12*	15.46*	17.26*	17.86*	20.64*	28.50*
Nb	2.7	11.7	16.0	4.5	16.6	14.9	12.6	67.0	2.2
Zr	40.3	70.9	45.4	57.4	77.5	68.1	46.1	102.4	32.0
Y	10.5	34.2	17.5	8.1	24.8	23.4	6.7	40.7	3.4
Sr	224.4	138.3	88.9	72.7	199.2	140.5	73.5	159.6	206.7
Rb	2.5	21.2	14.7	26.4	50.9	30.9	27.0	85.8	34.4
As^+	57.9	25.6	2078.1	61.2	1254.2	152.2	45.5	296.8	442.6
Zn	36.5	86.4	128.2	115.3	55.3	80.4	94.1	81.1	35.9
Cu	11.3	38.6	27.5	11.4	14.8	39.3	10.1	14.5	13.5
Ni	18.3	21.2	25.3	18.3	19.5	21.8	16.4	44.9	8.4
Co	7.6	24.2	8.5	25.4	9.8	20.4	14.8	12.4	9.0
Cr	44.9	60.1	66.6	55.2	80.1	62.5	83.6	96.3	34.2
Ba	371.5	48.0	226.6	48.0	891.0	89.0	107.9	961.9	407.0
V	83.6	183.7	92.7	165.1	131.7	170.2	[illegible].7	111.7	54.4
S	109.8	610.3	2182.2	55.6	311.4	271.5	108.1	99.8	309.6

Whole Rock Analysis

Ferroan Dolomite Chlorite-Sericite-Biotite-Quartz Schist

	159-9	159-10	159-13	156-5	156-7	156-9	159-11
SiO_2	45.62	41.34	46.27	35.48	47.66	35.67	37.69
TiO_2	1.20	0.92	1.21	1.13	0.83	0.77	0.54
Al_2O_3	15.47	11.95	13.13	13.36	16.69	9.60	6.62
FeO	12.34	8.03	11.51	10.17	6.46	8.44	6.33
MnO	0.16	0.13	0.15	0.16	0.09	0.25	0.19
MgO	9.40	7.44	7.42	7.10	4.54	7.06	8.42
CaO	11.28	10.13	5.29	11.01	7.19	13.78	15.35
Na_2O	1.26	0.15	2.19	1.61	3.96	0.57	0.58
K_2O	1.97	2.52	0.36	2.21	1.45	1.49	0.78
P_2O_5	0.11	0.08	0.06	0.04	0.06	0.07	0.20
total	100.25	99.59	99.25	97.11	97.58	98.72	99.97
LOI/CO_2*	14.06*	16.90*	12.04*	15.54*	7.72*	20.56*	22.12*
Nb	31.9	24.7	23.9	12.0	7.7	8.3	15.5
Zr	83.5	77.2	86.0	71.7	59.0	51.4	46.9
Y	28.2	21.5	21.7	17.6	3.4	11.6	17.4
Sr	170.7	141.3	114.3	168.3	179.9	139.1	108.5
Rb	77.6	67.6	18.7	51.3	46.1	33.5	39.1
As+	534.1	480.3	82.4	1194.2	356.4	72.7	51.6
Zn	207.5	86.5	98.2	65.4	59.2	48.3	40.2
Cu	19.4	15.6	14.3	29.3	16.3	75.3	19.3
Ni	24.4	28.4	44.2	16.0	19.2	13.6	9.2
Co	15.4	9.7	22.1	11.3	17.7	10.2	8.5
Cr	100.4	78.4	87.7	59.3	45.1	44.6	34.2
Ba	804.5	1314.6	102.1	487.2	324.0	1420.0	590.6
V	190.9	161.0	195.4	156.2	98.2	155.6	78.7
S	488.4	466.7	124.1	1595.2	288.8	142.9	128.1

Whole Rock Analysis

Massive Ferroan Dolomite

	159-11	159-17	159-21	159-26	159-27	159-42	60-9-1	60-1	156-13	57-3	88-7
SiO_2	15.48	16.33	15.75	24.49	31.74	14.11	22.30	20.11	19.24	24.45	17.10
TiO_2	0.23	0.14	0.52	0.25	0.39	0.59	0.38	0.27	0.45	0.51	0.55
Al_2O_3	5.87	1.33	3.35	3.29	11.29	9.09	4.79	3.04	5.41	4.08	8.37
FeO	5.67	4.59	14.71	9.51	8.10	16.98	5.74	4.70	5.10	6.28	9.39
MnO	0.25	0.32	0.38	0.39	0.17	0.56	0.46	0.15	0.17	0.17	0.87
MgO	12.39	13.70	10.65	13.13	7.85	10.61	12.28	13.82	11.71	11.16	23.69
CaO	21.53	24.68	20.53	19.37	14.10	16.54	19.27	22.67	20.53	21.09	38.08
Na_2O	0.17	0.00	0.01	0.00	0.54	0.26	0.96	0.96	2.19	0.29	0.18
K_2O	1.38	0.41	0.00	0.24	2.59	0.21	0.20	0.64	1.37	0.87	2.26
P_2O_5	0.28	1.27	0.12	0.08	0.10	0.14	0.10	0.12	0.28	1.01	0.10
total	98.00	99.31	100.00	100.45	100.00	98.77	96.38	99.60	98.80	99.84	101.66
LOI/CO_2*	34.12*	34.82*	32.48*	28.60	22.02*	22.58*	29.68*	33.66*	33.06*	28.91	38.98
Nb	2.2	68.5	4.1	2.2	7.2	11.5	10.6	15.2	23.5	0.0	27.1
Zr	20.3	74.6	29.0	14.3	38.8	45.7	35.1	38.5	50.2	24.1	51.2
Y	8.2	44.1	19.1	3.4	10.9	13.0	8.0	15.1	19.1	4.6	18.7
Sr	14.2	253.6	46.4	73.0	169.2	131.5	129.0	97.6	113.6	186.0	224.4
Rb	88.3	70.3	5.6	9.0	55.7	12.8	21.7	24.7	52.5	3.6	51.1
As$^+$	88.3	163.1	103.1	5112.4	589.5	19.3	99.2	93.7	61.4	46.8	77.4
Zn	40.9	64.3	52.5	65.7	43.0	212.1	43.5	33.4	43.8	29.4	59.8
Cu	8.7	16.7	11.3	9.7	21.9	10.1	7.4	11.6	12.3	6.8	8.9
Ni	9.2	19.6	16.8	4.2	14.6	7.7	7.5	10.8	17.3	9.5	10.6
Co	4.3	0.0	5.6	15.4	7.4	5.3	10.4	4.5	5.8	5.6	4.4
Cr	29.4	62.8	66.4	30.4	65.5	75.7	31.2	40.9	50.7	26.4	34.2
Ba	607.1	376.1	48.0	109.0	1898.7	48.0	48.0	306.1	509.0	308.8	932.5
V	70.6	45.6	211.4	60.8	156.4	209.0	53.8	37.0	49.5	30.1	65.9
S	19.7	52.9	48.4	364.4	600.2	76.2	41.4	37.2	128.0	56.2	36.6

Whole Rock Analysis

Sericite Chlorite Schist

	159-7	159-8	159-16	159-19	159-24	159-28	159-44	74-9	67-6
SiO_2	43.88	43.75	44.45	47.22	31.10	29.30	34.22	60.33	49.26
TiO_2	1.06	0.91	1.26	2.27	2.23	1.68	2.57	1.07	0.81
Al_2O_3	12.41	11.17	14.76	34.30	26.75	23.91	27.96	15.00	15.83
FeO	9.25	8.84	12.30	4.14	21.85	8.51	19.76	6.97	5.57
MnO	0.18	0.13	0.09	0.02	0.05	0.07	0.07	0.14	0.05
MgO	10.04	6.88	9.81	0.13	5.30	10.10	2.36	3.20	3.10
CaO	6.51	7.96	3.71	0.06	0.28	0.62	0.97	3.35	6.54
Na_2O	0.11	0.20	0.04	0.92	0.22	0.38	0.49	0.65	1.99
K_2O	1.10	2.09	1.42	8.82	3.64	2.81	4.64	3.73	3.08
P_2O_5	0.09	0.09	0.11	0.07	0.13	0.00	0.14	0.04	0.03
total	99.05	99.52	99.00	98.43	99.37	97.07	99.62	98.68	94.82
LOI/CO_2*	13.39*	16.44*	9.97*	4.03	5.81	7.59	4.26	3.44*	7.93*
Nb	10.0	8.4	10.7	23.0	15.2	2.2	11.0	41.9	2.2
Zr	63.4	59.9	79.5	174.3	121.1	54.8	134.0	156.7	36.5
Y	10.6	9.1	17.9	132.8	3.4	3.4	9.0	84.6	3.4
Sr	46.6	69.9	28.0	89.6	33.9	2.6	82.1	151.7	177.6
Rb^+	20.6	60.4	36.9	166.2	67.9	40.7	61.1	184.8	46.0
As	74.4	129.2	104.4	309.4	1127.3	2709.7	99.9	172.6	8909.8
Zn	119.6	121.2	155.1	14.1	178.2	151.6	196.2	55.4	18.4
Cu	10.9	8.8	14.8	10.7	11.3	5.5	24.6	12.5	14.5
Ni	39.8	21.0	28.9	40.1	19.6	36.3	80.4	18.7	17.4
Co	18.1	21.3	26.1	5.7	12.4	76.8	4.5	1.2	8.4
Cr	88.4	57.2	73.9	124.2	118.9	147.9	176.1	90.8	72.4
Ba	930.1	886.9	633.0	6195.0	3339.5	4142.6	4302.5	3671.7	2238.6
V	118.2	186.9	250.4	452.3	449.9	430.7	523.6	328.8	153.1
S	72.2	70.9	122.3	60.0	92.5	150.0	1430.4	254.8	1045.4

Whole Rock Analysis

Chlorite-Magnetite Schist

	159-18	159-20	159-23	159-43	60-9-2	60-9-3	60-9-4
SiO_2	45.07	26.00	19.48	45.15	18.96	31.87	26.88
TiO_2	0.95	2.06	1.79	1.80	3.54	2.22	0.25
Al_2O_3	[illegible]	23.12	6.36	16.81	8.26	11.81	10.80
FeO	[illegible]	30.44	57.85	25.00	58.97	30.31	29.05
MnO	0.09	0.06	0.17	0.26	0.12	0.24	0.26
MgO	5.72	3.98	2.19	2.63	4.32	5.06	10.42
CaO	2.92	0.29	1.91	1.12	1.94	8.60	10.47
Na_2O	0.06	0.17	0.01	0.20	0.10	2.62	0.72
K_2O	0.43	1.00	0.00	1.08	2.97	1.87	0.07
P_2O_5	0.17	0.11	0.41	0.11	0.52	0.48	0.17
total	96.52	96.89	90.60	97.70	100.00	100.00	100.00
LOI/CO_2 *	2.31	6.20	2.17	3.46	1.57	4.32	8.81
Nb	12.3	2.2	2.2	15.2	2.2	19.1	2.2
Zr	54.3	94.2	27.4	89.7	37.6	87.0	4.7
Y	13.8	3.4	3.4	21.6	3.4	30.8	11.3
Sr	4.2	2.6	2.6	15.2	2.6	104.8	81.9
Rb	16.1	9.4	2.3	28.0	58.2	65.1	2.3
Ag +	7334.2	19.8	14401.0	55.6	23.6	30.2	18888.9
Zn	163.1	214.1	168.4	239.2	304.2	144.6	205.2
Cu	165.7	12.6	51.8	20.1	91.9	202.2	370.6
Ni	13.9	29.4	47.9	31.7	67.3	25.3	15.9
Co	5.3	11.9	1.2	6.4	1.2	1.2	1.2
Cr	83.2	110.5	160.7	145.6	238.1	172.3	29.9
Ba	106.4	739.5	48.0	992.2	430.6	241.9	48.0
V	270.7	406.9	591.1	241.1	859.0	635.2	195.5
S	6899.2	75.9	2661.5	975.3	5008.9	8536.8	5370.6

Whole Rock Analyses

Silicified Dolomite

	159-29	159-31	159-32	159-34	159-39	159-48	159-50	159-54	159-56	159-57a	60-3	60-6
SiO_2	16.21	11.14	11.43	30.65	6.02	16.36	9.95	57.52	64.59	19.30	20.22	9.91
TiO_2	0.12	0.10	0.10	0.18	0.10	0.10	0.12	0.10	0.14	0.15	0.13	0.17
Al_2O_3	2.48	1.31	0.36	1.54	0.66	0.47	0.94	0.39	1.44	2.80	0.10	0.58
FeO	5.90	3.20	1.77	3.88	4.22	1.93	2.37	1.51	1.50	0.13	1.02	1.33
MnO	0.30	0.33	0.17	0.19	0.41	0.17	0.25	0.19	0.75	0.30	0.18	0.16
MgO	14.55	15.15	18.65	9.83	16.87	16.43	17.08	8.25	6.52	15.11	16.70	18.01
CaO	23.35	25.32	26.26	21.21	27.94	25.12	25.72	12.65	9.99	21.94	24.88	28.13
Na_2O	0.05	0.01	0.01	0.01	0.07	0.01	0.07	0.02	0.06	0.03	0.00	0.00
K_2O	0.46	0.35	0.00	0.05	0.00	0.01	0.07	0.02	0.31	0.84	0.11	0.25
P_2O_5	0.60	0.97	0.27	3.61	1.73	0.89	0.12	0.16	0.16	0.22	0.31	1.02
total	100.00	96.32	100.00	97.70	100.00	100.00	100.00	100.00	100.00	100.00	98.95	98.81
CO_2	35.94	38.40	41.47	26.11	42.07	38.59	43.24	19.39	15.69	34.71	35.39	39.34
Nb	42.4	4.9	2.8	22.4	40.1	0.1	17.6	25.1	16.9	20.5	6.5	10.8
Zr	55.7	18.1	13.5	32.3	46.4	14.3	30.2	35.4	30.1	35.7	18.1	19.2
Y	27.5	9.3	6.1	87.2	23.7	7.6	13.0	16.2	11.4	16.4	3.4	3.4
Sr	210.1	132.8	112.9	158.1	188.1	239.4	190.1	162.7	83.4	130.7	65.7	108.1
Rb[+]	51.0	21.3	0.1	39.1	37.1	0.0	20.9	29.2	27.0	41.0	18.9	22.9
As	1295.2	35.8	36.6	91.6	43.7	19.0	50.8	38.0	94.0	146.4	24.0	40.4
Zn	58.1	26.9	34.2	36.6	52.5	35.2	31.9	26.2	20.8	56.6	8.4	21.5
Cu	112.4	6.1	8.2	13.7	10.9	7.9	11.3	8.5	8.4	11.4	7.2	7.2
Ni	17.2	37.1	3.6	13.2	6.9	4.9	7.9	5.1	6.6	9.4	0.6	3.6
Co	1.8	1.9	0.7	1.2	2.2	0.6	2.1	3.3	3.6	2.8	6.1	8.3
Cr	32.3	11.4	11.3	16.1	14.1	17.8	24.0	44.5	55.9	35.6	6.7	13.4
Ba	430.7	244.1	100.8	162.4	110.7	112.0	119.7	133.3	322.7	864.3	133.5	278.8
V	64.1	23.7	12.6	3.1	18.0	12.0	17.9	15.4	29.3	30.3	13.7	17.1
S	196.3	37.6	18.8	40.5	33.9	16.3	24.6	29.4	57.2	78.4	29.9	30.4

Whole Rock Analysis

Silicified Dolomite

	60-11	60-19	60-21	74-12	49-4	49-5	49-9	77-4	79-2	156-14	156-15	156-20
SiO_2	12.17	24.62	7.96	45.36	86.11	14.01	11.77	10.33	25.22	24.30	49.74	38.17
TiO_2	0.15	0.13	0.15	1.39	0.17	0.14	0.16	0.48	0.10	0.12	0.11	0.12
Al_2O_3	0.71	1.65	1.50	17.73	1.36	1.22	0.47	4.02	0.57	0.93	2.17	0.10
FeO	2.27	1.97	3.46	21.58	0.13	2.27	2.28	7.22	4.84	4.49	6.23	4.37
MnO	0.30	0.19	0.33	0.15	1.68	0.21	0.20	0.32	0.65	0.20	0.17	0.16
MgO	15.82	14.72	18.41	1.98	1.68	16.76	17.40	25.95	24.18	12.80	6.94	11.88
CaO	25.20	20.95	28.91	3.59	0.48	26.83	27.54	42.98	42.33	23.28	13.79	18.22
Na_2O	0.00	0.02	0.03	0.22	0.00	0.08	0.03	0.13	0.04	0.06	0.18	0.01
K_2O	0.33	0.46	0.43	0.00	0.48	0.32	0.18	0.66	0.00	0.29	0.67	0.05
P_2O_5	0.75	0.36	0.60	0.07	0.11	1.11	0.96	3.58	0.55	0.84	0.84	0.26
total	96.53	96.50	99.71	97.45	100.51	99.67	99.61	101.74	98.42	98.77	100.28	99.33
CO_2	38.62	31.54	37.93	5.46	39.51	37.55	39.35	38.29	48.58	31.95	19.25	26.25
Nb	6.0	7.6	9.7	82.9	3.9	18.8	13.8	33.6	1.7	12.5	11.4	18.4
Zr	20.2	19.0	28.0	194.3	32.4	36.3	26.6	61.2	10.1	26.7	21.2	28.9
Y	3.4	3.4	6.8	99.9	6.6	16.1	12.2	28.5	6.2	15.5	14.0	12.5
Sr	118.8	66.5	216.9	201.9	49.2	158.7	151.3	409.3	333.3	163.8	108.1	116.4
Rb^+	18.6	30.4	26.0	21.5	12.5	23.5	15.8	40.6	0.0	13.8	21.7	16.8
As	44.2	15.0	50.7	234.5	93.5	37.1	34.0	212.8	22.5	71.9	111.7	21.2
Zn	23.2	16.5	47.5	196.3	11.2	32.7	36.9	55.1	36.5	40.3	29.2	25.8
Cu	9.8	10.9	7.8	37.0	8.4	8.1	8.4	10.1	8.0	8.8	9.4	10.1
Ni	2.5	1.6	4.2	21.6	8.5	6.4	6.5	20.4	3.1	7.7	14.0	6.5
Co	2.6	3.4	7.4	1.2	4.9	0.2	1.7	4.7	0.6	2.4	2.7	0.1
Cr	13.2	36.4	15.2	106.2	95.3	28.6	27.9	39.9	25.7	35.3	80.3	44.0
Ba	361.4	94.5	189.8	1063.7	379.5	352.5	262.8	228.2	78.9	132.9	368.7	144.8
V	15.4	15.8	19.1	168.4	16.1	23.6	12.3	32.9	12.6	30.6	34.9	7.6
S	91.7	176.4	44.3	918.0	40.7	25.4	29.6	34.5	28.5	32.3	35.9	25.2

Whole Rock Analysis

Graphitic Pelite

	156-1	156-3	159-37	159-46	159-47	159-66	159-67	159-73	60-12	60-13	60-15	60-17
SiO_2	60.67	53.31	57.44	60.16	54.50	56.14	56.98	49.67	60.72	65.77	60.83	60.83
TiO_2	0.82	0.66	0.79	0.65	0.64	0.60	0.63	1.03	0.73	0.66	0.73	0.70
Al_2O_3	18.28	14.74	14.99	12.86	13.10	12.45	13.40	18.73	14.30	15.11	14.48	13.90
FeO	6.50	6.39	8.49	7.47	6.81	8.46	6.11	9.49	7.75	6.26	7.57	8.20
MnO	0.06	0.06	0.17	0.27	0.33	0.13	0.18	0.13	0.17	0.07	0.26	0.27
MgO	3.13	3.23	3.32	3.33	3.24	3.77	3.51	5.71	3.08	2.70	3.06	3.28
CaO	1.87	1.99	2.06	3.65	7.77	5.80	5.79	2.64	2.31	1.26	2.78	3.53
Na_2O	2.29	1.41	1.44	1.27	1.88	0.38	0.93	0.49	1.94	1.79	1.73	1.83
K_2O	2.56	2.94	2.56	2.21	1.82	2.75	3.23	3.79	2.20	2.40	2.26	2.12
P_2O_5	0.25	0.21	0.10	0.14	0.16	0.19	0.08	0.27	0.14	0.14	0.14	0.13
total	99.71	99.40	97.80	99.07	98.80	97.42	98.20	99.72	98.55	99.23	99.41	100.55
LOI/CO_2*	3.25	15.41	6.38	7.01	9.71	6.69	7.31	7.69	5.16	3.03	5.51	5.71
Nb	17.4	8.4	553.3	16.4	16.0	15.0	11.3	21.1	8.9	21.0	21.3	19.2
Zr	144.7	117.5	941.8	127.2	129.6	112.0	124.7	182.4	102.6	172.8	151.1	147.8
Y	23.1	15.0	56.8	29.5	23.4	24.4	19.2	49.0	7.0	28.8	45.4	35.4
Sr	133.2	64.5	723.1	100.2	174.9	133.2	209.6	91.2	223.3	77.0	121.4	135.0
Rb	76.8	79.8	685.7	78.5	57.1	83.6	81.3	103.7	33.1	76.0	86.9	78.2
+As	95.0	78.5	1021.9	89.4	160.7	1939.2	103.2	25.6	193.8	45.1	209.8	140.3
Zn	87.6	80.5	929.5	135.3	122.7	108.5	37.1	225.5	34.3	83.9	136.1	154.6
Cu	13.4	11.0	179.2	25.9	26.7	25.1	22.0	25.1	19.8	9.0	28.3	24.6
Ni	19.4	9.1	60.3	19.2	32.2	20.2	11.9	23.9	9.9	18.0	23.3	23.2
Co	14.7	11.6	1.2	12.2	10.2	25.1	7.5	16.0	1.2	14.3	17.1	14.0
Cr	44.8	36.3	58.9	55.8	83.4	55.8	43.7	85.8	27.9	66.1	62.3	59.8
Ba	2601.5	1909.5	3152.0	1133.2	942.5	1037.6	1500.8	1342.1	466.1	1288.8	1278.6	817.8
V	108.5	91.5	179.0	77.2	88.6	94.4	92.2	132.8	35.2	62.4	90.3	82.4
S	276.1	420.2	2475.5	996.9	1500.1	3047.3	2770.9	1403.6	2072.2	81.3	1011.6	1145.2

Whole Rock Analysis[a]

Graphitic Pelite

	74-4	74-5	74-6	74-7	67-1	67-9	67-10	67-11b	67-14	67-18
SiO_2	60.59	57.78	60.23	53.03	62.38	59.48	60.50	57.23	47.89	55.08
TiO_2	0.52	0.86	0.68	0.44	0.79	0.47	0.76	0.79	0.67	0.74
Al_2O_3	14.15	15.73	14.64	10.78	16.15	12.53	16.98	17.64	13.74	12.99
FeO	5.63	7.62	7.33	6.47	6.87	6.88	7.54	7.38	12.10	9.19
MnO	0.15	0.23	0.14	0.35	0.06	0.18	0.12	0.07	0.24	0.14
MgO	2.05	3.35	2.81	3.87	2.90	2.89	2.23	2.31	4.58	3.44
CaO	3.18	3.40	2.32	8.51	2.13	2.59	1.97	2.17	8.39	5.36
Na_2O	0.02	1.60	2.33	2.60	2.71	0.52	2.90	3.98	2.52	0.59
K_2O	2.81	2.71	2.42	1.08	2.41	2.86	2.48	2.94	1.95	2.05
P_2O_5	0.14	0.18	0.19	0.14	0.19	0.11	0.19	0.17	0.10	0.20
total	96.88	99.08	98.23	97.05	98.78	96.79	98.55	96.26	100.00	98.03
LOI/CO_2*	7.11	3.90	5.08	9.79	2.14	8.32	1.89	1.51	8.27	8.20
Nb	14.3	22.1	21.0	9.1	16.0	3.9	16.7	15.9	2.2	13.8
Zr	126.5	174.0	143.2	104.1	135.7	118.7	155.5	154.7	70.8	116.3
Y	23.5	32.0	39.0	7.3	23.5	13.0	18.3	23.9	3.4	33.0
Sr	131.2	127.2	130.1	22.7	115.2	85.9	160.2	176.2	103.8	113.8
Rb	90.8	96.8	87.7	32.5	83.5	89.1	88.3	99.9	30.2	66.4
As+	74.1	110.1	144.4	196.5	94.1	40.3	59.2	104.8	21275.0	47.4
Zn	47.3	159.7	113.7	33.4	95.5	97.1	136.3	79.3	78.3	140.8
Cu	21.2	13.0	22.4	19.6	22.7	22.8	13.7	17.9	44.7	24.9
Ni	12.0	23.3	17.3	9.6	10.9	15.6	8.9	8.7	18.3	23.8
Co	11.4	14.6	11.5	6.3	12.7	11.6	11.7	8.1	5.5	18.9
Cr	30.3	97.9	51.3	28.9	44.9	28.5	34.0	36.9	42.5	63.4
Ba	1425.6	1075.2	1089.3	555.8	1839.9	1522.8	1298.1	1874.6	761.1	721.6
V	80.1	92.9	83.3	55.8	85.6	69.5	82.7	95.4	76.3	99.1
S	2829.6	370.9	2179.8	1901.1	1007.1	3124.0	519.7	1040.5	2236.2	1134.9

Whole Rock Analysis

Chlorite-Plagioclase-Quartz -Ferroan Dolomite Schist

	159-64	159-65	60-20
SiO_2	48.27	47.39	50.92
TiO_2	2.58	2.26	0.56
Al_2O_3	15.72	15.76	19.96
FeO	13.79	14.54	8.67
MnO	0.29	0.24	0.08
MgO	6.30	6.24	3.33
CaO	9.04	9.20	3.93
Na_2O	1.84	1.21	2.07
K_2O	0.12	0.40	5.47
P_2O_5	0.43	0.37	0.28
total	99.93	99.26	100.00
LOI/CO_2 *	3.93*	8.46	9.02*
Nb	98.7	45.5	27.2
Zr	221.5	161.2	163.5
Y	56.3	30.6	34.0
Sr	365.0	277.5	163.1
Rb	91.3	43.0	170.9
As+	100.0	96.3	109.9
Zn	189.1	188.6	182.8
Cu	18.7	13.5	18.9
Ni	41.8	52.0	9.5
Co	17.0	17.2	1.2
Cr	69.9	77.2	29.2
Ba	101.1	155.4	1951.6
V	107.8	72.5	87.8
S	952.5	187.0	1036.5

Whole Rock Analysis

Banded Chlorite-Sericite-Garnet Schist

	159-71	74-13	67-19	60-29
SiO_2	52.29	64.10	51.48	52.19
TiO_2	1.31	0.82	1.47	01.42
Al_2O_3	16.57	15.09	19.99	18.62
FeO	15.07	6.89	14.37	18.00
MnO	0.13	0.06	0.12	0.16
MgO	4.37	2.94	2.21	2.46
CaO	0.80	1.45	1.35	1.86
Na_2O	1.77	0.76	0.45	0.22
K_2O	2.10	2.43	4.38	2.94
P_2O_5	0.10	0.16	0.11	0.17
total	99.36	97.13	98.81	100.88
LOI/CO_2*	4.75	2.57*	2.84*	2.82*
Nb	77.3	2.2	25.1	30.9
Zr	278.7	12.0	108.4	105.7
Y	101.7	3.4	42.8	36.1
Sr	339.9	18.3	113.8	64.2
Rb+	137.2	2.3	130.4	106.8
As	89.2	12.3	773.4	62.2
Zn	139.6	107.7	182.8	232.5
Cu	19.8	6.9	33.9	46.2
Ni	37.9	14.2	30.7	38.4
Co	1.2	60.5	15.2	12.8
Cr	78.0	118.6	155.6	130.3
Ba	1001.0	665.7	964.2	635.4
V	50.8	335.3	55.2	256.8
S	62.2	1473.6	1532.0	374.7

4 of/de 4

Whole Rock Analysis

Quartz Cemented Graphitic Pelite Breccia

	159-59	159-61	60-24	74-12
SiO_2	72.97	42.06	50.25	45.36
TiO_2	0.42	1.79	0.76	1.39
Al_2O_3	8.61	28.41	17.00	17.73
FeO	3.84	14.78	8.13	19.55
MnO	0.07	0.15	0.21	0.15
MgO	2.13	3.23	5.65	1.98
CaO	3.05	6.33	3.73	3.59
Na_2O	0.28	1.13	0.41	0.22
K_2O	1.73	6.45	3.80	1.48
P_2O_5	0.18	0.00	0.17	0.07
total	98.46	100.00	98.67	99.16
LOI/CO_2*	4.96	7.00	8.51	5.46
Nb	2.8	2.2	15.1	2.2
Zr	73.9	48.1	152.2	12.0
Y	3.4	3.4	11.7	3.4
Sr	73.2	76.2	76.0	18.3
Rb	44.3	65.6	89.8	196.4
As+	866.2	46773.9	353.8	12.3
Zn	92.3	89.2	144.1	107.7
Cu	15.9	95.4	22.4	6.9
Ni	9.7	19.9	16.3	14.2
Co	10.1	1.2	13.1	60.5
Cr	32.6	184.3	66.1	118.6
Ba	4302.5	2328.8	1833.4	665.7
V	523.6	228.5	128.8	335.3
S	1430.4	7118.4	1550.9	1473.6

Whole Rock Analysis

Banded Quartz-Biotite-Chlorite-Plagioclase Schist

	159-77	159-79	74-15
SiO_2	58.26	61.18	46.03
TiO_2	0.79	0.85	1.14
Al_2O_3	18.35	15.63	14.06
FeO	6.92	7.06	11.15
MnO	0.08	0.07	0.31
MgO	3.71	3.68	7.39
CaO	1.20	1.21	6.99
Na_2O	0.20	1.90	1.86
K_2O	2.53	2.11	4.06
P_2O_5	0.16	0.15	0.07
total	96.94	99.20	96.57
LOI/CO_2*	3.89	4.56	2.26*
Nb	2.2	34.5	72.0
Zr	66.2	179.9	269.3
Y	3.4	37.5	81.7
Sr	5.8	186.9	275.9
Rb	28.6	84.2	144.8
As^+	11.9	49.4	82.0
Zn	287.4	104.6	141.8
Cu	16.0	9.9	16.2
Ni	17.3	27.8	31.0
Co	45.6	16.7	1.2
Cr	141.6	105.2	106.4
Ba	912.0	868.0	913.9
V	267.4	86.1	58.3
S	713.5	60.4	61.1

APPENDIX II

MINERAL ANALYSIS TECHNIQUES

II-1 ELECTRON MICROPROBE TECHNIQUES

Electron microprobe analyses were carried out using a M.A.C. model 400 electron microprobe with an on line automated Kreisel Control Microprobe V4C-M6SP1 System. ZAF (atomic number, absorption and flourescence) corrections using the computor program Magic IV were employed in data reduction.

Routine operating conditions for silicate analysis was 15 kv, 20,000 counts for 30 seconds and for carbonate analysis 15 kv, 10,000 counts for 10 seconds.

Structural formulae were calculated using programs written by the author after the method suggested by Deer et al., (1966)

Mineral Name Abbreviations

plag	- plagioclase	gnt	- garnet
ab	- albite	alm	- almandine
olig	- oligoclase	mu	- muscovite
act	- actinolite	pa	- paragonite
hb	- hornblende	bi	- biotite
zo	- zoisite	ann	- annite
qtz	- quartz	rt	- rutile
carb	- carbonate	il	- ilmenite
cc	- calcite	po	- pyrrhotite
dol	- dolomite	cpy	- chalcopyrite
FD	- ferroan dolomite	aspy	- arsenopyrite
chl	- chlorite	py	- pyrite
chtd	- chloritoid	graph	- graphite

AMPHIBOLE - Foliated Amphibolite

	159-1-1	159-1-2	159-1-3	159-1-4	159-1-5	159-1-6	159-1-7
SiO_2	47.79	46.98	47.87	47.22	45.11	50.04	46.24
TiO_2	0.30	0.22	0.23	0.29	0.33	0.18	0.26
Al_2O_3	10.28	9.04	9.63	19.20	11.75	6.83	10.02
Cr_2O_3	0.11	0.14	0.50	00.00	0.00	0.00	0.00
FeO	7.84	16.34	16.55	16.00	17.29	15.03	16.30
MnO	0.13	0.26	0.16	0.01	0.07	0.05	0.10
MgO	11.59	12.52	11.30	11.35	9.87	12.03	10.36
CaO	11.70	11.34	11.07	11.55	11.25	11.68	11.59
Na_2O	1.30	1.54	1.77	1.28	1.71	1.46	1.36
K_2O	0.18	0.27	0.27	0.11	0.27	0.15	0.18
total	99.01	98.66	97.68	98.30	97.65	97.45	96.41

structural formulae based on 20 oxygen

	159-1-1	159-1-2	159-1-3	159-1-4	159-1-5	159-1-6	159-1-7
Si	6.34	7.02	7.20	7.21	6.70	7.29	6.73
Al^{iv}	1.66	0.98	0.80	0.79	1.30	0.71	1.27
Al^{iv}	-0.05	0.62	0.91	0.88	0.76	0.46	0.45
Ti	0.03	0.02	0.03	0.01	0.04	0.02	0.03
Cr	0.01	0.02	0.06	0.00	0.00	0.00	0.00
Fe	0.87	2.04	2.08	2.06	2.15	1.83	1.98
Mn	0.01	0.03	0.02	0.01	0.01	0.01	0.01
Mg	2.29	2.79	2.53	2.54	2.19	2.61	2.25
Ca	1.66	1.82	1.78	1.79	1.79	1.82	1.81
Na	0.14	0.18	0.21	0.02	0.02	0.17	0.16
K	0.05	0.08	0.08	0.07	0.08	0.04	0.05

AMPHIBOLE - Foliated Amphibolite

	159-1-8	159-1-9	159-1-10	k4-2-1	k4-2-2	k4-2-3	K2-7-1	K2-7-2	k2-7-3	k2-7-4
SiO_2	45.00	44.00	45.09	40.29	40.95	41.85	45.47	47.87	45.14	45.42
TiO_2	0.36	0.29	0.25	0.28	0.30	0.24	0.33	0.36	0.33	0.29
Al_2O_3	12.01	11.88	9.68	15.82	15.54	15.06	11.41	10.91	11.12	10.51
Cr_2O_3	0.00	0.00	0.00	0.06	0.02	0.08	0.18	0.04	0.09	0.10
FeO	17.28	16.68	17.09	22.20	21.72	21.33	16.24	15.49	15.84	16.25
MnO	0.01	0.14	0.05	0.18	0.27	0.30	0.25	0.13	0.21	0.16
MgO	9.83	9.15	11.02	4.82	4.76	4.80	10.18	10.57	10.44	11.05
CaO	11.52	11.11	11.21	9.66	9.12	10.20	11.41	11.36	11.38	11.61
Na_2O	1.32	1.82	1.43	1.55	1.94	1.66	1.62	1.36	1.64	1.52
K_2O	0.27	0.24	0.26	0.33	0.28	0.29	0.43	0.23	0.26	0.20
total	97.62	96.46	96.07	95.38	95.38	94.90	97.52	98.32	96.45	97.09

structural formulae based on 20 oxygen

	159-1-8	159-1-9	159-1-10	k4-2-1	k4-2-2	k4-2-3	K2-7-1	K2-7-2	k2-7-3	k2-7-4
Si	6.67	6.38	6.59	5.96	6.02	6.21	6.72	7.05	6.59	6.69
Al^{iv}	1.33	1.62	1.41	2.04	1.98	1.79	1.28	0.95	1.41	1.31
Al^{iv}	0.76	0.40	0.25	0.72	0.72	0.84	0.71	0.94	0.50	0.51
Ti	0.04	0.03	0.03	0.03	[illegible]	0.03	0.04	0.04	0.04	0.03
Cr	0.00	0.00	0.00	0.01	0.00	0.01	0.02	0.00	0.01	0.01
Fe	2.14	2.02	2.09	2.75	2.67	2.84	2.01	1.91	1.93	2.00
Mn	0.00	0.02	0.01	0.02	0.03	0.04	0.03	0.02	0.03	0.02
Mg	2.17	1.98	2.40	1.06	1.04	1.08	2.24	2.32	2.27	2.42
Ca	1.83	1.72	1.75	1.53	1.44	1.62	1.81	1.79	1.78	1.83
Na	0.15	0.21	0.16	0.18	0.22	0.19	0.19	0.16	0.19	0.18
K	0.08	0.07	0.07	0.09	0.08	0.08	0.12	0.07	0.07	0.06

AMPHIBOLE - Regional Amphibolite

	CR-39-1	CR-39-2	CR-39-3	CR-39-4	CR-39-5	CR-52-1	CR-52-2	CR-52-3
SiO_2	49.56	51.39	51.55	49.24	48.02	44.14	42.58	44.58
TiO_2	0.21	0.39	0.28	0.20	0.20	0.37	0.39	0.41
Al_2O_3	6.79	5.38	5.44	7.56	9.95	12.78	13.61	13.62
Cr_2O_3	0.08	0.07	0.02	0.29	0.17	0.13	0.14	0.07
FeO	10.58	10.39	10.21	10.53	11.38	16.17	16.12	15.98
MnO	0.23	0.31	0.25	0.33	0.21	0.18	0.19	0.24
MgO	15.39	14.67	14.75	16.00	12.57	9.28	8.99	8.79
CaO	12.38	12.06	12.16	11.81	11.91	11.97	11.58	11.66
Na_2O	0.39	0.08	0.52	0.65	0.75	1.43	1.33	1.25
K_2O	0.05	0.05	0.04	0.08	0.07	0.25	0.29	0.23
total	95 .67	95.52	95.21	96.69	95.21	96.70	95.22	96.83

structural formulae based on 20 oxygen

	CR-39-1	CR-39-2	CR-39-3	CR-39-4	CR-39-5	CR-52-1	CR-52-2	CR-52-3
Si	6.94	7.08	7.15	6.97	6.72	6.47	6.15	6.51
Al^{iv}	1.06	0.92	0.85	1.03	1.28	1.53	1.85	1.49
Al^{iv}	0.06	-0.04	0.04	0.24	0.36	0.68	0.47	0.85
Ti	0.02	0.04	0.03	0.02	0.02	0.04	0.04	0.05
Cr	0.01	0.01	0.00	0.03	0.02	0.02	0.02	0.01
Fe	1.24	1.20	1.18	1.25	1.33	1.98	1.95	1.95
Mn	0.03	0.04	0.03	0.04	0.02	0.02	0.02	0.03
Mg	3.21	3.01	3.05	3.38	2.62	2.0[illegible]	1.94	1.91
Ca	1.86	1.78	1.81	1.79	1.78	1.88	1,79	1.82
Na	0.04	0.01	0.06	0.07	0.08	0.16	0,15	0.14
K	0.01	0.01	0.01	0.02	0.02	0.07	0.08	0.07

AMPHIBOLE - Chlorite-Magnetite Schist

	159-22-1	159-22-2	159-22-3	159-22-4	159-23-1	159-23-2	159-23-3
SiO_2	50.61	50.15	50.86	51.54	50.77	50.69	48.71
TiO_2	0.05	0.10	0.05	0.10	0.10	0.13	0.12
Al_2O_3	0.03	0.62	0.04	0.13	0.39	0.83	3.61
Cr_2O_3	0.11	0.20	0.15	0.16	0.07	0.14	0.12
FeO	39.98	40.59	40.67	39.76	39.67	40.49	38.38
MnO	0.32	0.43	0.30	0.36	0.40	0.21	0.22
MgO	7.02	7.61	7.25	7.31	7.16	6.25	6.22
CaO	0.08	0.20	0.13	0.11	0.26	0.29	0.29
Na_2O	0.00	0.00	0.00	0.00	0.00	0.20	0.33
K_2O	0.04	0.02	0.04	0.05	0.05	0.05	0.14
total	98.25	99.92	99.49	99.50	99.13	99.39	98.25

structural formulae based on 20 oxygen

Si	8.01	8.14	8.19	8.25	8.08	8.28	7.67
Al^{iv}	-0.01	-0.14	-0.19	-0.25	-0.08	-0.28	0.33
Al^{iv}	0.02	0.25	0.20	0.28	0.16	0.44	0.34
Ti	0.01	0.01	0.01	0.01	0.01	0.02	0.01
Cr	0.01	0.03	0.02	0.02	0.01	0.02	0.01
Fe	5.29	5.51	5.48	5.32	5.28	5.67	5.05
Mn	0.04	0.06	0.04	0.05	0.05	0.03	0.03
Mg	1.66	1.84	1.74	1.75	1.70	1.52	1.46
Ca	0.01	0.03	0.02	0.02	0.04	0.05	0.05
Na	0.00	0.00	0.00	0.00	0.00	0.03	0.04
K	0.01	0.01	0.01	0.02	0.02	0.02	0.04

PLAGIOCLASE - Foliated Amphibolite

	159-3-1	159-3-2	159-3-3	159-4-1-1	159-4-1-2	159-4-2	K2-7-1-1	K2-7-2-1	K2-7-2-2	K2-7-2-3	K2-7-2-4
SiO_2	70.12	68.96	68.84	64.09	67.08	66.40	67.91	68.85	68.83	68.05	68.05
Al_2O_3	19.50	20.14	19.61	21.83	20.01	20.00	19.20	19.25	20.07	19.89	20.02
FeO	0.43	0.00	0.00	0.00	0.00	0.03	0.00	0.00	0.00	0.00	0.00
CaO	0.34	0.48	0.55	1.93	0.39	0.51	0.45	0.14	0.18	0.20	0.32
BaO	0.00	0.00	0.00	0.00	0.00	0.00	0.00	0.00	0.00	0.00	0.00
Na_2O	11.16	11.38	11.14	11.49	11.53	11.68	12.09	12.51	12.24	11.36	12.62
K_2O	0.02	0.05	0.05	0.02	0.02	0.01	0.04	0.00	0.00	0.05	0.03
total	101.56	101.56	100.18	99.35	99.04	98.63	99.83	00.86	101.52	99.73	101.31
% An	1.65	2.27	2.65	8.49	2.45	2.35	2.01	0.68	0.80	0.96	1.38

	K4-2-1-1	K4-2-1-2	K4-2-2-1	K4-2-2-2	K4-2-3-1	K2-2-3-2
SiO_2	67.28	69.06	69.21	68.36	69.08	68.80
Al_2O_3	18.79	18.75	18.76	19.17	18.66	18.19
FeO	1.01	0.05	0.05	0.34	0.27	0.12
CaO	0.43	0.20	0.24	0.36	0.36	0.44
BaO	0.00	0.00	0.00	0.00	0.00	0.00
Na_2O	10.27	11.36	11.21	10.50	11.39	11.35
K_2O	0.05	0.05	0.05	0.05	0.15	0.04
total	97.83	99.47	99.52	98.78	99.91	98.94
% An	2.25	0.96	1.85	1.85	1.79	2.09

PLAGIOCLASE - Ferroan Dolomite Schist

	159-10-1	159-10-2	159-10-3	159-10-4	159-13-1	159-13-2	159-13-3	159-13-4	156-5-1	156-5-2
SiO_2	58.90	58.99	61.43	58.47	66.81	65.20	65.78	68.20	62.03	62.29
Al_2O_3	26.92	25.89	24.94	26.68	21.66	21.64	20.53	18.77	23.31	24.96
FeO	0.04	0.04	0.16	0.02	0.21	0.23	0.37	0.07	0.00	0.00
CaO	7.39	8.13	6.11	8.28	4.17	4.02	1.84	0.74	4.99	4.30
BaO	0.02	0.03	0.04	0.00	0.00	0.00	0.00	0.00	0.05	0.00
Na_2O	7.37	6.93	8.22	7.02	9.01	9.23	11.52	11.39	8.48	9.59
K_2O	0.10	0.09	0.08	0.11	0.13	0.12	0.06	0.04	0.07	0.09
total	100.72	100.07	100.96	100.59	100.99	100.44	100.10	99.21	99.01	99.29
% An	35.45	39.13	28.99	39.22	20.21	19.27	8.08	3.46	24.44	19.76

PLAGIOCLASE -- Sericite-Chlorite Schist

	159-24-1-1	159-24-1-2	159-24-1-3	159-24-2-1	159-24-2-2	159-24-3	159-24-4-1	159-24-4-28
SiO_2	60.93	61.02	63.73	60.65	62.30	68.49	61.13	60.39
Al_2O_3	25.25	25.78	22.98	24.98	23.34	20.33	24.27	24.81
FeO	0.08	0.02	0.22	0.00	0.04	0.16	0.04	0.25
CaO	7.49	7.70	4.59	7.75	4.32	0.89	6.74	7.88
BaO	0.08	0.00	0.07	0.06	0.00	0.04	0.00	0.02
Na_2O	7.70	7.30	8.74	7.55	9.97	11.52	8.18	7.48
K_2O	0.10	0.13	0.09	0.11	0.11	0.08	0.13	0.14
total	101.62	101.95	100.43	101.10	101.07	101.50	100.48	100.98
% An	34.77	36.55	22.38	35.97	19.21	4.08	31.06	36.51

	159-28-1-1	159-28-1-2	159-28-1-3	159-28-1-4	159-28-2
SiO_2	61.48	59.48	61.10	61.02	67.25
Al_2O_3	24.80	25.15	24.18	23.09	20.48
FeO	0.14	0.11	0.07	0.33	0.23
CaO	6.44	7.11	6.25	4.75	1.35
BaO	0.00	0.00	0.00	0.00	0.00
Na_2O	8.28	7.52	8.22	9.11	11.50
K_2O	0.08	0.04	0.06	0.30	0.05
total	101.23	98.41	99.88	98.59	100.86
% An	29.93	34.24	29.49	22.00	6.08

PLAGIOCLASE - Chlorite-Magnetite Schist

	159-18-1	159-18-2	159-18-3	159-19-1-1	159-19-1-2	159-19-2	S80-595-1	S80-595-2	S80-595-3	S80-595-4
SiO_2	58.90	59.37	58.37	61.45	61.32	59.96	69.65	68.98	68.01	70.67
Al_2O_3	24.53	25.55	25.81	24.50	24.27	24.16	17.95	17.95	18.81	18.15
FeO	0.00	0.09	0.04	0.00	0.00	0.00	0.24	0.09	0.22	0.16
CaO	6.09	6.63	6.85	6.66	5.96	5.99	0.12	0.02	0.15	0.13
BaO	0.05	0.01	0.03	0.00	0.00	0.00	0.00	0.00	0.00	0.00
Na_2O	7.63	7.19	7.46	8.02	7.84	8.01	11.86	11.29	11.44	11.18
K_2O	0.24	0.05	0.11	0.05	0.09	0.07	0.06	0.05	0.05	0.04
total	99.45	98.90	98.76	100.67	99.48	98.19	99.88	98.38	98.68	100.33
Z An	30.17	33.65	33.45	31.37	29.43	29.12	0.55	0.97	0.72	0.64

	60-9-1-1-1	60-9-1-1-2	60-9-1-2	60-9-5-1-3	60-9-5-2-1	60-9-5-2-2	60-9-5-2-3	60-9-5-3
SiO_2	67.46	67.64	68.05	68.93	67.34	67.27	68.78	68.08
Al_2O_3	18.65	18.56	18.79	18.43	18.77	18.73	18.07	18.82
FeO	0.00	0.00	0.00	0.00	0.00	0.00	0.00	0.00
CaO	0.00	0.00	0.00	0.00	0.00	0.00	0.00	0.00
BaO	0.00	0.00	0.00	0.00	0.00	0.00	0.00	0.00
Na_2O	12.14	12.07	11.91	11.29	11.68	11.72	11.43	11.70
K_2O	0.06	0.06	12.07	0.07	0.07	0.05	0.22	0.07
total	98.43	98.37	98.86	99.38	97.89	97.85	98.50	99.79
Z An	0.00	0.00	0.00	0.00	0.00	0.00	0.00	0.00

	60-9-6-1-1	60-9-6-1-2	60-9-6-2	60-9-6-3	60-9-5-1-1	60-9-5-1-2
SiO_2	66.71	68.21	67.80	68.43	67.50	67.65
Al_2O_3	18.96	19.52	18.96	19.05	19.93	18.43
FeO	0.00	0.05	0.00	0.00	0.00	0.00
CaO	0.46	0.32	0.14	0.15	0.00	0.01
BaO	0.00	0.00	0.00	0.00	0.00	0.00
Na_2O	11.71	12.05	11.53	10.93	11.52	12.06
K_2O	0.05	0.04	0.05	0.05	0.00	0.00
total	97.95	100.30	98.54	98.77	99.00	98.34
Z An	2.12	1.44	0.66	1.03	0.00	0.05

PLAGIOCLASE - Quartz Cemented Graphitic Pelite Breccia (1.0%)

	159-61-1	159-61-2	159-61-3	159-61-4	159-61-5-1	159-61-5-2	159-61-6	60-24-1-1	60-24-1-2	60-24-1-3	60-24-1-4
SiO_2	68.24	65.06	63.88	64.51	64.10	62.98	63.78	60.23	59.02	60.39	59.67
Al_2O_3	20.53	23.24	23.57	23.19	23.10	23.61	23.41	25.21	26.03	25.13	25.91
FeO	0.00	0.00	0.00	0.02	0.00	0.14	0.03	0.09	0.00	0.00	0.11
CaO	0.53	4.05	4.08	4.35	4.28	4.55	4.10	6.46	7.71	6.57	7.72
BaO	0.00	0.00	0.05	0.00	0.00	0.06	0.03	0.00	0.02	0.09	0.05
Na_2O	11.63	9.04	9.32	8.83	9.37	9.51	9.21	7.88	7.36	7.73	7.86
K_2O	0.05	0.16	0.12	0.10	0.10	0.13	0.11	0.08	0.15	0.05	0.05
total	100.98	101.56	101.02	101.00	101.25	100.98	100.67	99.9	100.29	99.87	101.32
% An	4.45	19.66	19.35	21.27	20.04	20.76	19.62	31.04	36.36	31.87	35.09

	60-24-2-1	60-24-2-2	60-24-2-3	60-24-4-1	60-24-4-2	60-24-5-1	60-24-5-2	60-24-6
SiO_2	59.31	60.46	65.29	60.98	59.55	60.31	59.52	61.10
Al_2O_3	25.69	25.84	22.61	24.06	26.23	24.50	23.82	24.32
FeO	0.00	0.00	0.00	0.00	0.00	0.16	0.17	0.05
CaO	7.23	7.17	3.39	6.14	7.61	6.22	5.95	6.35
BaO	0.05	0.16	0.02	0.14	0.02	0.00	0.00	0.00
Na_2O	7.85	7.26	9.56	7.67	7.63	7.46	8.14	8.25
K_2O	0.08	0.35	0.11	0.10	0.08	0.09	0.18	0.05
total	100.16	101.24	100.98	98.95	101.12	98.74	97.78	100.14
% An	33.58	34.60	16.28	30.49	35.38	31.37	28.48	29.76

	60-24-7-1	60-24-7-2	60-24-7-3	60-24-7-4	67-14-1	67-14-2
SiO_2	59.15	58.77	60.87	61.55	61.07	71.73
Al_2O_3	24.94	25.16	24.49	23.16	24.34	24.89
FeO	0.01	0.11	0.04	0.15	0.00	0.00
CaO	6.73	7.52	6.15	5.22	4.63	5.55
BaO	0.00	0.00	0.00	0.00	0.00	0.00
Na_2O	7.99	7.40	8.51	8.97	9.75	7.91
K_2O	0.04	0.05	0.05	0.10	0.00	0.00
total	98.89	99.00	100.11	99.16	99.88	100.01
% An	31.66	35.86	28.46	24.20	20.70	27.94

PLAGIOCLASE - Banded Chlorite-Sericite-Garnet Schist

	67-19-1-1	67-19-1-2	67-19-2-1	67-19-2-2	159-75-1	159-75-2	159-75-3	73-13-1	73-13-2	73-13-3
SiO_2	60.45	60.92	64.05	59.88	62.91	60.31	60.37	59.68	60.28	60.00
Al_2O_3	24.23	22.91	23.13	25.21	22.78	25.81	25.67	24.36	23.54	23.45
FeO	0.16	0.13	0.21	0.25	0.01	0.00	0.06	1.83	0.04	0.00
CaO	5.79	4.07	4.43	7.11	4.28	7.75	7.73	5.45	4.41	4.43
BaO	0.00	0.00	0.00	0.00	0.00	0.00	0.00	0.00	0.00	0.01
Na_2O	8.66	9.04	8.89	7.74	9.33	7.73	7.39	9.86	9.08	9.36
K_2O	0.10	0.13	0.07	0.06	0.10	0.05	0.07	0.57	0.04	0.11
total	99.39	97.19	100.80	100.25	99.41	101.36	101.28	101.74	97.39	98.35
% An	26.83	19.77	21.50	33.56	20.11	35.56	36.49	22.74	21.11	20.61

PLAGIOCLASE - Silicified Dolomite

	159-50-1	159-50-2	159-50-3
SiO_2	61.25	67.46	69.14
Al_2O_3	26.16	20.24	19.45
FeO	0.17	0.19	0.30
CaO	1.19	1.38	0.15
BaO	0.00	0.00	0.00
Na_2O	10.12	9.74	11.27
K_2O	0.29	1.02	0.09
total	99.71	100.03	100.4
% An	6.00	6.83	0.73

PLAGIOCLASE - Graphitic Pelite

	K2-14-1	K2-14-2-1	K2-14-2-2	K2-14-3
SiO_2	62.46	59.50	62.59	61.55
Al_2O_3	23.08	24.38	23.38	23.40
FeO	0.00	0.05	0.00	0.00
CaO	4.40	5.52	4.34	4.41
BaO	0.00	0.00	0.00	0.00
Na_2O	8.84	7.20	9.63	9.14
K_2O	0.07	1.49	0.07	0.05
total	98.85	98.15	100.00	98.56
% An	21.48	27.16	19.86	20.99

CHLORITE - Foliated Amphibolite

	159-1-1	159-1-2	159-4-1	159-4-2	159-4-3	159-4-4	159-4-5	159-4-6	159-4-7	159-6-1	159-6-2
SiO_2	25.70	26.79	22.72	23.49	20.45	21.90	21.46	21.14	23.80	24.90	24.66
TiO_2	0.12	0.08	0.06	0.15	0.04	0.14	0.05	0.04	0.07	0.09	0.14
Al_2O_3	22.25	20.63	31.03	30.82	29.00	29.15	0.00	29.89	30.89	28.33	28.02
Cr_2O_3	0.00	0.00	0.05	0.08	0.00	0.05	0.07	0.13	0.24	0.00	0.00
FeO	20.15	21.06	21.18	21.20	20.91	21.92	21.46	21.14	20.89	22.89	23.30
MnO	0.05	0.00	0.03	0.00	0.00	0.02	0.00	0.00	0.00	0.20	0.06
MgO	16.59	15.26	11.89	11.77	11.63	11.92	11.74	11.84	11.58	12.80	12.85
CaO	0.02	1.19	0.00	0.00	0.05	0.00	0.00	0.00	0.00	0.12	0.12
Na_2O	0.39	0.83	0.00	0.00	0.00	0.99	0.00	0.00	0.00	0.09	0.04
K_2O	0.03	0.07	0.00	0.00	0.00	0.04	0.00	0.00	0.00	0.04	0.00
total	85.31	85.90	87.12	87.52	82.54	86.14	87.04	86.46	86.95	89.80	89.46

structural formulae based on 28 oxygens

Si	5.49	5.64	5.02	5.13	4.79	4.87	6.10	4.83	5.21	5.22	5.17
Al^{iv}	2.51	2.36	2.98	2.87	3.21	3.13	1.90	3.17	2.79	2.78	2.83
Al^{vi}	2.57	2.86	2.53	2.60	2.56	2.61	5.29	2.53	2.59	2.87	2.93
Ti	0.02	0.01	0.01	0.02	0.01	0.02	0.01	0.01	0.01	0.01	0.02
Cr	0.00	0.00	0.01	0.01	0.00	0.01	0.02	0.02	0.04	0.00	0.00
Fe	3.98	3.63	5.73	5.63	5.68	5.42	0.00	5.71	5.65	4.97	4.91
Mn	0.01	0.00	0.01	0.00	0.00	0.00	0.00	0.00	0.00	0.04	0.01
Mg	5.29	4.79	3.92	3.84	4.06	3.95	4.97	4.03	3.78	4.00	4.02
Ca	0.00	0.27	0.00	0.00	0.01	0.00	0.00	0.00	0.00	0.03	0.03
Na	0.16	0.34	0.00	0.00	0.00	0.43	0.00	0.00	0.00	0.04	0.02
K	0.01	0.02	0.00	0.00	0.00	0.01	0.00	0.00	0.00	0.01	0.00

CHLORITE — Veined FDCSBQ Schist

	159-9-1	159-10-1	159-10-2	159-10-3	159-10-4	159-10-5
SiO_2	24.98	24.13	23.39	24.26	25.36	23.40
TiO_2	0.06	0.13	0.13	0.07	0.09	0.13
Al_2O_3	24.17	34.31	32.87	33.97	32.85	33.48
Cr_2O_3	0.00	0.00	0.00	0.00	0.00	0.00
FeO	22.98	21.97	22.24	21.31	22.66	21.68
MnO	0.00	0.00	0.00	0.00	0.00	0.00
MgO	15.32	9.01	9.09	8.53	9.89	8.28
CaO	0.00	0.01	0.04	0.01	0.01	0.03
Na_2O	0.25	0.15	0.00	0.16	0.30	0.14
K_2O	0.12	0.01	0.07	0.04	0.09	0.02
total	87.88	89.72	87.83	88.35	91.26	87.16

structural formulae based on 28 oxygens

	159-9-1	159-10-1	159-10-2	159-10-3	159-10-4	159-10-5
Si	5.22	5.21	5.14	5.32	5.32	5.21
Al^{iv}	2.78	2.79	2.86	2.68	2.68	2.79
Al^{vi}	2.88	2.81	2.90	2.83	2.92	2.89
Ti	0.01	0.02	0.02	0.01	0.01	0.02
Cr	0.00	0.00	0.00	0.00	0.00	0.00
Fe	4.22	6.20	6.04	6.23	5.76	6.23
Mn	0.00	0.00	0.00	0.00	0.00	0.00
Mg	4.77	2.90	2.98	2.79	3.09	2.75
Ca	0.00	0.00	0.01	0.00	0.00	0.01
Na	0.10	0.06	0.00	0.07	0.12	0.06
K	0.03	0.00	0.02	0.01	0.02	0.01

CHLORITE - Massive Ferroan Dolomite

	159-21-1	159-21-2	159-21-3	159-21-4	159-21-5	159-21-6	159-21-7	159-21-8	159-21-9	159-21-10
SiO_2	22.53	23.49	23.69	23.54	24.11	24.36	24.38	22.82	23.03	23.71
TiO_2	0.18	0.04	0.10	0.09	0.09	0.11	0.16	33.89	32.96	33.85
Al_2O_3	22.26	21.01	21.07	20.63	20.41	20.69	21.04	0.11	0.10	0.08
Cr_2O_3	0.00	0.00	0.00	0.00	0.00	0.00	0.00	21.42	21.39	20.75
FeO	33.52	33.74	33.06	32.70	32.66	31.59	32.05	0.00	0.00	0.00
MnO	0.18	0.04	0.10	0.09	0.09	0.11	0.16	0.11	0.18	0.07
MgO	9.18	9.55	9.37	9.58	9.62	10.26	10.17	9.18	9.36	9.15
CaO	0.04	0.00	0.05	0.02	0.04	0.07	0.05	0.04	0.12	0.05
Na_2O	0.02	0.00	0.00	0.00	0.01	0.00	0.03	0.00	0.03	0.00
K_2O	0.00	0.00	0.00	0.00	0.00	0.00	0.00	0.04	0.00	0.01
total	88.17	88.16	87.71	86.91	87.29	87.60	88.81	88.02	87.59	88.07

structural formulae based on 28 oxygen

	159-21-1	159-21-2	159-21-3	159-21-4	159-21-5	159-21-6	159-21-7	159-21-8	159-21-9	159-21-10
Si	4.99	5.19	5.24	5.26	5.35	5.35	5.28	5.08	5.12	5.26
Al^{iv}	3.01	2.81	2.76	2.74	2.65	2.65	2.72	2.92	2.88	2.74
Al^{vi}	2.80	2.66	2.74	2.68	2.68	2.71	2.66	2.69	2.73	2.68
Ti	0.01	0.01	0.02	0.02	0.02	0.02	0.12	0.02	0.02	0.01
Cr	0.00	0.00	0.00	0.00	0.00	0.00	0.00	0.00	0.00	0.00
Fe	6.21	6.24	6.12	6.11	6.06	5.81	5.81	6.31	6.13	6.28
Mn	0.03	0.01	0.02	0.02	0.02	0.02	0.03	0.02	0.03	0.01
Mg	3.03	3.15	3.09	3.19	3.18	3.36	3.29	3.04	3.10	3.02
Ca	0.01	0.00	0.01	0.00	0.01	0.02	0.01	0.01	0.03	0.01
Na	0.01	0.00	0.00	0.00	0.00	0.00	0.01	0.00	0.01	0.00
K	0.00	0.00	0.00	0.00	0.00	0.00	0.00	0.01	0.00	0.00

CHLORITE - Sericite-Chlorite Schist

	159-20-1	159-20-2	159-20-3	159-20-4	159-20-5	159-20-6	159-20-7
SiO_2	22.66	10.73	23.02	23.20	22.68	23.03	22.89
TiO_2	0.07	0.07	0.07	0.06	0.07	0.08	0.08
Al_2O_3	22.10	11.36	22.06	22.77	21.88	21.92	21.72
Cr_2O_3	0.16	0.06	0.09	0.13	0.14	0.16	0.13
FeO	39.10	30.32	38.36	38.79	37.98	38.66	38.26
MnO	0.06	0.07	0.03	0.04	0.06	0.07	0.00
MgO	5.79	3.43	5.81	6.02	5.80	5.74	5.93
CaO	0.00	0.00	0.01	0.00	0.00	0.00	0.00
Na_2O	0.00	0.02	0.00	0.09	0.23	0.19	0.23
K_2O	0.06	0.06	0.09	0.04	0.02	0.02	0.04
total	89.99	88.00	89.54	90.74	88.84	89.87	89.29

structural formulae based on 28 oxygen

Si	5.03	4.16	5.11	5.06	5.08	5.11	5.11
Al^{iv}	2.97	3.84	2.88	2.94	2.92	1.89	2.89
Al^{vi}	2.81	1.34	2.89	2.91	2.86	2.84	2.81
Ti	0.01	0.02	0.01	0.01	0.01	0.01	0.01
Cr	0.03	0.02	0.02	0.02	0.02	0.03	0.02
Fe	7.26	9.82	7.12	7.07	7.11	7.17	7.14
Mn	0.01	0.02	0.01	0.01	0.01	0.01	0.00
Mg	1.92	1.98	1.92	1.96	1.94	1.90	1.97
Ca	0.00	0.00	0.00	0.00	0.00	0.00	0.00
Na	0.00	0.02	0.00	0.04	0.10	0.08	0.10
K	0.02	0.03	0.03	0.01	0.01	0.01	0.01

CHLORITE - Sericite-Chlorite Schist

	159-24-1	159-24-2	159-24-3	159-24-4	159-28-1	159-28-2	159-28-3	159-28-4
SiO_2	24.70	24.48	23.48	23.96	25.55	24.72	25.27	24.26
TiO_2	0.06	0.07	0.11	0.07	0.09	0.07	0.08	0.09
Al_2O_3	22.23	22.73	22.15	22.44	22.27	21.69	21.19	22.05
Cr_2O_3	0.64	0.52	0.11	0.16	0.00	0.00	0.00	0.00
FeO	36.71	36.89	36.20	37.08	26.16	26.03	24.68	25.55
MnO	0.01	0.07	0.00	0.02	0.12	0.07	0.07	0.05
MgO	9.20	9.06	9.00	8.71	14.32	14.04	14.76	13.64
CaO	0.00	0.00	0.00	0.00	0.00	0.00	0.02	0.02
Na_2O	0.49	0.41	0.37	0.42	0.00	0.00	0.00	0.00
K_2O	0.03	0.39	0.04	0.06	0.01	0.03	0.04	0.01
total	91.38	92.23	89.46	90.92	88.62	86.71	86.23	85.84

structural formulae based on 28 oxygen

	159-24-1	159-24-2	159-24-3	159-24-4	159-28-1	159-28-2	159-28-3	159-28-4
Si	5.14	5.08	5.04	5.07	5.34	5.30	5.41	5.25
Al^{iv}	2.86	2.92	2.96	2.93	2.66	2.70	2.59	2.75
Al^{vi}	2.60	2.64	2.64	2.66	2.83	2.77	2.75	2.87
Ti	0.01	0.01	0.02	0.01	0.01	0.01	0.01	0.01
Cr	0.11	0.09	0.02	0.03	0.00	0.00	0.00	0.00
Fe	6.39	6.40	6.50	6.56	4.57	4.66	4.42	4.62
Mn	0.00	0.01	0.00	0.00	0.02	0.01	0.01	0.01
Mg	2.86	2.80	2.88	2.75	4.46	4.49	4.71	4.40
Ca	0.00	0.00	0.00	0.00	0.00	0.00	0.00	0.00
Na	0.20	0.16	0.15	0.17	0.00	0.00	0.00	0.03
K	0.01	0.10	0.01	0.02	0.00	0.01	0.01	0.00

CHLORITE - Sericite-Chlorite Schist

	159-44-1	159-44-2	159-44-3	159-44-4	159-44-5	159-44-6	159-44-7	159-44-8	K2-9-1-1	K2-9-1-2
SiO_2	23.11	22.86	23.30	24.29	22.77	23.38	22.04	23.23	22.82	22.89
TiO_2	0.11	0.09	0.09	0.09	0.11	0.08	0.08	0.08	0.04	0.05
Al_2O_3	20.79	20.00	21.35	22.71	21.25	22.33	20.88	21.49	21.75	21.78
Cr_2O_3	0.05	0.04	0.03	0.11	0.08	0.11	0.05	0.13	0.00	0.12
FeO	33.68	34.05	34.96	32.11	33.72	34.65	33.50	33.87	37.82	37.90
MnO	0.09	0.11	0.02	0.04	0.07	0.10	0.04	0.04	0.03	0.00
MgO	8.04	7.37	7.63	7.26	7.93	8.00	7.38	7.85	4.90	4.66
CaO	0.05	0.05	0.05	0.05	0.05	0.05	0.03	0.09	0.00	0.00
Na_2O	0.02	0.00	0.00	0.00	0.00	0.00	0.00	0.00	0.20	0.20
K_2O	0.05	0.10	0.06	0.23	0.07	0.04	0.11	0.09	0.00	0.00
total	85.98	84.67	87.49	86.89	86.05	88.74	84.11	86.86	87.66	87.68

structural formulae based on 28 oxygen

Si	5.24	5.29	5.21	5.36	5.16	5.13	5.13	5.21	5.18	5.20
Al^{iv}	2.76	2.71	2.79	2.64	2.84	2.87	2.87	2.79	2.82	2.80
Al^{vi}	2.79	2.75	2.84	3.26	2.84	2.91	2.86	2.88	3.00	3.02
Ti	0.02	0.02	0.02	0.01	0.02	0.01	0.01	0.01	0.01	0.01
Cr	0.01	0.01	0.01	0.02	0.01	0.02	0.01	0.02	0.00	0.02
Fe	6.38	6.59	6.54	5.92	6.39	6.36	6.52	6.35	7.18	7.20
Mn	0.02	0.02	0.00	0.01	0.01	0.02	0.01	0.01	0.01	0.00
Mg	2.72	2.54	2.54	2.39	2.68	2.62	2.56	2.62	1.66	1.58
Ca	0.01	0.01	0.01	0.01	0.01	0.01	0.01	0.02	0.00	0.00
Na	0.01	0.00	0.00	0.00	0.00	0.00	0.00	0.00	0.09	0.09
K	0.01	0.03	0.02	0.06	0.02	0.01	0.03	0.03	0.00	0.00

CHLORITE - Chlorite-Magnetite Schist

	159-18-1	159-18-2	159-18-3	159-18-4	159-18-5	159-20-1	159-20-2	159-20-3	159-20-4	159-20-5	159-20-6	159-20-7
SiO_2	23.76	22.79	23.34	23.32	23.16	23.45	23.18	23.69	23.24	23.79	22.91	23.52
TiO_2	0.16	0.17	0.07	0.08	0.08	0.07	0.02	0.10	0.07	0.11	0.05	0.07
Al_2O_3	21.57	20.79	19.18	21.57	21.23	23.08	21.91	22.25	22.47	22.70	22.27	22.88
Cr_2O_3	0.00	0.00	0.00	0.00	0.00	0.00	0.06	0.00	0.00	0.00	0.00	0.00
FeO	31.53	33.36	32.24	32.31	32.78	37.64	37.23	38.05	36.96	37.86	36.63	37.09
MnO	0.07	0.04	0.10	0.13	0.07	0.06	0.09	0.05	0.01	0.11	0.02	0.06
MgO	10.46	9.18	9.66	9.34	8.96	5.53	5.60	5.64	5.68	5.70	5.52	5.56
CaO	0.06	0.00	0.00	0.02	0.00	0.00	0.00	0.00	0.00	0.00	0.00	0.00
Na_2O	0.01	0.02	0.00	0.00	0.00	0.00	0.00	0.00	0.00	0.00	0.00	0.00
K_2O	0.01	0.02	0.03	0.03	0.04	0.00	0.00	0.01	0.00	0.00	0.00	0.07
total	87.93	86.55	85.52	86.97	85.43	90.43	88.23	90.00	88.88	90.48	87.83	89.52

structural formulae based on 28 oxygen

	159-18-1	159-18-2	159-18-3	159-18-4	159-18-5	159-20-1	159-20-2	159-20-3	159-20-4	159-20-5	159-20-6	159-20-7
Si	5.31	5.14	5.30	5.18	5.23	5.03	5.07	5.11	5.06	5.08	5.11	5.11
Al^{iv}	2.69	2.86	2.70	2.82	2.77	2.97	2.93	2.89	2.94	2.92	2.89	2.89
Al^{vi}	3.00	2.66	2.60	2.83	2.88	2.81	2.85	2.89	2.91	2.86	2.84	2.81
Cr	0.00	0.00	0.00	0.00	0.00	0.03	0.00	0.02	0.02	0.02	0.03	0.02
Ti	0.03	0.03	0.01	0.01	0.01	0.01	0.01	0.01	0.01	0.01	0.01	0.01
Fe	5.90	6.29	6.12	6.01	6.00	7.26	7.24	7.12	7.07	7.11	7.17	7.14
Mn	0.00	0.01	0.02	0.02	0.01	0.01	0.01	0.00	0.01	0.01	0.01	0.00
Mg	2.89	3.08	3.27	3.09	3.02	1.92	1.89	1.92	1.96	1.94	1.90	1.97
Ca	0.01	0.00	0.00	0.00	0.00	0.00	0.00	0.00	0.00	0.00	0.00	0.00
Na	0.00	0.01	0.00	0.00	0.00	0.00	0.00	0.00	0.04	0.00	0.00	0.00
K	0.00	0.01	0.01	0.01	0.01	0.00	0.00	0.01	0.01	0.00	0.00	0.01

CHLORITE – Chlorite-Magnetite Schist

	60-9-6-1	60-9-6-2	60-9-6-3	60-9-6-4	60-9-6-5
SiO_2	25.34	25.35	25.04	25.33	25.91
TiO_2	0.04	0.03	0.01	0.07	0.02
Al_2O_3	21.98	22.20	21.84	22.07	22.35
Cr_2O_3	0.05	0.00	0.09	0.00	0.03
FeO	28.59	27.59	27.70	27.59	28.91
MnO	0.00	0.00	0.12	0.0[illegible]	0.01
MgO	12.61	13.36	13.17	13.84	13.61
CaO	0.00	0.00	0.00	0.00	0.00
Na_2O	0.16	0.31	0.14	0.11	0.07
K_2O	0.00	0.00	0.00	0.00	0.00
total	88.76	88.86	88.12	89.11	90.91

structural formulae based on 28 oxygen

Si	5.35	5.33	5.32	5.31	5.34
Al^{iv}	2.65	2.67	2.68	2.69	2.66
Al^{vi}	2.83	2.82	2.78	2.76	2.76
Ti	0.01	0.00	0.00	0.01	0.00
Cr	0.01	0.00	0.02	0.00	0.00
Fe	5.05	4.85	4.92	4.84	4.98
Mn	0.00	0.00	0.02	0.00	0.00
Mg	3.97	4.18	4.17	4.32	4.18
Ca	0.00	0.00	0.00	0.00	0.00
Na	0.07	0.13	0.06	0.04	0.03
K	0.00	0.00	0.00	0.00	0.00

CHLORITE - Chlorite-Magnetite Schist

	60-9-3-1	60-9-3-2	60-9-5-1	60-9-5-2	60-9-5-3	60-9-6-1	60-9-6-2	60-9-6-3	60-9-6-4	60-9-6-5
SiO_2	23.66	23.88	24.50	24.73	25.02	25.34	25.35	25.04	25.33	25.91
TiO_2	0.00	0.06	0.07	0.03	0.04	0.08	0.03	0.01	0.07	0.02
Al_2O_3	21.38	22.61	21.23	21.47	21.81	21.98	22.20	21.84	22.07	22.35
Cr_2O_3	0.00	0.00	0.01	0.00	0.03	0.05	0.00	0.09	0.00	0.03
FeO	27.66	27.91	28.27	27.98	27.59	28.59	27.59	27.70	27.59	28.91
MnO	0.04	0.04	0.09	0.01	0.00	0.00	0.00	0.12	0.00	0.01
MgO	12.47	11.63	11.93	12.16	12.71	12.61	13.36	13.17	13.84	13.61
CaO	0.00	0.00	0.00	0.00	0.00	0.00	0.00	0.00	0.00	0.00
Na_2O	0.24	0.13	0.05	0.37	1.02	0.16	0.31	0.14	0.11	0.07
K_2O	0.00	0.02	0.00	0.00	0.00	0.00	0.00	0.00	0.00	0.00
total	86.48	86.89	86.18	86.88	88.29	88.76	88.86	88.12	89.11	90.91

structural formulae based on 28 oxygen

Si	5.35	5.28	5.35	5.35	5.32	5.35	5.33	5.32	5.31	5.34
Al^{iv}	2.65	2.72	2.65	2.65	2.68	2.65	2.67	2.68	2.69	2.66
Al^{vi}	2.81	3.02	2.82	2.83	2.78	2.83	2.82	2.78	2.76	2.76
Ti	0.00	0.01	0.01	0.00	0.01	0.01	0.00	0.00	0.01	0.00
Cr	0.00	0.00	0.00	0.00	0.01	0.01	0.00	0.02	0.00	0.00
Fe	5.02	5.03	5.16	5.06	4.91	5.05	4.85	4.92	4.84	4.98
Mn	0.01	0.01	0.02	0.00	0.00	0.00	0.00	0.02	0.00	0.00
Mg	4.03	3.74	3.88	3.92	4.03	3.97	4.18	4.17	4.32	4.18
Ca	0.00	0.00	0.00	0.00	0.00	0.00	0.00	0.00	0.00	0.00
Na	0.10	0.05	0.02	0.16	0.42	0.07	0.13	0.06	0.04	0.03
K	0.00	0.01	0.00	0.00	0.00	0.00	0.00	0.00	0.00	0.00

CHLORITE - Graphitic Pelite

	159-37-1	159-37-2	159-37-3	159-37-4	159-37-5	159-37-7	60-12-1	60-12-2	60-12-3	60-12-4
SiO_2	24.62	24.77	24.75	24.66	25.44	25.49	24.38	24.58	25.03	25.29
TiO_2	0.06	0.07	0.04	0.06	0.07	0.11	0.09	0.04	0.07	0.04
Al_2O_3	20.25	20.40	20.61	20.75	21.42	21.66	20.92	21.44	21.38	21.37
Cr_2O_3	0.02	0.02	0.09	0.08	0.00	0.00	0.13	0.20	0.15	0.06
FeO	25.23	24.89	25.43	24.41	26.04	25.59	25.88	25.43	25.79	25.25
MnO	0.32	0.32	0.20	0.24	0.30	0.35	0.28	0.15	0.27	0.44
MgO	14.04	13.90	13.96	13.66	13.33	14.45	13.39	13.87	13.60	13.88
CaO	0.04	0.08	0.05	0.08	0.00	0.01	0.05	0.05	0.02	0.10
Na_2O	0.00	0.00	0.00	0.00	0.00	0.00	0.00	0.00	0.00	0.00
K_2O	0.03	0.06	0.04	0.09	0.01	0.01	0.04	0.04	0.28	0.05
total	84.60	84.50	85.16	84.02	86.64	87.73	85.15	85.80	86.58	86.47

structural formulae based on 28 oxygen

	159-37-1	159-37-2	159-37-3	159-37-4	159-37-5	159-37-7	60-12-1	60-12-2	60-12-3	60-12-4
Si	5.41	5.43	5.40	5.42	5.45	5.38	5.34	5.31	5.37	5.41
Al^{iv}	2.59	2.57	2.60	2.58	2.55	2.62	2.66	2.69	2.63	2.59
Al^{vi}	2.65	2.71	2.69	2.80	2.85	2.77	2.73	2.78	2.78	2.80
Ti	0.01	0.01	0.01	0.01	0.01	0.02	0.01	0.01	0.01	0.01
Cr	0.00	0.00	0.02	0.01	0.00	0.00	0.02	0.03	0.03	0.01
Fe	4.63	4.57	4.64	4.49	4.66	4.52	4.74	4.60	4.63	4.52
Mn	0.06	0.06	0.04	0.04	0.05	0.06	0.05	0.03	0.05	0.08
Mg	4.60	4.54	4.54	4.48	4.26	4.55	4.37	4.47	4.35	4.43
Ca	0.01	0.02	0.01	0.02	0.00	0.00	0.01	0.01	0.00	0.02
Na	0.00	0.00	0.00	0.00	0.00	0.00	0.00	0.00	0.00	0.00
K	0.01	0.02	0.01	0.03	0.00	0.00	0.01	0.01	0.08	0.01

CHLORITE - Graphitic Pelite

	60-15-1	60-15-2	60-15-3	60.15-4	60-15-5	60-15-6	67-10-1	67-10-2	67-10-3	67-10-4	67-10-5	67-10-6
SiO_2	25.13	25.28	24.96	24.96	25.04	25.70	25.20	24.38	24.69	25.71	25.44	25.63
TiO_2	0.04	0.09	0.05	0.05	0.07	0.07	0.08	0.94	0.07	0.07	0.09	0.05
Al_2O_3	21.71	21.44	21.09	20.45	20.45	21.06	21.53	21.07	20.57	22.23	22.01	22.09
Cr_2O_3	0.08	0.03	0.10	0.02	0.10	0.15	0.01	0.07	0.04	0.08	0.02	0.00
FeO	25.53	25.91	25.01	25.62	25.18	25.59	29.73	28.57	29.21	29.05	29.22	29.21
MnO	0.21	0.29	0.34	0.27	0.23	0.34	0.02	0.16	0.07	0.13	0.09	0.11
MgO	14.10	14.75	14.32	14.52	14.25	14.70	12.32	12.14	11.83	12.73	13.18	12.64
CaO	0.04	0.02	0.05	0.02	0.09	0.06	0.04	0.05	0.07	0.05	0.05	0.04
Na_2O	0.00	0.00	0.00	0.00	0.00	0.00	0.00	0.00	0.07	0.00	0.00	0.00
K_2O	0.03	0.01	0.01	0.04	0.16	0.03	0.05	0.04	0.07	0.09	0.02	0.13
total	87.66	86.24	85.95	88.75	85.57	87.69	88.98	86.53	86.76	90.14	90.12	89.90

structural formulae based on 28 oxygen

	60-15-1	60-15-2	60-15-3	60.15-4	60-15-5	60-15-6	67-10-1	67-10-2	67-10-3	67-10-4	67-10-5	67-10-6
Si	5.29	5.32	5.42	5.40	5.43	5.43	5.35	5.26	5.39	5.36	5.31	5.36
Al^{iv}	2.71	2.68	2.58	2.60	2.57	2.57	2.65	2.74	2.61	2.64	2.69	2.64
Al^{vi}	2.78	2.67	2.74	2.61	2.65	2.67	2.73	2.62	2.69	2.81	2.72	2.81
Ti	0.01	0.01	0.01	0.01	0.01	0.01	0.01	0.15	0.01	0.01	0.01	0.01
Cr	0.01	0.01	0.02	0.00	0.02	0.03	0.00	0.01	0.01	0.01	0.00	0.00
Fe	4.58	4.59	4.48	4.63	4.57	4.52	5.28	5.16	5.33	5.06	5.10	5.11
Mn	0.04	0.05	0.06	0.05	0.04	0.06	0.00	0.03	0.01	0.02	0.02	0.02
Mg	4.51	4.65	4.58	4.68	4.61	4.63	3.90	3.91	3.85	3.95	4.10	3.94
Ca	0.01	0.00	0.01	0.00	0.02	0.01	0.01	0.01	0.02	0.01	0.01	0.01
Na	0.00	0.00	0.00	0.00	0.00	0.00	0.00	0.00	0.03	0.00	0.00	0.00
K	0.01	0.00	0.00	0.01	0.04	0.01	0.01	0.01	0.02	0.02	0.01	0.03

CHLORITE - Banded Chlorite-Sericite-Garnet Schist

	67-19-6	67-19-7	67-19-8	159-71-1	159-71-2	159-71-3	159-71-4	159-71-5
SiO_2	24.21	23.87	26.45	23.88	22.19	23.76	22.71	25.78
TiO_2	0.07	0.09	0.10	0.04	0.05	0.09	0.09	0.01
Al_2O_3	20.92	21.59	21.58	22.21	22.61	23.09	22.27	22.43
Cr_2O_3	0.09	0.13	0.11	0.56	0.53	0.12	0.59	0.04
FeO	31.21	31.17	29.38	30.83	36.07	32.93	37.85	24.30
MnO	0.07	0.03	0.01	0.04	0.05	0.02	0.07	0.02
MgO	10.27	10.87	10.31	12.04	7.78	7.71	7.74	17.38
CaO	0.05	0.03	0.02	0.02	0.00	0.00	0.00	0.04
Na_2O	0.00	0.00	0.00	0.00	0.00	0.00	0.00	0.00
K_2O	0.05	0.05	0.56	0.05	0.05	0.49	0.09	0.03
total	86.95	87.82	88.51	89.25	88.93	88.02	89.02	90.03

structural formulae based on 28 oxygen

	67-19-6	67-19-7	67-19-8	159-71-1	159-71-2	159-71-3	159-71-4	159-71-5
Si	5.33	5.20	5.63	5.08	4.90	5.20	4.93	5.25
Al^{iv}	2.67	2.80	2.37	2.92	3.10	2.80	3.07	2.75
Al^{vi}	2.76	2.74	3.03	2.65	2.78	3.15	2.63	2.63
Ti	0.01	0.01	0.02	0.01	0.01	0.01	0.01	0.00
Cr	0.02	0.02	0.02	0.09	0.09	0.02	0.10	0.01
Fe	5.75	5.68	5.23	5.49	6.66	6.03	6.87	4.14
Mn	0.01	0.01	0.00	0.01	0.01	0.00	0.01	0.00
Mg	3.37	3.53	3.27	3.82	2.56	2.51	2.51	5.27
Ca	0.01	0.01	0.00	0.00	0.00	0.00	0.00	0.01
Na	0.00	0.00	0.00	0.00	0.00	0.00	0.00	0.00
K	0.01	0.01	0.15	0.01	0.01	0.14	0.02	0.01

CHLORITE - Banded Chlorite-Sericite-Garnet Schist

	60-29-1	60-29-2	60-29-3	60-29-4	60-29-5	60-29-6	67-19-1	67-19-2	67-19-1	67-19-2	67-19-3	67-19-4	67-19-5
SiO_2	25.49	26.23	24.42	24.21	24.64	24.37	23.23	23.18	23.61	24.18	23.95	24.21	23.95
TiO_2	0.05	0.05	0.02	0.05	0.01	0.04	0.07	0.07	0.06	0.05	0.09	0.07	0.09
Al_2O_3	23.89	23.61	22.94	23.25	23.64	23.54	20.93	19.90	21.19	20.24	22.05	20.92	22.05
Cr_2O_3	0.04	0.07	0.11	0.18	0.04	0.13	0.14	0.15	0.20	0.08	0.02	0.09	0.02
FeO	27.96	29.05	30.95	30.78	30.32	29.09	30.56	31.34	31.61	31.26	31.52	31.21	31.52
MnO	0.01	0.00	0.00	0.00	0.00	0.00	0.00	0.01	0.00	0.02	0.01	0.07	0.01
MgO	9.86	9.49	10.11	10.66	10.81	10.47	10.42	9.93	10.64	10.67	10.69	10.27	10.69
CaO	0.00	0.00	0.00	0.00	0.00	0.00	0.08	0.04	0.08	0.08	0.13	0.05	0.13
Na_2O	0.32	0.35	0.30	0.29	0.09	0.21	0.00	0.00	0.00	0.00	0.00	0.00	0.00
K_2O	0.62	0.51	0.00	0.00	0.00	0.00	0.05	0.04	0.03	0.09	0.00	0.05	0.00
total	88.26	89.36	88.93	89.48	89.70	87.86	85.48	84.65	87.41	86.68	88.46	86.95	87.82

structural formulae based on 28 oxygen

	60-29-1	60-29-2	60-29-3	60-29-4	60-29-5	60-29-6	67-19-1	67-19-2	67-19-1	67-19-2	67-19-3	67-19-4	67-19-5
Si	5.40	5.50	5.23	5.15	5.20	5.22	5.21	5.28	5.19	5.35	5.18	5.33	5.18
Al^{iv}	2.60	2.50	2.77	2.85	2.80	2.78	2.79	2.72	2.81	2.65	2.82	2.67	2.82
Al^{vi}	3.37	3.34	3.02	2.97	3.08	3.16	2.73	2.62	2.68	2.63	2.80	2.76	2.80
Ti	0.01	0.01	0.00	0.01	0.00	0.01	0.01	0.01	0.01	0.01	0.01	0.01	0.01
Cr	0.01	0.01	0.02	0.03	0.01	0.02	0.02	0.03	0.03	0.01	0.00	0.02	0.00
Fe	4.95	5.10	5.54	5.47	5.35	5.21	5.73	5.97	5.81	5.79	5.70	5.	5.70
Mn	0.00	0.00	0.00	0.00	0.00	0.00	0.00	0.00	0.00	0.00	0.00	0.01	0.00
Mg	3.11	2.97	3.23	3.38	3.40	3.34	3.48	3.37	3.49	3.52	3.45	3.37	3.45
Ca	0.00	0.00	0.00	0.00	0.00	0.00	0.02	0.01	0.02	0.02	0.03	0.01	0.03
Na	0.13	0.14	0.12	0.12	0.04	0.09	0.00	0.00	0.00	0.00	0.00	0.00	0.00
K	0.17	0.14	0.00	0.00	0.00	0.00	0.01	0.01	0.01	0.03	0.00	0.01	0.00

Carbonate Probe Analysis

CARBONATE - Foliated Amphibolite

	159-1-2	159-1-2	159-1-3	159-1-4	159-1-5	159-1-6	159-1-7	159-1-8	159-3-1	159-4-1	159-4-2	159-4-3	159-4-4
FeO	01.60	02.22	03.14	02.37	02.55	02.04	02.48	02.68	01.27	04.03	05.04	04.52	04.11
MnO	00.87	00.91	00.76	00.77	00.87	00.68	00.87	00.73	01.00	00.62	00.60	00.59	00.49
MgO	01.05	01.13	01.78	01.38	01.58	01.20	01.44	01.66	00.59	01.14	01.26	01.50	01.13
CaO	55.32	55.16	55.52	54.98	55.99	56.71	56.14	54.93	58.54	55.10	57.09	53.88	56.02

	159-4-5	159-4-6	159-4-7	159-6-1	159-6-2	159-6-3	159-6-4	159-6-5	159-6-6	159-6-7
FeO	04.71	04.42	04.30	03.68	03.70	03.73	03.77	03.72	03.18	03.01
MnO	00.46	00.49	00.53	00.33	00.31	00.27	00.37	00.32	00.26	00.32
MgO	01.28	01.43	01.47	01.33	01.30	01.32	01.14	01.11	01.36	01.16
CaO	55.22	55.75	53.80	52.00	52.48	53.61	53.12	52.76	52.57	52.33

CARBONATE - Ferroan Dolomite Schist

159-9-1	159-9-2	159-9-3	159-9-4	159-9-5	159-9-6	159-9-7	159-9-8
11.61	11.96	12.32	12.04	12.43	11.64	10.75	11.90
00.51	00.55	00.46	00.55	00.24	00.61	00.50	00.39
13.63	12.54	13.30	12.74	13.57	13.37	13.68	13.47
29.63	30.35	28.92	29.07	28.74	29.26	28.44	29.14

	159-9-9	159-9-10	159-10-1	159-10-2	159-10-3	159-10-4	159-10-5	159-10-6	159-10-7	159-10-8
FeO	13.31	12.22	11.21	06.86	11.42	12.32	11.29	11.19	11.70	13.45
MnO	00.76	00.41	00.35	00.43	00.37	00.33	00.46	00.39	00.44	00.25
MgO	12.51	13.41	13.40	17.51	13.63	13.55	14.64	14.00	13.30	11.57
CaO	29.02	29.52	29.06	29.25	28.82	28.98	29.05	29.40	29.15	27.28

	159-11-1	159-11-2	159-11-3	159-11-4
FeO	06.47	04.58	00.20	06.56
MnO	00.16	00.26	00.00	00.09
MgO	16.77	18.26	21.11	17.30
CaO	29.08	28.86	30.07	29.05

CARBONATE - Massive Ferroan Dolomite

	159-11-1	159-11-2	159-11-3	159-11-4	159-11-5	159-11-6	159-11-7	159-11-8	159-11-9	159-11-10
FeO	06.47	04.58	00.20	06.56	06.61	04.18	07.23	05.07	07.28	07.95
MnO	00.16	00.26	00.00	00.09	00.16	00.45	00.27	00.46	00.28	00.16
MgO	16.77	18.26	21.11	17.30	16.95	18.36	16.90	17.97	16.96	16.57
CaO	29.08	28.86	30.07	29.05	28.29	28.94	28.97	27.98	29.18	28.26

	159-15-1	159-15-2	159-15-3	159-15-4	159-15-5	159-15-6	159-15-7	159-15-8	159-15-9	159-15-10	159-15-11
FeO	11.91	11.74	11.14	12.30	11.12	12.15	11.55	09.08	09.59	13.07	10.96
MnO	01.20	00.90	00.53	00.91	00.98	00.84	00.89	00.15	00.15	00.70	00.73
MgO	13.17	15.26	12.42	13.23	14.34	13.56	14.63	17.68	17.96	15.25	12.41
CaO	28.45	27.91	25.85	28.66	25.65	25.38	26.22	24.90	27.64	27.30	24.10

	159-17-1	159-17-2	159-17-3	159-17-4	159-17-5	159-17-6	159-17-7	159-21-1	159-21-2	159-21-3	159-21-4
FeO	04.31	09.38	10.36	11.27	07.67	07.01	08.88	20.40	18.20	21.10	20.30
MnO	01.18	00.89	00.77	00.66	01.24	01.26	00.71	00.60	00.80	00.70	00.80
MgO	18.64	14.45	14.43	15.28	17.83	17.12	16.11	00.00	10.30	00.00	00.00
CaO	28.85	28.55	29.13	28.07	28.94	28.32	28.00	26.10	27.10	26.50	25.40

	159-21-5	159-21-6	159-21-7	159-21-8	159-21-9	159-21-10	159-21-11
FeO	17.40	20.30	00.40	22.50	18.70	20.90	21.10
MnO	00.50	00.50	00.00	00.50	00.70	00.50	00.60
MgO	12.00	00.00	21.60	00.00	11.20	00.00	00.00
CaO	25.50	26.70	29.90	26.20	26.40	26.50	25.80

	159-23-1	159-23-2	159-32-3	159-23-4	159-23-5	159-27-1	159-27-2	159-27-3
FeO	23.80	24.10	22.90	22.30	23.90	00.00	11.10	10.90
MnO	00.00	00.00	00.00	00.20	00.80	00.40	00.30	00.30
MgO	00.00	00.00	00.00	00.00	00.00	18.50	14.90	14.00
CaO	26.60	26.80	26.70	27.20	25.70	27.00	[illegible]	29.00

	159-27-4	159-27-5	159-27-6	159-27-7	159-27-8	159-27-9
FeO	11.00	11.10	10.80	13.20	11.20	11.30
MnO	00.30	00.30	00.30	00.20	00.50	00.30
MgO	13.80	14.60	14.30	12.50	14.80	14.00
CaO	28.00	28.30	27.80	28.40	28.50	29.20

CARBONATE - Sericite-Chlorite Schist

	159-7-1	159-7-2	159-7-3	159-7-4	159-7-5	159-7-6	159-7-7	159-7-8	159-7-9	159-7-10	159-7-11
FeO	04.75	09.15	09.68	04.05	05.04	08.98	10.52	09.94	04.08	04.07	04.94
MnO	00.86	00.70	00.80	00.93	00.86	00.70	00.87	00.77	00.77	00.65	01.03
MgO	17.98	14.53	14.17	17.45	17.18	15.09	13.25	14.14	17.32	17.19	18.18
CaO	29.93	29.44	29.52	30.14	29.79	29.07	30.04	29.59	29.33	28.82	29.59

	159-28-1	159-28-2	159-28-3	159-28-4
FeO	11.[illegible]5	12.28	12.22	12.13
MnO	0.73	0.97	0.83	0.56
MgO	12.58	13.11	12.98	13.16
CaO	27.34	27.83	28.27	26.93

CARBONATE - Chlorite-Magnetite Schist

	159-23-1	159-23-2	159-23-3	159-23-3	159-23-5
FeO	23.82	24.18	22.93	21.30	21.95
MnO	1.43	1.67	1.41	0.28	0.85
MgO	7.86	7.99	8.39	7.[illegible]2	8.39
CaO	26.61	26.89	26.67	27.27	25.71

	60-9-1-1	60-9-1-2	60-9-1-3	60-9-1-4	60-9-1-5	60-9-1-6	60-9-1-7	60-9-1-8	60-9-1-9	60-9-1-10	60-9-1-11
FeO	15.04	17.67	14.56	14.18	15.19	13.18	14.36	14.46	13.72	13.26	13.44
MnO	1.23	1.04	1.28	1.13	1.29	1.39	1.05	1.39	1.12	1.54	1.51
MgO	11.59	9.56	11.59	12.04	11.70	12.27	11.91	12.23	12.06	12.52	11.93
CaO	27.86	27.27	28.05	27.13	27.62	27.94	27.80	28.10	27.13	17.38	27.93

	60-9-1-12	60-9-3-1	60-9-3-2	60-9-2-3	60-9-2-4	60-9-2-5	60-9-2-6	60-9-2-7	60-9-6-1	60-9-6-2
FeO	11.64	16.47	16.64	15.72	16.46	17.71	16.20	14.75	15.71	14.50
MnO	1.25	1.51	1.50	1.[illegible]7	1.36	1.28	1.14	1.43	0.48	0.48
MgO	13.58	11.09	10.85	11.26	10.41	9.96	11.02	12.09	18.56	16.91
CaO	28.04	27.59	27.36	27.27	27.45	27.74	27.13	27.65	29.27	28.32

	60-9-6-3	60-9-6-4	60-9-6-5	60-9-6-6	60-9-6-7	60-9-6-8	60-9-6-9	60-9-6-10
FeO	8.44	8.01	13.28	13.17	13.90	11.86	11.58	11.68
MnO	0.67	0.66	0.54	0.18	0.41	1.06	0.87	0.82
MgO	16.39	16.57	13.31	12.72	13.11	13.59	12.63	14.62
CaO	29.03	28.71	27.90	25.59	28.54	28.66	28.85	28.70

CARBONATE - Silicified Dolomite

	159-29-1	159-29-2	159-29-3	159-29-4	159-29-5	159-36-1	159-36-2	159-36-3	159-36-4	159-36-5	159-36-6
FeO	00.70	00.00	00.00	00.00	00.00	00.00	10.30	10.20	11.00	11.80	00.00
MnO	00.00	01.00	00.20	00.00	00.50	00.80	00.00	00.00	00.00	00.00	00.00
MgO	19.70	19.10	17.90	19.60	17.20	22.40	16.40	17.50	18.00	16.30	19.20
CaO	29.20	29.10	28.30	29.20	28.40	30.60	28.70	29.00	29.20	28.50	29.60

	159-36-7	159-36-8	159-36-9	159-36-10	159-36-11	159-36-12	159-36-13	159-36-14	159-37-1	159-37-2
FeO	00.00	10.10	10.60	10.40	13.00	00.00	11.10	13.10	12.40	12.50
MnO	00.00	00.00	00.30	00.00	00.00	00.60	00.00	00.00	00.00	00.00
MgO	24.70	17.60	13.60	17.10	14.90	23.60	13.50	12.00	11.20	11.60
CaO	29.20	24.80	24.10	25.20	24.40	26.60	25.00	27.40	24.50	24.00

	159-37-3	159-37-4	159-37-5	159-37-6	159-39-1	159-39-2	159-39-3	159-39-4	159-39-5	159-39-6
FeO	13.20	13.30	12.60	12.70	00.00	00.00	00.70	11.50	11.00	00.00
MnO	00.00	00.00	00.00	00.00	00.40	00.20	00.30	00.00	00.00	00.40
MgO	11.10	11.00	10.10	12.70	19.20	20.10	19.40	13.40	13.10	20.50
CaO	27.10	25.10	23.30	24.90	28.40	30.20	29.10	28.10	29.00	30.20

	159-39-7	159-39-8	159-39-9	159-39-10	159-39-11	159-39-12	159-48-1	159-48-2	159-48-3	159-48-4
FeO	00.00	10.30	00.00	10.70	11.30	10.20	00.10	00.00	00.00	00.80
MnO	00.30	00.00	00.00	00.00	00.00	00.00	00.00	00.20	00.10	00.10
MgO	20.20	12.80	14.20	13.60	13.30	14.20	21.30	19.40	20.40	19.10
CaO	29.60	27.70	28.10	27.50	27.30	28.30	30.50	30.50	30.00	31.30

	159-48-5	159-48-6	159-48-7	159-48-8	159-48-9	159-48-10	159-48-11	159-50-1	159-50-2	159-50-3
FeO	00.00	00.90	00.00	00.00	00.60	00.00	00.00	00.00	00.10	00.00
MnO	00.20	00.00	00.20	00.20	00.10	00.20	00.20	00.20	00.00	00.20
MgO	20.40	19.00	20.00	20.20	20.30	20.00	19.50	18.90	21.40	18.90
CaO	30.60	28.70	30.30	30.50	31.00	30.20	30.50	30.10	32.30	29.80

CARBONATE - Silicified Dolomite

	159-50-4	159-50-5	159-50-6	159-50-7	159-50-8	159-50-9	159-50-10	159-50-11	159-50-12	159-50-13
FeO	00.40	00.00	00.00	00.40	00.00	00.00	00.00	00.00	00.00	00.00
MnO	00.00	00.00	00.00	00.20	00.20	00.30	00.20	00.20	00.20	00.40
MgO	21.50	19.30	21.10	20.70	17.90	19.00	18.70	19.50	18.80	19.70
CaO	30.90	31.00	31.20	31.60	27.60	30.90	30.60	30.00	29.60	30.30

	159-50-14	159-50-15	159-53a-1	159-53a-2	159-53a-3	159-54-1	159-54-2	159-54-3	159-54-4	159-54-5
FeO	00.90	00.00	00.00	10.80	00.00	00.00	00.00	00.30	00.00	00.00
MnO	00.70	00.10	00.40	00.40	00.20	00.30	00.40	00.40	00.30	00.30
MgO	20.70	18.00	14.80	16.60	14.40	20.10	20.70	21.10	19.70	19.90
CaO	30.60	91.00	28.20	28.80	28.60	29.70	31.00	30.80	30.40	30.20

	159-54-6	159-54-7	159-54-8	159-56-1	159-56-2	159-56-3	159-56-4	159-56-5	159-56-6	159-56-7	159-56-8
FeO	00.00	00.30	00.00	00.00	00.00	00.00	00.00	00.00	00.00	00.00	00.00
MnO	00.40	00.00	00.10	00.00	00.40	00.30	00.30	00.40	00.30	00.40	00.00
MgO	20.10	21.00	20.50	19.10	20.10	19.60	19.20	20.20	19.70	19.90	21.60
CaO	30.40	31.70	30.90	29.30	29.70	29.00	29.50	29.40	29.40	30.00	30.80

	159-56-9	159-56-10	159-56-11	159-57a-1	159-57a-2
FeO	00.00	00.30	00.00	00.00	00.10
MnO	00.20	00.40	00.30	00.40	00.20
MgO	19.60	21.40	20.10	16.80	21.00
CaO	30.50	30.60	29.30	29.60	31.50

CARBONATE - Graphitic Pelite

	159-36-1	159-36-2	159-36-3	159-36-4	159-36-5	159-36-6	159-36-7	159-36-8	159-36-9	159-36-10	159-36-11
FeO	00.00	10.30	10.20	11.00	11.80	00.00	00.00	10.10	10.60	10.40	13.00
MnO	00.80	00.00	00.00	00.00	00.00	00.00	00.00	00.00	00.30	00.00	00.00
MgO	22.40	16.40	17.50	18.00	16.30	19.20	24.70	17.60	13.60	17.10	14.90
CaO	30.60	28.70	29.00	29.20	28.50	29.60	29.20	24.80	24.10	25.20	24.40

	159-36-12	159-36-13	159-36-14	159-37-1	159-37-2	159-37-3	159-37-4	159-37-5	159-37-6	60-12-1	60-12-2
FeO	00.00	11.10	13.10	12.40	12.50	13.20	13.30	12.60	12.70	11.71	12,57
MnO	00.60	00.00	00.00	00.00	00.00	00.00	00.00	00.00	00.00	3.91	2.95
MgO	23.60	13.50	12.00	11.20	11.60	11.10	11.00	10.10	12.70	11.74	11.32
CaO	26.60	25.00	27.40	24.50	24.00	27.10	25.10	23.30	24.90	27.39	28.05

	60-12-3	60-12-4	60-12-5	60-12-6	60-12-7	60-15-1	60-15-2	60-15-3	60-15-4	60-15-5	60-15-6	67-10-1	67-10-2
FeO	12.61	11.87	12.30	12.99	12.52	12.96	14.16	14.65	12.39	11.38	12.05	3.53	12.92
MnO	4.11	1.21	4.36	2.86	4.49	1.76	2.66	2.70	3.38	3.42	3.34	1.53	2.12
MgO	11.04	13.00	11.66	10.37	11.50	12.82	12.11	9.47	11.30	12.02	12.05	1.33	11.29
CaO	27.59	27.69	27.33	27.08	21.35	27.64	27.39	27.55	28.08	27.55	27.72	55.82	28.18

CARBONATE - Lower Ore Zone

	159-61-1	159-61-2	159-61-3	159-61-4	159-61-5	159-61-6	159-61-7
FeO	14.25	13.70	9.43	9.26	0.99	2.63	2.04
MnO	0.55	1.81	1.26	1.14	1.14	1.17	1.38
MgO	11.43	11.49	13.87	13.73	0.43	1.74	1.74
CaO	27.77	27.86	28.01	28.88	50.23	50.30	52.32

	159-61-8	159-61-9	159-61-10	159-61-11	159-61-12	159-61-13
FeO	0.64	0.99	2.22	1.15	12.29	11.45
MnO	1.19	1.31	1.32	1.29	0.54	1.14
MgO	0.21	0.14	1.89	0.42	12.41	13.01
CaO	52.62	51.87	51.55	53.22	27.09	29.12

BIOTITE - Foliated Amphibolite

	159-4-1	159-4-2	159-4-3	159-4-4	159-6-1	159-6-2	159-6-3	159-6-4
SiO_2	31.82	31.57	32.99	34.85	34.84	34.45	35.12	33.37
TiO_2	1.78	1.81	1.66	1.70	1.55	1.63	1.59	1.77
Al_2O_3	17.45	17.30	17.17	16.52	17.99	18.09	18.20	17.54
Cr_2O_3	0.11	0.03	0.18	0.05	0.14	0.04	0.04	0.04
FeO	22.36	22.84	23.09	23.02	21.16	22.41	22.32	22.33
MnO	0.00	00.00	0.00	0.00	0.05	0.00	0.00	0.00
MgO	0.41	8.29	8.91	8.23	8.39	8.77	8.68	8.45
CaO	0.00	0.00	0.00	0.00	0.00	0.00	0.00	0.00
Na_2O	1.13	1.07	1.00	1.05	0.68	0.59	0.80	0.86
BaO	0.11	0.10	0.09	0.02	0.08	0.24	0.13	0.09
K_2O	8.87	8.66	8.50	8.66	8.75	9.05	9.22	8.82
total	92.03	91.67	93.59	94.11	93.63	95.25	96.00	93.26

structural formulae based on 22 oxygen

	159-4-1	159-4-2	159-4-3	159-4-4	159-6-1	159-6-2	159-6-3	159-6-4
Si	5.67	5.16	5.26	5.49	5.43	5.45	5.40	5.31
Al^{iv}	2.33	2.84	2.74	2.51	2.54	2.65	2.60	2.69
Al^{vi}	1.34	0.50	0.48	0.56	0.78	0.66	0.69	0.60
Ti	0.24	0.22	0.20	0.20	0.18	0.19	0.18	0.21
Cr	0.02	0.00	0.02	0.01	0.02	0.00	0.00	0.01
Fe	3.33	3.12	3.08	3.03	2.77	2.91	2.87	2.97
Mn	0.00	0.00	0.00	0.00	0.01	0.00	0.00	0.00
Mg	0.11	2.02	2.12	1.93	1.96	2.03	1.99	2.00
Ca	0.00	0.00	0.00	0.00	0.00	0.00	0.00	0.00
Na	0.39	0.34	0.31	0.32	0.21	0.18	0.24	0.27
Ba	0.01	0.01	0.01	0.00	0.00	0.01	0.01	0.01
K	1.60	1.81	1.73	1.74	1.75	1.79	1.81	1.79

BIOTITE - Veined FDCSBQ Schist

	159-9-1	159-9-2	159-9-3	159-9-4	159-9-5	159-13-1	159-13-2	159-13-3	159-13-4	159-13-5	159-13-6
SiO_2	37.10	37.28	36.02	36.74	36.86	35.38	35.72	34.98	35.00	35.16	35.14
TiO_2	1.51	1.50	1.96	1.54	1.49	1.70	1.69	1.57	1.64	1.84	1.61
Al_2O_3	17.07	16.97	17.33	16.47	17.81	18.56	17.86	17.64	17.14	18.11	17.70
Cr_2O_3	0.00	0.00	0.00	0.00	0.00	0.05	0.06	0.09	0.22	0.14	0.18
FeO	17.85	17.34	16.79	17.76	17.28	18.44	19.17	18.04	19.27	17.74	18.20
MnO	0.00	0.00	0.00	0.00	0.00	0.02	0.07	0.05	0.07	0.08	0.11
MgO	11.60	11.75	10.93	11.81	11.39	10.07	10.28	1.00	0.00	9.63	9.72
CaO	0.00	0.00	0.08	0.00	0.01	0.03	0.04	0.02	0.04	0.05	0.07
Na_2O	0.00	0.00	0.00	0.00	0.00	0.35	0.32	0.34	0.32	0.23	0.23
BaO	0.78	0.44	0.38	0.36	0.57	0.17	0.11	0.11	0.10	0.12	0.25
K_2O	9.66	9.77	9.95	9.36	9.48	9.14	8.81	8.96	8.72	8.57	8.75
total	95.58	95.06	93.43	93.80	94.88	93.92	94.13	91.81	92.15	91.77	92.10

structural formulae based on 22 oxygen

	159-9-1	159-9-2	159-9-3	159-9-4	159-9-5	159-13-1	159-13-2	159-13-3	159-13-4	159-13-5	159-13-6
Si	5.62	5.65	5.66	5.63	5.59	5.67	5.16	5.26	5.49	5.51	5.51
Al^{iv}	2.38	2.35	2.44	2.37	2.41	2.55	2.51	2.49	2.48	2.49	2.49
Al^{vi}	0.66	0.68	0.71	0.61	0.77	0.81	0.73	0.78	0.70	0.85	0.79
Ti	0.17	0.17	0.23	0.18	0.17	0.20	0.20	0.19	0.19	0.22	0.19
Cr	0.00	0.00	0.00	0.00	0.00	0.01	0.01	0.01	0.03	0.02	0.02
Fe	2.26	2.20	2.17	2.28	2.19	2.37	2.47	2.37	2.54	2.32	2.39
Mn	0.00	0.00	0.00	0.00	0.00	0.00	0.01	0.01	0.01	0.01	0.01
Mg	2.62	2.65	2.51	2.70	2.57	2.31	2.36	2.35	2.26	2.27	2.31
Ca	0.00	0.00	0.01	0.00	0.00	0.00	0.01	0.00	0.01	0.01	0.01
Na	0.00	0.00	0.00	0.00	0.00	0.10	0.10	0.10	0.10	0.07	0.07
Ba	0.05	0.03	0.02	0.02	0.03	0.01	0.01	0.01	0.01	0.01	0.02
K	1.87	1.89	1.96	1.83	1.83	1.80	1.73	1.80	1.75	1.71	1.75

BIOTITE - Massive Ferroan Dolomite

	159-15-1	159-15-2	159-15-3	159-15-4
SiO_2	36.83	37.42	37.14	37.21
TiO_2	1.63	1.72	1.59	1.68
Al_2O_3	18.64	19.01	18.53	19.20
Cr_2O_3	0.05	0.09	0.17	0.25
FeO	18.06	17.65	17.77	18.30
MnO	0.13	0.09	0.04	0.09
MgO	11.09	11.11	11.10	11.23
CaO	0.05	0.03	0.10	0.02
Na_2O	0.60	0.46	0.54	0.30
BaO	0.20	0.17	0.23	0.26
K_2O	9.25	9.50	9.08	9.62
total	96.52	97.24	96.28	98.15

structural formulae based on 22 oxygen

Si	5.49	5.52	5.54	5.46
Al^{iv}	2.51	2.48	2.46	2.54
Al^{vi}	0.77	0.82	0.79	0.76
Ti	0.18	0.19	0.18	0.19
Cr	0.01	0.01	0.02	0.03
Fe	2.25	2.18	2.22	2.25
Mn	0.02	0.01	0.01	0.01
Mg	2.47	2.44	2.47	2.46
Ca	0.01	0.00	0.02	0.00
Na	0.17	0.13	0.16	0.09
Ba	0.01	0.01	0.01	0.01
K	1.76	1.79	1.73	1.80

BIOTITE - Sericite-Chlorite Schist

	159-28-1	159-28-2	159-28-3	159-28-4	159-28-5	159-28-6
SiO_2	36.21	35.49	37.52	37.65	36.15	37.66
TiO_2	1.45	1.55	1.53	1.51	1.47	1.46
Al_2O_3	17.27	16.97	18.51	17.86	18.51	18.82
Cr_2O_3	0.00	0.00	0.07	0.09	0.05	0.05
FeO	17.17	17.35	17.45	17.54	19.33	17.71
MnO	0.12	0.05	0.11	0.15	0.05	0.13
MgO	11.73	11.66	11.49	11.65	11.23	11.42
CaO	0.00	0.00	0.00	0.00	0.00	0.00
Na_2O	0.00	0.11	0.77	0.64	0.57	0.69
BaO	0.14	0.00	0.31	0.25	0.22	0.19
K_2O	9.59	9.50	9.65	9.70	9.34	9.68
total	93.84	92.87	97.41	97.04	96.92	95.50

structural formulae based on 22 oxygen

	159-28-1	159-28-2	159-28-3	159-28-4	159-28-5	159-28-6
Si	5.56	5.52	5.54	5.58	5.42	5.53
Al^{iv}	2.44	2.48	2.46	2.42	2.58	2.47
Al^{vi}	0.69	0.63	0.76	0.71	0.68	0.79
Ti	0.17	0.18	0.17	0.17	0.17	0.16
Cr	0.00	0.00	0.01	0.01	0.01	0.01
Fe	2.21	2.26	2.15	2.18	2.42	2.18
Mn	0.02	0.01	0.01	0.02	0.01	0.02
Mg	2.69	2.70	2.53	2.58	2.51	2.50
Ca	0.00	0.00	0.00	0.00	0.00	0.00
Na	0.00	0.03	0.22	0.18	0.17	0.20
Ba	0.01	0.00	0.02	0.01	0.01	0.[illegible]
K	1.88	1.89	1.82	1.84	1.79	1.81

BIOTITE - Sericite-Chlorite Schist

	k2-9-1-1	k2-9-1-2	k2-9-1-3	k2-9-1-4	k2-9-1-5	k2-9-1-6	k2-9-1-7	k2-9-1-8	k2-9-1-9	k2-9-1-10
SiO_2	33.35	33.14	33.27	31.98	33.95	32.38	33.54	33.34	33.74	33.67
TiO_2	1.95	1.94	1.96	2.25	1.80	1.98	1.79	1.82	2.13	1.96
Al_2O_3	18.03	19.00	17.41	14.90	18.42	17.23	18.07	17.62	18.20	17.69
Cr_2O_3	0.25	0.13	0.05	0.17	0.29	8.18	0.20	0.23	0.34	0.09
FeO	28.99	28.58	27.23	29.95	27.92	28.42	28.01	29.54	28.23	28.77
MnO	0.05	0.02	0.13	.00	0.00	0.05	0.07	.00	0.09	0.14
MgO	3.33	3.29	3.23	3.34	3.67	3.35	2.05	3.95	3.82	3.94
CaO	.00	.00	.00	.00	0.00	.00	.00	.00	.00	.00
Na_2O	0.82	0.67	0.93	0.89	0.73	0.69	0.79	0.63	0.64	0.61
BaO	0.35	0.31	0.45	0.29	0.35	0.15	0.25	0.28	0.37	0.24
K_2O	8.76	8.75	8.77	7.96	8.82	8.65	7.54	8.83	8.98	9.08
total	95.87	95.83	95.39	91.73	95.95	93.07	92.33	96.23	96.53	95.99

structural formulae based on 22 o   structural formulae based on 22 oxygen

Si	5.43	5.28	5.43	5.41	5.38	4.98	5.50	5.32	5.33	5.34
Al^{iv}	2.67	2.72	2.57	2.59	2.62	3.02	2.50	2.68	2.67	2.66
Al^{vi}	0.73	0.85	0.79	0.39	0.82	0.11	0.99	0.64	0.73	0.67
Ti	0.23	0.23	0.24	0.29	0.21	0.23	0.22	0.22	0.25	0.24
Cr.	0.03	0.02	0.01	0.02	0.04	1.00	0.03	0.03	0.04	0.01
Fe	3.88	3.81	3.72	4.24	3.70	3.66	3.84	3.94	3.73	3.84
Mn	0.01	0.00	0.02	0.00	0.00	0.01	0.01	0.00	0.01	0.02
Mg	0.79	0.78	0.79	0.84	0.87	0.77	0.50	0.94	0.90	0.94
Ca	0.00	0.00	0.00	0.00	0.00	0.00	0.00	0.00	0.00	0.00
Na	0.25	0.21	0.29	0.29	0.22	0.21	0.25	0.20	0.20	0.19
Ba	0.02	0.02	0.03	0.02	0.02	0.01	0.02	0.02	0.02	0.02
K	1.79	1.78	1.83	1.72	1.78	1.70	1.58	1.80	1.81	1.85

BIOTITE - Sericite-Chlorite Schist

	K2-9-2-1	K2-9-2-2	K2-9-2-3	K2-9-2-4	K2-9-2-5
SiO_2	31.22	32.91	32.61	31.73	31.97
TiO_2	1.93	1.89	1.80	1.89	1.80
Al_2O_3	20.18	20.47	18.83	19.05	18.56
Cr_2O_3	0.02	0.02	0.04	0.00	0.02
FeO	27.71	27.46	29.44	29.95	27.66
MnO	0.00	0.06	0.06	0.04	0.04
MgO	2.79	2.73	2.79	2.55	2.49
CaO	0.00	0.00	0.00	0.00	0.00
Na_2O	1.00	0.71	0.88	0.81	0.84
BaO	0.42	0.57	0.31	0.53	0.29
K_2O	7.95	8.79	8.92	8.18	8.19
total	93.23	95.62	95.67	94.73	91.30

structural formulae based on 22 oxygen

	K2-9-2-1	K2-9-2-2	K2-9-2-3	K2-9-2-4	K2-9-2-5
Si	5.10	5.23	5.25	5.17	5.26
Al^{iv}	2.90	2.77	2.75	2.83	2.74
Al^{vi}	0.99	1.06	0.82	0.82	0.92
Ti	0.24	0.23	0.22	0.23	0.23
Cr	0.00	0.00	0.01	0.00	0.00
Fe	3.79	3.65	3.96	4.08	3.87
Mn	0.00	0.01	0.01	0.01	0.01
Mg	0.68	0.65	0.67	0.62	0.62
Ca	0.00	0.00	0.00	0.00	0.00
Na	0.32	0.22	0.27	0.26	0.27
Ba	0.03	0.04	0.02	0.03	0.02
K	1.66	1.78	1.83	1.70	1.75

BIOTITE - Chlorite-Magnetite Schist

	60-9-1-1	60-9-1-2	60-9-1-3	60-9-1-4	60-9-1-5	60-9-3-1	60-9-3-2	60-9-3-3	60-9-3-4	60-9-3-5	60-9-3-6
SiO_2	32.98	34.82	34.88	34.57	34.73	34.44	34.73	34.47	34.12	34.93	34.27
TiO_2	1.91	1.11	1.81	1.08	1.77	1.93	2.00	1.92	1.43	1.97	1.95
Al_2O_3	16.50	17.10	16.33	17.05	15.81	16.20	16.09	15.52	16.15	16.20	15.86
Cr_2O_3	0.26	0.25	0.17	0.07	0.16	0.07	0.16	0.21	0.18	0.14	0.07
FeO	25.99	25.23	24.83	24.70	23.89	27.25	26.66	26.72	26.78	27.12	27.65
MnO	.00	0.00	.00	.00	.00	.00	.00	.00	0.00	.00	.00
MgO	7.97	8.22	8.27	7.63	8.38	6.73	6.70	6.64	7.07	6.62	7.65
CaO	.00	0.00	.00	.00	.00	.00	.00	.00	0.00	.00	.00
Na_2O	0.33	0.43	0.42	0.33	0.40	0.39	0.38	0.36	0.39	0.34	0.34
BaO	0.12	0.16	0.14	0.67	0.96	0.21	0.14	0.12	0.06	0.20	0.21
K_2O	9.50	9.40	9.60	9.15	9.46	9.22	9.03	9.45	9.23	9.44	9.27
total	97.79	97.41	96.46	95.25	95.56	96.43	95.90	95.41	95.40	96.96	96.43

structural formulae based on 22 oxygen

	60-9-1-1	60-9-1-2	60-9-1-3	60-9-1-4	60-9-1-5	60-9-3-1	60-9-3-2	60-9-3-3	60-9-3-4	60-9-3-5	60-9-3-6
Si	5.42	5.41	5.43	5.45	5.48	5.42	5.47	5.49	5.42	5.47	5.37
Al^{iv}	2.58	2.59	2.57	2.55	2.52	2.58	2.53	2.51	2.58	2.53	2.63
Al^{vi}	0.42	0.54	0.43	0.62	0.41	0.43	0.46	0.40	0.45	0.45	0.30
Ti	0.22	0.13	0.21	0.13	0.21	0.23	0.24	0.23	0.17	0.23	0.23
Cr	0.03	0.03	0.02	0.01	0.02	0.01	0.02	0.03	0.02	0.02	0.01
Fe	3.35	3.28	3.23	3.26	3.15	3.59	3.51	3.56	3.56	3.55	3.62
Mn	0.00	0.00	0.00	0.00	0.00	0.00	0.00	0.00	0.00	0.00	0.00
Mg	1.83	1.90	1.92	1.79	1.97	1.58	1.57	1.58	1.68	1.54	1.79
Ca	0.00	0.00	0.00	0.00	0.00	0.00	0.00	0.00	0.00	0.00	0.00
Na	0.10	0.13	0.13	0.10	0.12	0.12	0.12	0.11	0.12	0.10	0.10
Ba	0.01	0.01	0.01	0.04	0.06	0.01	0.01	0.01	0.00	0.01	0.01
K	1.87	1.86	1.91	1.84	1.90	1.85	1.82	1.92	1.87	1.88	1.85

BIOTITE - Graphitic Pelite

	159-37-1	159-37-2	159-37-3	159-37-4	67-10-1	67-10-2	67-10-3	67-10-4	67-10-5	67-10-6	67-10-7
SiO_2	36.39	36.55	35.73	36.59	35.69	34.16	35.12	35.72	35.66	36.14	35.32
TiO_2	1.62	1.50	1.67	1.57	1.94	1.53	1.51	1.92	1.97	1.91	1.72
Al_2O_3	17.07	17.51	17.83	17.0	18.78	18.57	16.33	17.76	17.17	17.36	17.74
Cr_2O_3	0.00	0.00	0.00	0.0	0.09	.00	0.11	.00	0.02	0.11	0.14
FeO	18.65	18.38	17.64	18.17	21.58	21.77	21.04	22.40	21.14	21.76	22.30
MnO	0.08	0.18	0.21	0.14	0.05	0.04	0.05	0.05	.00	0.20	0.04
MgO	10.64	10.40	9.96	10.97	8.50	8.55	8.80	9.44	9.70	9.24	8.84
CaO	0.00	0.02	0.00	0.00	0.03	0.01	.00	.00	.00	0.00	.00
Na_2O	0.00	0.00	0.00	0.11	0.57	0.52	0.59	0.36	0.48	0.44	0.38
BaO	0.13	0.13	0.06	0.00	0.14	0.07	0.16	0.24	0.17	0.18	0.26
K_2O	9.48	9.43	9.17	9.19	9.40	9.66	9.27	9.64	9.45	9.38	9.16
total	94.13	94.19	92.43	93.82	96.78	94.88	92.99	97.54	95.76	96.71	95.80

structural formulae based on 22 oxygen

Si	5.60	5.61	5.57	5.62	5.41	5.32	5.57	5.61	5.47	5.50	5.44
Al^{iv}	2.40	2.39	2.43	2.3	2.59	2.68	2.43	2.59	2.53	2.50	2.56
Al^{vi}	0.69	0.77	0.84	0.7	0.77	0.74	0.62	0.59	0.58	0.61	0.65
Cr	0.00	0.00	0.00	0.00	0.01	0.00	0.01	0.00	0.00	0.01	0.02
Ti	0.19	0.17	0.20	0.18	0.22	0.18	0.18	0.22	0.23	0.22	0.20
Fe	2.40	2.36	2.30	2.33	2.74	2.84	2.79	2.84	2.71	2.77	2.87
Mg	2.44	2.38	2.31	2.51	1.92	1.99	2.08	2.13	2.22	2.10	2.03
Mn	0.01	0.02	0.03	0.02	0.01	0.01	0.01	0.01	0.00	0.03	0.01
Ca	0.00	0.00	0.00	0.00	0.00	0.00	0.00	0.00	0.00	0.00	0.00
Na	0.00	0.00	0.00	0.03	0.17	0.16	0.18	0.11	0.14	0.13	0.11
Ba	0.00	0.01	0.00	0.00	0.01	0.00	0.01	0.01	0.01	0.01	0.02
K	1.86	1.85	1.82	1.80	1.82	1.92	1.87	1.86	1.85	1.82	1.80

BIOTITE - Graphitic Pelite

	60-12-1	60-12-2	60-12-3	60-12-4	60-12-5	60-12-6	60-15-1	60-15-2	60-15-3	60-15-4
SiO_2	35.88	35.67	35.24	35.59	35.79	36.37	35.48	35.00	36.11	36.52
TiO_2	1.80	2.05	2.21	1.73	1.81	1.71	1.59	1.62	1.39	1.58
Al_2O_3	19.13	20.14	19.00	17.55	18.38	18.18	18.41	17.63	17.83	18.18
Cr_2O_3	0.19	0.09	0.17	0.23	0.10	0.00	0.05	0.09	0.04	0.03
FeO	19.31	18.38	19.46	20.86	18.26	19.48	18.32	18.49	18.78	18.43
MnO	.00	.00	.00	.00	0.00	0.00	0.05	0.04	0.15	0.04
MgO	9.98	9.30	9.67	10.00	9.79	10.30	9.27	10.15	9.86	10.24
CaO	.00	0.63	.00	.00	0.00	0.00	0.06	0.01	0.03	0.02
Na_2O	0.41	0.62	0.34	0.37	0.38	0.40	0.35	0.52	0.42	0.40
BaO	0.09	0.17	0.24	0.20	0.21	0.16	0.30	0.10	0.18	0.13
K_2O	9.62	5.88	9.32	9.24	8.91	9.64	9.10	9.75	9.25	9.74
total	96.41	92.93	95.64	95.77	93.64	96.23	96.78	94.88	92.99	97.54

structural formulae based on 22 oxygen -

	60-12-1	60-12-2	60-12-3	60-12-4	60-12-5	60-12-6	60-15-1	60-15-2	60-15-3	60-15-4
Si	5.40	5.43	5.36	5.45	5.51	5.49	5.52	5.46	5.56	5.54
Al^{iv}	2.60	2.57	2.64	2.55	2.49	2.51	2.48	2.54	2.44	2.46
Al^{vi}	0.80	1.05	0.77	0.61	0.84	0.73	0.89	0.70	0.80	0.79
Cr	0.02	0.01	0.02	0.03	0.01	0.00	0.01	0.01	0.00	0.00
Ti	0.20	0.23	0.25	0.20	0.21	0.19	0.19	0.19	0.16	0.18
Fe	2.43	2.34	2.48	2.67	2.35	2.47	2.38	2.41	2.42	2.34
Mg	2.24	2.11	2.19	2.29	2.25	2.32	2.15	2.36	2.26	2.32
Mn	0.00	0.00	0.00	0.00	0.00	0.00	0.01	0.01	0.02	0.01
Ca	0.00	0.10	0.00	0.00	0.00	0.00	0.01	0.00	0.00	0.00
Na	0.12	0.18	0.10	0.11	0.11	0.12	0.11	0.16	0.13	0.12
Ba	0.01	0.01	0.01	0.01	0.01	0.01	0.02	0.01	0.01	0.01
K	1.85	1.14	1.81	1.80	1.75	1.86	1.81	1.94	1.82	1.89

BIOTITE - Graphitic Pelite

	k2-13-1	k2-13-2	k2-13-3	k2-14-1	k2-14-2	k2-14-3	k2-14-4	k2-14-5	k4-7-1	k4-7-2	k4-7-3	k4-7-4	k4-7-5
SiO_2	34.79	34.55	35.60	34.70	35.28	36.26	35.88	35.38	36.24	35.68	35.74	35.62	34.11
TiO_2	1.81	1.48	1.63	1.46	1.34	1.46	1.33	1.53	1.71	1.48	1.59	1.41	1.43
Al_2O_3	18.79	18.44	18.23	18.56	17.36	18.60	18.20	18.17	19.73	19.19	18.72	19.91	19.36
Cr_2O_3	0.00	0.10	0.04	0.02	0.00	0.00	0.04	0.08	20.25	20.89	19.05	17.63	19.98
FeO	18.83	17.82	19.43	17.80	19.18	18.69	16.90	17.38	0.00	0.00	0.00	0.03	0.00
MnO	0.08	0.03	0.10	0.14	0.11	0.21	0.20	0.10	0.12	0.06	0.14	0.09	0.15
MgO	10.53	10.17	10.95	10.88	11.12	10.89	11.46	10.83	8.93	9.52	10.01	9.76	10.07
CaO	0.00	0.00	0.00	0.00	0.00	0.00	0.00	0.00	0.00	0.00	0.00	0.00	0.00
Na_2O	0.45	0.48	0.40	0.31	0.31	0.40	0.35	0.38	0.48	0.54	0.35	0.49	0.48
BaO	0.22	0.19	0.17	0.36	0.21	0.21	0.38	0.36	0.25	1.48	0.18	0.27	0.18
K_2O	9.23	9.01	9.08	9.42	9.34	9.33	9.12	9.49	8.26	9.25	9.66	9.24	9.39
total	94.74	92.28	95.62	93.64	94.25	96.06	93.85	93.69	95.96	96.83	95.44	94.45	95.14

structural formulae based on 22 oxygen

	k2-13-1	k2-13-2	k2-13-3	k2-14-1	k2-14-2	k2-14-3	k2-14-4	k2-14-5	k4-7-1	k4-7-2	k4-7-3	k4-7-4	k4-7-5
Si	5.34	5.41	5.41	5.37	5.45	5.46	5.49	5.46	5.46	5.59	5.44	5.43	5.47
Al^{iv}	2.66	2.59	2.59	2.63	2.55	2.54	2.51	2.54	2.54	2.41	2.56	2.57	2.53
Al^{vi}	0.73	0.82	0.67	0.76	0.62	0.76	0.78	0.76	0.96	1.13	0.80	1.00	1.13
Cr	0.00	0.01	0.00	0.00	0.00	0.00	0.00	0.01	0.00	0.00	0.00	0.00	0.00
Ti	0.21	0.17	0.19	0.17	0.16	0.17	0.15	0.18	0.19	0.17	0.18	0.16	0.17
Fe	2.42	2.33	2.47	2.30	2.48	2.35	2.16	2.24	2.55	2.74	2.43	2.25	2.68
Mg	2.41	2.38	2.48	2.51	2.56	2.45	2.62	2.49	2.00	2.22	2.27	2.22	2.41
Mn	0.01	0.00	0.01	0.02	0.01	0.03	0.03	0.01	0.02	0.01	0.02	0.01	0.02
Ca	0.00	0.00	0.00	0.00	0.00	0.00	0.00	0.00	0.00	0.00	0.00	0.00	0.00
Na	0.13	0.15	0.12	0.09	0.09	0.12	0.10	0.11	0.14	0.16	0.10	0.14	0.16
Ba	0.01	0.01	0.01	0.02	0.01	0.01	0.02	0.02	0.01	0.09	0.01	0.02	[illegible]
K	1.81	1.80	1.76	1.86	1.84	1.79	1.78	1.87	1.59	1.85	1.88	1.80	1.84

BIOTITE - Silicified Dolomite

	159-29-1	159-29-2	159-57a-1	159-57a-2	159-57a-3	159-57a-4	159-57a-5	159-57a-6	159-57a-7	159-57a-8
SiO_2	39.81	40.96	37.80	39.17	40.10	40.09	40.71	40.16	39.61	40.33
TiO_2	0.72	0.72	0.86	0.87	0.84	0.86	0.86	0.76	0.95	0.51
Al_2O_3	16.77	16.48	16.18	16.13	16.22	16.27	16.30	16.02	16.71	16.17
Cr_2O_3	0.06	0.11	0.06	0.00	0.00	0.07	0.00	0.00	0.00	0.08
FeO	7.96	7.98	10.55	10.56	10.92	10.63	10.70	10.31	10.30	10.63
MnO	0.09	0.10	0.00	0.00	0.00	0.00	0.00	0.00	0.00	0.00
MgO	18.74	19.04	16.69	17.13	16.93	17.22	16.86	17.70	17.32	16.81
CaO	0.00	0.00	0.00	0.00	0.00	0.00	0.00	0.00	0.00	0.00
Na_2O	0.29	0.29	0.39	0.29	0.31	0.32	[illegible]	0.36	0.43	0.32
BaO	0.26	0.29	0.09	0.09	0.09	0.04	0.15	0.18	0.07	0.17
K_2O	9.63	9.85	9.23	9.58	9.15	9.63	8.91	9.09	9.33	8.97
total	94.33	95.82	91.84	93.82	94.56	95.12	94.83	94.59	94.73	94.43

structural formulae based on 22 oxygen

	159-29-1	159-29-2	159-57a-1	159-57a-2	159-57a-3	159-57a-4	159-57a-5	159-57a-6	159-57a-7	159-57a-8
Si	5.78	5.85	5.71	5.79	5.85	5.83	5.90	5.85	5.77	5.90
Al	2.22	2.15	2.29	2.21	2.15	2.17	2.10	2.15	2.23	2.10
Al^{vi}	0.64	0.62	0.59	0.59	0.65	0.61	0.69	0.60	0.64	0.69
Ti^{vi}	0.08	0.08	0.10	0.10	0.09	0.09	0.09	0.08	0.10	0.06
Cr	0.01	0.01	0.01	0.00	0.00	0.01	0.00	0.00	0.00	0.01
Fe	0.97	0.95	1.33	1.30	1.33	1.29	1.30	1.26	1.25	1.30
Mn	0.01	0.01	0.00	0.00	0.00	0.00	0.00	0.00	0.00	0.00
Mg	4.05	4.05	3.76	3.77	3.68	3.73	3.65	3.84	3.76	3.69
Ca	0.00	0.00	0.00	0.00	0.00	0.00	0.00	0.00	0.00	0.00
Na	0.08	0.08	0.11	0.08	0.09	0.09	0.10	0.10	0.12	0.09
Ba	0.01	0.02	0.01	0.01	0.01	0.00	0.01	0.01	0.00	0.01
K	1.78	1.79	1.78	1.81	1.70	1.79	1.65	1.69	1.73	1.67

BIOTITE - LOZ

	159-61-1	159-61-2
SiO_2	35.98	36.12
TiO_2	1.56	1.47
Al_2O_3	17.73	18.25
Cr_2O_3	0.02	0.07
FeO	14.23	14.89
MnO	0.05	0.16
MgO	13.52	12.62
CaO	0.00	0.00
Na_2O	0.50	0.45
BaO	0.25	0.12
K_2O	9.58	9.39
total	93.42	93.54

structural formulae based on 22 oxygen

Si	5.48	5.44
Al^{iv}	2.52	2.56
Al^{vi}	0.66	0.67
Ti	0.18	0.17
Cr	0.00	0.01
Fe	1.81	1.87
Mn	0.01	0.02
Mg	3.07	3.06
Ca	0.00	0.00
Na	0.15	0.13
Ba	0.01	0.01
K	1.86	1.80

BIOTITE - Banded Chlorite-Sericite-Garnet Schist

	60-29-1	60-29-2	60-29-3	60-29-4	60-29-5	60-29-6	60-29-7	67-19-1	67-19-2	67-19-3	67-19-4	67-19-5
SiO_2	36.36	33.67	36.81	36.64	37.43	36.28	35.80	35.12	35.88	35.55	36.03	35.46
TiO_2	1.81	1.75	1.73	1.80	1.79	1.84	1.75	1.63	1.63	1.73	1.71	1.67
Al_2O_3	18.65	18.93	18.86	18.99	18.38	18.65	18.46	17.65	18.64	18.16	18.14	17.89
Cr_2O_3	0.25	0.06	0.06	0.02	0.16	0.08	0.07	0.08	0.11	0.07	0.06	0.08
FeO	23.16	24.43	22.89	23.61	24.43	22.98	25.52	23.06	22.23	22.28	21.49	23.31
MnO	0.01	.00	.00	.00	.00	.00	.00	0.00	.00	.00	.00	.00
MgO	7.46	7.23	7.44	7.76	7.41	7.45	8.30	7.55	7.70	7.77	7.88	7.68
CaO	0.00	0.02	0.02	0.02	.00	0.01	.00	0.10	0.05	0.06	.00	.00
Na_2O	0.37	0.37	0.37	0.36	0.30	0.36	0.31	0.25	0.27	0.25	0.28	0.26
BaO	0.10	0.11	0.07	0.10	0.09	0.07	0.11	0.18	0.11	0.09	0.05	.00
K_2O	8.55	9.20	9.04	9.01	8.93	9.06	7.94	8.51	8.77	9.04	8.75	8.58
total	96.72	98.75	97.28	98.32	98.93	96.77	98.26	94.14	95.38	94.99	94.41	94.93

structural formulae based on 22 oxygen

	60-29-1	60-29-2	60-29-3	60-29-4	60-29-5	60-29-6	60-29-7	67-19-1	67-19-2	67-19-3	67-19-4	67-19-5
Si	5.48	5.44	5.55	5.48	5.57	5.51	5.38	5.50	5.51	5.50	5.37	5.50
Al^{iv}	2.49	2.75	2.45	2.52	2.43	2.49	2.62	2.50	2.49	2.50	2.43	2.50
Al^{vi}	0.85	0.73	0.89	0.83	0.80	0.85	0.67	0.76	0.88	0.81	0.87	0.77
Ti	0.21	0.21	0.20	0.20	0.20	0.21	0.20	0.19	0.19	0.20	0.20	0.19
Cr	0.03	0.01	0.01	0.00	0.02	0.01	0.01	0.01	0.01	0.01	0.01	0.01
Fe	2.94	3.19	2.89	2.95	3.04	2.92	3.21	3.02	2.85	2.88	2.78	3.02
Mn	0.00	0.00	0.00	0.00	0.00	0.00	0.00	0.00	0.00	0.00	0.00	0.00
Mg	1.69	1.68	1.67	1.73	1.65	1.69	1.86	1.76	1.76	1.79	1.82	1.78
Ca	0.00	0.00	0.00	0.00	0.00	0.00	0.00	0.02	0.01	0.01	0.00	0.00
Na	0.11	0.11	0.11	0.10	0.09	0.11	0.09	0.08	0.08	0.07	0.08	0.08
Ba	0.01	0.01	0.00	0.01	0.01	0.00	0.01	0.01	0.01	0.01	0.00	0.00
K	1.65	1.83	1.74	1.72	1.70	1.76	1.53	1.70	1.72	1.79	1.73	1.70

BIOTITE - Banded Chlorite-Sericite-Garnet Schist

	73-13-1	73-13-2	73-13-3	73-13-4	73-13-5	73-13-6	73-13-7
SiO_2	34.09	33.94	34.69	33.61	34.54	34.22	34.48
TiO_2	2.08	2.07	2.02	2.16	2.53	2.63	2.45
Al_2O_3	17.45	17.62	18.17	17.94	17.95	17.66	18.53
Cr_2O_3	0.18	0.17	0.21	0.10	0.20	0.23	0.12
FeO	25.96	24.46	24.86	24.27	25.84	26.42	25.34
MnO	0.03	.00	0.00	0.05	0.04	.00	.00
MgO	5.25	5.95	5.83	5.94	5.24	5.29	4.96
CaO	0.02	.00	0.01	0.02	0.04	0.07	0.04
Na_2O	0.44	0.44	0.43	0.46	0.46	0.60	0.52
BaO	0.06	0.05	0.05	0.08	0.02	0.08	0.12
K_2O	7.24	8.63	9.16	8.77	9.08	8.92	8.48
total	94.28	93.32	95.43	93.39	95.92	96.13	95.04

structural formula based on 22 oxygen

Si	5.47	5.43	5.43	5.37	5.40	5.37	5.54
Al^{iv}	2.53	2.57	2.57	2.63	2.60	2.63	2.59
Al^{vi}	0.78	0.75	0.78	0.75	0.71	0.63	0.04
Ti	0.25	0.25	0.24	0.26	0.30	0.31	0.29
Cr	0.02	0.02	0.03	0.01	0.02	0.03	0.01
Fe	3.49	3.27	3.25	3.25	3.38	3.47	3.33
Mn	0.00	0.00	0.00	0.01	0.01	0.00	0.00
Mg	1.26	1.42	1.36	1.42	1.22	1.24	1.16
Ca	0.00	0.00	0.00	0.00	0.01	0.01	0.01
Na	0.14	0.14	0.13	0.14	0.14	0.18	0.16
Ba	0.00	0.00	0.00	0.01	0.00	0.00	0.01
K	1.48	1.76	1.83	1.79	1.81	1.79	1.70

MUSCOVITE - Ferroan Dolomite Schist

	159-9-1	159-9-2	159-9-3	159-9-4	159-10-1	159-10-2	159-10-3	159-10-4	159-17-1	159-17-2
SiO_2	49.28	48.10	48.49	47.34	46.59	48.90	47.57	47.70	44.33	44.23
TiO_2	0.38	0.38	0.38	0.39	0.49	0.44	0.52	0.45	0.37	0.48
Al_2O_3	34.44	32.51	35.31	33.58	34.39	32.25	34.20	31.97	31.34	33.21
Cr_2O_3	0.01	0.06	0.00	0.24	0.09	0.07	0.17	1.30	1.36	1.20
FeO	1.83	1.88	1.81	2.14	1.20	1.40	1.30	0.07	0.08	0.11
MnO	0.00	0.00	0.00	0.00	0.00	0.00	0.00	0.00	0.00	0.00
MgO	1.82	1.85	1.57	1.83	1.00	1.70	1.30	1.60	1.63	1.38
CaO	0.00	0.00	0.00	0.00	0.00	0.00	0.00	0.00	0.03	0.00
BaO	0.34	0.28	0.41	0.57	0.61	0.48	0.47	0.47	0.45	0.59
Na_2O	0.44	0.70	0.36	0.59	0.79	0.79	0.61	0.68	0.92	0.72
K_2O	9.88	10.29	6.57	10.10	9.40	9.30	10.23	10.08	9.19	9.70
total	98.42	96.06	94.89	98.79	94.68	95.43	96.41	94.42	89.70	91.64

structural formulae based on 22 oxygen

	159-9-1	159-9-2	159-9-3	159-9-4	159-10-1	159-10-2	159-10-3	159-10-4	159-17-1	159-17-2
Si	6.34	6.38	6.33	6.25	6.23	6.47	6.27	6.42	6.28	6.15
Al^{iv}	1.66	1.62	1.67	6.75	1.77	1.53	1.73	1.58	1.72	1.85
Al^{vi}	3.56	3.46	3.77	3.48	3.66	3.50	3.58	3.38	3.52	3.60
Ti	0.04	0.04	0.04	0.04	0.05	0.04	0.05	0.05	0.04	0.05
Cr	0.00	0.01	0.00	0.03	0.01	0.01	0.02	0.01	0.01	0.01
Fe	0.20	0.21	0.20	0.24	0.14	0.16	0.14	0.15	0.16	0.14
Mn	0.00	0.00	0.00	0.00	0.00	0.00	0.00	0.00	0.00	0.00
Mg	0.35	0.37	0.31	0.36	0.20	0.34	0.26	0.33	0.34	0.29
Ca	0.00	0.00	0.00	0.00	0.00	0.00	0.00	0.00	0.00	0.00
Ba	0.01	0.01	0.02	0.02	0.03	0.02	0.02	0.02	0.02	0.03
Na	0.11	0.18	0.09	0.15	0.20	0.20	0.16	0.18	0.25	0.19
K	1.62	1.74	1.09	1.70	1.62	1.58	1.71	1.73	1.66	1.72

MUSCOVITE - Ferroan Dolomite Schist

	159-17-3	159-17-4	159-17-5	159-17-6	159-17-7	156-5-1	156-5-2	156-5-3
SiO_2	45.06	45.21	45.36	46.74	46.24	45.04	46.00	49.19
TiO_2	0.37	0.38	0.32	0.38	0.28	0.30	0.27	0.32
Al_2O_3	32.22	32.01	33.38	31.63	31.14	34.39	35.41	33.31
Cr_2O_3	0.12	0.11	1.02	1.37	1.11	1.19	1.11	1.84
FeO	1.30	1.21	0.13	0.04	0.08	0.23	0.14	0.09
MnO	0.00	0.00	0.07	0.02	0.08	0.00	0.00	0.00
MgO	1.54	1.71	1.21	1.61	1.70	1.24	1.11	1.84
CaO	0.03	0.04	0.00	0.02	0.02	0.00	0.00	0.00
BaO	0.37	0.36	0.40	0.29	0.33	0.27	0.22	0.22
Na_2O	0.86	0.88	1.03	0.82	0.87	0.70	1.00	0.46
K_2O	8.99	9.32	9.30	9.05	9.57	10.70	10.44	11.10
total	90.88	91.32	92.22	91.96	91.43	94.05	95.90	97.96

structural formulae based on 22 oxygen

	159-17-3	159-17-4	159-17-5	159-17-6	159-17-7	156-5-1	156-5-2	156-5-3
Si	6.28	6.29	6.23	6.42	6.41	6.11	6.11	6.39
Al^{iv}	1.72	1.71	1.77	1.58	1.59	1.89	1.89	1.61
Al^{vi}	3.57	3.67	3.64	3.53	3.50	3.62	3.65	3.49
Ti	0.04	0.04	0.03	0.04	0.03	0.03	0.03	0.03
Cr	0.01	0.01	0.01	0.00	0.01	0.02	0.01	0.01
Fe	0.15	0.14	0.12	0.16	0.13	0.14	0.14	0.15
Mn	0.00	0.00	0.01	0.00	0.01	0.00	0.00	0.00
Mg	0.32	0.35	0.25	0.33	0.35	0.25	0.22	0.36
Ca	0.00	0.01	0.00	0.00	0.00	0.00	0.00	0.00
Ba	0.02	0.02	0.02	0.01	0.02	0.01	0.01	0.01
Na	0.23	0.24	0.27	0.22	0.23	0.18	0.26	0.12
K	1.60	1.65	1.63	1.58	1.69	1.85	1.77	1.84

MUSCOVITE - Sericite-Chlorite Schist

	159-24-1	159-24-2	159-24-3	159-24-4	159-24-5
SiO_2	45.52	46.93	46.49	47.00	46.83
TiO_2	35.67	34.70	36.50	34.26	34.73
Al_2O_3	0.30	0.32	0.36	0.28	0.48
Cr_2O_3	0.00	0.00	0.00	0.00	0.00
FeO	1.90	2.30	1.90	2.00	2.60
MnO	0.11	0.15	0.11	0.07	0.18
MgO	0.54	0.68	0.46	0.86	0.75
CaO	0.00	0.00	0.00	0.00	0.00
BaO	1.50	0.98	0.87	1.00	1.00
Na_2O	1.00	1.10	1.10	0.62	1.10
K_2O	9.90	10.04	10.29	9.90	10.25
total	96.52	97.37	98.09	96.19	97.93

structural formulae based on 22 oxygen

Si	6.07	6.19	6.07	6.25	6.16
Al^{iv}	1.93	1.81	1.93	1.75	1.84
Al^{vi}	3.87	3.58	3.69	3.62	3.54
Ti	0.03	0.03	0.04	0.03	0.05
Cr	0.01	0.02	0.01	0.01	0.02
Fe	0.21	0.26	0.21	0.23	0.29
Mn	0.00	0.00	0.00	0.00	0.00
Mg	0.11	0.13	0.09	0.17	0.15
Ca	0.00	0.00	0.00	0.00	0.00
Ba	0.08	0.05	0.04	0.05	0.05
Na	0.26	0.30	0.28	0.16	0.28
K	1.69	1.69	1.71	1.69	1.72

MUSCOVITE - Sericite-Chlorite Schist

	159-19-6	159-19-7	159-20-1	159-20-2	159-20-3	159-20-4	159-20-5	159-20-6	159-20-7
SiO_2	45.16	47.71	46.59	45.70	46.13	44.73	45.72	47.93	46.50
TiO_2	0.41	0.30	0.34	0.24	0.23	0.20	0.21	0.26	0.22
Al_2O_3	34.73	32.38	34.81	36.03	36.71	36.02	35.50	36.11	35.02
Cr_2O_3	0.00	0.00	0.12	0.06	0.14	0.17	0.05	0.04	0.11
FeO	2.06	3.23	2.50	2.10	1.70	2.00	1.70	2.40	2.20
MnO	0.52	1.25	0.00	0.00	0.00	0.00	0.00	0.00	0.08
MgO	0.00	0.09	0.41	0.46	0.38	0.32	0.44	0.47	0.41
CaO	0.00	0.00	0.00	0.00	0.00	0.00	0.00	0.00	0.00
BaO	0.84	0.46	1.10	0.69	0.85	1.00	0.86	0.72	0.80
Na_2O	0.84	0.78	1.00	0.89	1.00	1.00	0.83	0.94	0.86
K_2O	9.49	9.91	9.80	9.80	9.40	10.27	10.23	10.04	10.31
total	96.45	95.78	96.82	96.02	96.72	95.88	95.61	98.92	96.52

structural formulae based on 22 oxygen

	159-19-6	159-19-7	159-20-1	159-20-2	159-20-3	159-20-4	159-20-5	159-20-6	159-20-7
Si	6.13	6.36	6.18	6.08	6.07	6.01	6.12	6.19	6.18
Al^{iv}	1.87	1.64	1.82	1.92	1.93	1.99	1.88	1.81	1.82
Al^{vi}	3.69	3.45	3.62	3.72	3.77	3.71	3.72	3.68	3.66
Ti	0.04	0.03	0.03	0.02	0.02	0.02	0.02	0.03	0.02
Cr	0.00	0.01	0.01	0.01	0.01	0.02	0.01	0.00	0.01
Fe	0.23	0.36	0.28	0.24	0.19	0.23	0.20	0.26	0.25
Mn	0.00	0.01	0.00	0.00	0.00	0.00	0.00	0.00	0.01
Mg	0.11	0.25	0.08	0.09	0.07	0.06	0.09	0.09	0.08
Ca	0.00	0.00	0.00	0.00	0.00	0.00	0.00	0.00	0.00
Ba	0.02	0.00	0.06	0.04	0.04	0.05	0.05	0.04	0.04
Na	0.22	0.20	0.27	0.23	0.27	0.28	0.22	0.24	0.22
K	1.64	1.69	1.66	1.67	1.59	1.76	1.75	1.65	1.75

MUSCOVITE - Sericite-Chlorite Schist

	K2-9-1-1	K2-9-1-2	K2-9-1-3	K2-9-1-4	K2-9-1-5	159-19-1	159-19-2	159-19-3	159-19-4	159-19-5
SiO_2	45.52	45.62	46.54	44.51	47.27	46.59	45.86	45.23	46.31	46.12
TiO_2	0.19	0.25	0.20	0.28	0.35	0.22	0.24	0.24	0.27	0.25
Al_2O_3	35.45	35.68	34.77	34.55	34.92	35.33	36.06	36.03	36.39	35.96
Cr_2O_3	1.78	2.08	2.03	3.08	2.11	0.00	0.14	0.04	0.01	0.02
FeO	0.18	0.17	0.13	0.11	0.11	1.85	1.89	1.88	2.11	2.24
MnO	0.32	0.34	0.48	0.42	0.45	0.45	0.36	0.36	0.45	0.49
MgO	0.00	0.00	0.00	0.00	0.00	0.00	0.09	0.04	0.02	0.04
CaO	0.00	0.00	0.00	0.00	0.00	0.00	0.00	0.00	0.00	0.00
BaO	1.03	0.98	0.80	1.20	0.80	0.88	0.63	0.72	0.74	0.60
Na_2O	0.73	0.71	0.54	3.08	0.66	0.91	0.91	0.96	0.88	1.07
K_2O	9.55	9.54	9.65	9.57	9.66	9.98	10.11	9.96	9.59	9.90
total	94.85	95.38	95.14	94.54	96.23	95.78	95.56	94.89	93.76	95.78

structural formulae based on 22 oxygen

	K2-9-1-1	K2-9-1-2	K2-9-1-3	K2-9-1-4	K2-9-1-5	159-19-1	159-19-2	159-19-3	159-19-4	159-19-5
Si	6.13	6.11	6.23	5.99	6.25	6.18	6.09	6.06	6.10	6.10
Al^{iv}	1.87	1.89	1.77	2.01	1.75	1.82	1.91	1.94	1.90	1.90
Al^{vi}	3.75	3.74	3.71	3.48	3.70	3.71	3.73	3.74	3.74	3.70
Ti	0.02	0.03	0.02	0.03	0.02	0.02	0.02	0.02	0.03	0.02
Cr	0.02	0.02	0.01	0.01	0.01	0.00	0.01	0.00	0.00	0.00
Fe	0.20	0.23	0.23	0.35	0.23	0.21	0.21	0.21	0.23	0.25
Mn	0.00	0.00	0.00	0.00	0.00	0.00	0.00	0.00	0.00	0.00
Mg	0.06	0.07	0.10	0.08	0.09	0.09	0.04	0.07	0.09	0.10
Ca	0.00	0.00	0.00	0.00	0.00	0.00	0.00	0.00	0.00	0.00
Ba	0.06	0.05	0.04	0.06	0.04	0.05	0.03	0.04	0.03	0.04
Na	0.19	0.18	0.14	0.80	0.17	0.23	0.23	0.25	0.22	0.27
K	1.64	1.63	1.65	1.64	1.63	1.69	1.71	1.70	1.61	1.67

MUSCOVITE - Sericite-Chlorite Schist

	159-28-1	159-28-2	159-28-3	159-28-4	159-28-5	159-28-6	159-28-7	159-28-8	159-28-9
SiO_2	44.30	44.79	44.30	46.01	47.45	46.12	46.78	47.39	46.52
TiO_2	0.40	0.38	0.34	0.40	0.43	0.63	0.44	0.38	0.39
Al_2O_3	33.47	34.04	32.94	34.02	32.07	32.03	33.88	33.50	36.02
Cr_2O_3	0.30	0.11	0.14	0.00	0.00	0.02	0.03	0.04	0.00
FeO	1.38	1.89	1.30	2.06	2.03	1.82	1.59	2.38	1.42
MnO	0.00	0.00	0.00	0.01	0.03	0.04	0.02	0.02	0.04
MgO	1.05	1.20	1.09	1.52	1.66	1.15	1.13	1.41	1.31
CaO	0.00	0.00	0.00	0.00	0.00	0.00	0.00	0.00	0.00
BaO	1.09	0.71	1.05	0.80	0.71	1.27	1.20	0.98	1.32
Na_2O	0.63	0.71	0.64	0.75	0.61	0.73	0.72	0.88	0.69
K_2O	8.86	9.85	9.79	10.09	10.09	10.02	10.30	9.84	9.29
total	92.09	92.63	92.72	93.76	95.09	95.74	97.38	96.85	97.03

structural formulae based on 22 oxygen

Si	6.18	6.09	6.06	6.10	6.10	6.13	6.36	6.18	6.09
Al^{iv}	1.82	1.91	1.94	1.90	1.90	1.87	1.64	1.73	1.89
Al^{vi}	3.71	3.73	3.74	3.74	3.70	3.69	3.45	3.50	3.68
Ti	0.04	0.04	0.04	0.04	0.04	0.06	0.04	0.04	0.04
Cr	0.03	0.01	0.02	0.00	0.00	0.00	0.00	0.00	0.00
Fe	0.16	0.22	0.15	0.24	0.24	0.20	0.18	0.26	0.16
Mn	0.00	0.00	0.00	0.00	0.00	0.00	0.00	0.00	0.00
Mg	0.22	0.25	0.22	0.31	0.33	0.23	0.22	0.26	0.26
Ca	0.00	0.00	0.00	0.00	0.00	0.00	0.00	0.00	0.00
Ba	0.06	0.04	0.06	0.04	0.04	0.07	0.06	0.05	0.07
Na	0.17	0.19	0.17	0.20	0.19	0.18	0.19	0.23	0.18
K	1.56	1.74	1.72	1.76	1.73	1.72	1.73	1.66	1.56

MUSCOVITE - Chlorite-Magnetite Schist

	595-1	595-2	595-3	595-4	595-5	595-6	595-7	596-1	596-2	596-3	596-4	596-5	596-6
SiO_2	46.17	46.12	47.59	44.67	45.79	44.64	46.24	45.67	44.55	46.45	45.68	44.12	43.71
TiO_2	0.49	0.46	0.43	0.42	0.14	0.52	0.39	0.13	0.13	0.14	0.19	0.11	0.19
Al_2O_3	35.29	33.08	33.06	33.97	34.82	31.27	30.83	35.89	36.31	35.66	36.53	34.98	36.07
Cr_2O_3	[illegible]20	0.33	0.42	0.33	0.43	2.56	2.45	0.05	0.06	0.06	0.00	0.04	0.04
FeO	1.70	1.52	1.68	1.67	1.18	2.09	1.59	2.75	2.02	2.82	2.42	3.25	3.22
MnO	0.00	0.00	0.00	0.00	0.00	0.00	0.00	0.00	0.00	0.00	0.00	0.00	0.00
MgO	1.20	1.85	1.48	0.92	0.92	1.55	1.54	0.51	0.54	0.52	0.55	0.39	0.49
CaO	0.00	0.00	0.00	0.00	0.00	0.00	0.00	0.00	0.00	0.00	0.00	0.00	0.00
BaO	0.96	0.93	0.92	0.74	0.34	0.66	0.66	0.80	0.83	0.65	0.69	0.69	0.95
Na_2O	0.74	0.59	0.59	0.59	0.89	0.36	0.60	1.13	1.11	1.29	1.29	0.98	0.93
K_2O	9.23	9.98	9.82	10.32	9.60	9.59	9.68	9.00	9.18	9.24	9.20	9.40	9.47
total	96.48	94.99	95.99	93.64	94.11	93.25	94.00	95.93	94.73	96.84	96.55	93.95	95.07

structural formulae based on 22 oxygen

	595-1	595-2	595-3	595-4	595-5	595-6	595-7	596-1	596-2	596-3	596-4	596-5	596-6
Si	6.08	6.22	6.32	6.12	6.17	6.17	6.31	6.08	6.13	6.04	6.04	5.93	6.22
Al^{iv}	1.92	1.78	1.68	1.88	1.83	1.83	1.69	1.92	1.87	1.96	1.96	2.07	1.78
Al^{vi}	3.56	3.48	3.50	3.60	3.70	3.26	3.28	3.71	3.67	3.73	3.68	3.69	3.54
Ti	0.05	0.05	0.04	0.04	0.01	0.05	0.26	0.01	0.01	0.00	0.00	0.00	0.01
Cr	0.12	0.04	0.04	0.04	0.05	0.28	0.04	0.01	0.01	0.02	0.01	0.02	0.01
Fe	0.19	0.17	0.19	0.19	0.13	0.24	0.18	0.31	0.31	0.27	0.37	0.37	0.46
Mn	0.00	0.00	0.00	0.00	0.00	0.00	0.00	0.00	0.00	0.00	0.00	0.00	0.00
Mg	0.24	0.37	0.29	0.19	0.18	0.32	0.31	0.10	0.10	0.11	0.08	0.10	0.16
Ca	0.00	0.00	0.00	0.00	0.00	0.00	0.00	0.00	0.00	0.00	0.00	0.00	0.00
Ba	0.04	0.04	0.04	0.04	0.02	0.04	0.04	0.04	0.03	0.04	0.04	0.05	0.03
Na	0.19	0.15	0.15	0.16	0.23	0.10	0.16	0.29	0.33	0.33	0.26	0.24	0.23
K	1.55	1.72	1.66	1.80	1.65	1.69	1.69	1.53	1.56	1.55	1.64	1.64	1.64

MUSCOVITE - Chlorite-Magnetite Schist

	159-44-1	159-44-2	159-44-3	159-44-4	159-44-5	159-44-6
SiO_2	42.30	44.13	44.37	44.75	44.50	43.32
TiO_2	0.24	0.25	0.22	0.22	0.25	0.35
Al_2O_3	35.35	35.09	35.38	36.29	36.18	36.10
Cr_2O_3	0.04	0.07	0.04	0.05	0.01	0.11
FeO	1.55	1.19	1.48	1.55	1.75	1.86
MnO	0.11	0.02	0.00	0.05	0.08	0.09
MgO	0.34	0.58	0.35	0.38	0.39	0.48
CaO	0.00	0.00	0.00	0.00	0.00	0.00
BaO	0.77	0.74	0.82	0.88	0.87	1.42
Na_2O	0.86	0.90	0.93	0.89	1.09	1.07
K_2O	9.98	9.69	9.80	9.93	9.89	9.65
total	91.57	93.42	92.42	94.99	95.04	94.47

structural formulae based on 22 oxygen

Si	1.93	6.05	6.07	6.02	6.00	5.91
Al^{iv}	2.07	1.95	1.93	1.98	2.00	2.09
Al^{vi}	3.77	3.71	3.77	3.78	3.75	3.72
Ti	0.03	0.03	0.02	0.02	0.03	0.04
Cr	0.00	0.01	0.00	0.01	0.00	0.01
Fe	0.18	0.22	0.17	0.17	0.20	0.21
Mn	0.01	0.00	0.00	0.01	0.01	0.01
Mg	0.07	0.12	0.07	0.08	0.09	0.10
Ca	0.00	0.00	0.00	0.00	0.00	0.00
Ba	0.04	0.04	0.04	0.05	0.05	0.08
Na	0.23	0.24	0.25	0.23	0.28	0.28
K	1.79	1.69	1.71	1.70	1.70	1.68

Silicified Dolomite

	159-29-1	159-29-2	159-29-3	159-29-4	159-29-5	159-39-1	159-39-2	159-50-1	60-7-1	60-7-2	60-7-3
SiO_2	44.54	47.34	47.90	48.11	45.87	47.53	47.87	46.89	51.08	51.04	49.13
TiO_2	0.54	0.48	0.40	0.41	0.39	0.45	0.41	0.46	0.18	0.16	0.18
Al_2O_3	28.64	33.68	33.79	32.89	34.19	34.65	36.63	34.73	32.38	33.30	35.19
Cr_2O_3	0.00	0.07	0.05	0.05	0.08	0.01	0.07	0.06	0.01	0.00	0.07
FeO	3.37	0.80	0.87	0.75	0.19	1.00	0.99	0.44	0.59	0.43	0.39
MnO	0.00	0.00	0.09	0.01	0.02	0.00	0.00	0.00	0.05	0.00	0.00
MgO	4.48	1.92	1.55	1.91	1.83	1.40	1.00	1.90	2.40	2.00	1.50
CaO	0.00	0.00	0.00	0.00	0.81	0.00	0.02	0.00	0.00	0.00	0.00
BaO	0.40	0.44	0.50	0.47	0.52	0.70	0.66	0.44	0.54	0.54	0.49
Na_2O	0.95	0.80	1.02	0.71	0.96	0.69	0.85	0.75	0.65	0.72	0.83
K_2O	9.85	9.97	9.78	10.09	9.57	10.67	10.02	10.55	9.70	9.10	9.70
total	92.83	95.57	96.01	95.47	95.76	97.20	98.60	96.27	97.62	97.41	97.50

strutural formulae based on 22 oxygen

Si	6.23	6.28	6.32	6.38	6.16	6.23	6.15	6.18	6.58	6.55	6.34
Al^{iv}	1.77	1.72	1.68	1.62	1.84	1.77	1.85	1.82	1.42	1.45	1.66
Al^{vi}	2.94	3.54	3.57	3.52	3.57	3.59	3.70	3.58	3.49	3.59	3.68
Ti	0.06	0.05	0.04	0.04	0.04	0.04	0.04	0.04	0.02	0.02	0.02
Cr	0.00	0.01	0.01	0.01	0.01	0.00	0.01	0.01	0.00	0.00	0.01
Fe	0.39	0.09	0.10	0.08	0.02	0.12	0.11	0.05	0.06	0.05	0.04
Mn	0.00	0.00	0.01	0.00	0.00	0.00	0.00	0.00	0.01	0.00	0.00
Mg	0.93	0.38	0.30	0.38	0.37	0.28	0.21	0.38	0.46	0.40	0.29
Ca	0.00	0.00	0.00	0.00	0.00	0.00	0.00	0.00	0.00	0.00	0.00
Ba	0.02	0.02	0.03	0.02	0.03	0.04	0.03	0.02	0.03	0.03	0.02
Na	0.26	0.21	0.26	0.18	0.25	0.18	0.21	0.19	0.16	0.18	0.21
K	9.85	9.97	9.78	10.09	9.57	1.78	1.64	1.77	1.60	1.50	1.60

MUSCOVITE - Graphitic Pelite

	159-37-1	159-37-1	60-12-1	K2-14-1	K2-14-2	K2-14-3	K2-14-4	60-15-1	60-15-2	60-15-3
SiO_2	46.32	45.59	46.41	47.71	47.04	47.15	48.06	49.60	46.89	46.40
TiO_2	0.40	0.36	0.21	0.16	0.42	0.40	0.38	0.27	0.33	0.32
Al_2O_3	33.57	35.38	32.68	35.37	34.93	34.48	34.26	33.18	35.49	35.89
Cr_2O_3	1.76	1.79	1.10	0.96	1.24	1.41	1.32	1.38	1.15	1.64
FeO	0.19	0.07	0.08	0.04	0.09	0.05	0.11	0.05	0.07	0.15
MgO	0.08	0.05	0.00	0.82	0.93	1.04	0.98	1.15	1.01	1.08
MnO	3.11	0.86	0.66	0.00	0.00	0.00	0.00	0.00	0.00	0.00
CaO	0.05	0.05	0.41	0.00	0.00	0.00	0.00	0.00	0.00	0.00
BaO	0.56	0.77	0.73	0.36	0.86	0.51	0.61	0.47	0.89	0.64
Na_2O	0.20	0.79	2.10	0.64	0.51	0.80	0.64	0.39	0.54	0.50
K_2O	9.08	9.57	9.10	10.16	10.19	10.23	10.74	7.05	9.90	9.61
total	95.30	95.28	91.82	96.22	96.21	96.09	97.11	93.55	96.28	96.24

structural formulae based on 22 oxygen

Si	5.17	6.10	6.32	6.27	6.24	6.24	6.31	1.44	1.81	1.88
Al^{iv}	1.83	1.90	1.68	1.73	1.76	1.76	1.69	3.74	3.71	3.70
Al^{vi}	3.44	3.68	3.56	3.74	3.67	3.63	3.61	0.03	0.03	0.03
Ti	0.04	0.04	0.02	0.02	0.04	0.04	0.04	0.01	0.01	0.02
Cr	0.02	0.01	0.01	0.00	0.01	0.01	0.01	0.15	0.13	0.18
Fe	0.20	0.20	0.13	0.11	0.14	0.16	0.14	0.00	0.00	0.00
Mn	0.01	0.01	0.00	0.00	0.00	0.00	0.00	0.23	0.20	0.21
Mg	0.62	0.17	0.13	0.16	0.18	0.21	0.19	0.00	0.00	0.00
Ca	0.01	0.01	0.06	0.00	0.00	0.00	0.00	0.02	0.04	0.03
Ba	0.03	0.04	0.04	0.02	0.04	0.02	0.03	0.10	0.14	0.13
Na	0.05	0.20	0.58	0.16	0.13	0.21	0.16	1.19	1.67	1.62
K	1.54	1.63	1.59	1.82	1.83	1.73	1.80			

MUSCOVITE – Lower Ore Zone

	67-14-1	67-14-2	67-14-3	67-14-4	60-24-1	60-24-2	159-61-1	159-61-2	159-61-3	159-61-4	159-61-5
SiO_2	46.18	46.91	48.69	48.68	45.76	48.04	44.29	44.09	45.71	45.48	46.10
TiO_2	0.50	0.28	0.32	0.42	0.52	0.40	0.47	0.59	0.62	0.38	0.59
Al_2O_3	35.84	36.06	32.82	33.65	33.43	34.83	34.24	33.04	34.46	33.17	33.86
Cr_2O_3	0.09	0.13	0.20	0.20	1.98	2.07	1.72	1.88	1.34	1.74	1.76
FeO	1.08	1.18	1.19	1.36	0.08	0.00	0.11	0.19	0.11	0.04	0.09
MnO	0.00	0.00	0.00	0.00	0.00	0.00	0.07	0.02	0.02	0.07	0.02
MgO	0.86	1.15	1.36	1.38	1.68	2.05	1.46	1.53	1.51	1.39	1.63
CaO	0.14	0.00	0.00	0.00	0.00	0.00	0.12	0.00	0.00	0.00	0.00
BaO	0.72	0.30	0.45	0.57	0.44	0.41	0.52	0.61	0.66	0.43	0.54
Na_2O	0.99	0.60	0.32	0.36	0.57	0.49	0.72	0.54	0.48	0.70	0.60
K_2O	7.71	10.29	10.04	9.98	10.04	10.20	9.73	10.07	10.45	10.19	10.11
total	94.24	96.89	95.38	96.58	94.52	98.50	93.45	92.55	95.37	93.59	95.29

structural formulae based on 22 oxygen

	67-14-1	67-14-2	67-14-3	67-14-4	60-24-1	60-24-2	159-61-1	159-61-2	159-61-3	159-61-4	159-61-5
Si	6.16	6.14	6.45	6.38	6.19	6.21	6.06	6.11	6.13	6.21	6.18
Al^{iv}	1.84	1.86	1.55	1.62	1.81	1.79	1.94	1.89	1.87	1.79	1.82
Al^{vi}	3.79	3.70	3.58	3.58	3.51	3.52	3.58	3.51	3.57	3.55	3.92
Ti	0.05	0.03	0.03	0.04	0.05	0.04	0.05	0.06	0.06	0.04	0.06
Cr	0.01	0.01	0.02	0.02	0.01	0.00	0.01	0.02	0.01	0.00	0.01
Fe	0.12	0.13	0.13	0.15	0.22	0.22	0.20	0.22	0.15	0.20	0.20
Mn	0.00	0.00	0.00	0.00	0.00	0.00	0.01	0.00	0.00	0.01	0.00
Mg	0.17	0.22	0.27	0.27	0.34	0.04	0.30	0.32	0.30	0.28	0.33
Ca	0.02	0.00	0.00	0.00	0.00	0.00	0.02	0.00	0.00	0.00	0.00
Ba	0.03	0.01	0.02	0.02	0.02	0.02	0.02	0.03	0.03	0.02	0.02
Na	0.26	0.15	0.08	0.09	0.15	0.12	0.19	0.15	0.12	0.19	0.16
K	1.31	1.72	1.70	1.67	1.73	1.68	1.70	1.78	1.79	1.77	1.73

MUSCOVITE - Banded Chlorite-Sericite-Garnet Schist

	67-19-1	67-19-2	67-19-3	67-19-4	67-19-5	60-29-1	60-29-2	60-29-3	60-29-4	74-13-1	74-13-2	159-71-1	159-71-2
SiO_2	47.62	46.19	46.94	48.25	46.56	46.99	47.23	47.63	46.77	47.3[illegible]	47.85	46.47	47.79
TiO_2	0.26	0.31	0.27	0.26	0.25	0.19	0.37	0.29	0.42	0.28	0.29	0.26	0.30
Al_2O_3	35.02	34.82	35.57	35.06	33.15	35.70	35.66	35.30	34.35	35.31	35.29	34.87	35.71
Cr_2O_3	0.00	0.09	0.15	0.13	0.10	0.16	0.16	0.34	0.05	0.20	0.06	0.13	0.08
FeO	1.70	1.60	1.60	2.30	3.30	1.40	1.50	1.70	1.80	3.20	1.80	2.10	1.90
MnO	0.00	0.00	0.02	0.03	0.00	0.00	0.00	0.04	0.00	0.00	0.00	0.00	0.00
MgO	0.53	0.65	0.61	0.61	0.81	0.55	0.64	0.69	0.77	0.86	0.61	0.94	0.79
CaO	0.00	0.00	0.00	0.00	0.00	0.00	0.00	0.00	0.00	0.00	0.00	0.00	0.00
BaO	0.32	0.34	0.33	0.32	0.33	0.24	0.44	0.30	0.30	0.48	0.47	0.37	0.39
Na_2O	0.66	0.45	0.57	0.81	2.00	0.92	0.67	0.57	0.59	0.70	0.57	0.71	0.70
K_2O	10.11	10.39	10.27	10.18	10.05	10.55	10.14	10.08	10.62	10.11	9.80	9.90	10.21
total	96.30	94.89	95.45	97.97	96.64	96.73	96.90	97.02	95.75	98.46	96.86	95.88	97.93

structural formulae based on 22 oxygen

	67-19-1	67-19-2	67-19-3	67-19-4	67-19-5	60-29-1	60-29-2	60-29-3	60-29-4	74-13-1	74-13-2	159-71-1	159-71-2
Si	6.19	6.19	6.19	6.27	6.22	6.18	6.19	6.23	6.23	6.16	6.26	6.18	6.29
Al^{iv}	1.81	1.81	1.81	1.73	1.78	1.82	1.81	1.77	1.77	1.84	1.74	1.82	1.71
Al^{vi}	3.70	3.70	3.72	3.64	3.44	3.71	3.70	3.67	3.62	3.58	3 71	3.64	3.61
Ti	0.03	0.03	0.03	0.03	0.03	0.02	0.04	0.03	0.04	0.03	0.03	0.03	0.03
Cr	0.01	0.01	0.02	0.01	0.01	0.02	0.02	0.04	0.01	0.02	0.01	0.01	0.01
Fe	0.19	0.19	0.18	0.25	0.37	0.16	0.17	0.19	0.21	0.35	0.21	0.17	0.16
Mn	0.00	0.00	0.00	0.00	0.00	0.00	0.00	0.00	0.00	0.00	0.00	0.00	0.00
Mg	0.13	0.13	0.12	0.12	0.16	0.11	0.13	0.13	0.15	0.17	0.12	0.19	0.18
Ca	0.00	0.00	0.00	0.00	0.00	0.00	0.00	0.00	0.00	0.00	0.00	0.00	0.00
Ba	0.02	0.02	0.02	0.02	0.02	0.01	0.02	0.02	0.02	0.02	0.02	0.02	0.04
Na	0.12	0.12	0.15	0.20	0.54	0.23	0.17	0.14	0.15	0.18	0.14	0.18	0.23
K	1.78	1.78	1.73	1.69	1.71	1.77	1.70	1.68	1.80	1.68	1.65	1.69	1.73

GARNET - Banded Chlorite-Sericite-Garnet Schist

	60-29-1-1 core	60-29-1-2 ---	60-29-1-3 ---	60-29-1-4 rim
SiO_2	37.44	36.98	36.67	37.29
Al_2O_3	21.04	21.26	21.27	20.78
FeO	33.23	33.65	32.43	34.17
MnO	0.00	0.09	0.06	0.13
MgO	1.23	0.99	0.89	0.84
CaO	6.75	6.77	7.34	6.54
	structural formulae based on 24 oxygen			
Si	6.03	5.98	5.97	6.04
Al	4.00	4.05	4.08	3.96
Fe^{2+}	4.48	4.55	4.42	4.63
Mn	0.00	0.01	0.01	0.02
Mg	0.30	0.24	0.22	0.20
Ca	1.17	1.17	1.28	1.13
endmember proportions				
Al	75.40	76.17	74.58	77.35
Py	4.98	3.99	3.65	3.39
Gr	19.62	19.63	21.63	18.96
Sp	0.00	0.21	0.14	0.30

	60-29-2-1 core	60-29-2-2 ---	60-29-2-3 ---	60-29-2-4 rim
SiO_2	36.96	36.43	36.69	36.97
Al_2O_3	21.04	21.00	20.98	21.11
FeO	32.82	32.59	33.06	34.09
MnO	1.29	2.41	1.20	0.11
MgO	0.55	0.42	0.47	0.74
CaO	6.22	6.19	6.96	6.46
	structural formulae based on 24 oxygen			
Si	6.03	5.97	5.98	6.00
Al	4.04	4.05	4.03	4.04
Fe^{2+}	4.48	4.46	4.50	4.63
Mn	0.18	0.33	0.17	0.02
Mg	0.13	0.10	0.11	0.18
Ca	1.09	1.09	1.22	1.12
endmember proportions				
Al	76.19	74.56	75.09	77.84
Py	2.28	1.71	1.90	3.01
Gr	18.50	18.14	20.25	18.90
Sp	3.03	5.58	2.81	0.25

GARNET - Banded Chlorite-Sericite-Garnet Schist

	67-19-2-1 rim	67-19-2-2 ---	67-19-2-3 ---	67-19-2-4 rim	67-19-2-5 rim	67-19-2-6 core
SiO_2	37.17	36.76	36.89	37.34	37.15	36.63
Al_2O_3	21.14	21.11	20.43	21.16	20.80	20.81
FeO	34.13	36.76	31.64	32.13	33.95	33.54
MnO	0.13	1.86	2.96	2.04	0.23	0.30
MgO	0.92	0.69	0.59	0.72	0.88	0.91
CaO	6.31	6.20	7.02	6.59	6.37	6.79
structural formulae based on 24 oxygen						
Si	6.01	5.85	6.01	6.02	6.03	5.98
Al	4.03	3.96	3.92	4.02	3.98	4.00
Fe^{2+}	4.61	4.89	4.31	4.33	4.61	4.58
Mn	0.02	0.25	0.41	0.28	0.03	0.04
Mg	0.22	0.16	0.14	0.17	0.21	0.22
Ca	0.09	1.06	1.23	1.14	1.11	1.19
endmember proportions						
Al	77.59	76.88	70.81	73.15	77.31	75.94
Py	3.73	2.57	2.35	2.92	3.57	3.67
Gr	18.38	16.61	20.13	19.22	18.58	19.70
Sp	0.30	3.94	6.71	4.71	0.53	0.69

CHLORITOID - Banded Sericite-Chlorite Schist

	k2-9-1-1	k2-9-1-2	k2-9-1-3	k2-9-1-4	k2-9-1-5	k2-9-1-6	159-20-1	159-20-2	159-20-3
SiO_2	23.98	24.79	24.34	25.11	24.30	24.31	23.42	23.07	24.57
TiO_2	0.02	0.02	0.00	0.03	0.02	0.05	0.01	0.03	0.12
Al_2O_3	39.25	40.13	39.64	38.03	39.55	39.6	40.04	39.33	40.39
Cr_2O_3	0.04	0.11	0.15	0.25	0.10	0.1	0.07	0.40	0.14
FeO	26.10	27.04	27.99	26.13	27.06	27.39	25.82	26.84	26.36
MnO	0.00	0.04	0.03	0.03	0.00	0.01	0.15	0.11	0.19
MgO	0.91	0.84	0.94	0.91	0.90	0.99	0.89	0.71	0.99
CaO	0.00	0.00	0.04	0.00	0.01	0.01	0.03	0.04	0.02
Na_2O	0.00	0.00	0.00	0.00	0.00	0.00	0.00	0.01	0.03
K_2O	0.01	0.01	0.03	0.01	0.00	0.00	0.00	0.00	0.00
total	90.30	92.97	93.19	90.52	91.94	92.58	90.44	90.54	92.79

sturctural formulae based on 14 oxgen

Si	2.05	2.07	2.04	2.15	2.05	2.00	2.00	1.99	2.05
Al^{iv}	2.95	2.93	2.96	2.85	2.95	2.90	3.00	3.01	2.95
Al^{vi}	1.02	1.01	0.95	0.98	0.99	0.97	1.04	0.98	1.02
Ti	0.00	0.00	0.00	0.00	0.00	0.00	0.00	0.00	0.01
Cr	0.00	0.01	0.01	0.02	0.01	0.01	0.00	0.03	0.01
Fe	1.87	1.88	1.96	1.87	1.91	1.93	1.85	1.93	1.84
Mn	0.00	0.00	0.00	0.00	0.00	0.00	0.01	0.01	0.01
Mg	0.07	0.06	0.07	0.07	0.06	0.07	0.06	0.05	0.07
Ca	0.00	0.00	0.00	0.00	0.00	0.00	0.00	0.00	0.00
Na	0.00	0.00	0.00	0.00	0.00	0.00	0.00	0.00	0.00
K	0.00	0.00	0.00	0.00	0.00	0.00	0.00	0.00	0.

CHLORITOID - Banded Chlorite-Sericite-Garnet Schist

	LaTour (1980)	74-13-1	74-13-2	74-13-3
SiO_2	24.85	23.39	23.69	24.66
TiO_2	0.00	0.02	0.00	0.00
Al_2O_3	40.62	39.38	39.60	40.11
Cr_2O_3	---	0.11	0.11	0.07
FeO	27.02	25.02	26.18	26.31
MnO	0.71	0.13	0.09	0.09
MgO	0.78	1.15	1.07	1.07
CaO	0.02	0.03	0.04	0.00
Na_2O	0.01	0.00	0.00	0.00
K_2O	0.00	0.01	0.01	0.00
total	94.01	89.25	90.79	92.30

structral formulae based on 14 oxygen

Si	2.04	2.03	2.02	2.07
Al^{iv}	3.00	2.97	2.98	2.93
Al^{vi}	0.94	1.04	1.01	1.02
Ti	0.00	0.00	0.00	0.00
Cr	0.00	0.01	0.01	0.00
Fe	1.86	1.81	1.87	1.84
Mn	0.05	0.01	0.01	0.01
Mg	0.10	0.08	0.08	0.08
Ca	0.00	0.00	0.00	0.00
Na	0.00	0.00	0.00	0.00
K	0.00	0.00	0.00	0.00

TOURMALINE - Veined FDCSBQ Schist

	159-13-1	159-13-2	159-13-3	159-13-4	159-13-5	159-17-1
SiO_2	39.79	36.25	36.13	33.79	36.34	35.75
TiO_2	0.37	0.25	0.13	0.49	0.49	0.48
Al_2O_3	30.30	34.83	33.41	33.48	33.88	33.96
Cr_2O_3	0.02	0.04	0.04	0.00	0.00	0.07
FeO	6.04	6.89	6.87	6.75	7.00	6.12
MnO	5.74	6.50	6.63	6.38	6.52	6.38
MgO	0.46	0.42	0.06	0.52	0.50	0.70
CaO	3.84	2.72	2.66	2.81	2.49	2.65
K_2O	.00	0.00	0.00	0.00	0.00	0.92
Na_2O	.00	0.00	0.00	0.00	0.00	0.00
total	86.56	87.91	85.92	84.23	87.24	87.02

TOURMALINE - Banded QBCP Schist

	159-79-1	159-79-2	159-79-3	159-79-4	159-79-5
SiO_2	36.23	36.35	34.63	36.18	36.57
TiO_2	0.64	0.11	0.58	0.36	0.13
Al_2O_3	32.75	33.59	31.72	32.82	33.05
Cr_2O_3	0.02	0.04	0.00	0.00	0.00
FeO	6.77	8.11	7.90	7.94	8.32
MnO	7.43	6.07	6.68	6.71	5.92
MgO	0.93	0.19	0.62	0.46	0.21
CaO	2.59	2.67	3.02	2.93	2.54
K_2O	0.05	.00	0.03	0.00	0.03
Na_2O	0.00	.00	0.00	0.00	0.00
total	86.80	87.43	87.14	85.19	87.40

APPENDIX III

Location of diamond drill holes at Minas III. Numbers are used as prefix to sample numbers used in study.

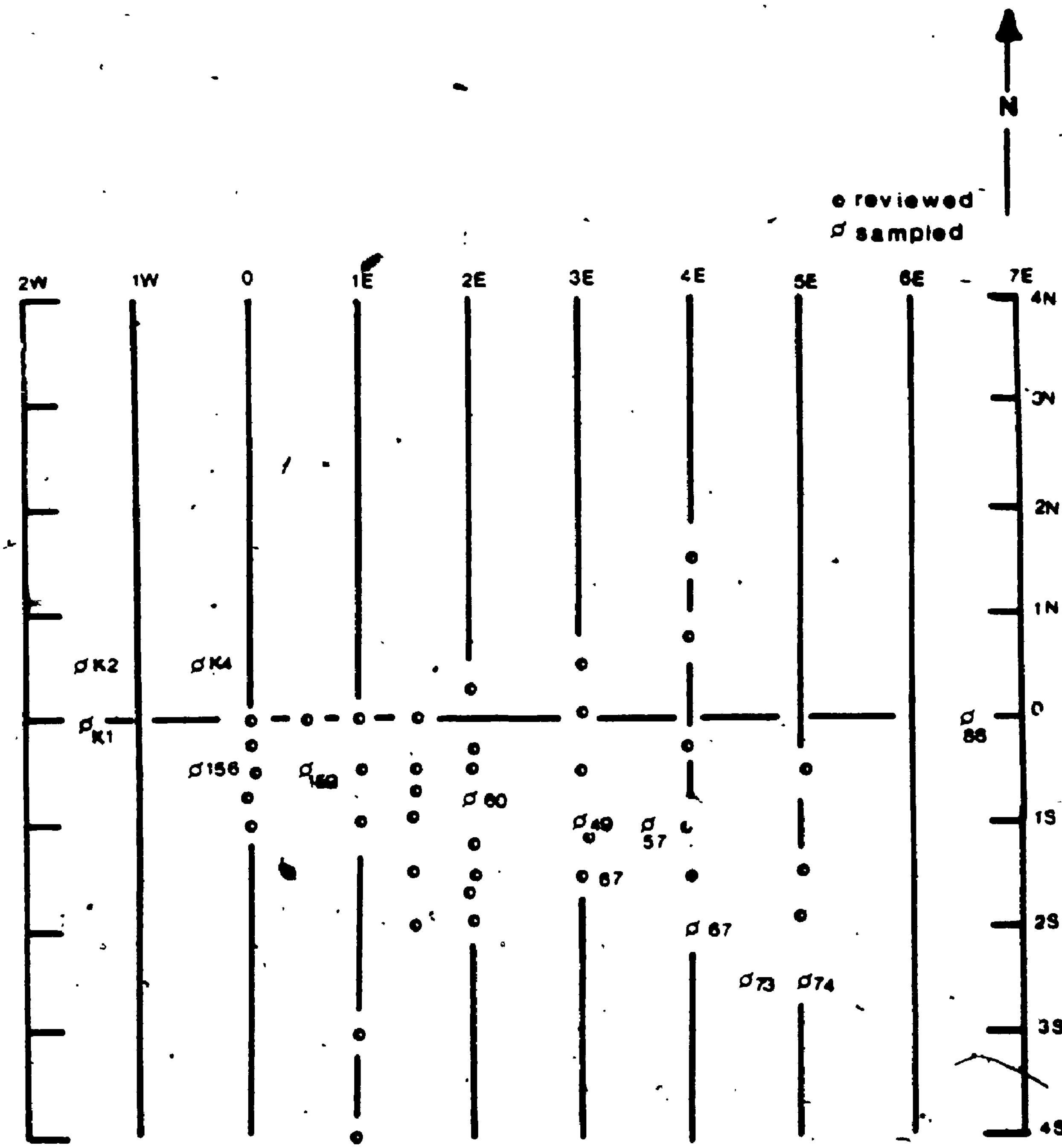

REFERENCES

Almeida, F.F.M., 1968. Evolucao teconica do Contor-Oeste Brasileiro no Proterozoico Superior. Anais Acad. Brasil Cienc., 40, 285-295.

Almeida, F.F.M., Hasuy, Y. and Nevess, B.B.B., 1976. The Upper Precambrian of South America. Bol. Inst. Geol USP, 7, 45-80.

Anhaeusser, C.R., Mason, R., Viljoen, M.J. and Viljoen, R.P., 1969. A reappraisal of some aspects of the Precambrain Shield geology. Bull. Geol. Soc. Amer., 80, 2175-2200.

Apted, M.J. and J.G. Liou, 1983. Phase relations among greenschist, epidote amphibolite and amphibolite in a basaltic system. A.J.S., 283-A, 328-354.

Arndt, N.T., 1976. Thick, layered peridotite-gabbro lava flows in Munro Township, Ontario. C.J.E.S., 14, 2620-2637.

Arndt, N.T., Naldrett, A. J., Pyke, D.R., 1977. Komatiitic and iron-rich tholeiitic lavas of Munro Township, Northeast Ontario. J. Petrol., 18, 319-369.

Atherton, M.P. and R.A. Smith, 1979. Chloritoid-Staurolite assemblages from Barrow's Zones in Central Perthshire, Scotland. Geol. Mag., 116, 469-476.

Beach, A. and W.S. Fyfe, 1972. Fluid Transport and Shear Zones at Scourie, Sutherland: Evidence of Overthrusting? Contr. Mineral. Petrol., 36, 175-180.

Bell, T.H., 1985. Deformation partitioning and porphyroblast rotation in metamorphic rocks: a radical reinterpretation. J. Metamorphic Geol., 3, 109-118.

Carmichael, D.M., 1969. On the mechanism of prograde metamorphic reaction in quartz-bearing pelitic rocks. Contr. Miner. Petrol., 20, 244-267.

Carmichael, D.M., 1984. Mineral equilibria in metabasites andmetagreywackes in the transition from greenschist to amphibolite facies. G.S.A., Abstracts with Programs, 16, 464.

Cathles, L.M., 1986. The gologic solubility of gold from 200-350°C, and its implications for gold-base metal ratios in vein and stratiform deposits. In: Clark, L.A. (ed.). Gold in the Western Shield. CIM Special Volume 38, pp.537.

Chinner, G.A., 1967. Chloritoid, and the isochemical character of Barrow's Zones. J. of Petrol., 8, 269-282.

Clark, M.E., Archibald, N.J. and Hodgson, C.J., 1986. The structural and metamorphic setting of the Victory Gold Mine, Kambalda Western Australia. In: Macdonald, A.J. (editor), Proceedings of Gold '86, an International Symposium on the Geology of Gold. Toronto, 1986, 243-254.

Clarke, F.W., 1924. Data of geochemistry. U.S.G.S. Bull., 770, pp 841.

Danni,J.C.M. and C.C.Ribeira,1978, Caracterizacao estratigrafica da sequencia vulcano-sedimentar de Pilar de Goias e de Guarinos, Goias: Anais XXX Cong. Bras. Geol., Recife,2,582-596.

Davis, J.C., 1976. Statistics andData Analysis in Geology. John Wiley & Sons, Toronto. pp. 550.

Deer, W.A., Howie, R.A. and J. Zussman, 1966. An introduction to the rock-forming minerals. Longman, London, pp. 528

Dempster, T.J., 1985. Garnet zoning and metamorphism of the Barrovian Type Area, Scotland. Contrib. Mineral. Petrol, 89,30-38.

Dreimanis, A., 1962. Quantitative gasometric determination of calcite and dolomite using Chittick apparatus. J. Sed. Petrol., 29, 520-529.

Essene, E.J., 1982. Geologic Thermometry and Barometry. In: Ferry, J.M. (editor). Characterization of Metamorphism through Mineral Equilibria. Reviews in Mineralogy, 10, 153-206.

Ferry, J.M., 1981. Petrology of graphitic sulphide-rich schists from South-Central Maine: an example of desulphidization during prograde regional metamorphism. Amer. Mineral., 66, 908-930.

Ferry, J.M., 1984. A biotite isograd in South-Central Maine, U.S.A.: mineral reactions, fluid transfer, heat transfer. J. Petrol., 25, 871-893.

Ferry, J.M. and Spear, F.S., 1978. Experimental calibration of the partitioning of Fe and Mg between biotite and garnet. contrib. Mineral. Petrol., 66, 113-117.

Floyd, P.A. and Winchester, J.A., 1977. Identification and discrimination of altered and metamorphosed volcanic rocks using immobile elements. Chemical Geology, 21, 291-306.

Floyd, P.A. and Winchester, J.A., 1982. Element mobility associated with meta-shear zones within the Ben Hope Amphibolite Suite, Scotland. Chemical Geology, 39,1-15.

Frey, M., 1978. Progressive low-grade metamorphism of a black shale formation, central Swiss Alps, with special reference to pyrophyllite and margarite bearing assemblages. J. of Petrology., 19, 95-135.

Froese, E., 1977. Oxidation and sulphidation reactions. In: H.J. Greenwood (ed). Short course in application of thermodynamics to petrology and ore deposits. Mineralogical Association of Canada. Volume 2., 84-98.

Fuck,R.A. and O.J.Marini,1981, O Grupo Araxa e unidades homostaxiais. In: Anais do simpios so sobre o craton do Sao Francisco e suas faixas marginais. Sociedade Brasileira de Geologia. pp.118-130.

Fyfe, W.S and R. Kerrich, 1984. Gold: Natural concentration processes. In: R.P. Foster (ed.). Gold '82: The Geology, Geochemistry and Genesis of Gold Deposits. Balkema, Rotterdam, 165-182.

Fyfe, W.S., Price, N.J. and A.B. Thompson, 1978. Fluids in the Earth's Crust. Development in Geochemistry, 1, Elsevier, Amsterdam, pp 383.

Garrels, R.M. and Mackenzie, F.T.,1971. Evolution of Sedimentary Rocks. W.W. Norton Company, Inc., New York, pp 841.

Gibbs,A.K. and C.N.Barron,1983, The Guiana Shield reviewed: Episodes,6,7-14.

Goldman, D.S. and Albee, A.L., 1977. Correlation of Mg/Fe partitioning between garnet and biotite with O^{18}/O^{16} partitioning between quartz and magnetite. A.J.S., 277, 750-767.

Goldsmith, J.R. and Newton, R.C., 1969. P-T-X relations in the system $CaCO_3$-$MgCO_3$ at high temperatures and pressures. A.J.S.,267-A,160-190.

Gole,M.J. and C.Klein,Jr.,1981, Banded iron-formations through much of Precambrian time: Journal of Geology,8,169-183

Goodwin, A.M., 1968. Archaean protocontinental growth and early crustal history of the Canadian Shield. 23rd Int. Geol. Congr., 1, 69-89.

Graham, C.M., Greig, K.M., Sheppard, S.M.F and B. Turi, 1983. Genesis and mobility of the H_2O-CO_2 fluid phase during regional greenschist and epidote amphibolite facies metamorphism: a petrological and stable isotope study in the Scottish Dalradian. J. Geol. Soc. London, 140, 577-599.

Grapes, R.H. and Graham, 1978. The actinolite-hornblende series in metabasites and the so-called miscibility gap: A review. Lithos, 6, 85-97.

Gresens, R.L., 1967, Composition-volume relations of metasomatism: Chemical Geology, 2, 47-65.

Gross, G.A., 1980. A classification of iron formations based on depositional enviroments. Can. Min., 18, 215-222.

Grigoryeva, T.A. and L.S. Sukneva, 1981. Effects of sulphur and of antimony and arsenic sulphides on the solubility of gold. Geochem. Inter., 152-158.

Hall, R.D., 1980. Meamorphism of Sulfide Schist, Limerick Township, Ontario. Unpublished Ph.D. Thesis. The Unveristy of Western Ontario. pp.441.

Hashimoto, M., 1972. Reactions producing actinolite in basic metamorphic rocks. Lithos, 5, 19-31.

Hasui, Y. and F.F.M de Almeida, 1985, The Central Brazil Shield. Reviewed: Episodes, 8, 29-37.

Hawthorne, F.C., 1983. The crystal chemistry of amphiboles. Can. Mineral., 21, 173-480.

Helgeson, H.C., 1968. Hydrothermal transport and deposition of gold. Econ. Geol., 63, 622-635.

Henley, R. W., 1973. Solubility of gold in hydrothermal chloride solutions. Chem. Geol., 11, 73-87.

Hobbs, B.E., Means, W.D. and Williams, P.F., 1976. An Outline of Structural Geology. John Wiley & Sons, Toronto. pp. 571.

Holland, H.D., 1984. The Chemical Evolution of the atmosphere and oceans. Princeton University Press, Princeton, N.J., pp. 582.

Holdaway, M.J., 1972. Thermal Stability of Al-Fe Epidote as a Function of f^{O2} and Fe content. Contr. Mineral and Petrol, 37, 307-340.

Hyndman,D.W.,1985, Petrology of igneous and metamorphic rocks(second edition). McGraw-Hill Book Company, New York.pp.786.

James, H.L., 1954. Sedimentary facies of iron formation. Econ. Geol., 49, 235-293.

Jensen, L.S. and F.F. Langford, 1983. Geology and petrogenesis of the Archean Abitibi Belt in the Kirkland Lake Area, Ontario. Ont. Geol. Sur. Open File Rep. 5455, pp520.

Karabinos, P., 1984. Polymetamorphic garnet zoning from southeastern Vermont. A.J.S., 284, 1008-1025.

Karabinos, P.,1985. Garnet and staurolite producing reactions in a chlorite-chloritoid schist. Contrib. Mineral. Petrol., 90, 262-275.

Kishida, A.,1984. Hydrothermal alteration zoning and gold concentration at the Kerr-Addison Mine, Ontario Canada. Unpublished Ph.D. Thesis. University of Western Ontario.

Kronberg, B.I. and H.W Nesbitt, 1981. Quantification of weathering, soil geochemistry and soil fertility. Journal of Soil Science, 32, 453-459.

Kuyumjian, R.M.,1981, Geologia e mineralizacoes auriferas do "greenstone belt" da Faixa Crixas-Go. Unpublished Masters of Science Thesis. University of Brazilia, Brazilia. pp.72.

Kuyumjian, R.M. and de Araujo Filho, J.O., 1984. Contribuicao a tectonica do greensotne belt do faixa Crixas. Revista Bradileira de Geociencias, 14, 92-96.

Laird, J., 1980. Phase equilibria in mafic Schist from Vermont. J. Petr., 21, 1-37.

Laird,J. and Albee,A.L.,1981, Pressure, temperature, and time indicators in mafic schists: their application to reconstructing the polymetamorphic history of Vermont. American Journal of Science,281,127-175.

LaTour, T.E., Kerrich, R. Hodder, R.W., Barnett, R.L., 1980. Chloritoid stability in very iron-rich altered pillow lavas. Contrib. Mineral. Petrol., 74, 165-173.

Liou, J.G., 1973. Synthesis and stability relations of epidote, $Ca_2Al_2FeSi_3O_12(OH)$. J. Petr., 14, 381-413.

Magalhaes, J.H.G., Castro,J.H.G.,de, and Borges,C.1985, Geologia, prospeccao e pesquisa de ouro no greenstone belt de Crixas--algumas consideracais. In: 1. Encentro Regional do Ouro de Goias, Goiania,Go. Sociedade Brasileira do Geologia Nucleo centro-oest.,26-51.

Maynard, 1983. Geochemistry of Sedimentary Ore Deposits. Springer-Verlag, New York, pp. 305.

McLennan,S.M, Taylor,S.R. and K.A. Eriksson,1983, Geochemistry of Archean shales from the Pilbara Supergroup, Western Australia: Geochemica et Cosmochimica Acta,47,1211-1222.

Moody, J.B., Meyer, D. and Jenkins, 1983. Experimental characteriztion of the greenschist/amphibolite boundary in mafic systems. A.J.S., 283, 48-92

Milling-Stanley, G., 1986. Gold. Mining Annual Review. Mining Journal, 15-20.

Miyashiro, A., 1973. Metamorphism and metamorphic belts. George Allen and Unvwin Ltd., London, pp. 492.

Nesbitt, B.E., 1986. Metamorphic sulfide-silicate equilibria in the massive sulfide deposits at Ducktown Tennessee. Econ. Geol., 77, 364-378.

Nesbitt, B.E., 1986. Oxide-sulphide-silicate equilibria associated with metamorphosed ore deposits. Part I: Theoretical considerations. Econ. Geol., 81, 831-840.

Nesbitt, B.E., 1986. Oxide-sulphide-silicate equilibria associated with metamorphosed ore deposits. Part II: Pelitic and felsic volcanic terrains. Econ. Geol., 81, 841-856.

Nicholas, A., and Poirier, J.P., 1976. Crystalline Plasticity and Solid State Flow in Metamorphic rocks. Wiley & Sons, New York. pp. 432.

de Oliveira, O.A.B., 1986. As falhas de empurrao e sual implicacoes na estratigrapfia e metalogenese do Quadrilatero Ferrifero--M.G. XXXIV Congresso Brasileiro de Geologia, Goiania, Goias, Brasil (pr-print)

Pearce, J.A. and J.R. Cann, 1973. Tectonic setting of basic volcanic rocks determined using trace elements analyses. Earth. Plant. Sci. Lett., 19, 290-300

Perchuk, L.L., 1977. Thermodynamic control of metamorphic processes. In: Saxena, S.K. and Bhattacharji, S. (editors). Energetics of Geologocal Processes. Soringer-Verlag, New York. pp. 285-352.

Pyke, D.R., Naldrett, A.J. and Eckstrand, O.R., 1973. Archaean ultramafic flows in Munro Mownhip, Ontario. Bull. Geol. Soc. Amer., 84, 955-978.

Rasse, P., 1974. Al and Ti contents of hornblende, indicators of pressure and temperature of regional metamorphism. Contr. Mineral. Petrol., 45, 231-236.

Ramsay, J.G., 1967. Folding and fracturing of rocks. McGraw-Hill Book Company, Toronto. pp.568.

Richardson, S.V., Kesler, S.E., Essene, E.J., and Jones, L.M., 1986. Origin and geochemistry of the Chapada Cu-Au Deposit, Goias, Brazil: A metamorphosed wall-rock porphyry copper deposit. Econ. Geol., 81, 1884-1898.

Ridler, R.H., 1970. Relationship of mineralization to volcanic stratigraphy in the Kirkland-Larder Lake area, Ontario. Ont. Proc. Geol. Assock. Can., 21, 33-42.

Reeder, R.J., 1983. Crystal Chemistry of the rhombohedral carbonates. In: Carbonates: Mineralogy and Chemistry. R.J. Reeder (Ed.). Reviews in Mineralogy, 11, Mineralogical Society of America. pp394.

Ribeiro Filho, W., 1984. Geolgia e alguns aspectos das mineralizacoes aurideras das faixas Pilar e Guarinos. Sociedade Brasileira do Geologia, Nucleo Centro-Oest., 14, 6-24.

Ribeiro Filho, W., Costa, J.F.G., Araujo, V.A., Valente, C.R. Machado, E.C., Matos, S.H.S., Rodrigues, R., Vivian, O, Sa, A.M. and Lina, P.F.C., 1978. Projecto Geologia da Regiao de Pilar - Mara Rosa, Goias. DNPM-CPRM, 3, Goiania, Goias.

Romberger, S.B., 1986. The solution chemistry of gold applied to the origin of hydrothermal deposits. In: Clark, L.A. (ed). Gold in the Western Shield. CIM Special Volume 38, pp537.

Ronov, A.B. and Migdisov, A.A., 1970. Evolution of the chemical composition of the rocks in the shields and sediment cover of the Russian and North American Platform. Geochemistry International, 7, 294-324.

Rumble, D. and Finnerty, T.A., 1974. Devonian grossularite-spessartine overgrowths on Ordovician almandine from eastern Vermont. Amer. Mineral., 59, 558-562.

de Saboia, L.A.,1979, Os "greenstone belts" de Crixas e Goias-Go: Sociedade Brasileira de Geologia, Nucleo centro-oest,9,43-72.

de Saboia, L.A, Teixeira, N.A., de Castro, J.H. and Teixeira, A.S., 1981. Geologia do "Greenstone Belt" de Crixas (Go) e suas implicacoes geotectonicas. In: Anais do simosio sobre o craton do Sao Francisco e suas faixas marginais. Soc. Brasileira de Geo., 39-50.

de Saboia, L.A. and Teixeira, N.A., 1983 Ultramafic flows of the Crixas Greenstone Belt, Goias - Brazil. Precambrian Research, 22 23-40.

Sakai, C., Banno, S., Torium, M. and T. Higashino, 1985. Growth history of garnet in pelitic schists of the Sanbagawa metamorphic terrain in central Shikoku. Lithos, 18, 81-95.

Seward, T. M., 1973. Thiocomplexes of gold and the transport of gold in hydrothermal ore solutions. Geochim. Cosmochim. Acta., 37, 379-399.

Seward, T.M., 1984. The transport and depostion of gold in hydrothermal systems. In: R.P. Foster (ed.) Gold '82: Geology, Geochemistry and Genesis of Gold Depostis, Balkema, Rotterdam, 165-182.

Shaw, D.M., 1956. Geochemistry of pelitic rocks, Part III: Major elements and general geochemistry. Bull., Geological Society of America, 67, 919-934.

Schobbenhaus, C., Campos, D. de A., Derze, G.R. and H. E. Asmus, 1984. (editors). Geologia do Brasil. DNPM, Brasilia, pp. 501.

Schobbenhaus, C., et al., 1975. Carta Geologica do Brasil ao Milionesimo. Brasila, DNPM.

Sibson, R.H.,1977. Fault rocks and fault mechanisms. Geo. Soc. of London Journal, 133, 191-213.

Spry,A., 1969. Metamorphic Textures. Pergamon, New York. pp.350.

Stanton, R.L., 1972. Ore Petrology. McGraw Hill Book Company, Toronto, pp 713.

Stanton, R.L. and K.L. Williams, 1978. Garnet compositions at Broken Hill, New South Wales, as indicators of metamorphic processes. J. of Petrol., 19, 514-529.

Streckeisen, A., 1976. Classification of the common igneous rocks by means of their chemical composition. N. Jb. Niner. Mh., H-1, 1-15.

Teixeira, N. A., Saboia, L.A., Ferreira, M.C.B., Teixeira, A.S. and Castro, J.H.G., 1981. Estruturas e texturas das lavas ultrasicas e basicas do greenstone belt de Crixas - Goias, Brasil. Soc. Bras. Geol. Nucleo Centro-Oeste., 10, 38-87.

Tassinari, C.C.G. and R.M.G. de Montalvao, 1980, Estudo geochronologico do "greenstone belt" Crixas: Anais. Cong. Bras. Geol. Balneario de Camboriu, 5, 2752-2759.

Thompson, A.B., 1976. Mineral reactions in pelitic rocks: II. Calculations of some P-T-X (Fe-Mg) phase relations. A.J.S., 276, 425-454.

Thompson, J.B., Tracy, R.J., Lyttle, P., and Thompson, J.B., Jr., 1977. Prograde reaction histories deduced from compositional zonation and mineral inclusions in garnet from the Gassetts schist, Vermont. A.J.S., 277, 1152-1167.

Thompson, J.B., 1957. The graphical analysis of mineral assemblages in pelitic schists. Amer. Min., 42, 842- 858.

Thomson, M.L., Barnett, R.L. Fleet, M.E. and Kerrich, R., 1985. Metamorphic assemblages in the south range norite and footwall mafic rocks near the Kirkwood Mine, Sudbury, Ontario. Can. Mineral., 23, 173-186.

Tracy, R,J., 1982. Compositional zoning and inclusions in metamorphic minerals. In: J.M. Ferry (editior). Characterization of metamorphism through mineral equilibria. Reviews in Mineralogy, Volume 10, pp397.

Veizer, J., 1983. Trace Elements and Isotopes in Sedimentary Carbonates. In: R.J. Reeder, (Ed.). Carbonates: Mineralogy and Chemsitry. Reviews in Mineralogy, 111, pp394.

Viljoen, M.J. and Viljoen, R.P., 1969. Evidence for the existence of mobile extrusive peridotitic magma form the Komati Formation of the Onverwacht Group. Trans., Geol. Soc. Afr. Spec Pub., 2, 89-123.

Viljeon, M.J., Viljoen, R.P., and T.N. Pearton, 1982. The Nature and distribution of Archean komatiite volcanics in South Africa. In: N.T. Arndt and E. G. Nisbet, editors. Komatiites, George Allen & Unwin, Boston. pp 526

Wedepohl, K.H., 1969. Composition and abundance of common sedimentary rocks. In: Wedepohl, K.H. (editor). Handbook of Geochemistry. Springer-Verlag, Berlin, 250-271.

Winkler, G.F., 1974. Petrogenesis of metamorphic rocks. Springer-Verlag, New York, pp. 334.

Yardley, B.W.D. Leake, B.E. and C.M Farrow, 1980. The metamorphism of Fe-rich pelites from Connemara, Ireland. J. Sed. Petrol., 21, 365-399.

Zen, E., 1960. Metamorphism of lower Paleozoic rocks in the vincinity of the Taconic range in the west-central Vermont. Amer. Min., 45, 129-175.